AD NUMBER

AD861847

LIMITATION CHANGES

TO:

Approved for public release; distribution is unlimited.

FROM:

Distribution authorized to U.S. Gov't. agencies and their contractors; Critical Technology; FEB 1969. Other requests shall be referred to Army Electronics Command, AMSEL-XL-C, Fort Monmouth, NJ 07703. This document contains export-controlled technical data.

AUTHORITY

usaec ltr, 30 jul 1971

Technical Report ECOM-02261-F

WAVEGUIDE, WAVEGUIDE CIRCUITS AND ANTENNA RESEARCH STUDY

FINAL REPORT

BY

E. H. SCHEIBE

FEBRUARY 1969

07703

ECOM

UNITED STATES ARMY ELECTRONICS COMMAND · FORT MONMOUTH, N.J.

CONTRACT DA36-039-AMC-02261(E)

THE UNIVERSITY OF WISCONSIN
DEPARTMENT OF ELECTRICAL ENGINEERING
MADISON, WISCONSIN

30.3

DISCLAIMER

The findings in this report are not to be construed as an official Department of the Army position unless so designated by other authorized document.

The citation of trade names and names of manufacturers in this report is not to be construed as official Government indorsement or approval of commercial products or services referenced herein.

Destroy this report when no longer needed. Do not return it to the originator.

TECHNICAL REPORT ECOM-02261-F FEBRUARY 1969

WAVEGUIDE, WAVEGUIDE CIRCUITS AND ANTENNA RESEARCH STUDY

Final Report

1 September 1964 to 31 January 1969

Report No. 17

Contract No. DA 36-039 AMC-02261 (E)

DA Project No. 3A99-25-004

Prepared by

Elmer H. Scheibe

University of Wisconsin

Department of Electrical Engineering

Madison, Wisconsin

for

U. S. Army Electronics Command

Fort Monmouth, New Jersey

TABLE OF CONTENTS

LIST OF ILLUSTRATIONS

LIST OF ILLUSTRATIONS

LIST OF ILLUSTRATIONS

TABLES

I. PURPOSE OF CONTRACT

An engineering research study on novel electromagnetic waveguides, antennas, filters and related devices is to be carried out to supplement in-house research. Work on surface waves, antennas based on surface waves, and microwave branching filters is to be continued when special problems arise. Special emphasis will be placed on studies concerning the beam waveguide and beam waveguide resonator. The program is to give special considerations to problems and structures which are important from the viewpoint of practical military application.

It is contemplated that this program will include the following subjects:

a. The determination of circuit properties of beam waveguide resonators.

b. A study of the coupling problem between beam waveguide resonators and conventional waveguides.

c. Investigation of antennas based on the beam waveguide.

d. Frequency stabilization with beam waveguide resonators.

e. Other problems related to the above which are agreed to by the contractor and contracting officer's representative.

II ABSTRACT

The research work that was carried out under this contract was a continuation of, but over and beyond, the studies made under Contract No. DA-36-039-sc-85188. This final report covers the period from September 1, 1964 to January 31, 1969. During this period three distinct studies were carried out. Two of these studies dealt with topics closely related to the beam waveguide. The third study was a separate one and was concerned with the theory and design of a new type of filter called a cut-off coupled microwave filter.

Part 1 of the report describes the general study made of beam waveguide resonators at millimeter wavelengths. An important result of this study was the derivation of the equivalent circuits for resonators with input and output coupling. An extensive bibliography on guided electromagnetic wave beams, beam waveguides, beam waveguide antennas, beam waveguide resonators, and Fabry-Perot resonators is included in Part 1 of this report.

Part 2 of this report describes a new type of waveguide filter called a cut-off coupled microwave filter. The theory, design and fabrication of these filters as well as the measurements made on them is described in some detail.

Part 3 of this report deals with two general applications of the beam waveguide of rectangular symmetry. One of the studies was concerned with the rectangular beam waveguide resonator and the other with a rectangular beam waveguide antenna formed from the resonator.

III. INTRODUCTION

The research work that was carried out under this contract was a continuation of, but over and beyond, the studies made under Contract No. DA-36-039-sc-85188. This final report covers the period from September 1, 1964 to January 31, 1969. During this period three distinct studies were carried out. Two of these studies dealt with topics closely related to the beam waveguide. The third study was a separate one and was concerned with the theory and design of a new type of filter called a cut-off coupled microwave filter.

These three studies are essentially independent of each other and hence each will be treated as a unit. This report will therefore be divided into three parts, each of which will be self contained and will include a bibliography, appendixes when necessary and the conclusions arrived at as the result of the study.

Part 1 of the report will describe the research carried out between September 1964 and June 1967.[1] Because of the large amount of experimental work detailed in the quarterly reports, the material will not be repeated here. Since the study was concerned in general with beam waveguide resonators at millimeter wavelengths, an overall view of the work will be given. An important result of this study was the derivation of the equivalent circuits for the coupled resonators. Since this derivation has not previously been reported, it will be given here in some detail. An extensive bibliography on guided electromagnetic wave beams, beam waveguides, beam waveguide antennas, beam waveguide resonators, and Fabry-Perot resonators is included in Part 1 of this report.

---

1. The research reported on in this section appears also as a part of the Ph.D. thesis of Arthur W. Murphy (107).

Part 2 of this report will be concerned with the research carried out between September 1965 and September 1966.[2] The research performed during this period dealt with a new type of waveguide filter called a cut-off coupled microwave filter. Conventional waveguides arranged in a special configuration were used to form the filter. The theory, design and fabrication of these filters as well as the measurements made on them will be described in some detail.

Part 3 of this report will describe the research carried out between September 1966 and January 1969.[3] The research performed during this period dealt with two general applications of the beam waveguide of rectangular symmetry. One of the studies was concerned with the rectangular beam waveguide resonator and the other with a rectangular beam waveguide antenna formed from the resonator.

---

2. The research reported on in this section appears also as a part of the M.S. thesis of John R. Brauer.

3. The research reported on in this section appears also as a part of the Ph.D. thesis of John R. Brauer.

PART 1

BEAM WAVEGUIDE RESONATORS

AT MILLIMETER WAVELENGTHS

Previous Studies

The investigation carried out under this phase of the contract was concerned with a general study of the characteristics and properties of the cylindrical beam waveguide developed by Dr. Georg Goubau of the U.S. Army Electronic Command. The work of Goubau and his associates is detailed in the literature.[4,5,6,7,8,9]

Briefly, the beam waveguide consists of a launching and receiving antenna, usually horns, and a number of equally spaced lenses or phase correcting plates placed between the antennas to reset the cross-sectional phase of the guided beam. The cross-sectional field distribution of the beam is not constant with distance along the beam as is the case in conventional

---

4. G. Goubau and J.R. Christian, "A New Waveguide for Millimeter Waves," presented at URSI-IRE Fall meeting, San Diego, California, October 1959.

5. G. Goubau and F. Schwering, "On the Guided Propagation of Electromagnetic Wave Beams," IRE Trans. on Antennas and Propagation, Vol. AP-9, May 1961. pp. 248-256. This paper was first presented at URSI-IRE Spring meeting, Washington, D.C., May 1960.

6. J.R. Christian and G. Goubau, "Experimental Studies on a Beam Waveguide for Millimeter Waves," IRE Trans. on Antennas and Propagation, Vol. AP-9, May 1961, pp. 256-263.

7. J.R. Christian and G. Goubau, "Some Measurements on an Iris Beam Waveguide", Proc. IRE, Vol. 49, November 1961, pp. 1679-1680.

8. G. Goubau, Optical Relations for Coherent Wave Beams, presented at Sym. on Electromagnetic Theory and Antennas, Copenhagen, Denmark, June 25, 1962: published in Electromagnetic Theory and Antennas, in International Series of Monographs on Electromagnetic Waves, E.C. Jordan, Ed., Vol. 6, part 2, Pergamon Press, New York, N.Y., 1963.

9. G. Goubau, and J.R. Christian, "Some Aspects of Beam Waveguides for Long Distance Transmission at Optical Frequences," IEEE Trans. on Microwave Theory and Techniques, Vol. MTT-12, March 1964, pp. 212-220.

waveguides. The amplitude and phase of the cross-sectional distribution vary with distance along the beam. The cross-sectional amplitude distribution however, is repeated at certain distances from the source. The original phase distribution at the source can be reconstituted by phase transformers placed at the point where the original amplitude distribution is repeated. Thus a reiterative system is formed which is called a beam waveguide. The beam waveguide can be made to have very small losses. The possible applications of the beam waveguide as a low loss transmission line for the millimeter through optical frequency range is of prime interest. The resonator formed from this transmission line, called the beam waveguide (or the Fabry-Perot) resonator, has among other desirable characteristics a very high Q in the millimeter through the optical frequency range. The beam waveguide resonator is therefore a very useful millimeter wave circuit element which makes possible the extension of resonator techniques into the millimeter and optical frequency ranges.

A brief review of the studies made on the beam waveguide and the beam waveguide resonator under previous contracts will be given. Such a review will assist in orienting the further investigations made under the present contract.

The first phase of the early investigations was concerned with the measurement of the very small diffraction losses of the waveguide. Work on the measurement of the diffraction losses of the beam waveguide has been completed and reported on previously.[10] In addition, measurements of the field

---

10. E.H. Scheibe, "Surface Wave, Antenna and Microwave Filter Engineering Research Study," Final Report on Contract No. DA-36-039-sc-78326, Department of Electrical Engineering, University of Wisconsin, Madison, Wisconsin, September 30, 1961.
Also see J.B. Beyer and E.H. Scheibe, "Loss Measurements of Beam Waveguides," IEEE Trans. on Microwave Theory and Techniques, Vol. MTT-11, January 1963, pp. 18-22.
and E.H. Scheibe, "Measurements on Resonators Formed from Circular Plane and Confocal Paraboloidal Mirrors," Proc. IRE, Vol. 49, June 1961, p. 1079.

distribution within the beam for the lowest mode, and an analytical study of the losses of the higher modes which will propagate on such a line have also been completed.[11]

The study of the diffraction loss for the lowest loss mode of the beam waveguide was made with a loop coupled resonator consisting of a paraboloidal mirror as one end plate and a flat mirror as the other end plate. Such a resonator simulates one iteration of the beam waveguide and the diffraction loss per iteration can be determined from the measured Q of the resonator. Since the diffraction loss to be measured was very small and hence the Q of the resonator was very high, special apparatus and techniques were devised to measure the Q. These studies and measurements were made at, or near, a frequency of 9 GHz.

The remainder of the studies completed thus far were made at, or near, a frequency of 35 GHz and are detailed in previous reports.[12] These studies are almost entirely concerned with applications of the beam waveguide or Fabry-Perot resonator.

Though a large number of modes may be present in the beam in many instances, only the lowest loss mode survives in a reasonable length of beam waveguide. In resonators formed from the beam waveguide it is possible, under proper conditions, to encourage the excitation of selected modes only.

---

11. J.B. Beyer and E.H. Scheibe, "Higher Modes in Guided Electromagnetic Wave Beams," IEEE Trans. on Antennas and Propagation, Vol. AP-10, May 1962, p. 349.

    See also J.W. Mink, "Higher Modes in Electromagnetic Wave Beams," M.S. Thesis, University of Wisconsin, Madison, Wisconsin, 1962.

12. E.H. Scheibe, "Surface Wave and Antenna Engineering Research Study," Final Report on Contract No. DA-36-039-sc-85188, Department of Electrical Engineering, University of Wisconsin, Madison, Wisconsin, November 30, 1964.

    See also J.W. Mink and E.H. Scheibe, "A Dual-Mode Beam Waveguide Resonator and Frequency Stabilizer at Millimeter-Wave Frequencies," IEEE Trans. on Microwave Theory and Techniques, Vol. MTT-14, May 1966, pp. 222-228.

In cases where a single mode or a selected number of modes exists it is advisable to know the field pattern or transverse field distribution in the cross-section of the beam of individual modes or mode combinations. The radial field distribution, which depends on the Laguerre polynomials that appear in the solution of the beam waveguide, was calculated on a computer for a number of the lowest loss modes. With the radial dependence of the field known, the most favorable position of the coupling elements for launching the desired higher modes can be determined. Because it is convenient to refer to individual modes at times, particularly the lower loss modes, it was necessary to devise a meaningful mode designation. A mode notation was chosen which used the degree and order of the Laguerre polynomial associated with each mode.

The frequency stabilization of microwave oscillators was one of the studies carried out which used the beam waveguide resonator as a microwave circuit element. The resonator was used as the frequency control or high Q reference cavity and was operated in a dual mode. The dual mode operation of the beam waveguide resonator made it possible to form a frequency discriminator which was then used in a feedback loop to stabilize the frequency of a microwave oscillator. A marker generator, consisting of a very stable low frequency crystal and a series of varactor multipliers, was developed in order to measure both the long term and short term stabilities of stabilized microwave oscillators operating near 35 GHz. The use of the beam waveguide resonator as a stalo cavity for oscillator stabilization was also investigated.

The work done on the frequency stabilization of microwave oscillators using the dual mode beam waveguide resonator led to a study of the measurement of the dielectric constant of gases at 35 GHz. In this application the dual mode beam waveguide resonator was put in an evacuated chamber to determine its resonant frequency. When a gas was admitted into the chamber

the change in the resonant frequency of the resonator was a measure of the dielectric constant of the gas. The dielectric constants of dry air, helium, nitrogen, oxygen and argon have so far been measured with an accuracy of a few parts in 10^7 at 35 GHz.

When the beam waveguide resonator operating in the low loss mode is fitted with one end plate which is partially transparent it becomes an antenna. A study of such an antenna was made in which the partially transparent end plate was fabricated from polystyrene sheets with air spaces between them. This type of construction makes it possible to control the value of the reflection coefficient of the end plate. The energy passing through the end plate will radiate into space.

The radiation pattern of this beam waveguide antenna was determined analytically from the field distribution in the aperture. Measurements of the radiation pattern of the antenna bore out the analysis made. Other forms of the beam waveguide antenna are possible and additional antenna studies have been carried out and are detailed in Part 3 of this report.

A problem which arises when using the beam waveguide is that of coupling energy into the system from a conventional waveguide system. Usually a conventional microwave horn along with a dielectric phase corrector is used. A method which has better launching efficiency uses a diagonal horn and a properly designed phase correcting lens. The field of the diagonal horn has an amplitude distribution which closely simulates the radial amplitude distribution of the lowest loss mode of the beam waveguide. When the diagonal horn is used with a properly designed phase corrector, the output of the combination very closely simulates the field of the lowest loss mode of the beam waveguide in both amplitude and phase.

Coupling energy from a conventional waveguide system into a beam waveguide resonator also raises problems and is the principal subject of Part 1 of this

report. Loop coupling can be used at a frequency of 9 GHz but is not practical at 35 GHz. The details of the coupling schemes possible at this frequency are given in another section of this part of the report.

IV. THEORETICAL CHARACTERISTICS OF BEAM WAVEGUIDE RESONATORS

A. General Considerations

A beam waveguide resonator in general consists of two reflecting surfaces mounted normal to and concentric about a common axis. Especially for microwave applications, it is advantageous to consider the fields in the resonator as being due to a traveling wave beam propagating along the axis of the resonator. The resonance condition then is that the total phase shift of the beam must be a multiple of 2π radians in traversing a path twice the physical length of the resonator. The resonance condition may also be defined in terms of a total phase shift of π radians in a path length equal to the physical length of the resonator.

The cross sectional energy distribution and the divergence properties of the wave beam will in general be a property of the shape of the reflecting surfaces and the separation between the surfaces. Due to the finite size of the reflectors, some energy will be lost past the reflectors. These diffraction losses are a function of the resonator size and the cross sectional energy distribution of the beam. The most common geometries used for beam waveguide resonators is shown in Fig. 4-1.

When all resonator dimensions are large compared to the wavelength and when the reflector separation is large compared to the size of the reflectors, Kirchoff's diffraction theory may be applied to the fields in order to obtain the resonator field distributions as the eigenfunctions of the general integral equations[13]

---

13. H. Kogelnik, T. Li, "Laser Beams and Resonators", Proc. IEEE, vol. 54, 10, October, 1966, p. 1314.

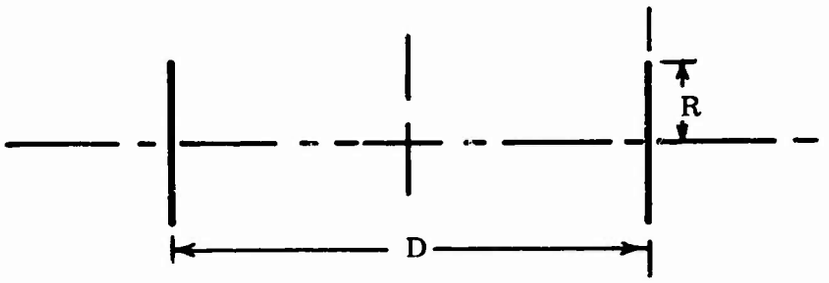

A. PARALLEL PLANE RESONATOR

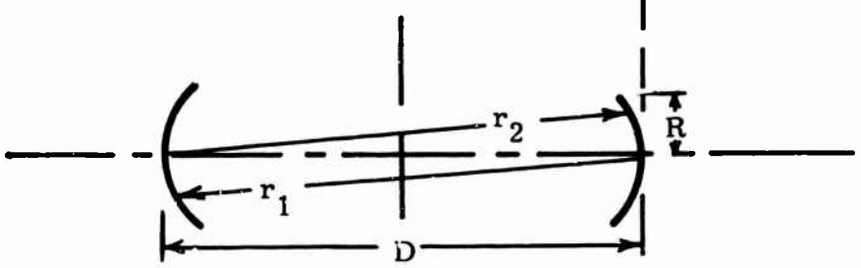

B. CONFOCAL RESONATOR
WHEN $r_1 = r_2 = D$

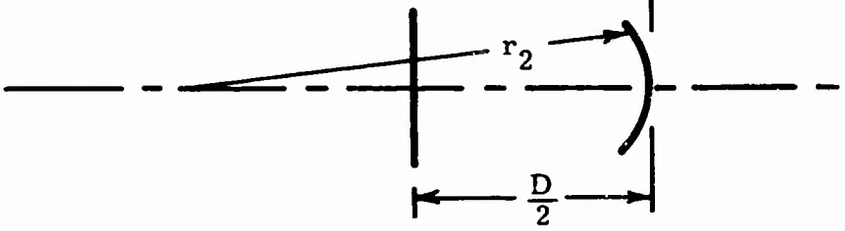

C. CONFOCAL HALF RESONATOR
WHEN $r_2 = D$

FIG. A - 1

MOST COMMON RESONATOR GEOMETRIES

$$\gamma^{(1)}E^{(1)}(s_1) = \int_{s_2} K^{(2)}(s_1,s_2)E^{(2)}(s_2)\, ds_2 \tag{4-1}$$

$$\gamma^{(2)}E^{(2)}(s_2) = \int_{s_1} K^{(1)}(s_2,s_1)E^{(1)}(s_1)\, ds_1 \tag{4-2}$$

where the eigenvalues $\gamma^{(1)}$ and $\gamma^{(2)}$ give the loss and phase change of a wave propagating between reflector surfaces s_1 and s_2. The form of the kernels K depends upon the choice of coordinate system in which the problem is to be solved.

In rectangular coordinates,[14]

$$K^{(1)}(x_2,x_1,y_2,y_1) = (\tfrac{j}{\lambda D})\exp\{-jk[(x_1-x_2)^2+(y_1-y_2)^2]/2D\} \tag{4-3}$$

where x_1 and y_1 are the coordinates on s_1

x_2 and y_2 are the coordinates on s_2

D is the reflector separation

$k = 2\pi/\lambda$.

Expressed in the cylindrical coordinate system, (ρ,ϕ,z)[15]

$$K^{(1)}(\rho_2,\rho_1,\phi_2,\phi_1) = (j/\lambda D)\exp\{-jk[\rho_2^2+\rho_1^2-2\rho_2\rho_1\cos(\phi_2-\phi_1)]/2D\} \tag{4-4}$$

In both rectangular and cylindrical coordinate systems it is possible to reduce the two dimensional equations into two orthogonal equations in one dimension. In rectangular coordinates, letting

$$E(x,y) = E_x(x)E_y(y) \tag{4-5}$$

then for Eq. 4-1:

$$\gamma_x^{(1)}E_x^{(1)}(x_1) = \int_X K^{(2)}(x_1,x_2)E_x^{(2)}(x_2)\, dx_2 \tag{4-6}$$

---

14. A. Fox, T. Li, "Resonant Modes in a Maser Interferometer", B.S.T.J., vol. 40, 1961, p. 485.

15. L. Bergstein, H. Schachter, "Resonant Modes of Optic Interferometer Cavities, I. Plane Parallel Reflectors", J. of the Opt. Soc. Am., vol. 54, July, 1964, p. 896.

$$\gamma_y^{(1)} E_y^{(1)}(y_1) = \int_Y K^{(2)}(y_1,y_2) E_y^{(2)}(y_2)\, dy_2 \tag{4-7}$$

$$K_x^{(2)} = (\lambda D)^{-1/2} e^{j\pi/4} e^{-jk(x_2-x_1)^2/2D} \tag{4-8}$$

$$K_y^{(2)} = (\lambda D)^{-1/2} e^{j\pi/4} e^{-jk(y_2-y_1)^2/2D} \tag{4-9}$$

$$\gamma^{(1)} = \gamma_x^{(1)} \gamma_y^{(1)} \tag{4-10}$$

Similar expressions can be written for Eq. 4-2 by interchanging superscripts (1) and (2) and subscripts 1 and 2 in the above equations.

In a cylindrical coordinate system, it has been shown that[16]

$$E(\rho,\phi) = R_n(\rho) e^{-jn\phi} \qquad n = \text{an integer} \tag{4-11}$$

$$\gamma_n R_n(\rho_2)(\rho_2)^{1/2} = \int_\rho K_n(\rho_2,\rho_1) R_n(\rho_1)(\rho_1)^{1/2} d\rho_1 \tag{4-12}$$

$$K_n(\rho_2,\rho_1) = \frac{j^{n+1} k}{D} J_n\left(k \frac{\rho_1\rho_2}{D}\right)(\rho_1,\rho_2)^{1/2} e^{-jk(\rho_1^2+\rho_2^2)/2D} \tag{4-13}$$

with J_n a Bessel function of the first kind and order n.

For solutions of Eqs. 4-1 and 4-2 to exist, it is necessary that the fields across one reflector of the resonator be related to the fields across the other reflector by a multiplicative constant. Whether this condition can be met or not determines the stability criterion for the particular resonator geometry as discussed by Fox and Li (30). Stability is determined by the relationship between the reflector curvatures and the separation between the reflectors. A stability diagram plotted in two dimensions in terms of the normalized coordinates G_1 and G_2 is shown in Fig. 4-2. The normalized coordinates G_1 and G_2 are defined by Gordon and Kogelnik as[17]

---

16. See p. 487 of reference in footnote 14.

17. J.P. Gordon, H. Kogelnik, "Equivalence Relations among Spherical Mirror Optical Resonators", B.S.T.J., vol. 43, November, 1964, p. 2875.

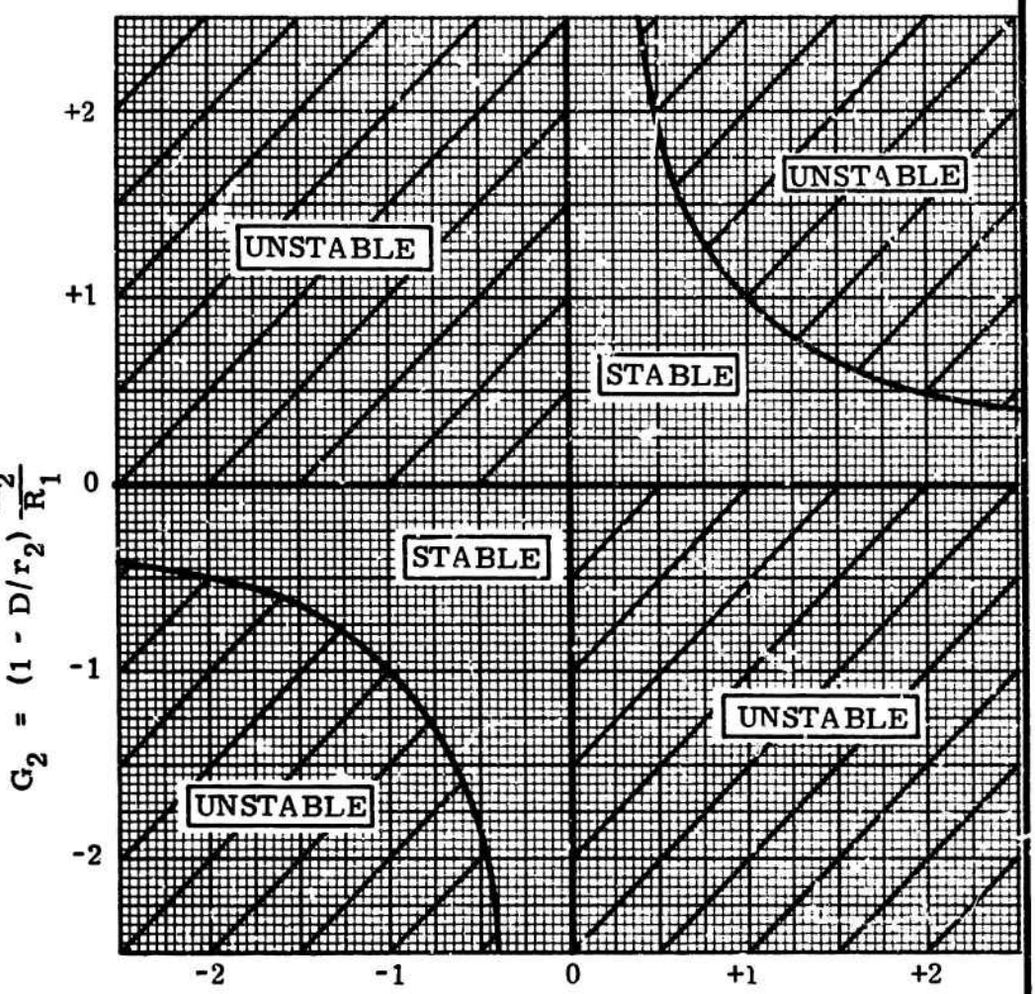

FIG. 4-2

STABILITY DIAGRAM

$$G_1 = \left(1 - \frac{D}{r_1}\right) \frac{R_1}{R_2} \tag{4-14}$$

$$G_2 = \left(1 - \frac{D}{r_2}\right) \frac{R_2}{R_1} \tag{4-15}$$

where r_1 and r_2 are the radii of curvature,

D is the separation,

and R_1 and R_2 are the radii of the circular reflectors. A particular resonator geometry will be stable only when

$$0<G_1G_2<1 \tag{4-16}$$

A third normalized coordinate formulated by Gordon and Kogelnik is given by

$$N = R_1R_2/\lambda D \tag{4-17}$$

Resonators which have the same G_1, G_2, and N are said to be equivalent in that they satisfy the same resonance conditions, have the same diffraction losses, and have field patterns on the reflectors which are related by a scale constant.

B. Plane Parallel Reflectors

For a resonator having identical plane parallel reflectors, $G_1=G_2=+1$. This resonator has inherently one of the highest losses for a particular value of N of any of the stable resonator configurations. Its losses are equaled by the concentric resonator, for which $G_1=G_2=-1$. Advantages which have led to the use of the parallel plane resonator in laser applications are the large percentage of the resonator volume which has substantial field components, and the dependance of the resonance condition on the mode number which allows control of the mode of operation by adjustment of the reflector spacing.

The losses for the dominant mode of a parallel plane resonator with identical reflectors of circular shape have been obtained by Fox and Li in terms of the percent power loss per transit length D of a traveling wave field as a function of the Fresnel number N characterizing the geometry.[18]

$$\text{Percent Power Loss} = 100(1 - |\gamma|^2) \tag{4-18}$$

where $\gamma = \gamma^{(1)} = \gamma^{(2)}$ is the eigenvalue of Eqs. 4-1 and 4-2. The loss characteristic for the dominant mode from Fox and Li is given in Fig. 4-3 in terms of the loss L expressed in db per transit as a function of N. The percentage power loss is related to the loss in db by

$$L_{db} = 10 \text{ Log}_{10} \left[1 - \frac{\% \text{ loss}}{100}\right]$$

In the linear region, it is claimed that the loss may be approximated by[19]

$$\frac{\% \text{ loss}}{100} = 0.207 \, N^{-1.4} \tag{4-19}$$

For N = 0, this gives $L_{db} = 0.0358$, which is in good agreement with Fig. 4-3.

The phase velocity of the wave beam in general is slightly different from the velocity of a plane wave in the medium occupying the resonator volume. For the parallel plane resonator, the beam undergoes an additional phase shift β beyond the free space value. This term depends upon the transverse field mode, the length of the resonator, and the size of the reflectors. The resonance condition for the dominant mode becomes

$$\ell\pi = \frac{2\pi}{\lambda_o} D + \beta\left(\frac{2\pi}{360}\right) \tag{4-20}$$

---

18. See p. 466 of reference in footnote 14.

19. See p. 481 of reference in footnote 14.

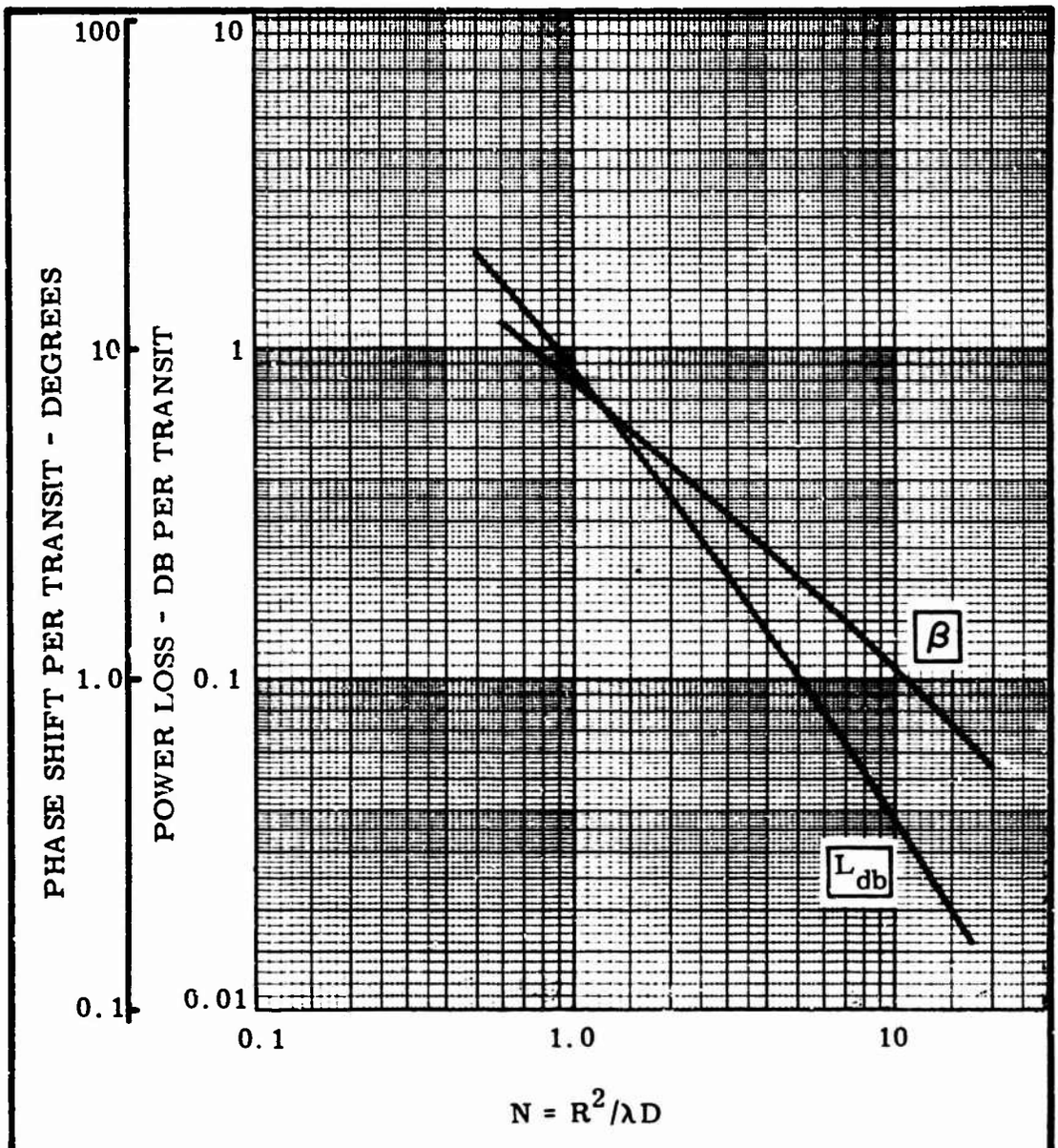

FIG. 4 - 3

DIFFRACTION LOSS FOR THE DOMINANT MODE OF A PARALLEL PLATE RESONATOR WITH CIRCULAR REFLECTORS

where ℓ = an integer

λ_o = free space wavelength

β = the additional phase shift in degrees.

The additional phase shift β is given in Fig. 4-3 as determined by Fox and Li.[20]

An analytical solution for a parallel plane resonator made by Vainshtein gives expressions for the losses and the phase shift for circular reflectors. With a change in notation, the losses are given by[21]

$$L_{db} = 10 \text{ Log}_{10} \left[1 - 8\chi_{mn}^2 \frac{A(M+A)}{[(M+A)^2+A^2]^2}\right] \qquad (4\text{-}21)$$

where $A = -\delta(1/2)/(\pi)^{1/2} = 0.824$

$\delta(1/2)$ is the zeta function of Riemann.

χ_{mn} = (m+1)th zero of J_n.

$M = (8\pi N)^{1/2}$ with N defined by Eq. 4-17.

m = n = 0 for the dominant mode.

The phase shift is given by

$$\beta = \left(\frac{360}{2}\right) \left[2\chi_{mn}^2 \frac{M(M+A)}{[(M+A)^2+A^2]^2}\right] \qquad (4\text{-}22)$$

For N = 10, Eqs. 4-21 and 4-22 give respectively a loss per transit of 0.0358 db and an additional phase shift β of 2.27° for the dominant mode. These values are in good agreement with the numerical values of Fox and Li. Equation 4-21 is expected to be valid over a larger range of N than Eq. 4-18.

It was also found by Vainshtein that the cross sectional field distribution at the reflectors was of the complex form

---

20. See p. 467 of reference in footnote 14.

21. L.A. Vainshtein, "Open Resonators for Lasers", J.E.T.P., (USSR), vol. 17, September, 1963, p. 717.

$$f(\rho,\phi) = \frac{c}{4\pi} J_m \left(\frac{x_{mn}\frac{\rho}{R}}{1+A(1+j)/M}\right) \cos m\phi \qquad (4\text{-}23)$$

where f may be either f_x or f_y.

Then:

$$\bar{E} = jk^{-1} (\text{grad div } \bar{f} + k^2\bar{f})$$

and $$\bar{H} = \text{curl } \bar{f}$$

where $k = 2\pi/\lambda_o$ = the free space propagation constant

and $j = \sqrt{-1}$.

For resonators having reflectors of rectangular shape and dimensions 2a X 2b, the eigenvalues and eigenfunctions may be obtained from those of the infinite strip resonator. The infinite strip reflector has a finite width, but is assumed to have an unlimited length. Such geometries have been extensively investigated. (2)(5)(30). The eigenvalue for a rectangular reflector 2a X 2b in size would be given by the product of the eigenvalue for a strip resonator of width 2a and the eigenvalue of a strip resonator of width 2b. The eigenfunctions may also be obtained as the eigenfunctions of one strip times those of another strip if one strip is assumed to extend along the x direction and the other along the y direction.

C. Confocal Geometry

Confocal geometry is characterized by the condition that the separation D between the two reflectors be given by

$$D = f_1 + f_2$$

where f_1 and f_2 are the focal lengths of reflectors 1 and 2 respectively. For spherical curvature

$$f = r/2$$

where r is the radius of curvature. The generalized values for a confocal resonator with f_1 equal to f_2 are

$$G_1 = G_2 = 0$$

Most of the theoretical work on beam waveguide resonator structures has been done for the confocal geometry. Some of the reasons for the concentration of effort on this particular geometry are, a) the confocal geometry is the only geometry in addition to the parallel plane case for which it has been shown possible to formulate analytical solutions, b) for a fixed value of the Fresnel number N, the confocal case has the lowest possible losses, and c) the confocal resonator may be considered a resonant section of the low loss beam waveguide developed by Goubau (99) (37) (40).

The first formulation of the fields in the confocal resonator was obtained by Goubau and Schwering (36). The method consisted of the solution of the wave equation in cylindrical coordinates under the restriction that, the propagation constant along the axis may have a spectrum of values limited to a narrow range and, that

$$|E(\rho,\phi,+z)| = |E(\rho,\phi,-z)|$$

Allowing the field to be of infinite extent in the transverse (ρ,ϕ) plane, the solution was found to be:[22]

$$E_{nv} = (\mu/\epsilon)^{1/2} H_{nv} = A_{nv}(1+u^2)^{-1/2}\left(\frac{\rho}{\rho_z}\right)^v L_n^v\left(\frac{\rho}{\rho_z}\right)^2$$

$$\cdot\{\exp[-1/2\left(\frac{\rho}{\rho_z}\right)^2 - j\psi] \quad \begin{pmatrix}\cos v\\ \sin v\end{pmatrix} \tag{4-24}$$

$$\psi = kz - (2n+v+1)\tan^{-1}u + 1/2u\left(\frac{\rho}{\rho_z}\right)^2 \tag{4-25}$$

where L_n^v are Laquerre polynomials of order v and degree n

$$u = \frac{z}{k\rho_o^2} \tag{4-26}$$

---

22. G. Goubau, "Optical Relations for Coherent Wave Beams," Sym. of Elect. Mag. Theory and Antennas, Pergammon Press, New York, 1963, p. 908, 915.

$$\rho_z^2 = \rho_o^2 (1+u^2) \tag{4-27}$$

where ρ_o, the mode parameter, is obtained from

$$(k\rho_o^2)^2 = (2 - \frac{d_1}{f_1}) f_1 d_1 = (2 - \frac{d_2}{f_2}) f_2 d_2 \tag{4-28}$$

with $\psi = 0$ at $z = 0$.

$k = 2\pi/\lambda_o$

λ_o = the free space wavelength

d_1 and d_2 are the distance from $z = 0$ of surfaces of constant phase

f_1 and f_2 are the equivalent focal lengths of the surfaces of constant phase at d_1 and d_2.

E_{nv} may be polarized in either the x or y direction, with H_{nv} then in the y or -x direction assuming propagation in the +z direction.

The amplitude functions of E_{nv} are plotted at $u = 1$ in Figs. 4-4, 4-5, and 4-6 as a function of the normalized radial coordinate x where

$$x = a \frac{\rho}{R}$$

R = the radius of the reflector.

The function a is given by

$$a = (k/D)^{1/2} R \tag{4-29}$$

when the resonator has two identical reflectors of radius R and separation D. The relation between a and N is

$$a = (2\pi N)^{1/2}$$

and is a more convenient parameter for use with confocal resonators than N. Due to the low diffraction losses a practical confocal resonator would have N less than 1.

The generalized Laguerre polynomials are given by

$$L_n^v = \sum_{i=0}^{n} \frac{(n+v)!}{(n-i)!(v+i)!} \frac{(-x^2)^i}{i!}$$

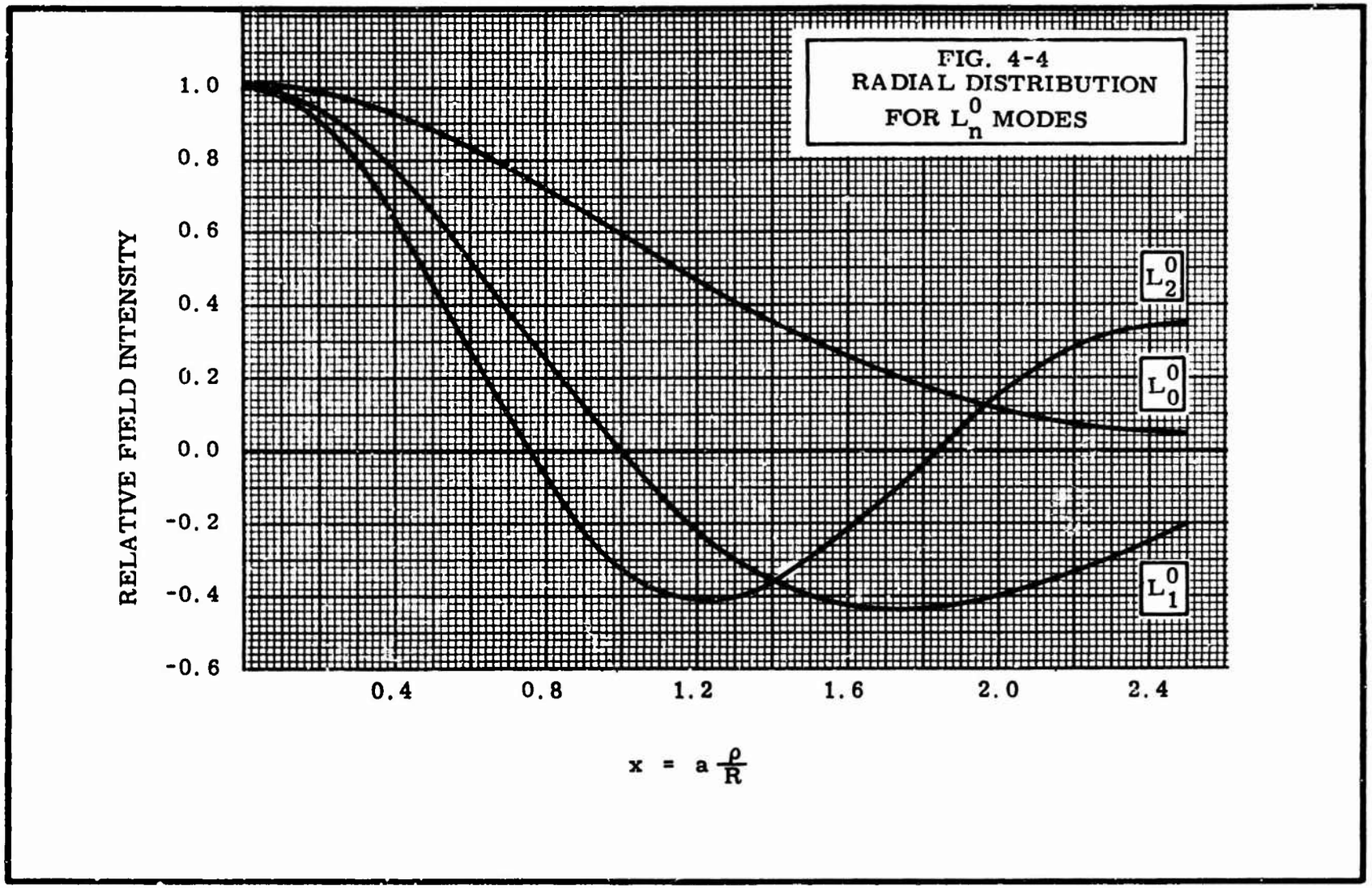
FIG. 4-4
RADIAL DISTRIBUTION
FOR L_n^0 MODES
RELATIVE FIELD INTENSITY
1.0
0.8
0.6
0.4
0.2
0.0
-0.2
-0.4
-0.6
0.4
0.8
1.2
1.6
2.0
2.4
L_2^0
L_0^0
L_1^0
$x = a\frac{\rho}{R}$

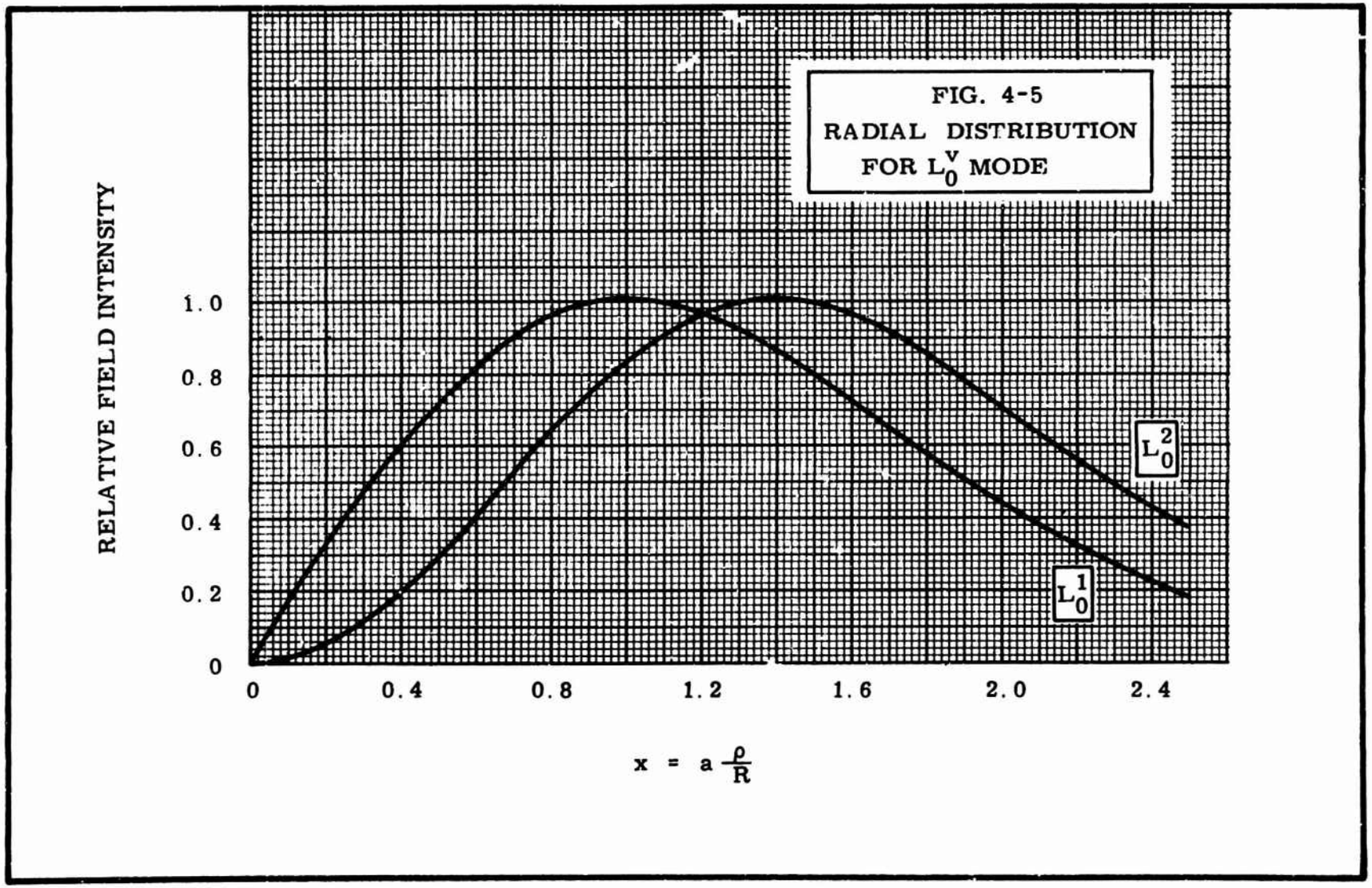
FIG. 4-5
RADIAL DISTRIBUTION
FOR L_0^v MODE
RELATIVE FIELD INTENSITY
1.0
0.8
0.6
0.4
0.2
0
0
0.4
0.8
1.2
1.6
2.0
2.4
L_0^2
L_0^1
$x = a\frac{\rho}{R}$

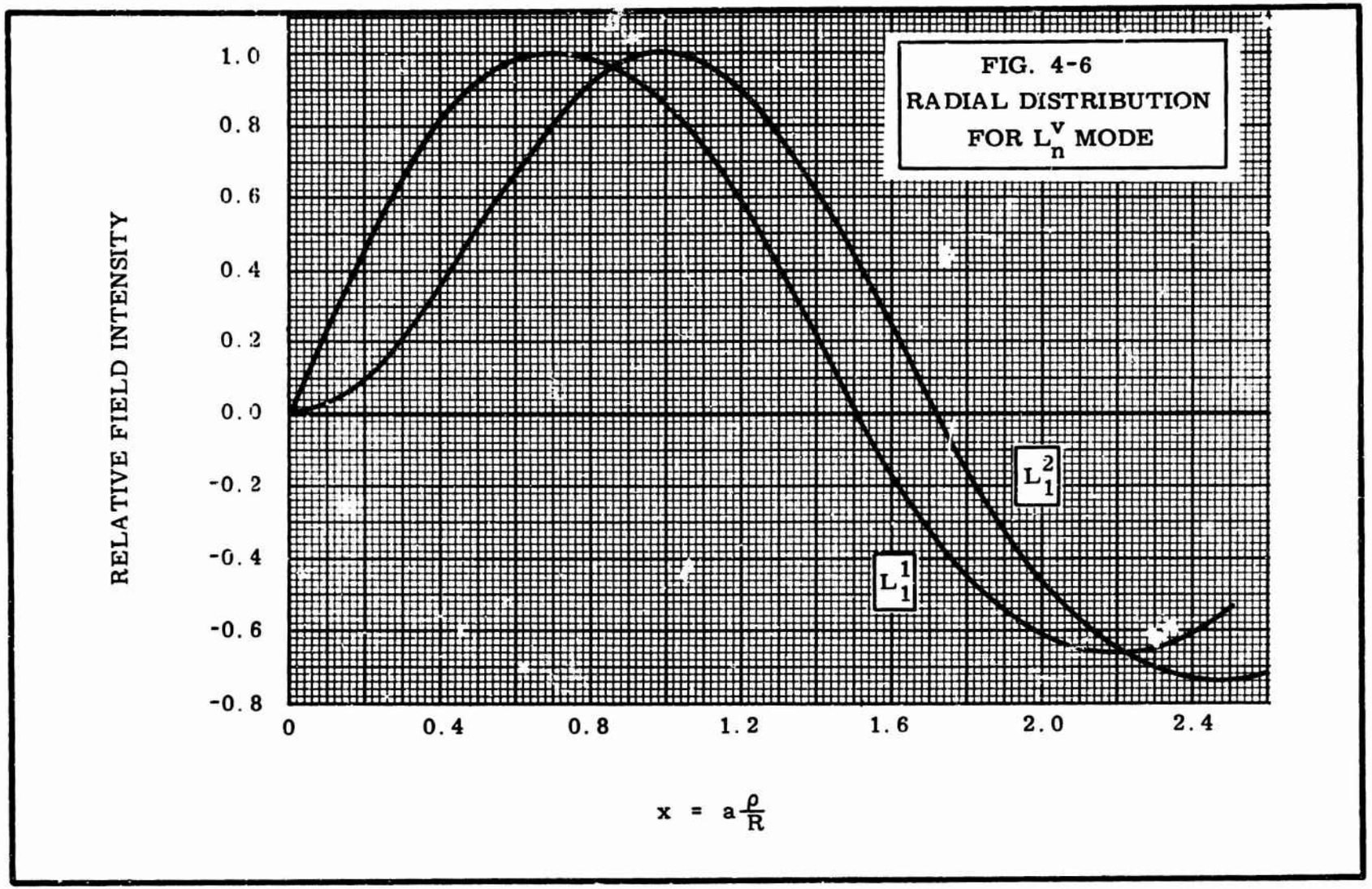
FIG. 4-6
RADIAL DISTRIBUTION
FOR L_n^v MODE
RELATIVE FIELD INTENSITY
1.0
0.8
0.6
0.4
0.2
0.0
-0.2
-0.4
-0.6
-0.8
0
0.4
0.8
1.2
1.6
2.0
2.4
L_1^2
L_1^1
$x = a\frac{\rho}{R}$

The modes for beam waveguide resonators are hybrid modes, that is, they are neither TE, TM, nor TEM to z, however the longitudinal components of the fields that do exist are small. The modes, which are determined by their Laguerre polynomials will be designed by the integers n and v. This has the advantage that the mode designation will tend to indicate the shape of the reflectors for the resonator under discussion. Thus the modes will be designated L_o^o, L_o^1, etc., for reflectors of circular symmetry.

For a confocal resonator, the reflector surfaces coincide with the surfaces of constant phase. These surfaces are parabolic, but for reflector diameters small compared to the radius of curvature, the constant phase surfaces may be approximated by spherical curvatures. Under the condition $f_1=f_2=D/2$, Eq. 4-23 becomes

$$k\rho_o^2 = D/2$$

and

$$\rho_z^2 = (D/2k)(1+u^2)$$

At the mid-plane of the resonator, taken as z = 0, Eq. 4-24 becomes

$$E_{nv}(z=0) = A_{nv}\left(\frac{2k\rho}{D}\right)^v L_n^v\left(\frac{2k\rho}{D}\right)^2 \cdot$$

$$\left[\exp\left\{-1/2\left(\frac{2k\rho}{D}\right)^2 - j\psi\right\}\right]\begin{pmatrix}\cos v\phi \\ \sin v\phi\end{pmatrix} \qquad (4\text{-}30)$$

where from Eqs. 4-25 and 4-26 it is found that $\psi = 0$ in the plane z = 0. At $z = \pm D/2$, u = 1 and $\rho_z^2 = D/k$. Then,

$$E_{nv}\left(z=\pm\frac{D}{2}\right) = A_{nv}(2)^{-1/2}\left(\frac{k\rho}{D}\right)^v L_n^v\left(\frac{k\rho}{D}\right)^2 \cdot$$

$$\left[\exp -1/2\left(\frac{k\rho}{2}\right)^2 - j\psi\right]\begin{pmatrix}\cos v\phi \\ \sin v\phi\end{pmatrix} \qquad (4\text{-}31)$$

and again using Eqs. 4-25 and 4-26

$$\psi = \pm k\frac{D}{2} - (2n+v+1)\frac{\pi}{4} + 1/2\left(\frac{k\rho}{D}\right)^2 \qquad (4\text{-}32)$$

The resonance condition for the confocal full resonator is that

$$\psi(z=\frac{D}{2}) - \psi(z=-\frac{D}{2}) = \ell\pi \tag{4-33}$$

where ℓ is an integer.

$$\ell\pi = kD - (2n+v+1)\frac{\pi}{2} \tag{4-34}$$

The last term in the expression for ψ may be neglected since the reflectors fit surfaces of constant phase. Therefore, ψ may be evaluated at $\rho = 0$.

When the reflecting surfaces for the resonator, or phase correctors for the beam waveguide, are of finite extent, the fields will be modified slightly and there will be a diffraction loss at each reflector. The value of this loss as a function of resonator size and mode number has been obtained by Goubau and Schwering (36) and Beyer and Scheibe (6) by an expansion of eigenvalue equations similar to Eqs. 4-12 and 4-13 in terms of the generalized Laguerre polynomials. The losses shown in Fig. 4-7 were obtained on a computer using the first ten terms of the expansion.[23]

The integral equations for the fields in the confocal resonator with circular reflectors of finite size have also been evaluated by numerical integration (31), and by power series expansion (62). The results obtained in these cases appear to be in good agreement with those presented in Fig. 4-7.

In an analysis similar to that used to determine the beam modes in a system of cylindrical symmetry, Schwering obtained the fields for beam modes in rectangular coordinates for a square or rectangular symmetry condition. For fields of infinite extent in the transverse plane[24]

---

23. J. Beyer, E. Scheibe, "Higher Modes in Guided Electromagnetic Wave Beams," Trans. IRE, AP-10, May 1962, p. 349.

24. F. Schwering, "Reiterative Wave Beams of Rectangular Symmetry," Archiv Elect. Ubertragung, vol. 15, December 1961, p. 558.

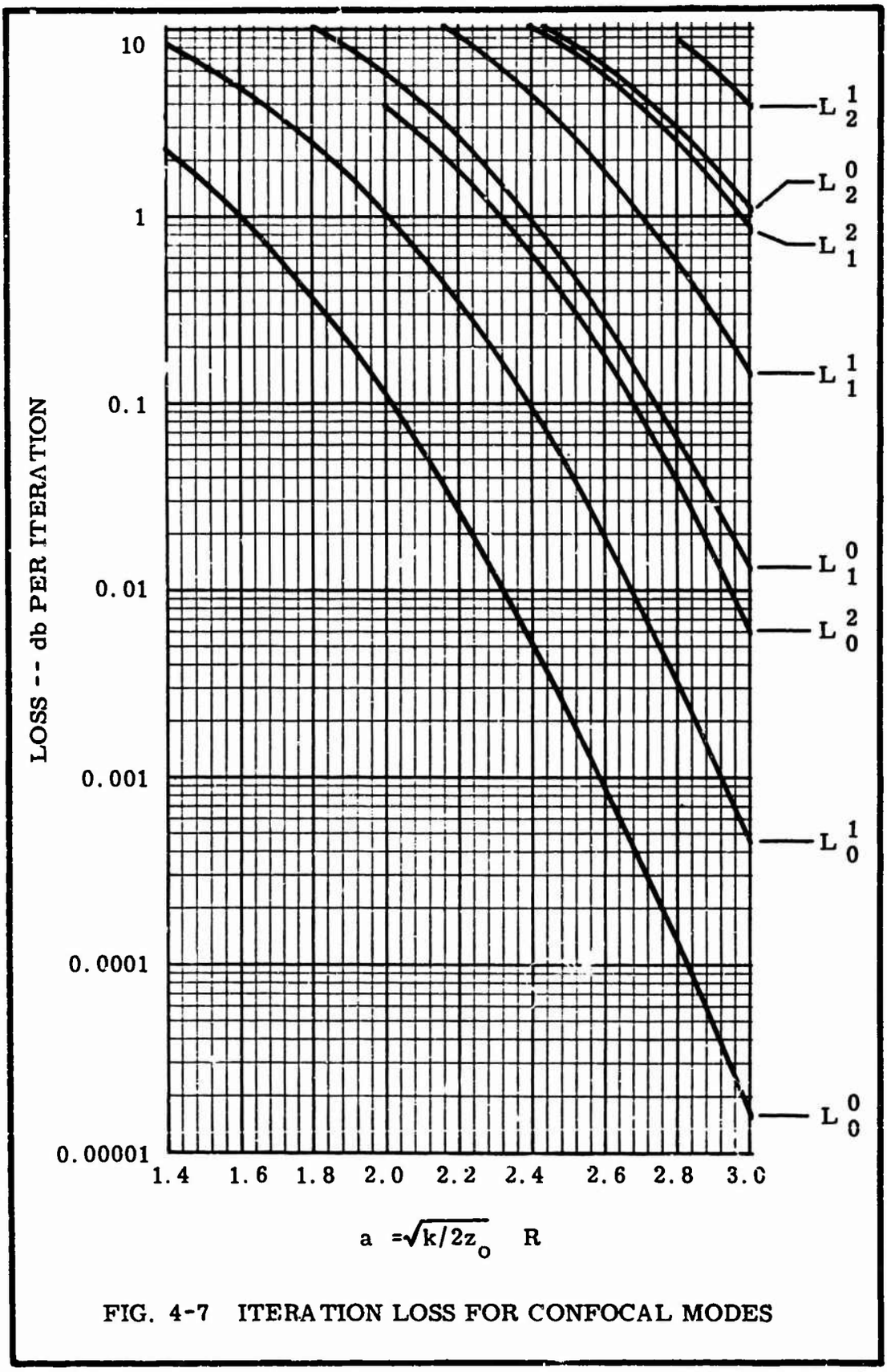

FIG. 4-7 ITERATION LOSS FOR CONFOCAL MODES

$$E_{nm} = 4\pi u_o v_o [1+z_u^2)(1+z_v^2)]^{-1/4} \cdot$$

$$\cdot He_n\{\frac{x'}{(1+z_u^2)^{1/2}}\} \cdot He_m\{\frac{y'}{(1+z_v^2)^{1/2}}\} \cdot \exp\{-1/4(\frac{x'^2}{1+z_u^2} +$$

$$\frac{y'^2}{1+z_v^2})\} \cdot \exp\{-j\ 1/4(\frac{z_u x'^2}{1+z_u^2}) + (\frac{z_v y'^2}{1+z_v^2}) +$$

$$j[(n+1/2)\tan^{-1} z_u + (m+1/2)\tan^{-1} z_v]\} \qquad (4\text{-}35)$$

$$x' = 2u_o x \qquad y' = 2v_o y$$

$$z_u = 2u_o^2 \frac{z}{k} \qquad z_v = 2v_o^2 \frac{z}{k}$$

u_o and v_o are analogous to the ρ_o of the cylindrical case. The confocal condition corresponds to

$$u_o = v_o = (k/2z_o)^{1/2} \qquad z_o = D/2$$

The $He_{nm}(w)$ are Hermit polynomials defined by

$$He_n(w) = (-1)^n \exp(w^2/2)\ \frac{d^n}{dw^n}\ (e^{-w^2/2}) \qquad (4\text{-}36)$$

Under confocal conditions, $Z_u = Z_v = 1$ for $z = z_o$ and $Z_u = Z_v = 0$ for $z = 0$. The resonance condition for the confocal case can be derived as

$$\ell\pi = kD - (n+1/2)\ \frac{\pi}{2} - (m+1/2)\ \frac{\pi}{2} \qquad \ell, m, n \text{ integers} \qquad (4\text{-}37)$$

Schwering has solved for the fundamental mode energy distribution and diffraction losses when the phase correctors of a beam waveguide are of finite extent by an expansion of an integral equation similar to Eqs. 4-2 and 4-3 in terms of the Gaussian Hermit functions characterizing the unlimited fields.

Boyd and Gordon have shown that the fields for the confocal resonator with finite rectangular reflectors can be formulated in terms of prolate

spheroidal wave functions (10). These functions are also shown to reduce to the Gaussian-Hermite functions obtained by Schwering when the reflectors are sufficiently large. Boyd and Gordon also give the diffraction losses for the six lowest loss modes for a square reflector 2a on a side, and for the three lowest loss modes of an infinite strip resonator of width 2a. By using the procedure mentioned on p. 17, the losses for any rectangular reflector can be determined.

D. Reflectors of Arbitrary Curvature

Analytical solutions for the eigenvalues and eigenfunctions of Eqs. 4-1 and 4-2 have not been obtained for arbitrary reflector separation and curvature. By the use of numerical integration, Li has solved for the eigenvalues and field distribution at the reflectors for both full and half resonators for several ratios of reflector curvature to reflector separation (48) (53). The ratios analyzed were for the radius of curvature variable from the separation length (confocal) to infinity (parallel plane).

Another approach for determining the losses of a resonator having arbitrary reflector curvature involves matching the reflector curvature and spacing to an equiphase surface of a beam mode defined by Eqs. 4-24 through 4-28. An equivalent a value for the resonator to be used in determining the diffraction loss is obtained by finding a confocal geometry which would have the same losses as the real resonator. Such a method was proposed by Boyd and Gordon during a study of resonators having rectangular reflectors (10).

The analysis is based on the assumption that two reflectors at equiphase surfaces will have the same diffraction loss if the field distributions and reflector dimensions are properly scaled versions of each other. That is, required that

$$R/w(z_o) = R'/w(z_o')$$

where $w(z_o)$ is the beam radius defined as the radius at which $\bar{E}$ falls to 1/e of its maximum value. The geometry and notation for this problem are shown in Fig. 4-8. By inspection of Eq. 4-24 for the L_o^o mode

$$w(z) = 2^{1/2}\rho_z = \left(\frac{2d'}{k}\right)^{1/2}\left(1 + \frac{z^2}{d'^2}\right)^{1/2} \tag{4-38}$$

where ρ_o has been chosen for the confocal condition at $z = d'$. In order to find

$$a' = (k/2d')^{1/2}R'$$

use

$$\frac{R'}{(2d'/k)^{1/2}\left(1+\frac{d'^2}{d'^2}\right)^{1/2}} = \frac{R}{(2d'/k)^{1/2}\left(1+\frac{d^2}{d'^2}\right)^{1/2}}$$

$$R' = \frac{2^{1/2}R}{\left(1+\frac{d^2}{d'^2}\right)^{1/2}}$$

$$a' = \frac{2^{1/2}(k/2d')^{1/2}R}{\left(1+\frac{d^2}{d'^2}\right)^{1/2}} = 2^{1/2}\,a\,\frac{(d/d')^{1/2}}{\left(1+\frac{d^2}{d'^2}\right)^{1/2}}$$

$$a' = 2^{1/2}\,a\,\left(\frac{d'}{d} + \frac{d}{d'}\right)^{-1/2} \tag{4-39}$$

where

$$a = (k/2d)^{1/2}R$$

for the resonator. It is now necessary to find the correct value of (d') in terms of the resonator parameters d, r, R.

From Eq. 4-25, define a constant phase surface by

$$\psi = kz+(1/2)u\left(\frac{\rho}{\rho_z}\right)^2 = \text{constant}$$

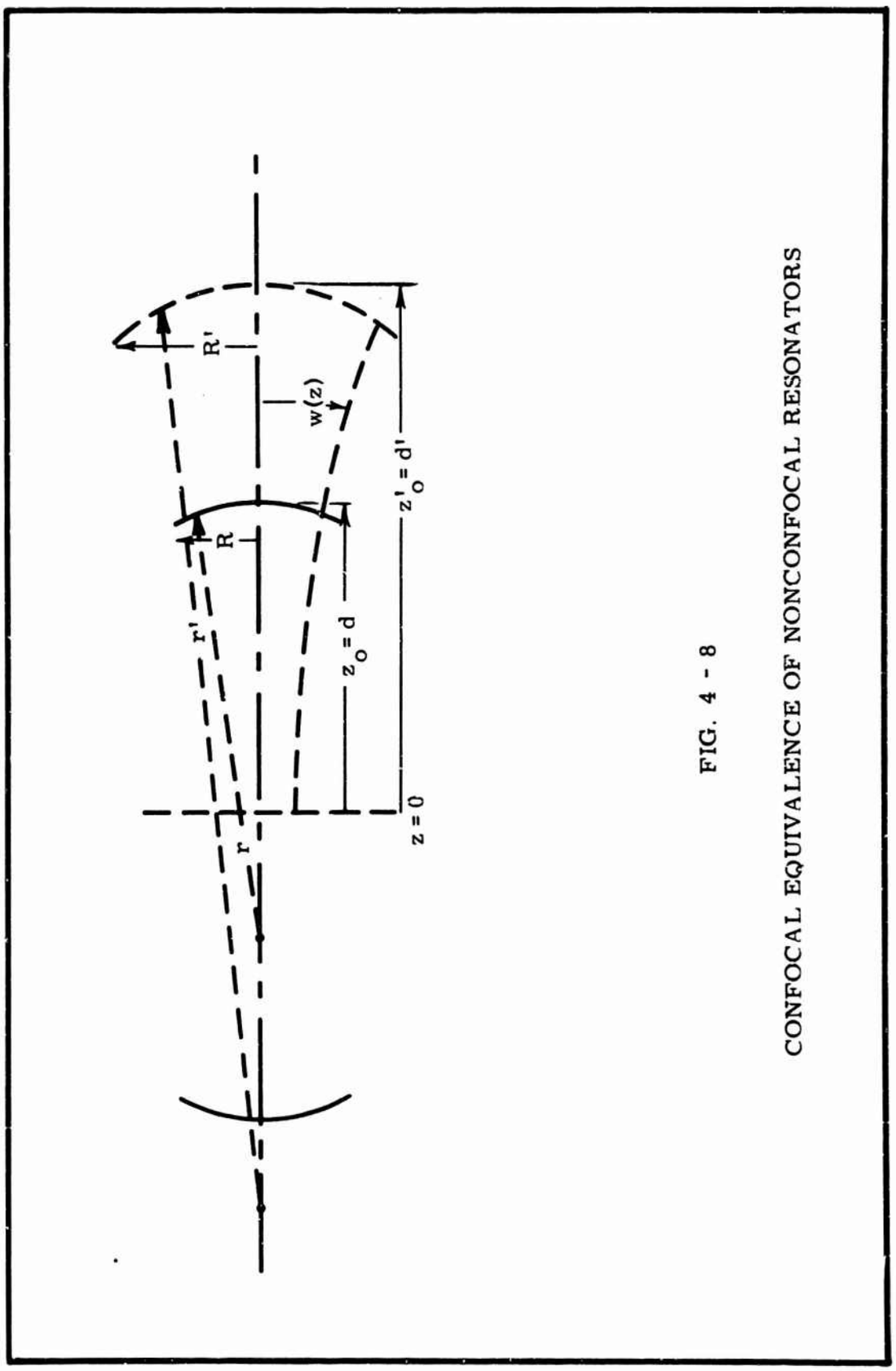

FIG. 4 - 8

CONFOCAL EQUIVALENCE OF NONCONFOCAL RESONATORS

where the small correction introduced by $\tan^{-1}u$ has been neglected. Then

$$z_o - z = \frac{1}{2k}\, u\left(\frac{\rho}{\rho_z}\right)^2 = \frac{u}{2k\rho_z^2}\,\rho^2 \tag{4-40}$$

where $kz_o = \psi$ for $\rho = 0$. This is of the form

$$z = f(\rho) = A\rho^2$$

and the radius of curvature is given by[25]

$$r = (1+f'^2(\rho))^{3/2}/f''(\rho)$$

Therefore

$$r = (1+4A^2\rho^2)^{3/2}/2A = 1/2A \qquad \rho \to 0$$

$$r = k\rho_z^2/u = k\rho_o^2(1+u^2)/u$$

For the confocal beam

$$u = z/d' \qquad\qquad k\rho_o^2 = d'$$

and

$$r = d'\,\frac{\left(1+\frac{z^2}{d'^2}\right)}{z/d'} = \frac{d'^2}{z} + z \tag{4-41}$$

Thus, as $z \to 0$, $r \to \infty$ and at $z = d'$, $r = 2d'$ which is the confocal condition. Now, matching this curvature to that of the resonator reflector at $z = d$

$$d' = (rd - d^2)^{1/2} \tag{4-42}$$

$$a' = 2^{1/2}\, a\left[\frac{(r-d)^{1/2}}{(d)^{1/2}} + \frac{(d)^{1/2}}{(r-d)^{1/2}}\right]^{-1/2}$$

$$a' = 2^{1/2}\, a\left(\frac{d}{r} - \frac{d^2}{r^2}\right)^{1/4} \tag{4-43}$$

Equation 4-42 indicates that d' for the equivalent confocal geometry may be defined for resonators satisfying the condition $(r-d) > 0$.

---

25. R.E. Johnson, F.L. Kichemeister, Calculus with Analytic Geometry, Allyn and Bacon, Boston, 1961, p. 431.

E. Resistive Losses

One of the more important features of beam waveguide resonator structures is the small amount of metallic surface necessary to confine a very large volume distribution of energy. However, the reflectors do introduce resistive losses in the resonator, and must be considered along with the diffraction losses in order to determine the operating characteristics of the device. For the purpose of evaluating the reflector losses, the traveling wave field in the resonator may be considered to be incident normally upon the reflector, although this will only be exact for cases where the reflectors are fitted to surfaces of constant phase.

By transmission line analogy, the load impedance represented by the reflector may be given for metallic reflectors as

$$Z_L = (\mu\omega/\sigma)^{1/2}\ 45^\circ = \frac{1+j}{\sqrt{2}}(\mu\omega/\sigma)^{1/2} \qquad (4\text{-}44)$$

σ = conductivity in mho/meter

$\omega = 2\pi f$ radians per second

$\mu = 4\pi X\ 10^{-7}$ henry/meter

The energy reflection coefficient may then be calculated as[26]

$$|\Gamma|^2 = 1 - 2(2\omega\epsilon/\sigma)^{1/2} \qquad (4\text{-}45)$$

under the condition that $2\omega\epsilon/\sigma \ll 1$. The loss in db per reflection may be expressed as

$$L_{db} = 10\ \text{Log}\ \{1 - 2(2\omega\epsilon/\sigma)^{1/2}\}$$

$$= 4.34\ \text{Ln}\ \{1 - 2(2\omega\epsilon/\sigma)^{1/2}\} \qquad (4\text{-}46)$$

which for $2\omega\epsilon/\sigma \ll 1$ reduces to

$$L_{db} = 8.68(2\omega\epsilon/\sigma)^{1/2} \quad \text{db loss/reflection} \qquad (4\text{-}47)$$

---

26. J.C. Slater, Microwave Transmission, Dover Publications, New York, 1959, p. 116.

Three of the common materials used for reflecting surfaces are silver, brass, and aluminum. The d.c. conductivities of these materials are:[27]

Silver: 61 X 10^6 mho/m.

Brass: 15 X 10^6 mho/m.

Aluminum: 35 X 10^6 mho/m.

The loss in db per reflection based on the d.c. values of conductivity for these materials at a frequency of 35 GHz would be

Silver: 2.2 X 10^{-3} db

Brass: 4.43 X 10^{-3} db

Aluminum: 2.9 X 10^{-3} db

Previous measurements have shown that with aluminum reflectors at 9 GHz the loss per reflection was 0.0021 db rather than the 0.0016 db predicted on the basis of the dc conductivity. This is equivalent to an effective increase in surface resistivity of 1.3, which is consistent with experimental investigations of microwave surfaces as reported by Lending (7) (50). Allowing this increase in surface resistivity due to surface imperfections, the following working values for the reflection losses are obtained

Silver: 2.86 X 10^{-3} db

Brass: 5.77 X 10^{-3} db

Aluminum: 3.77 X 10^{-3} db

V. DERIVATION OF THE COUPLED RESONATOR EQUIVALENT CIRCUIT

A. General Considerations

In order to better predict the effects of variations in the resonator parameters and variations in the size of the coupling apertures, a lumped element equivalent circuit for the resonator together with the coupling

27. The Microwave Engineers' Handbook, Horizon House, Massachusetts, 1966, p. 332.

networks would be helpful. Prediction of measureable characteristics and the design of efficient coupling networks could then be achieved using standard network theory.

The derivation of the equivalent circuit for the resonator, will start with the relation between the unloaded Q, Q_u, of the resonator and the total power loss P_{loss} of the resonator

$$P_{loss} = \frac{\omega W}{Q_u} \tag{5-1}$$

where W is the energy stored in the resonator.

The power lost must be supplied to the resonator by the magnetic dipole in the coupling aperture, and is given by

$$P_{loss} = 1/2\mathrm{Re}[j\omega \bar{B}_o' \cdot \bar{m}^*] \tag{5-2}$$

where $\bar{B}_o'$ is the magnetic flux density

and $\bar{m}$ is the magnetic dipole moment.

All field, and field related, quantities are peak values and B_o and m are considered to be at the plane z = 0. Due to the presence of the reflecting surface in which the coupling aperture is located, the total field at the aperture, B_o', will be equal to $2B_o$ where B_o is the peak amplitude of the resonator traveling wave field.

B. Confocal Half Resonator

The energy stored in the dominant mode of a half resonator of length D/2 is with the aid of Eq. 4-24 given by

$$W = \pi\epsilon E_o^2 \rho_z^2 D/2$$

where E_o is the field of the dominant mode.

Using

$$E_o^2 = \frac{\mu}{\epsilon} H_o^2 = \frac{1}{\mu\epsilon} B_o^2$$

then

$$W = \pi B_o B_o^* \rho_o^2 D/2\mu \tag{5-3}$$

Inserting Eqs. 2-2 and 2-3 into Eq. 2-1, with $B_o' = 2B_o$

$$j\omega B_o\, m^* = \frac{\omega\pi B_o B_o^* \rho_o^2 D}{2\mu Q_u}$$

Solving for B_o^*

$$B_o^* = \frac{2j\mu Q_u m^*}{\pi\rho_o^2 D} \tag{5-4}$$

or

$$B_o = \frac{-2j\mu Q_u m}{\pi\rho_o^2 D}$$

and since $B = \mu H$

$$H_o = \frac{-2jQ_u m}{\pi\rho_o^2 D} \tag{5-5}$$

The field obtained is the maximum field at resonance. The general expression for the field is a function of frequency, and decreases in magnitude below the maximum value obtained above, as the frequency deviates from the resonant frequency.

$$H_o(\omega) = \frac{-2jQ_u m}{\pi\rho_o^2 D} f(\omega) \qquad f(\omega) \leq 1 \tag{5-6}$$

According to Goubau, the following useful definitions for equivalent currents and voltages may be made[28]

$$I = k^2 m \quad \text{where } k^2 = \omega^2 \mu\varepsilon$$

and

$$V = j \frac{1}{k} \sqrt{\frac{\mu}{\varepsilon}}\, H$$

With these definitions an equivalent resonator impedance can be found and is,

$$\frac{H}{m} = -jk^3 \sqrt{\frac{\varepsilon}{\mu}} \frac{V}{I} = -jk^3 \sqrt{\frac{\varepsilon}{\mu}}\, Z_o \tag{5-7}$$

---

28. G. Goubau, Unpublished notes.

From Eq. 5-6 for $H = 2H_o(\omega)$ in the plane of m

$$\frac{2H_o(\omega)}{m} = \frac{-4jQ_u}{\pi\rho_o^2 D} f(\omega) \tag{5-8}$$

and the impedance presented by the resonator at the point of excitation is

$$Z_o = \frac{4}{k^3}\sqrt{\frac{\mu}{\varepsilon}}\frac{Q_u}{\pi\rho_o^2 D} f(\omega) \tag{5-9}$$

The impedance is real and reaches a maximum at the resonant frequency f_o. Therefore the equivalent circuit is a parallel resonant circuit with

$$R_o = \frac{4}{k^3}\sqrt{\frac{\mu}{\varepsilon}}\frac{Q_u}{\pi\rho_o^2 D} \tag{5-10}$$

From the relations

$$Q_u = \frac{R_o}{\omega_o L_o} \quad \text{and} \quad \omega_o^2 = \frac{1}{LC}$$

for a parallel resonant circuit, obtain

$$L_o = \frac{R_o}{\omega_o Q_u} \tag{5-11}$$

and

$$C_o = \frac{Q_u}{\omega_o R_o} \tag{5-12}$$

In addition to exciting the resonator fields, the magnetic coupling also causes a radiation field. The amount of power coupled into the radiation field may be obtained by using the relation

$$P_{loss} = 1/2\,\mathrm{Re}\,[j\omega\bar{B}_o' \cdot \bar{m}^*]$$

where B_o' is equal to twice the magnitude of the homogeneous B field of the dipole moment m because of the presence of the reflector. The magnetic field components of a magnetic dipole are given by[29]

---

29. See reference in footnote 28.

$$B_R = \frac{mk^3}{4\pi}\mu\left(\frac{2}{(kR)^3} + \frac{2j}{(kR)^2}\right)e^{-jkR}\cos\theta \qquad (5\text{-}13)$$

and

$$B_\theta = \frac{mk^3}{4\pi}\mu\left(\frac{1}{(kR)^3} + \frac{j}{(kR)^2} - \frac{1}{kR}\right)e^{-jkR}\sin\theta$$

Expanding the exponential term in a power series in R

$$e^{-jkR} = 1 - jkR - 1/2(kR)^2 + j\frac{(kR)^4}{3!} + \frac{(kR)^4}{4!} \ldots. \qquad (5\text{-}14)$$

and considering only the component B_R with $\theta=0$ since the dot product is to be taken with m, and m is R directed when $\theta=0$.

$$B_R = \frac{mk^3}{4\pi}\mu\left(\frac{2}{(kR)^3} + \frac{1}{(kR)} - j\frac{2}{3} - \frac{1}{4}kR + \ldots.\right) \qquad (5\text{-}15)$$

The homogeneous field of the dipole is the R independent portion of the total field

$$B = -j\frac{mk^3\mu}{6\pi} \qquad (5\text{-}16)$$

and B_o' is equal to two times B. Then the power radiated is given by

$$P_{loss} = \frac{2k^3\omega\mu^2}{2\cdot 4\pi\cdot 3}\bar{m}\cdot\bar{m}^* = \frac{k^4}{3\pi}\sqrt{\frac{\mu}{\varepsilon}}\,\bar{m}\cdot\bar{m}^* \qquad (5\text{-}17)$$

The impedance represented by this radiation loss is obtained by arranging Eq. 5-16 in the form of Eq. 5-7. Thus, using the total field at the reflector

$$\frac{H}{m} = -j\frac{2k^3}{6\pi} \qquad (5\text{-}18)$$

then from Eq. 5-7

$$Z(\text{radiation}) = Rd = \sqrt{\frac{\mu}{\varepsilon}}\,\frac{1}{3\pi} \qquad (5\text{-}19)$$

Since m is related to the current, and the same m excites both fields, the equivalent circuit will be a radiation resistance in series with the shunt resonant circuit representing the resonator mode.

The elements of the equivalent circuit have been derived from the ratio of H to m for the resonator and for the radiation fields. The dipole

moment m is proportional to the incident field on the aperture and to the size and shape of the aperture,

$$m = - m \cdot \overline{H}_i \tag{5-20}$$

where m is the polarizability of the aperture and H_i is the magnetic field strength incident on the aperture. For a small circular aperture of radius a_o

$$m = - \frac{8}{6} a_o^3 \quad \text{and} \quad m = - \frac{8}{3} a_o^3 (2H_i) \tag{5-21}$$

The polarizabilities for other common small aperture shapes also have been determined and tabulated.[30,31] From Eq. 5-21 with $H = 2H_i$ combined with Eq. 5-7

$$\frac{H}{m} = - \frac{3}{8} a_o^{-3} = - jk^3 \sqrt{\frac{\mu}{\epsilon}} Z_o$$

Using this form a value of Z_a,

$$Z_a = - j \frac{3}{8} \sqrt{\frac{\mu}{\epsilon}} \left(\frac{a_o}{\lambda}\right)^{-3} \frac{1}{8\pi^3} = - j0.572 \left(\frac{a_o}{\lambda}\right)^{-3} = - j4.56 \left(\frac{d}{\lambda}\right)^{-3} \tag{5-22}$$

referred to the field on one side of the aperture is obtained. For transmission through the aperture, the total Z is twice Z_a

$$Z = 2Z_a = - j9.12 \left(\frac{d}{\lambda}\right)^{-3} = - j1.144 \left(\frac{a_o}{\lambda}\right)^{-3} \tag{5-23}$$

and is in agreement with the equivalent circuit element given by Goubau.[32]

Also according to Goubau, when the coupling through an iris is from a waveguide section, there is an impedance transformation from the impedance of the waveguide. This is represented by a quarter wavelength line section whose characteristic impedance is given by

---

30. S.B. Cohn, "Determination of Aperture Parameters by Electrolytic Tank Measurements," Proc. IRE, vol. 39, 1951, pp. 1416-1421.

31. G. Matthaei, L. Young, E. Jones, Microwave Filters, Impedance Matching Networks and Coupling Structures, McGraw-Hill, New York, 1964, pp. 232-235.

32. G. Goubau, Electromagnetische Wellenleiter und Hohlraume, Wissenschaftliche Verlagsgesellschaft, M.B.H., Stuttgart, Germany, 1955, p. 402.

$$z_t^2 = 7200 \frac{\lambda}{ab} \tag{5-24}$$

where a and b are respectively the width and the height of the waveguide, and λ is the free space wavelength at the frequency of operation. The complete equivalent circuit for the singly coupled confocal half resonator is shown in Fig. 5-1.

When coupling is performed at the curved reflector, the magnitude of the power coupled into the resonator for a fixed m is reduced due to the wider distribution of the beam. Since at the curved surface the magnitude of the B field will be $1/\sqrt{2}$ of its value at the plane z=0, the effective real part of the impedance seen by the coupling aperture will be reduced by a factor of $1/\sqrt{2}$ also.

This reduction in coupling strength at the curved reflector can be included in the equivalent circuit by using an ideal transformer of turns ratio $2^{1/4}$:1. A complete equivalent circuit for a confocal half resonator with small circular apertures and fed from a waveguide at both input and output ports is shown in Fig. 5-2.

In order to reduce the circuit of Fig. 5-2 and simplify analysis, all elements except the parallel tank circuit are transformed to the source or load sides of the $\lambda/4$ transformers at the input and output respectively. The transformed aperture impedance becomes

$$Z' = \frac{Z_t^2}{R_d + 2j\omega L_a} \tag{5-25}$$

or

$$Y' = \frac{R_d}{Z_t^2} + \frac{2j\omega L_a}{Z_t^2} \tag{5-26}$$

A shunt parallel resonant circuit to which input and output coupling is performed via quarter wave transformers will appear as a series resonant circuit in series with the line, and of the transformed impedance

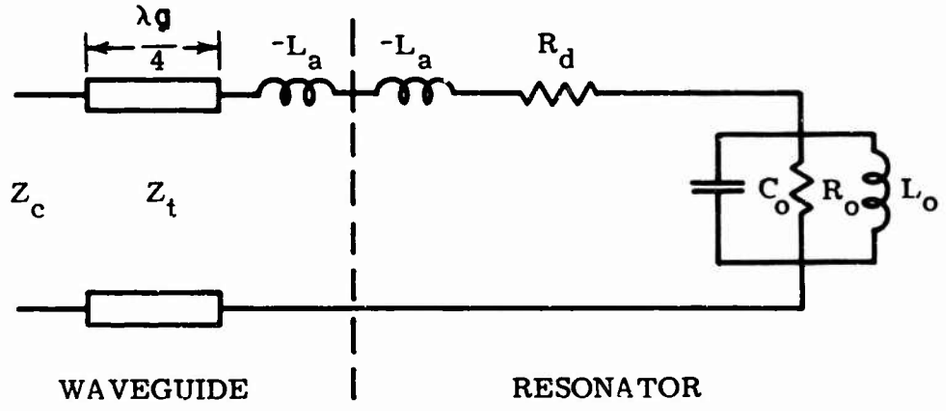

$$-L_a = j\frac{\sqrt{\mu/\epsilon}}{2\omega k^3 m}$$

$$R_o = \frac{4}{k^3}\sqrt{\frac{\mu}{\epsilon}}\,\frac{Q_u}{\pi \rho_o^2 D}$$

$$L_o = \frac{R_o}{\omega_o Q_u}$$

$$C_o = \frac{Q_u}{R_o \omega_o}$$

$$R_d = \sqrt{\frac{\mu}{\epsilon}}\,\frac{1}{3\pi}$$

FIG. 5 - 1

EQUIVALENT CIRCUIT TO SINGLY
COUPLED CONFOCAL HALF RESONATOR

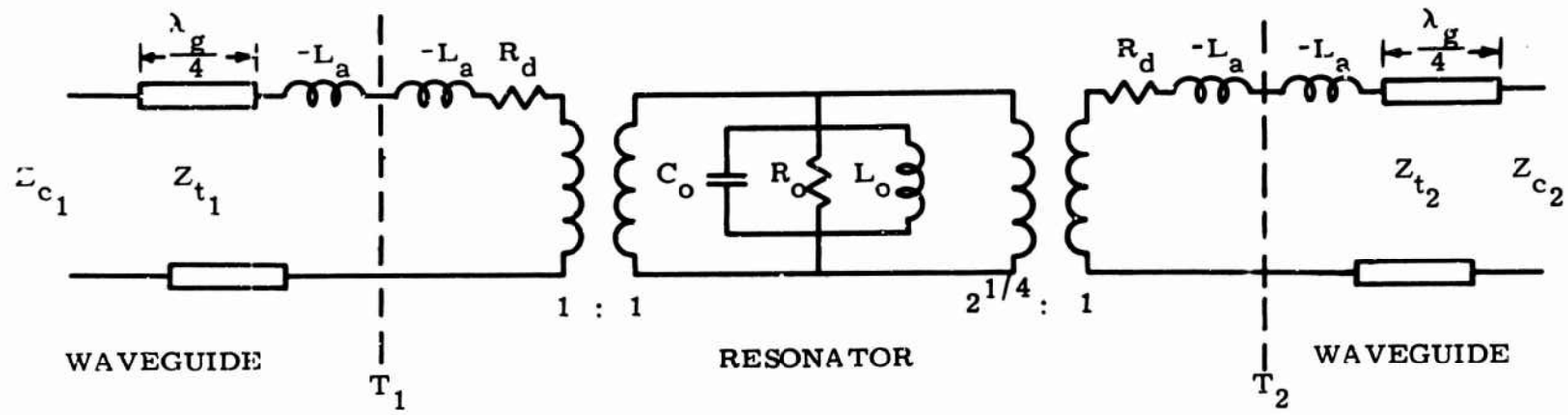

FIG. 5 - 2

EQUIVALENT CIRCUIT

DOUBLY COUPLED CONFOCAL HALF RESONATOR

$$Z_o' = \frac{Z_t^2}{Z_o} = Z_t^2 Y_o$$

From Eq. 5-11

$$j\omega L_o = \frac{j\omega R_o}{\omega_o Q_u} = j\,\frac{(\omega_o + \delta\omega)R_o}{\omega_o Q_u} = j\,\frac{R_o}{Q_u}\left(1 + \frac{\delta\omega}{\omega_o}\right) \tag{5-27}$$

where $\delta\omega$ is the deviation of ω from ω_o, and $\delta\omega/\omega_o$ is constrained to be much less than unity in magnitude.

Similarly, from Eq. 5-12

$$\frac{1}{j\omega C_o} = \frac{\omega_o R_o}{j\omega Q_u} = \frac{\omega_o R_o}{j(\omega_o+\delta\omega)Q_u} = \frac{R_o}{jQ_u}\left(1 - \frac{\delta\omega}{\omega_o}\right) \tag{5-28}$$

Combining Eqs. 5-10, 5-24, and 5-25,

$$Y_o = \frac{1}{R} + j\,\omega C_o - j\,\frac{1}{\omega L_o}$$

$$Y_o = \frac{1}{R_o} + j\,\frac{2Q_u}{R_o}\,\frac{\delta\omega}{\omega} \tag{5-29}$$

and

$$Z_o' = \frac{Z_t^2}{R_o} + j\,\frac{2Z_o^2 Q_u}{R_o}\,\frac{\delta\omega}{\omega_o} \tag{5.30}$$

in the vicinity of $\omega = \omega_o$.

A further reduction will bring the output coupling elements and the load impedance Z_c from the secondary to the primary side of the $2^{1/4}$:1 transformer. The reduced equivalent circuit now appears as in Fig. 5-3 and is of the form of the circuit analysed in Appendix B of this report and shown in Fig. B-1.

C. Confocal Full Resonator

In order to formulate the equivalent circuit for the full confocal resonator, no change in the coupling elements is required, nor is the radiation resistance R_a affected since these quantities are not functions of the resonator geometry as derived. Ideal transformers with $2^{1/4}$:1 turns ratios are employed both at the input and the output since both couplings

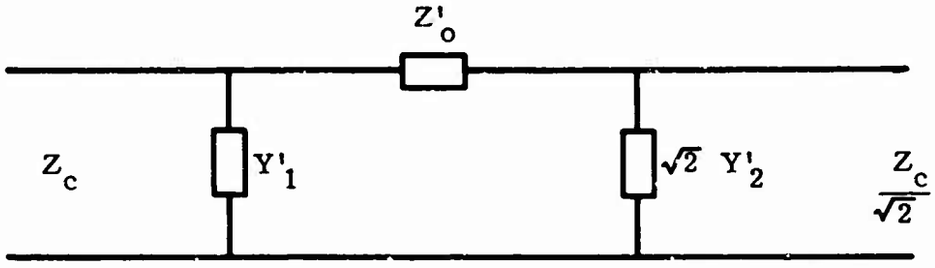

$$Z_c = 120\pi\frac{\lambda_g}{\lambda}$$

$$Y'_a = \frac{R_d}{Z_t^2} + j\,\frac{2\omega L_a}{Z_t^2}$$

$$Z_o' = \frac{Z_t^2}{R_o} = j\,\frac{2Z_t^2 Q_u}{R_o}\,\frac{\delta\omega}{\omega_o}$$

$$R_o = \frac{8}{k^2}\sqrt{\frac{\mu}{\epsilon}}\,\frac{Q_u}{\pi D^2}$$

$$Z_t^2 = 7200\frac{\lambda}{ab}$$

FIG. 5 - 3

REDUCED EQUIVALENT CIRCUIT

CONFOCAL HALF RESONATOR

are in curved reflectors where the beam density is reduced below that used in calculating the resistance of the resonator equivalent circuit. For fixed field amplitudes, the energy stored in the full resonator is twice that stored in the half resonator for equal field amplitudes at the plane z=0. An inspection of Eqs. 5-3 through 5-10 shows this change in energy storage appears as a reduction by a factor of 2 in R_o of Eq. 5-10. Thus for the full resonator

$$R_o = \frac{2}{k^3}\sqrt{\frac{\mu}{\epsilon}}\frac{Q_u}{\pi\rho_o^2 D} = \frac{4}{k^2}\sqrt{\frac{\mu}{\epsilon}}\frac{Q_u}{D^2\pi} \qquad (5\text{-}31)$$

The quantities L_o and C_o are still determined from Eqs. 5-11 and 5-12. The reduced equivalent circuit for the full confocal resonator is shown in Fig. 5-4.

D. Equivalent Circuits for Higher Modes

To complete the analysis for the equivalent circuit of a coupled confocal resonator, the effect of higher order modes must be added to the resonator equivalent circuit. Calculations show that for both full and half confocal resonators there will be higher mode excitation when there is a coupling aperture in one of the reflectors. The presence of higher mode fields has also been indicated by the field perturbation measurements. Furthermore calculations indicated that the field amplitude of the higher order mode will be a function of the aperture size. In these calculations it has been assumed that most of the energy is transferred into these higher order modes from the high energy field of the low loss dominant mode through the perturbation caused by the coupling apertures.

Measurements show that for the full resonator with fixed aperture sizes, the field distribution is distorted from that of the lowest or L_o^o mode and the measured (unloaded, uncoupled Q) Q_{oo} values are lower at the confocal spacing of 114 cm. than those measured at a reflector separation of 108 cm.

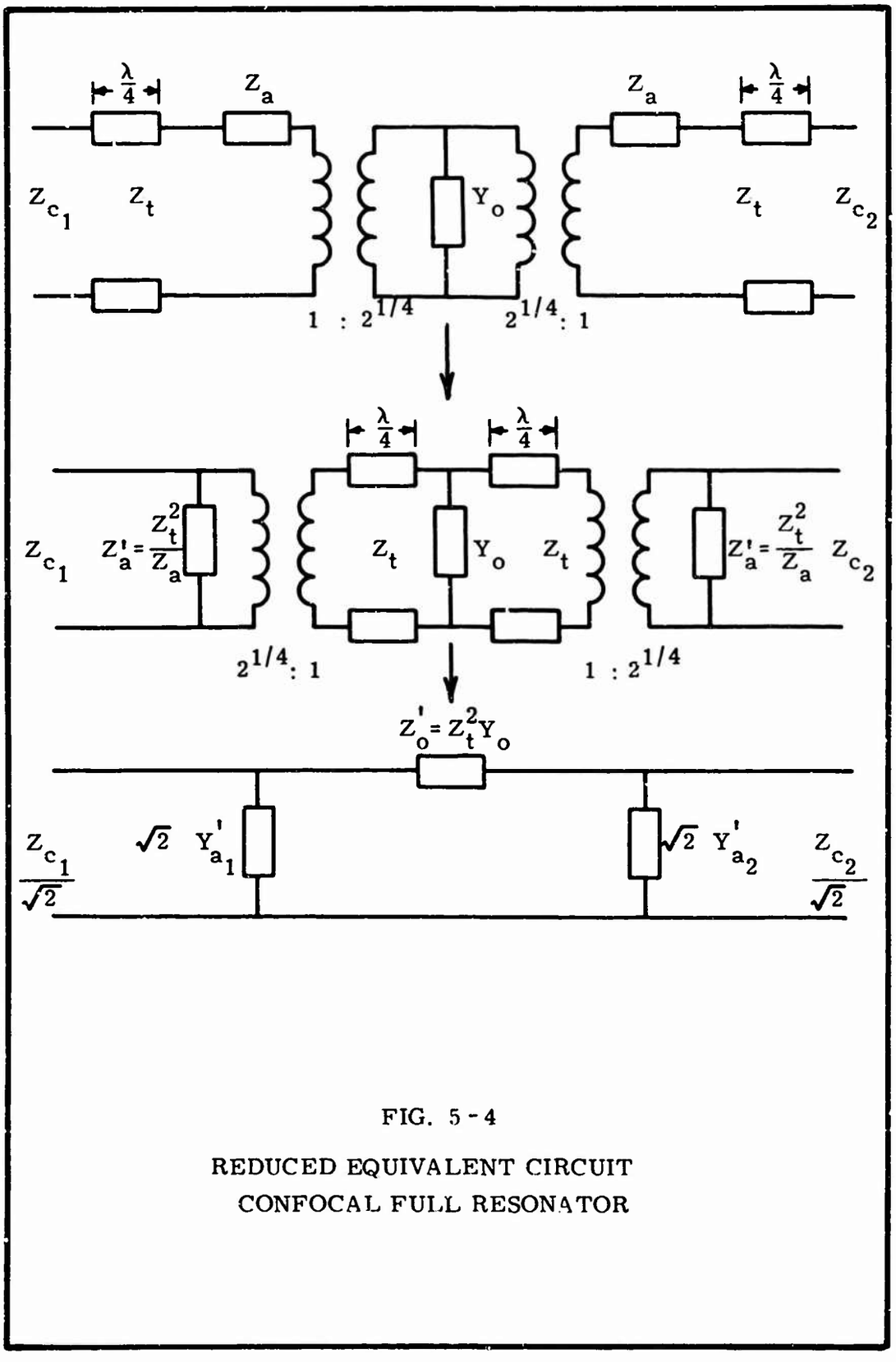

FIG. 5 - 4

REDUCED EQUIVALENT CIRCUIT
CONFOCAL FULL RESONATOR

The calculations show that the cross-mode coupling is strongest to the L_1^o mode from the L_o^o mode. Since the degree of coupling between the two modes is a function of the amount of overlap in their respective resonant responses, and since the resonance conditions are functions of both the mode numbers and the reflector separation, the coupling between modes will be a function of reflector separation. The relative coupling will be a maximum when both modes are resonant at the same reflector spacing and frequency. For a fixed frequency, the coupling will approach zero when the resonances are separated far enough so that the responses no longer overlap.

It will be assumed that a fifty percent reduction in coupling will take place at a reflector separation where the peak of the low Q mode response coincides with the 3 db point on the dominant mode response as illustrated in Fig. 5-5. Thus the resonant frequency of the L_o^o mode is separated from the resonant frequency of the L_1^o mode by a frequency difference equal to one-half of the 3 db bandwidth of the L_o^o mode. In order to calculate the amount that the reflector separation must be changed from the confocal condition to achieve this frequency separation of the modes, the resonance condition given by Eq. 4-25 will be used with M being the number of integer half wavelengths of reflector separation,

$$M\frac{\pi}{2} = kD/2 - (2n+v+1)\tan^{-1}\left(\frac{D}{2k\rho_o^2}\right)$$

with v=0, and using the relation

$$k\rho_o^2 = \left[\left(2 - \frac{D}{2b}\right) b \frac{D}{2}\right]^{1/2}$$

which is identical to Eq. 4-28 under the condition of identical reflectors separated by a length D and with the change of notation that b = focal length of the reflectors. Then

$$k\frac{D}{2} - (2n+1)\tan^{-1}\left(\frac{1}{\sqrt{\frac{4b}{D} - 1}}\right) = M\frac{\pi}{2} \qquad (5\text{-}32)$$

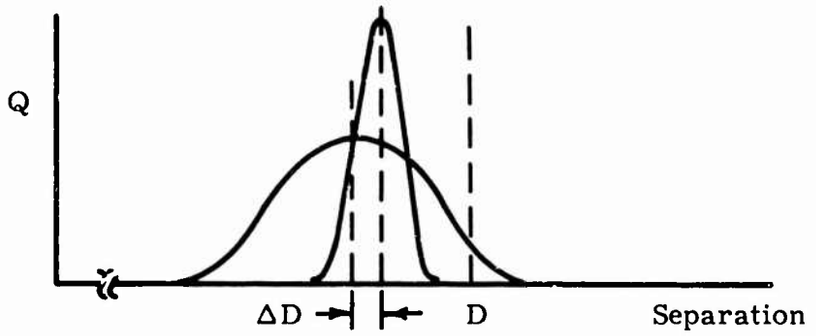

a) INDIVIDUAL MODE RESPONSES

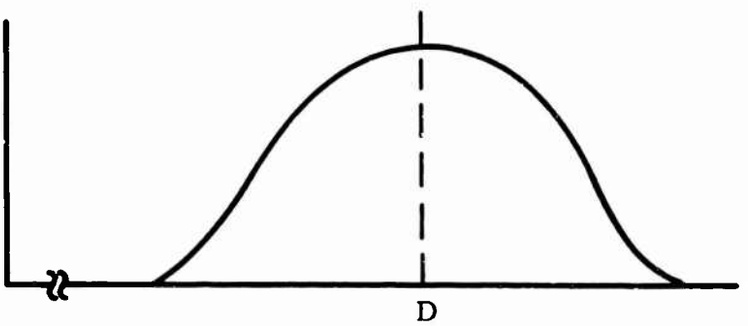

b) RELATIVE MODE COUPLING VERSUS SEPARATION

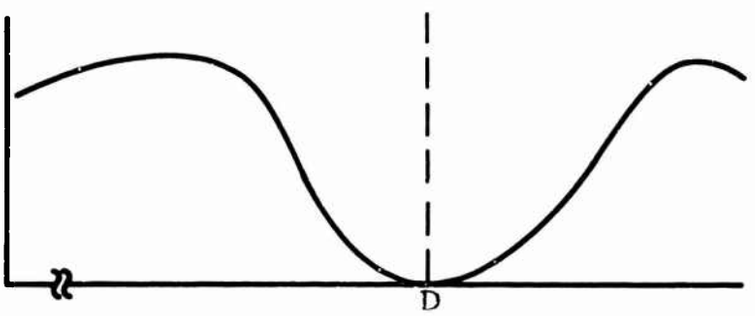

c) COUPLED MODE MEASURED Q VERSUS SEPARATION

FIG. 5-5

MULTIPLE MODE RESPONSE VERSUS SEPARATION

From $k = 2\pi/\lambda = 2\pi f/c$,

$$f = \frac{c}{2D}\left[M + \frac{2}{\pi}(2n+1)\tan^{-1}\left(\frac{1}{\sqrt{\frac{4b}{D} - 1}}\right)\right] \tag{5-33}$$

Evaluating the rate of change of frequency with variation in the reflector separation in the neighborhood of confocal operation

$$\frac{\partial f}{\partial D} = \frac{c}{2D}\left\{\frac{2}{\pi}(2n+1)\frac{1}{1 + \frac{1}{\frac{4b}{D} - 1}}\frac{1}{2}\frac{1}{\left(\frac{4b}{D} - 1\right)^{3/2}}\frac{4b}{D^2}\right\}$$
$$- \frac{c}{2D}\frac{1}{D}\left[M + \frac{2}{\pi}(2n+1)\tan^{-1}\frac{1}{\sqrt{\frac{4b}{D} - 1}}\right] \tag{5-34}$$

Simplifying,

$$\frac{\partial f}{\partial D} = \left(\frac{c}{2D^2}\right)\left\{M + \frac{2}{\pi}(2n+1)\left(\frac{1}{\sqrt{\frac{4b}{D} - 1}} - \tan^{-1}\frac{1}{\sqrt{\frac{4b}{D} - 1}}\right)\right\} \tag{5-35}$$

Evaluated at D=2b (confocal operation) Eq. 5-35 becomes

$$\frac{\partial f}{\partial D} = \left(\frac{c}{2D^2}\right)\left\{M + (2n+1)\left(\frac{2}{\pi} - 1\right)\right\} \tag{5-36}$$

Note that the partial derivative of the resonant frequency with respect to the reflector separation is a function of the mode number n; a condition that is necessary if the resonant frequencies of the modes for non-confocal reflector spacing are to be separated.

For the L_o^o mode (n=0),

$$\Delta f_1 = \frac{\partial f}{\partial D}\Delta D = \frac{c}{2D^2}\left[M + \frac{2}{\pi} - 1\right]\Delta D \tag{5-37}$$

where ΔD is the deviation from confocal spacing of the reflectors and Δf_i is the corresponding shift in resonant frequency for the L_o^o mode. For the L_1^o mode (n=1)

$$f_2 = \frac{c}{2D^2}\left[M + \frac{4}{\pi} - 2\right]\Delta D \tag{5-38}$$

Then

$$\Delta f_2 - \Delta f_1 = \frac{c\Delta D}{2D^2}\left(1 - \frac{2}{\pi}\right) \qquad (5\text{-}39)$$

It is now desired to find the value of ΔD which will cause the resonance frequencies for the two modes to differ by one half on the 3 db bandwidth of the fundamental mode. Recall that this is the condition under which the coupling between the modes is assumed to have been reduced by fifty percent from its maximum value.

Measurements made on a particular resonator show that half the difference between the minimum and maximum values of Q was approximately 150,000. Also for a resonant frequency of 35.07 GHz, one half on the 3 db bandwidth was 1.17 MHz. Solving Eq. 5-39 for ΔD with

$$c = 3 \times 10^8 \text{ m/sec}$$

and $$D = 114 \text{ cm.}$$

yields $$\Delta D = 2.82 \text{ cm.}$$

The changes in reflector spacing on either side of confocal spacing at which Q values of 150,000 were measured, were 3.5 cm and 3.0 cm. Within the limits of experimental error and the approximations made, the calculated and measured values are in excellent agreement. This is further proof that in the full resonator, a decrease in Q for the dominant mode takes place in the vicinity of confocal spacing and is due to coupling to the L_1^o mode. It also appears that the dominant coupling mechanism between the two modes is the perturbation introduced by the presence of the coupling apertures in the reflectors.

The lumped element equivalent circuit for a higher order mode may be formulated in the same manner as that used for the dominant mode. For equal field magnitudes, the energy stored in the L_o^o and L_1^o modes will have

the same total energy for the same field amplitude constant E_{n0}^2 (E_{nv} for confocal spacing with v=0, Eq. 4-24). In Eqs. 5-3 through 5-10 the expression for R_o is the same for both modes. The quantity Q_u is, with the exception of the resonance conditions of frequency versus reflector separation, the only mode dependent factor. The coupling element values are not functions of the resonator mode, and hence the equivalent circuit of the second mode becomes a parallel tuned resonant circuit Y_{o2} in series with the Y_o calculated for the fundamental mode. This is shown in Fig. 5-6. In the reduced equivalent circuit also shown in Fig. 5-6, the L_1^o mode is represented as a series resonant circuit in parallel with Z_o'. This series circuit is given by

$$Z_{o2}' = \frac{Z_t^2}{R_{o_2}} + \frac{2Z_t^2 Q_{u2}\delta\omega}{R_{o_2}\omega_{o_2}} \tag{5-40}$$

where the subscript 2 refers to the elements of the L_1^o mode circuit. ω_{o_2} will only be equal to ω_o at confocal spacing of the resonator reflectors.

E. Applications of the Equivalent Circuits

An example of the application of the equivalent circuit will be given which will also serve to confirm the validity of the representation. The full resonator equivalent circuit shown in Fig. 5-4 will be treated. It will be assumed that the resonator length has been changed just enough from the confocal length so that the L_o^o mode resonates alone. The output waveguide is to be terminated in a variable position short circuit. Then the unloaded Q measured at the input port will be a function of Z_o' in series with the parallel combination of $Y_2'/\sqrt{2}$ and the variable position short circuit which presents values of reactance between the extremes of an open circuit and a short circuit. Actual measurements made on such a configuration are plotted in Fig. 5-7 and show the unloaded Q versus the position of

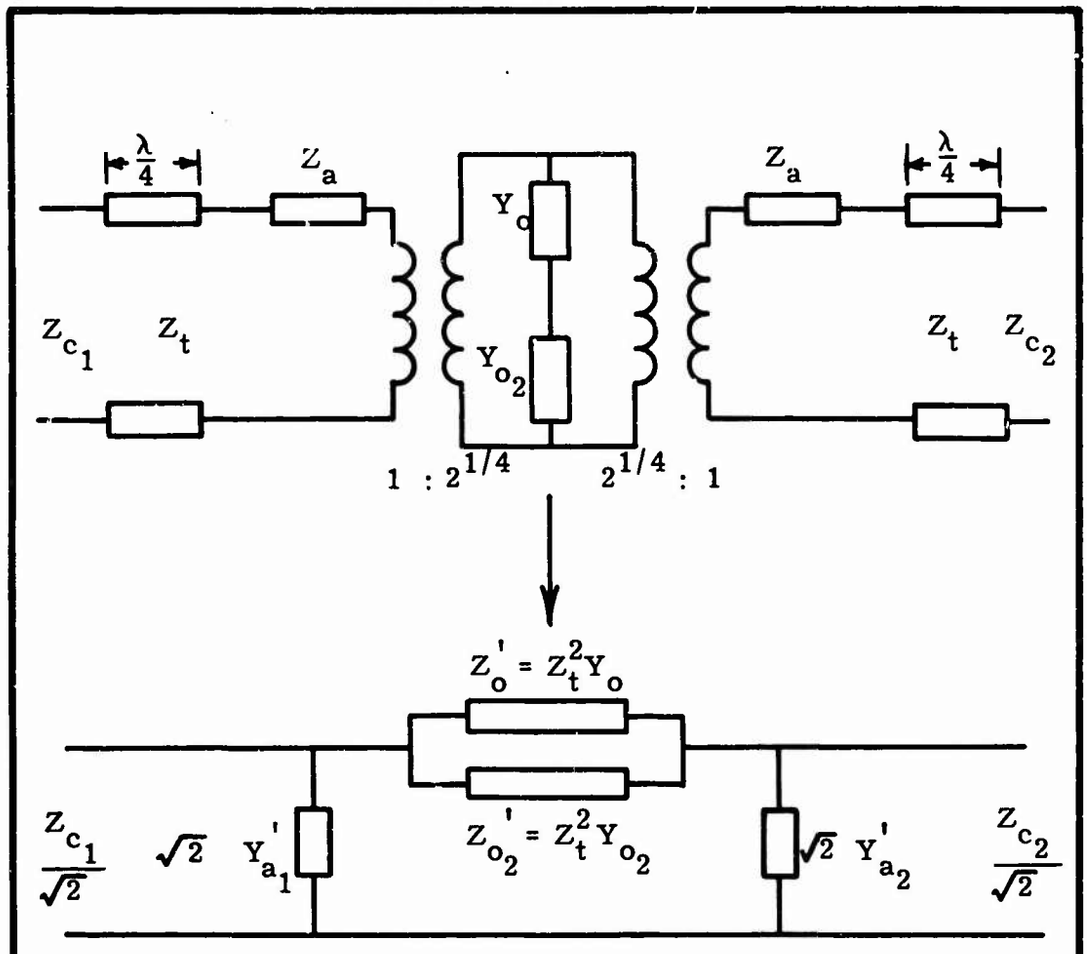

$$Y_o = \frac{1}{R_o} + j\omega C_o - j\frac{1}{\omega_o L_o}$$

$$Y_{o2} = \frac{1}{R_{o2}} + j\omega_{o2} C_{o2} - j\frac{1}{\omega_{o2} L_{o2}}$$

FIG. 5 - 6

MULTIPLE MODE RESONATOR

EQUIVALENT CIRCUIT

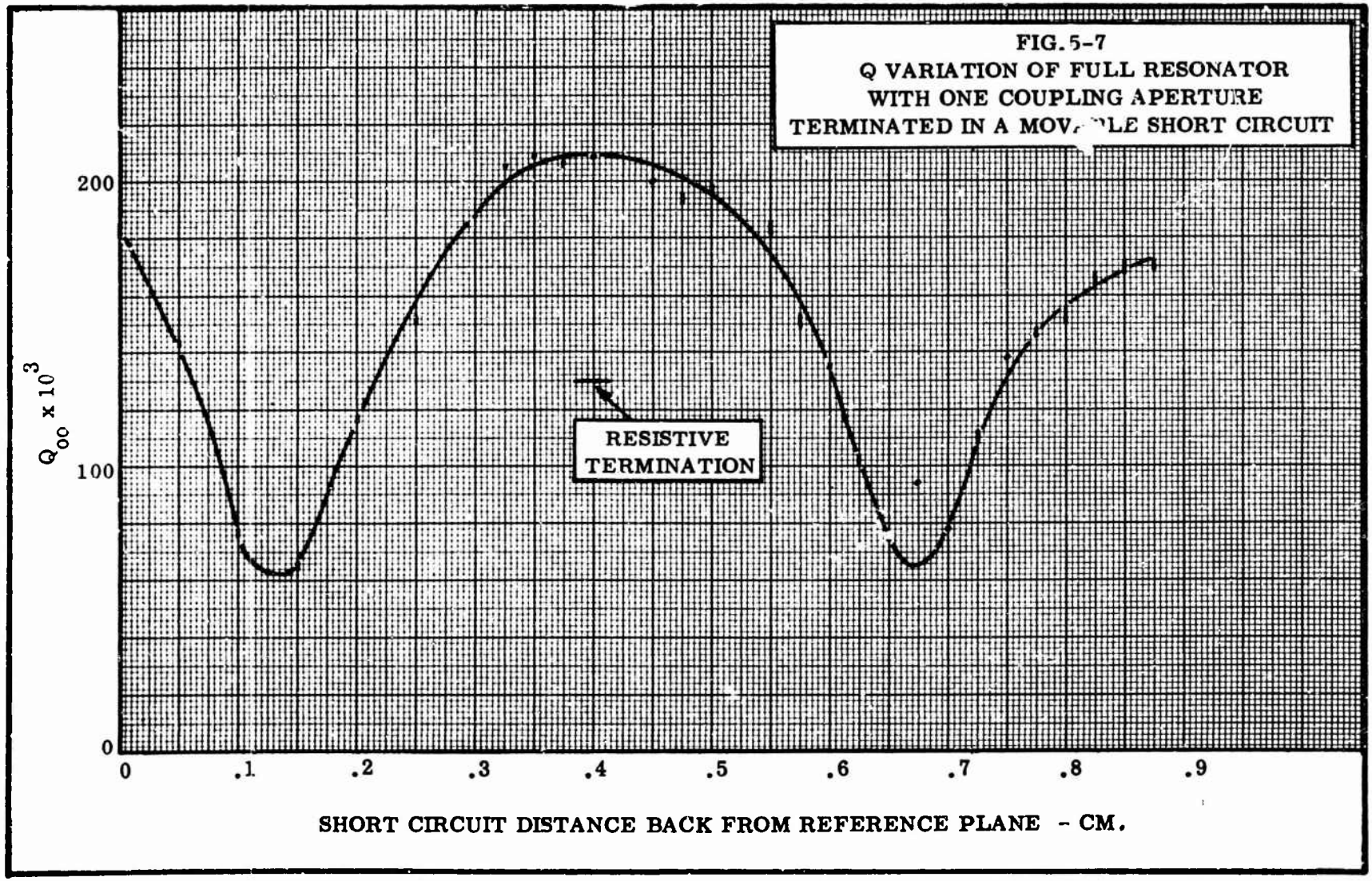
FIG. 5-7
Q VARIATION OF FULL RESONATOR
WITH ONE COUPLING APERTURE
TERMINATED IN A MOV
LE SHORT CIRCUIT
200
100
0
$Q_{oo} \times 10^3$
RESISTIVE
TERMINATION
0
.1
.2
.3
.4
.5
.6
.7
.8
.9
SHORT CIRCUIT DISTANCE BACK FROM REFERENCE PLANE - CM.

the variable short circuit terminating the output coupling aperture. The test resonator had a D = 108 cm., an f_o = 35.0 GHz, and RG96/u waveguides at each port by means of which coupling to the resonator was accomplished. In RG96/u waveguide at f_o,

$$\frac{\lambda g}{\lambda} = 1.25$$

therefore $Z_{c_z} = 377(1.25) = 472$ ohms

From Eq. 5-31 with D = 108 cm, $k = 2\pi/\lambda$ and $\lambda = 0.855$ cm,

$$R_o = \frac{4(377)Q_u}{54\pi(108)^2} = 7.64 \times 10^{-4} Q_u \qquad (5\text{-}41)$$

and from Eq. 5-19

$$R_d = \sqrt{\frac{\mu}{\varepsilon}} \frac{1}{3\pi} = 40 \text{ ohms}$$

The maximum value of measured unloaded Q will occur at the input port when the position of the short circuit is such that an effective open circuit is present at the reference plane T_2 of the equivalent circuit (Fig. 5-2) which separates the output waveguide elements from the resonator elements. Under this condition, the internal losses are due only to R_o which is given by Eq. 5-41 as

$$R_o = 7.54 \times 10^{-4} \, Q_{u\,max} \qquad (5\text{-}42)$$

When $Q_{u\,max}$ is 553,000, obtained from theoretical loss calculations, then R_o = 422 ohms. The lowest measured value of Q_u will be obtained when the short circuit is so positioned that the radiation resistance effectively shunts the resonator. On the resonator side of the coupling transformer

$$\sqrt{2}\, R_d = 56.6 \text{ ohms}$$

The parallel combination of R_o and $\sqrt{2}\, R_d$ gives an effective R_o' of

$$R_o' = [R_o, || \sqrt{2} R_d] = 50 \text{ ohms}$$

For negligible change in the reactive components of the parallel resonant circuit; i.e., constant stored energy, the unloaded Q and the effective value of R_o are still related by Eq. 5-41.

$$Q_u = \frac{50}{7.64 \times 10^{-4}} = 65,300$$

The measured minimum Q shown in Fig. 5-7 was approximately 62,000, although there is some uncertainty in this value due to a scarcity of data points in the minimum Q region.

When the output waveguide is terminated in its characteristic impedance, the load impedance is transformed by a $\lambda/4$ transformer and appears in series with R_d giving an effective load impedance of

$$R_L' = R_d + \frac{Z_t^2}{Z_c}$$

where

$$Z_t^2 = 7200 \frac{\lambda}{ab}$$

Now for RG96/u waveguide at 35 GHz

$$a = 0.7112 \text{ cm}, \quad b = 0.3556 \text{ cm}, \text{ and } \lambda = 0.855 \text{ cm}.$$

Then

$$Z_t^2 = 7200 \frac{(0.855)^2}{(0.711)(0.3556)} = 20,800$$

and

$$R_L' = 40 + \frac{20,800}{472} = 84 \text{ ohms}$$

The quantity $\sqrt{2}R_L'$ will appear in shunt with R_o and the effective resonator real impedance becomes

$$R_o' = [R_o || \sqrt{2}R_L'] = [422 || 119] = 92.8 \text{ ohms}$$

Then $Q_u = 93/7.64 \times 10^{-4} = 121,000$. The measured Q when the resonator was terminated in its characteristic impedance was 130,000 from Fig. 5-7.

The results obtained by this application of the equivalent circuit are consistent with the approximations involved and the degree of experimental error that may be expected. It has been assumed that the L_1^o mode was not

resonating and that the tapered waveguide and slot feed used was approximated by the circular iris equivalent circuit. The degree to which this can be expected to hold would depend on the validity of representing the aperture field by a single dipole moment m, and the degree to which the iris equivalent inductance L_a effected the matched load condition.

A second application illustrating the usefulness of the equivalent circuit for a beam waveguide resonator, will compare Q measurements made on a half resonator with the behavior of the equivalent circuit of Fig. 5-2. The input coupling is at the curved reflector and is also where the measurements were made. The size of an aperture in the flat reflector (at z=0) was varied. Due to the thickness of the plate in which the aperture was located (approx. 1/16 inch), the aperture was non-transmitting until the aperture diameter was made greater than the thickness. The radiation resistance of the aperture for radiation into a half space was shown to be 40 ohms in the previous application of the equivalent circuit. If the aperture is free to radiate into all space, i.e., both transmission through and reflection from the aperture, the radiation resistance would be 20 ohms.

By Eq. 5-10

$$R_o = \frac{4}{k^3}\sqrt{\frac{\mu}{\epsilon}}\,\frac{1}{\pi\rho_o^2 D}\,Q_u = \frac{8}{k^2}\sqrt{\frac{\mu}{\epsilon}}\,\frac{1}{\pi D^2}\,Q_u = \frac{4(377)}{54\pi(114)^2}\,Q_u \qquad (5\text{-}43)$$

$$R_o = 1.77 \times 10^{-3} Q_u$$

For a parallel resonant circuit

$$Q = \frac{\omega_o C}{G} = \frac{R}{\omega_o L} \qquad (5\text{-}44)$$

Thus by comparison of Eq. 5-43 and Eq. 5-44,

$$\omega_o L = 1.77 \times 10^{-3} \text{ ohms}$$

The presence of the aperture in the flat reflector adds

$$Z_a = R_d + 2j\omega L_a$$

in parallel with R_o. The effective value of R_o as measured at the input port is given by

$$R_o' = \frac{1}{\frac{1}{R_o} + \mathrm{Re}\left[\frac{1}{R_d+2j\omega L_a}\right]} = \frac{1}{\frac{1}{R_o} + \frac{R_d}{(R_d)^2+(2\omega L_a)^2}} \tag{5-45}$$

and

$$Q_u = \frac{1}{\omega_o L_o}\left[\frac{1}{\frac{1}{R_o} + \frac{R_d}{(R_d)^2+(2\omega L_a)^2}}\right] = \frac{1}{\frac{1}{Q_{u_{max}}} + \frac{\omega_o L_o R_d}{(R_d)^2+(2\omega L_a)^2}} \tag{5-46}$$

Equation 5-46 for Q_u is plotted in Fig. 5-8 as a function of the iris radius a_o for the reflection loss case. Also shown in Fig. 5-8 is the case of the combined transmission and reflection loss represented by Eq. 5-48 where the effective resistance shunting R_o is

$$R_a' = 1/2\ \mathrm{Re}\ \frac{1}{R_d + 2j\omega L_a} \tag{5-47}$$

and

$$Q_u = \frac{1}{\frac{1}{Q_{u_{max}}} + \frac{\omega_o L_o R_d/2}{(R_d)^2+(2\omega L_a)^2}} \tag{5-48}$$

Also plotted for comparison is the measured data for this configuration. The constants used for the calculated values were

$$Q_{u_{max}} = 294{,}000$$

$$2\omega L_a = 1.144\left(\frac{a_o}{\lambda}\right)^{-3} = 0.71\ a_o^{-3}$$

$$\lambda = 0.855\ \mathrm{cm}.$$

A transition from the behavior expected when reflection losses alone are present, to that predicted when transmission losses through the aperture are also present is shown in Fig. 5-8. The measured curve shows reasonably

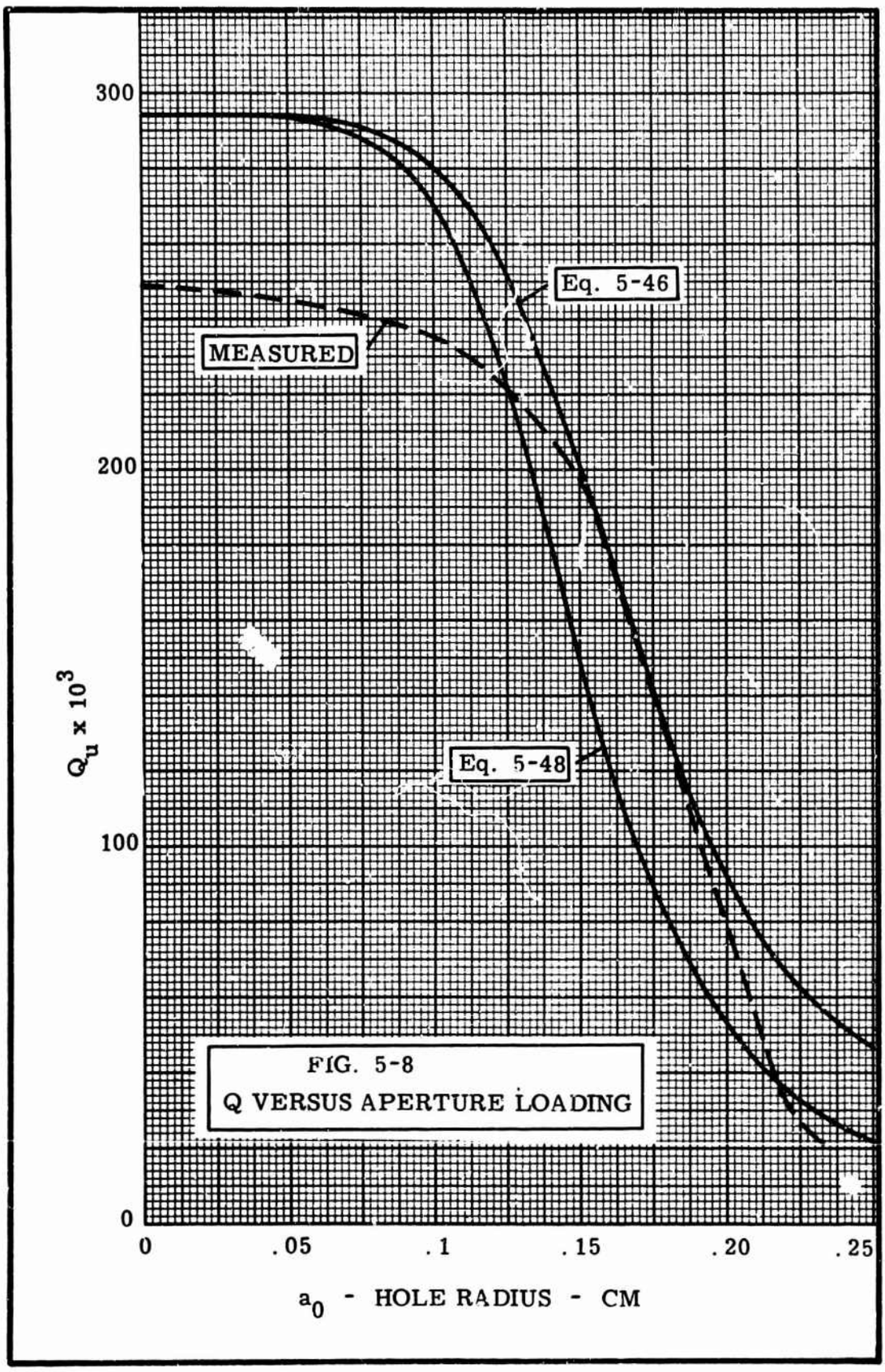

FIG. 5-8
Q VERSUS APERTURE LOADING

good agreement with predicted values. The predicted Q for the resonator when $a_o=0$ is much higher than the measured value. This discrepancy is believed due to an unaccounted for factor in calculating the theoretical losses, and may lie either in the value of the end plate resistance or in the fact that the L_2^o mode may have been present in the resonator.

VI. CONCLUSIONS AND RECOMMENDATIONS

The principle objective of this research has been to explore the use of beam waveguide resonators as circuit elements at millimeter wave frequencies. While a detailed summary of the derivation of the resonator characteristics described in section IV was not presented, the extensive bibliography referenced throughout will aid in locating an analysis for a particular geometry if such an analysis is desired.

The emphasis in the presentation of the resonator characteristics of section IV was on the diffraction losses and resonant frequencies as functions of the geometry and the mode number. The equations governing the energy distribution for the various modes and plots of the field distributions for some low loss modes are presented for the confocal geometry. An analysis has also been presented of an equivalence relation by means of which the diffraction losses for non-confocal resonators of either full length or half length may be determined from the diffraction loss versus geometry function of Fig. 4-7 for a confocal resonator.

Generally neglected in many analytical studies, but important in resonators designed to have high unloaded Q values at microwave frequencies are the resistive losses due to the metal reflecting surfaces. These losses are calculated for the three most common reflector materials in terms of a db power loss per reflection.

Early experimental difficulties were encountered; the principle one was the inability to obtain the theoretically predicted high Q values at 35 GHz. Coupling to the resonator was with circular apertures excited through a circular transition from standard rectangular waveguide. This coupling problem has not been reported on in other experimental studies that have been made on open resonators, and it did not appear when coaxial loop coupling was used with these resonators in a series of X-band experiments. A calculation was made of the power loss from the resonator due to radiation from an equivalent magnetic dipole induced in a small circular aperture by the resonator field, and rough agreement between this loss and the unaccounted for losses of the test resonator was obtained.

A series of experiments was performed to study in greater detail the departures from the theoretically predicted behavior of the resonators which might be due entirely or in part to the presence of the coupling apertures in the reflectors. The equipment used for these experiments, which was a swept frequency generator and a generator for point by point response measurements, is described in Appendix A. A discussion of the reflected response of a coupled resonant circuit is given in Appendix B. The equations presented in Appendix B were used to obtain information about the resonator properties from measurements.

With respect to the radiation loss caused by an aperture in a reflector, agreement was obtained with the predicted values from small aperture theory, within the limits of experimental error. This applies to circular apertures with radii approaching a quarter wavelength. Since this aperture was essentially a circular waveguide operating in the cutoff frequency region and of finite length, the radiation loss was predominantly backscatter from the aperture.

For thin apertures, the radiation loss is due to backscatter and to transmission through the aperture. This latter loss was verified by the increase in loss measured as a function of aperture size. This increase in loss is in general agreement with the difference in loss obtained between a transmitting and non-transmitting aperture shown in Fig. 5-8.

The experimental data (shown in Fig. 5-7) obtained when a small aperture in the center of the curved reflector of a full resonator was terminated in a variable position short circuit and when it was terminated in a matched load showed the drastic effect on the characteristics of an open resonator which can take place. A comparison of the maximum and minimum Q values obtained as a function of the position of the short circuit with the Q value obtained when the aperture was terminated in a matched load indicates that the phase angle of the effective reflection coefficient of the resonator load is more important than the magnitude. Coupling energy out of the resonator into a resistive load causes a decrease in the Q below the value obtainable with a reactive termination, but it is not a condition which leads to minimum Q. The calculations of pp. 52 through 53 show that the minimum and maximum values of measured Q are related to whether the radiation resistance of one aperture is effectively open circuited or short circuited by the reactive load.

The low Q values obtained at confocal spacing, coupled with the fact that the Q appeared to rise when the reflectors were moved in either direction from confocal separation led to investigation of the unloaded Q versus reflector spacing. It was found that the Q decreased in the area of confocal operation for the full resonator, but no noticeable decrease in Q was found for the half confocal resonator. The possible existence of an optical instability region of operation for a full resonator is

described on pp. 12 and 13. This unstable operation occurs when the radii of curvature for the two reflectors are different, and the separation between the reflectors falls between the two radii of curvature. Measurements of the radii of curvature of the reflectors for the test resonator showed that they were identical to within $\pm$ 0.5 inch. If present, this region of instability would occur over too narrow a range of reflector separations to account for the broad decrease in Q measured near confocal spacing.

A discussion of the multiple mode operation of the full and half resonator is given in Appendix C. The tabulation in Table C-2 of Appendix C shows that the two resonators are not equivalent in their resonance characteristics. In particular, the L_2^o mode is simultaneously resonant with the L_o^o mode in the half resonator, while both the L_1^o and L_2^o modes are simultaneously resonant with the L_o^o dominant mode in the full resonator. Both of these modes have the same angular symmetry as the dominant mode and are the next most likely modes to be excited. Calculations indicate that the presence of coupling apertures in either type of resonator can cause transfer of energy from the dominant mode to the higher loss mode. The presence of these higher loss modes was also indicated from measurements made of the radial fields in the resonator for various aperture diameters. The calculations in section V concerning the range of reflector separation over which the L_o^o mode and the L_1^o mode in the full resonator can interact are in good agreement with the range of separation over which the low Q values were actually measured.

As a result of this investigation, emphasis must be placed on two differences which exist between the beam waveguide resonators and conventional closed cavity resonators. The first of these is the predominantly real impedance introduced into the resonator by the coupling apertures. Whereas

in a closed cavity resonator a perturbation of the boundary conditions can generally be represented as a reactance and primarily affects only the resonant frequency or cut-off frequency, in the beam waveguide or beam waveguide resonator a perturbation of the boundary conditions will cause radiation and will be primarily represented by a resistive effect. The perturbation in an open resonator will primarily affect the Q of the device rather than the resonant frequency. The second difference which must be emphasized is the inherent multi-mode nature of the confocal full and half resonators. While the modes are, in the ideal sense, orthogonal, the coupling apertures in the reflectors couple energy from the dominant low loss mode to the higher order high loss modes. The experiments have shown that this coupling can become quite strong when aperture sizes approach the dimensions of a half wavelength at the resonant frequency.

To complete this investigation of beam waveguide resonators for millimeter wave circuit applications, lumped element equivalent circuits for both full and half resonators are derived in section V. The effects of small circular coupling apertures are accounted for in the equivalent circuits including the radi tion losses introduced by the apertures. The analysis made will apply to any point source excitation, if suitable expressions for the coupling element impedance are used, and a relation between the induced magnetic moment in the aperture and the field quantities can be found as a function of the geometry. While the equivalent circuits that were derived are for single mode operation of the resonators, a discussion is included concerning the addition of resonant circuits to represent higher mode effects.

With the aid of the equivalent circuits and by application of standard network analysis, it is believed that the radiation losses introduced by the coupling apertures can be minimized for desired operating

conditions of Q and insertion loss. In order to minimize multi-mode operation and the attendant problems, it is recommended that the confocal half resonator be used whenever possible. When the full resonator is used operation at a reflector separation slightly different from confocal spacing is recommended. The change in reflector separation necessary from confocal spacing will depend on the Q for the fundamental mode, and may be calculated by the method used on pp. 45 through 48 keeping in mind the approximations involved.

VII SELECTED BIBLIOGRAPHY

Periodicals

1. V. Ya. Balakhov, V. K. Zhivotor, A. R. Striganov, "Diffraction Losses and Resonance-type Oscillations in Open Resonators with Cylindrical Mirrors", Soviet Physics-Doklady, vol. 9, #8, Feb., 1965, pp. 692-694.

2. S. R. Barone, "Resonances of the Fabry-Perot Laser", J. Appl. Phys., vol. 34, 1963, p. 831.

3. S. R. Barone, M. C. Newstein, "Fabry-Perot Resonators at Small Fresnel Numbers", Appl. Opt., vol. 3, Oct., 1964, p. 1194.

4. M. Bertolotti, "Matrix Representation of Geometrical Properties of Laser Cavities", Nuovo Cimento, vol. 32, June, 1964, pp. 1242-1257.

5. L. Bergstein, H. Schackter, "Resonant Modes of Optic Interferometer Cavities, I. Plane Parallel End Reflectors", Journ. of the Opt. Soc. of Amer., vol. 54, July, 1964, p. 887.

6. J. B. Beyer, E. H. Scheibe, "Higher Modes in Guided Electromagnetic Wave Beams", Trans. IEEE, AP-10, May, 1962, p. 349.

7. J. B. Beyer, E. H. Scheibe, "Loss Measurements of the Beam Waveguide", Trans. IEEE, MTT-11, Jan., 1963, pp. 18-22.

8. A. Boivin, R. Tremblay, "Interferometer Micro-onde a Fond Coherent", Canadian Journ. of Phys., vol. 39, 1961, pp. 393-408.

9. G. Boivin, R. Tremblay, "Canalisation d'ondes Electromagnetiques par Diffraction Iterée", Canadian Journ. of Phys., vol. 41, 1963, pp. 1604-1613.

10. G. D. Boyd, J. P. Gordon, "Confocal Multimode Resonator for Millimeter through Optical Wavelength Masers", B.S.T.J., vol. 40, 1961, pp. 489-509.

11. G. D. Boyd, H. Kogelnik, "Generalized Confocal Resonator Theory", B.S.T.J., vol. 41, July, 1962, pp. 1347-1369.

12. V. P. Bykov, L. A. Vainshtein, "Geometrical Optics of Open Resonators", J.E.T.P., vol. 47, Aug., 1964, pp. 508-517.

13. P. T. Checcacci, A. M. Scheggi, T. Di Francia, "Microwave Model of a Laser Resonator", Alta Frequenza, vol. 33, Nov., 1964, pp. 720-722.

14. P. F. Checcacci, A. M. Scheggi, "Microwave Models of Optical Resonators", Appl. Opt., vol. 4, 1965, p. 1529.

15. P. F. Checcacci, A. M. Scheggi, G. T. Di Francia, "Experimental Verification of Fox and Li Patterns in Open Resonators", Electronics Letters, Feb., 1966, vol. 2, #2, pp. 63-64.

16. T. S. Chu, "Geometrical Representation of Gaussian Beam Propagation", B.S.T.J., vol. 45, Feb., 1966, pp. 287-299.

17. J. R. Christian, G. Goubau, "Experimental Studies of a Beam Waveguide for Millimeter Waves", Trans. IRE, AP-9, May, 1961, pp. 256-263.

18. J. R. Christian, G. Goubau, "Some Measurements on an Iris Beam Waveguide", Proc. IRE, vol. 49, Nov., 1961, pp. 1679-1680.

19. P. O. Clark, "A Self-consistent Field Analysis of Spherical Mirror Fabry-Perot Resonators", Proc. IEEE, vol. 53, Jan., 1965, p. 36.

20. W. Culshaw, "Reflectors for a Microwave Fabry-Perot Interferometer", Trans. IRE, MTT-7, April, 1959, pp. 221-228.

21. W. Culchaw, "High Resolution Millimeter Wave Fabry-Perot Interferometer", Trans. IRE, MTT-8, March, 1960, pp. 182-189.

22. W. Culshaw, "Resonators for Millimeter and Submillimeter Wavelengths", Trans. IRE, MTT-9, March, 1961, pp. 135-144.

23. W. Culshaw, M. V. Anderson, "Measurements of Dielectric Constants and Losses with a Millimeter Wave Fabry-Perot Interferometer", Proc. Conf. Microwave Measurements Tech., IEE, London, England, Sept., 1961.

24. W. Culshaw, "Measurements of Permittivity and Dielectric Loss with a Millimeter Wave Fabry-Perot Interferometer", Proc. IEE, vol. 109, Pt. B, Suppl. 23, 1961, p. 820.

25. W. Culshaw, "Further Considerations on Fabry-Perot Type Interferometers", Trans. IEEE, MTT-10, Sept., 1962, pp. 331-339.

26. J. E. Degenford, M. D. Sirkos, and W. H. Steier, "The Reflecting Beam Waveguide", IEEE Trans. on Microwave Theory and Techniques, vol. MTT-12, July, 1964, pp. 445-453.

27. S. F. Dyublo, V. V. Kamyshan, V. P. Sheiko, "Instability of Confocal Systems", Soviet Physics-Technical Physics, vol. 10, #10, April, 1966.

28. C. C. Eaglesfield, "Mode Conversion Loss in a Sequential Confocal Lense System", Proc. Inst. Elect. Eng., III, 1964, pp. 610-615.

29. A. G. Fox, T. Li, "Resonant Modes in an Optical Maser", Proc. IRE, vol. 48, Nov., 1960, pp. 1904-1905.

30. A. G. Fox, T. Li, "Resonant Modes in a Maser Interferometer", B.S.T.J., vol. 40, 1961, pp. 453-488.

31. A. G. Fox, T. Li, "Modes in a Maser Interferometer with Curved and Tilted Mirrors", Proc. IEEE, vol. 51, Jan., 1963, pp. 80-88.

32. D. Gloge, "Calculation of Fabry-Perot Resonators by Scattering Matrices", Arch. Elect. Ubertragung, vol. 18, March, 1964, p. 197.

33. D. Gloge, "Ein allgemeines Verfakren zur Berechnung Optischer Resonatorer und Periodischer Linsensysteme", Arch. Elect. Ubertragung, vol. 19, 1965, pp. 13-26.

34. J. P. Gordon, "A Circle Diagram for Optical Resonators", B.S.T.J., vol. 43, July, 1964, pp. 1826-1827.

35. J. P. Gordon, H. Kogelnik, "Equivalence Relations Among Spherical Mirror Optical Resonators", B.S.T.J., vol. 43, Nov., 1964, pp. 2873-2886.

36. G. Goubau, F. Schwering, "On the Guided Propagation of Electromagnetic Wave Beams", Trans. IRE, AP-9, May, 1961, pp. 248-256.

37. G. Goubau, "Optical Relations for Coherent Wave Beams", Symp. on Elect. Mag. Theory and Antennas, Copenhagen, June 1962, Pergamon Press, 1963.

38. G. Goubau, J. R. Christian, "Some Aspects of Beam Waveguides for Long Distance Transmission at Optical Frequencies", IEEE Trans., MTT-12, March, 1964, pp. 212-220.

39. G. Goubau, J. R. Christian, "Loss Measurements with a Beam Waveguide for Long-Distance Transmission at Optical Frequencies", Proc. IEEE, vol. 52, Dec., 1964, p. 1739.

40. G. Goubau, "Lenses Guide Optical Frequencies to Low Loss Transmission", Electronics, vol. 39, May, 1966, pp. 83-89.

41. D. R. Hericott, "Spherical Mirror Oscillating Interferometer", Appl. Opt., vol. 2, Aug., 1963, pp. 865-866.

42. J. C. Heurtley, W. Streifer, "Optical Resonator Modes-Circular Reflectors of Spherical Curvature", J. Opt. Soc. Am., vol. 55, Nov., 1965, pp. 1472-1479.

43. J. C. Heurtley, "Optical Resonators with Circular Mirrors", J. Opt. Soc. Am., vol. 54, Nov., 1964, p. 1400.

44. W. K. Kahn, "Geometric Optical Derivation of Formula for the Variation of the Spot Size in a Spherical Mirror Resonator", Appl. Opt., vol. 4, June, 1965, pp. 758-759.

45. B. Z. Katsenelenbaum, "Quasioptical Methods of Generation and Transmission of Millimeter Waves", Soviet Physics, USPEKHI, vol. 7, #3, Nov., Dec., 1964, p. 385.

46. H. Kogelnik, W. W. Rigrod, "Visual Display of Isolated Optical Resonator Modes", Proc. IRE, vol. 50, Feb., 1962, p. 220.

47. H. Kogelnik, S. P. Morgan, "Equivalence of Different Integral Equations for the Confocal Resonators", Trans. IEEE, MTT-12, Nov., 1964, p. 624.

48. H. Kogelnik, T. Li, "Laser Beams and Resonators", Proc. IEEE, vol. 54, #10, October, 1966, pp. 1312-1329.

49. H. Kogelnik, "On the Propagation of Gaussian Beams of Light Through Lense-like Media Including Those with a Loss or Gain Variation", Appl. Opt., vol. 4, Dec., 1965, pp. 1562-1569.

50. R. D. Lending, "New Criteria for Microwave Component Surfaces", Microwave Tubes and Components, 1965 NEC Proc., Chicago, p. 391.

51. T. Li, "Mode Selection in an Aperture Limited Concentric Maser Interferometer", B.S.T.J., vol. 42, Nov., 1963, pp. 2609-2620.

52. T. Li, "Dual Forms of the Gaussian Beam Chart", Appl. Opt., vol. 3, Nov., 1964, pp. 1315-1317.

53. T. Li, "Diffraction Loss and Selection of Modes in Maser Resonators with Circular Mirrors", B.S.T.J., vol. 44, May, 1965, p. 917.

54. H. Lotsch, "The Confocal Resonator System with a Large Fresnel Number", Trans. IEEE, MTT-12, July, 1964, pp. 482-483.

55. H. K. Lotsch, "The Spherical and Hemi-spherical Resonator Systems with a Large Fresnel Number", Zeitschrift fur angewandte Physik, vol. 18, Heft 3, 1964, pp. 241-245.

56. H. K. Lotsch, "Note Concerning the Analogy between the Fabry-Perot Interferometer and the Iris Type Beam Waveguide", Phys. Letters, vol. 11, #3, Aug., 1964, pp. 221-222.

57. H. K. Lotsch, "On the Physical Formulation of the Fabry-Perot Interferometer used as a Laser Resonator", Phys. Letters, vol. 12, #2, Sept., 1964, pp. 99-101.

58. H. K. Lotsch, "An Elementary Theory for Beam Waveguides", Zeitschrift fur Naturforschung, vol. 19, Heft 13, 1964, pp. 1438-1446.

59. H. K. Lotsch, "Comments on the Self Consistent Field Technique for Optical Resonators", Phys. Letters, vol. 13, #3, Dec. 1, 1964, pp. 220-221.

60. H. K. Lotsch, "Multimode Resonators with a Small Fresnel Number (Lowest Order Eigenmodes)", Zeitschrift for Naturforschung, vol. 20, Heft 1, 1965, pp. 38-48.

61. B. Macke, "Laser Cavities in Geometrical Optics Approximation", J. Physics, (Paris), vol. 26, March, 1965, pp. 104a-112a.

62. D. E. McCumber, "Eigenmodes of a Symmetric Cylindrical Confocal Laser Resonator and Their Perturbation by Output Coupling Apertures", B.S.T.J., vol. 44, Feb., 1965, pp. 333-363.

63. J. W. Mink, E. H. Scheibe, "A Dual Mode Beam Waveguide Resonator and Frequency Stabilizer at Millimeter-wave Frequency", Trans. IEEE, MTT-14, #5, May, 1966, pp. 222-228.

64. S. P. Morgan, "On the Integral Equations of Laser Theory", Trans. IEEE, MTT-11, May, 1963, p. 191.

65. D. J. Newmann, S. Morgan, "Existence of Eigenvalues of a Class of Integral Equations Arising in Laser Theory", B.S.T.J., vol. 43, Jan., 1964, pp. 113-126.

66. A. G. van Nie, "Rigorous Calculation of the Electromagnetic Field of Wave Beams", Phillips Res. Repts., vol. 19, Aug., 1964, pp. 378-394.

67. M. J. Offerhaus, "Geometry of the Radiation Field for a Laser Interferometer", Phillips Res. Repts., vol. 19, Dec., 1964, pp. 520-523.

68. Hisanco Ogura, Y. Yoshida, Y. Furukama, Joni-ichi Ikenocee, "Slight Deformation of Confocal Fabry-Perot Resonator", Japanese Journ. of Appl. Phys., vol. 5, #3, March, 1966, pp. 225-233.

69. G. Oltmann, "A 2 mm. (Non)-Confocal Resonator for Use as a Wavemeter or Filter Element", IRE Wescon Conv. Record, 1963.

70. A. M. Prophorov, "Molecular Amplifier and Generator for Submillimeter Waves", J.E.T.P., vol. 34, 1958, p. 1658.

71. A. L. Schawlow, C.H. Towns, "Infrared and Optical Masers", Phys. Rev., vol. 112, Dec., 1958, pp. 1940-1949.

72. E. H. Scheibe, B. King, A. van Zeeland, "Loss Measurements of Surface Wave Transmission Lines", J. Appl. Phys., vol. 25, June, 1954, pp. 790-797.

73. E. H. Scheibe, "Measurements on Resonators Formed from Circular Plane and Confocal Paraboloidal Mirrors", Proc. IRE, vol. 49, June, 1961, p. 1079.

74. F. Schwering, "Reiterative Wave Beams of Rectangular Symmetry", Archiv Elect. Ubertragung, vol. 15, Dec., 1961, pp. 555-564.

75. A. E. Siegmann, "Unstable Optical Resonators for Laser Applications", Proc. IEEE, vol. 53, March, 1965, p. 277.

76. D. C. Sinclair, "Choice of Mirror Curvatures for Gas Laser Cavities", Appl. Opt., vol. 3, Sept., 1964, p. 1067.

77. D. Slepian, "Prolate Spheroidal Wave Functions, Fourier Analysis and Uncertainty- IV, Extensions to Many Dimensions, Generalized Prolate Spheroidal Functions", B.S.T.J., vol. 43, p. 3009, Nov., 1964.

78. H. Statz, C. L. Tang, "Problem of Mode Deformation in Optical Masers", J. Appl. Phys., vol. 35, June, 1965, pp. 1816-1819.

79. R. J. Strain, P. D. Coleman, "Millimeter Wave Cavity Coupling by Quarter Wave Transformer", Trans. IRE, MTT-10, Nov., 1962, p. 612.

80. W. Streifer, "Modes in Spherical Resonators with Rectangular Mirrors", J. Opt. Soc. Am., vol. 54, Nov., 1964, p. 1399.

81. W. Streifer, H. Gamo, "On the Schmidt Expansion for Optical Resonator Modes", Proc. of Symp. on Quasi-Optics, Brooklyn Polytechnic Press, New York, 1964.

82. W. Streifer, "Optical Resonator Modes-Rectangular Reflectors of Spherical Curvature", J. Opt. Soc. Am., vol. 55, July, 1965, pp. 868-877.

83. K. F. Sooho, "Nonconfocal Multimode Resonators for Masers", Proc. IEEE, vol. 51, Jan., 1963, pp. 70-75.

84. W. A. Specht, "Modes in Spherical Mirror Resonators", Journ. Appl. Phys., vol. 36, #4, April, 1965, pp. 1306-1313.

85. P. Szulkin, "On the Theory of the Open Resonator", Buli. Acad. Polon. Sci. Ser. Sci. Tech., (Poland), vol. 8, 1960, p. 639.

86. C. L. Tang, "On Diffraction Losses in Laser Interferometers", Appl. Opt., vol. 1, 1962, p. 768.

87. M. J. Taylor, G. R. Hanes, K. M. Baird, "Diffraction Loss and Beam Size in Lasers with Spherical Mirrors", Journ. Opt. Soc. of Amer., vol. 54, #11, Nov., 1964, pp. 1310-1314.

88. J. F. La Tourette, S. F. Jacobs, R. Rabinowitz, "Improved Laser Angular Brightness through Diffraction Coupling", Appl. Opt., vol. 3, Aug., 1964, p. 981.

89. L. A. Vainshtein, "Open Resonators for Lasers", J.E.T.P., (USSR), vol. 17, Sept., 1963, p. 709.

90. L. A. Vainshtein, "Open Resonators with Spherical Mirrors", J.E.T.P., vol. 18, Feb., 1964, pp. 371-479.

91. R. W. Zimmerer, "New Wavemeter for Millimeter Wavelengths", Rev. Sci. Instr., vol. 33, 1962, p. 858.

92. R. W. Zimmerer, M. V. Anderson, G. L. Strine, Y. Beers, "Millimeter Wavelength Resonant Structures", Trans. IRE, MTT-11, March, 1963, p. 142.

93. R. W. Zimmerer, "Spherical Mirror Fabry-Perot Resonators", Trans. IRE, MTT-11, Sept., 1963, p. 371.

94. R. W. Zimmerer, "Experimental Investigation of Fabry-Perot Interferometers", Proc. IRE, vol. 51, March, 1963, pp. 475-476.

95. Books

G. Goubau, "Beam Waveguides", Advances in Microwaves, Academic Press, New York, Ed. by L. Young, vol. 3, pp. 67-126, 1968.

G. Goubau and P. D. Coleman, "Beam Waveguides", Microwave Power Engineering, Academic Press, New York, Ed. by E. C. Okress, vol. 1, pp. 228-240, 1968.

H. Kogelnik, "Modes in Optical Resonators", Lasers, A. K. Levine, Ed., New York, Dekker, 1966.

Miscellaneous

96. J. B. Beyer, "A Study of the Beam Waveguide", Ph.D. Thesis, Univ. of Wis., Madison, Wis., 1961.

97. R. H. Dicke, "Molecular Amplification and Generation Systems and Methods", U.S. Patent 2,851,652, Sept., 1958.

98. G. Goubau, J. R. Christian, "A New Waveguide for Millimeter Waves", presented at URSI-IRE Fall Meeting, San Diego, Cal., Oct., 1959; Army Science Conf., West Point, New York, June, 1959.

99. G. Goubau, "Transmission of Electromagnetic Wave Beams", U.S. Patent 2,651,715, Sept. 8, 1963.

100. B. King, T. Tatsuguchi, E. Scheibe, G. Goubau, "Pseudo-Resonance Between Parallel Plates", presented at URSI-IRE Spring Meeting, Washington, D.C., May, 1955.

101. B. King, "A Study of Cylindrical Surface Waves and of the Parallel Plane Open Resonator", Ph.D. Thesis, Univ. of Wis., Madison, Wis., 1955.

102. J. W. Mink, "Higher Modes in Electromagnetic Wave Beams", M.S. Thesis, Univ. of Wis., Madison, Wis., 1962.

103. J. W. Mink, "A Study of the Beam Waveguide Resonator", Ph.D. Thesis, Univ. of Wis., Madison, Wis., 1964.

104. E. H. Scheibe, "Study of Surface Wave Transmission Lines", Univ. of Wis., Madison, Wis., Final Report on Contract DA-36-039-sc-56734, June 30, 1955.

105. E. H. Scheibe, "Surface Wave, Antenna and Microwave Filter Engineering Research Study", Final Report on Contract No. DA-36-039-sc-78326, Sept. 30, 1961.

106. E. H. Scheibe, "Surface Wave and Antenna Engineering Research Study", Final Report on Contract DA-36-039-sc-85188, Nov. 30, 1964.

107. J. W. Sherman, "Research for Open Resonators, Diode Array Harmonic Generators, and Optical Beam Steering", Final Report on Contract AF 19(628)-397 by Advanced Technology Corp, April, 1965.

108. A. W. Murphy, "Investigation of Beam Waveguide Resonators at Millimeter Wavelengths", Ph.D. Thesis, Univ. of Wis., Madison, Wis., 1967.

109. E. H. Scheibe, "Waveguide, Waveguide Circuits and Antenna Research Study", Final Report on Contract No. DA-36-039-AMC-02261(E), Feb. 28, 1969.

110. J. R. Brauer, "A Rectangular Beam Waveguide Resonator and Antenna", Ph.D. Thesis, Univ. of Wis., Madison, Wis., 1969.

VIII. APPENDIX A

MEASURING EQUIPMENT AND PROCEDURES

During the course of the experimental study on which this report is based, it was necessary to perform certain measurements repeatedly on many open resonator structures. In order to facilitate these measurements certain special equipment was constructed, and measurement procedures were standardized.

All of the data obtained on resonant structures required only that relative power and frequency be measured. A block diagram of the signal generator portion of the test equipment is shown in Fig. A-1. As much of the microwave circuitry as possible was mounted on a portable chassis to achieve flexibility. As assembled, the generator is capable of delivering 14 milliwatts from 34.0 GHz to 35.5 GHz.

Any one of several modes of operation may be selected by using the waveguide switches and the klystron repeller control switches. With the aid of the Dymec Model 2650A Frequency Synchronizer, the VA-97 klystron may be locked in phase 30 MHz away from a stable, spectrally pure signal from a frequency multiplier chain. The 30 MHz difference signal generated by the klystron and the frequency multiplier is phase locked to a 30 MHz reference signal. For fixed frequency operation, the third harmonic of a 10 MHz crystal oscillator contained in the Dymec may be used as a reference. For variable frequency operation over a narrow range while phase locked, an external variable frequency oscillator near 30 MHz may be used. The phase comparison circuit permits the difference frequency to be varied from 28 MHz to 32 MHz. Since the frequency change is direct, i.e., a 1 MHz change in the 30 MHz reference frequency produces a

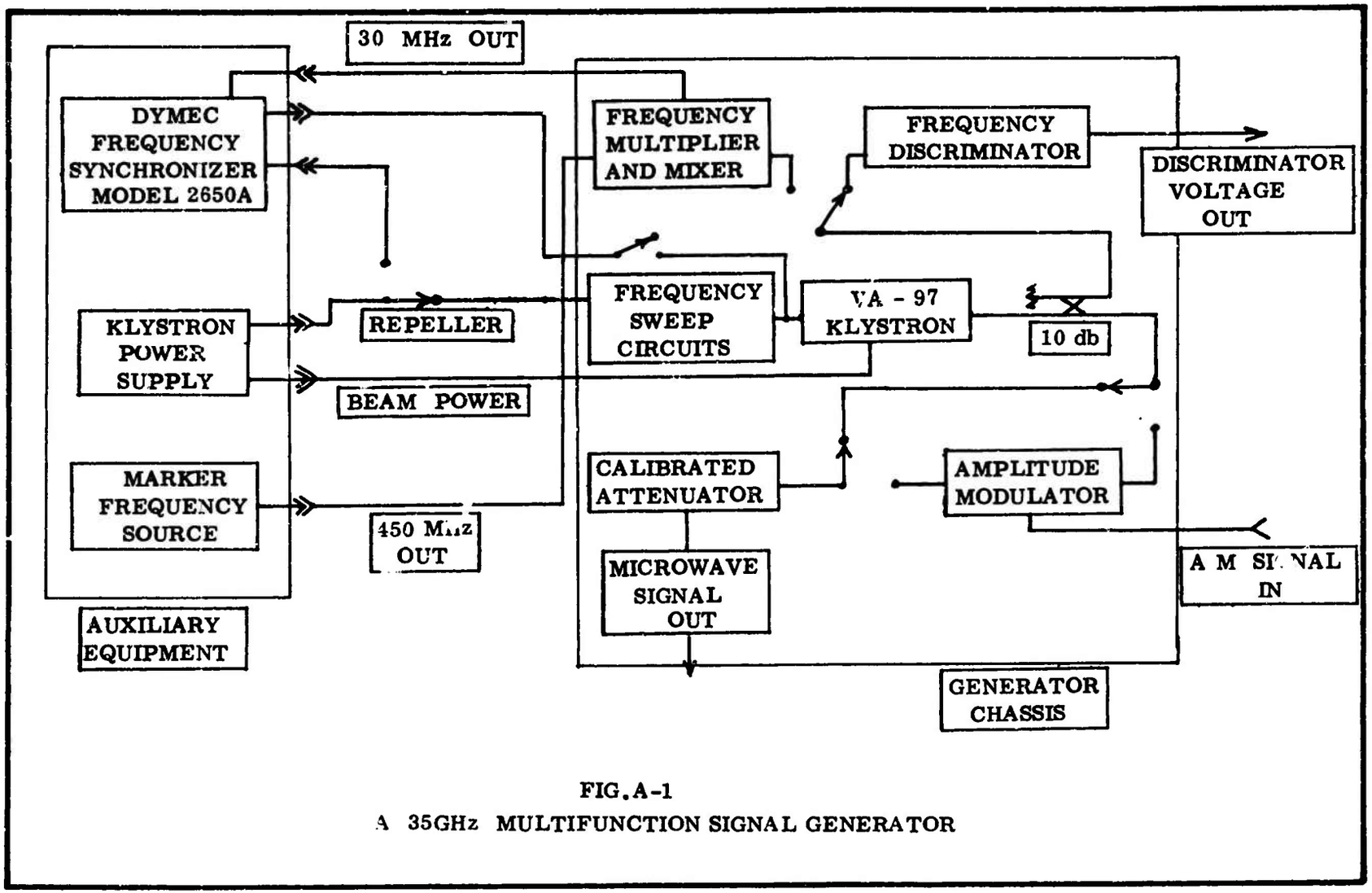

FIG. A-1

A 35GHz MULTIFUNCTION SIGNAL GENERATOR

1 MHz change in the klystron frequency, the 30 MHz reference oscillator need only be stable to one part in 10^4 for a klystron stability of one part in 10^7.

With the phase lock loop disconnected, the repeller of the klystron may be modulated to obtain either swept frequency or pulse operation. As shown in Fig. A-2a, 60 Hz power may be switched to the repeller to obtain a variable width 60 Hz swept frequency from the klystron. The 60 Hz signal is also fed to a terminal on the rear of the chassis and may be used for the blanking voltage on an oscilloscope.

The diode modulator of Fig. A-2b inserted after the frequency control loop, permits the klystron output to be amplitude modulated in either the phase locked or swept frequency modes of operation. The variable position short circuit permits the amplitude of the carrier relative to the amplitude of the sidebands to be controlled up to complete carrier suppression. The modulation range is from a few kilohertz to 50 MHz using a 1N53 microwave diode; the modulating signal being supplied from an external source.

Incorporating the frequency discriminator shown in Fig. A-3 and monitoring part of the klystron output, makes available an output voltage which is a function of the klystron frequency. The discriminator output is used to drive the horizontal amplifier of an oscilloscope when the klystron frequency is being swept.

Much of the circuitry of the generator was designed to facilitate the use of a swept frequency response measurement procedure shown in Fig. A-4. When the signal is amplitude modulated, three responses due to the resonator are displayed on the oscilloscope, one each as the carrier and two sidebands are swept through the response. When the modulating frequency is

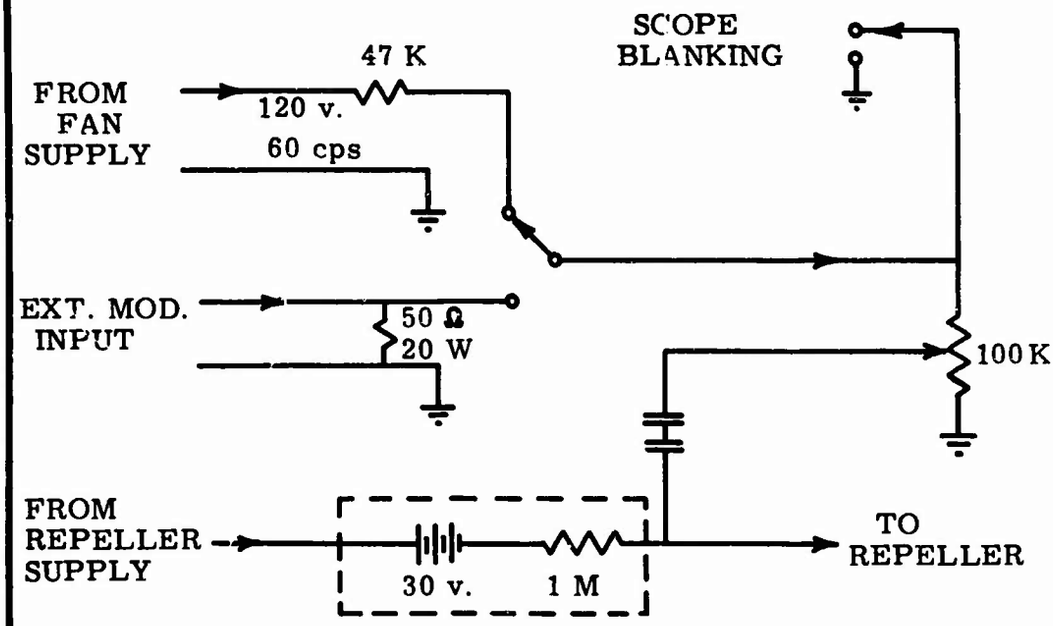

FIG. A - 2a

REPELLER MODULATION CIRCUITS

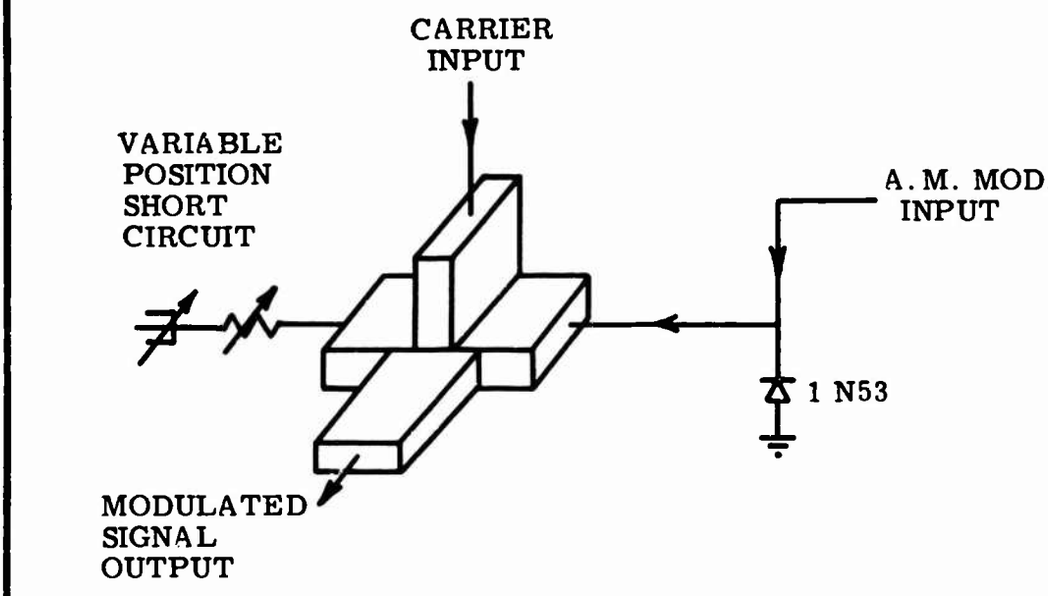

FIG. A - 2b

AMPLITUDE MODULATOR

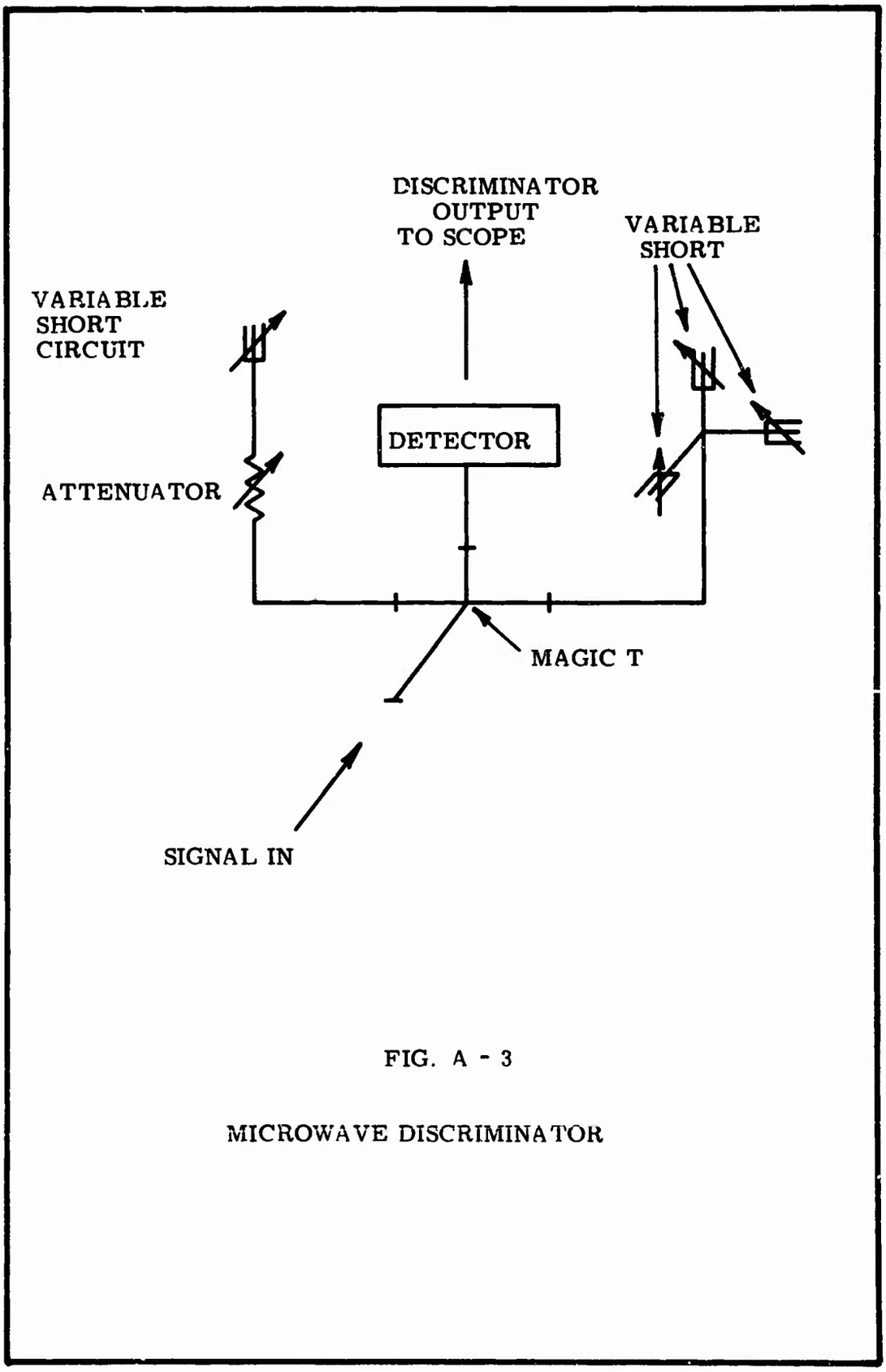

FIG. A - 3

MICROWAVE DISCRIMINATOR

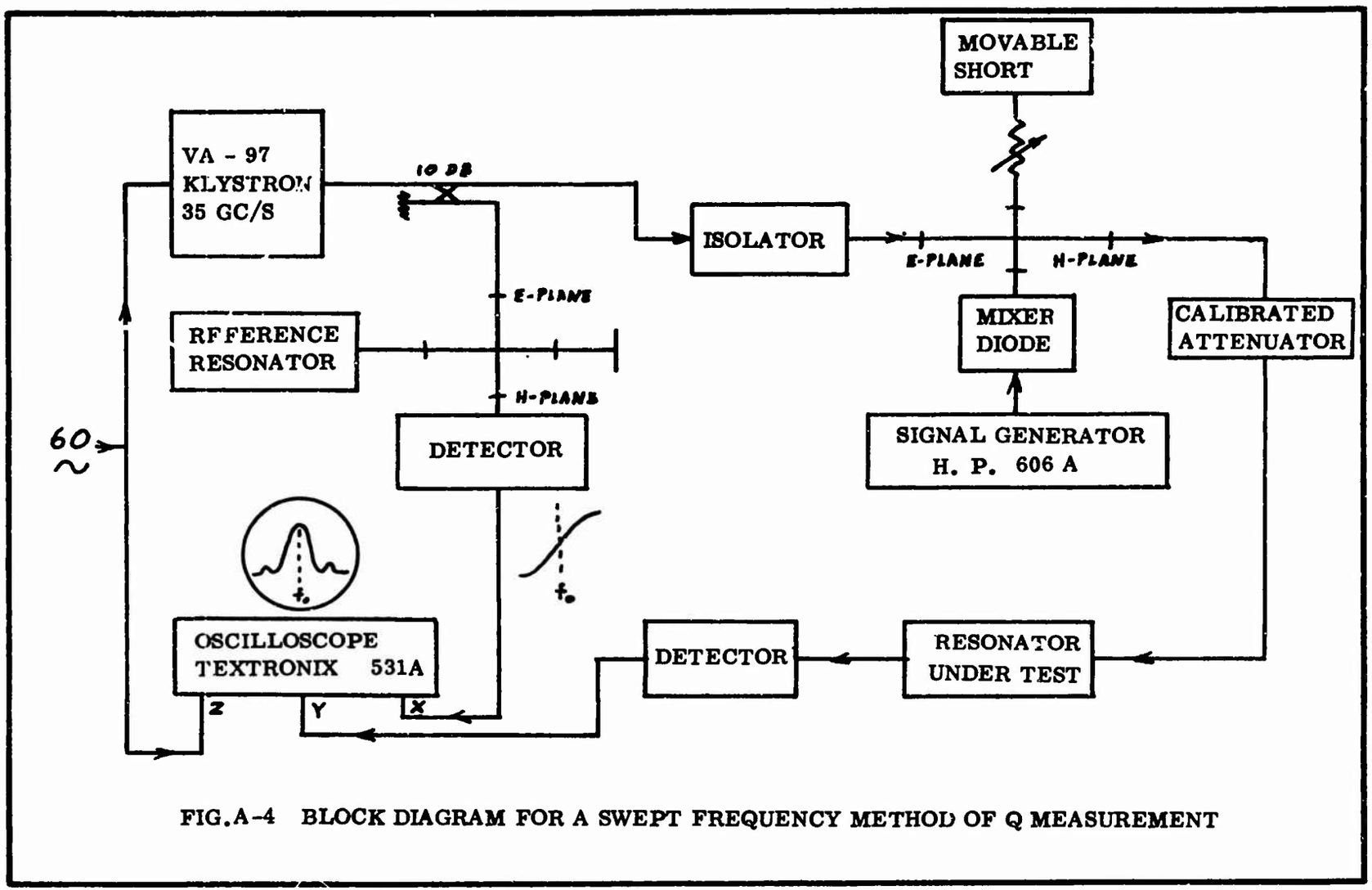

FIG.A-4 BLOCK DIAGRAM FOR A SWEPT FREQUENCY METHOD OF Q MEASUREMENT

known, the linearity of the display may be adjusted by tuning the discriminator and thus a frequency calibration of the horizontal scope scale can be obtained.

When more accuracy than can be obtained by the swept frequency method is required, a point by point measurement of amplitude response versus frequency is necessary. The anticipated resonator Q's in these measurements was as high as 500,000. At 35 GHz, the half power band width of such a response is only 70 KHz. For an accurate measurement of such a response the spectral purity and stability of the source must be better than 10 KHz.

Although there will be a degrading of the klystron stability due to noise in the phase lock loop, the most important consideration is the stability of the reference signal to which the klystron is locked. This signal is supplied by the combination of the marker frequency source and the frequency multiplier and mixer shown in Fig. A-1. The marker frequency source is driven by a crystal oscillator using a Bliley type BG 61A-5, 5 MHz crystal mounted in a proportional control oven. The oscillator is followed by two buffer amplifiers. The crystal stability as quoted by the manufacturer to be 0.001 ppm/day. Using vacuum tube multipliers and amplifiers, the 5 MHz reference is raised to 150 MHz at 10 watts. A varactor tripler circuit converts this to 450 MHz at 5 watts. The final multiplier is driven at 450 MHz and 150 milliwatts. The excess power is dissipated in resistive padding between the multiplier stages. The input power to the final stage must be limited to the dissipation rating of the Microwave Associates MA 4361 pill varactor which is mounted in a section of 35 GHz waveguide.

The marker frequency used for phase-locking was 35.01 GHz, and is the 78th harmonic of 450 MHz. Markers are also available for phase-locking at all other multiples of 450 MHz within the pass band of the waveguide.

Based on the 5 MHz oscillator stability, the stability of the marker is one part in 10^9 short term. Checks with an HP 851A/8551A Spectrum Analyzer showed that the marker was atable to within 10 MHz at 35 GHz, and the phase locked klystron was also found to have a dispersion of less than 10 KHz.

The receiver used to measure the resonator response consisted of a VA-97 klystron as a local oscillator, a balanced mixer, a 60 MHz I.F. amplifier with 100 db gain and a 12 MHz bandwidth, a second detector, and a microammeter. To prevent variations in the gain of the I.F. amplifier over its passband from affecting the signal level indication on the microammeter, the local oscillator was frequency locked 60 MHz from the received signal by means of a Micro-Now Model 201 Microwave Frequency Stabilizer. The microammeter at the receiver output was set at a reference level, and the change in the received signal level was determined by returning to the reference level by using a calibrated microwave attenuator in the signal path between the transmitter and the receiver.

Both the transmitted and reflected responses of resonators were measured. The reflected response however yielded the most information about the resonator under test. The transmitted response provides measured values of the loaded Q and total insertion loss. When the coupling to the resonator is sufficiently weak, the measured Q approximates the unloaded Q. The reflected response yields values of the loaded and unloaded Q, the degree of coupling, and the losses associated with the coupling network. The data necessary and the procedures for the data evaluation are given in Appendix B. The majority of the data presented in this report has been obtained from the measurement of the reflected response of the resonators. The block diagram for the general measurement setup is given in Fig. A-5. A coupling network used quite extensively is shown in Fig. A-6.

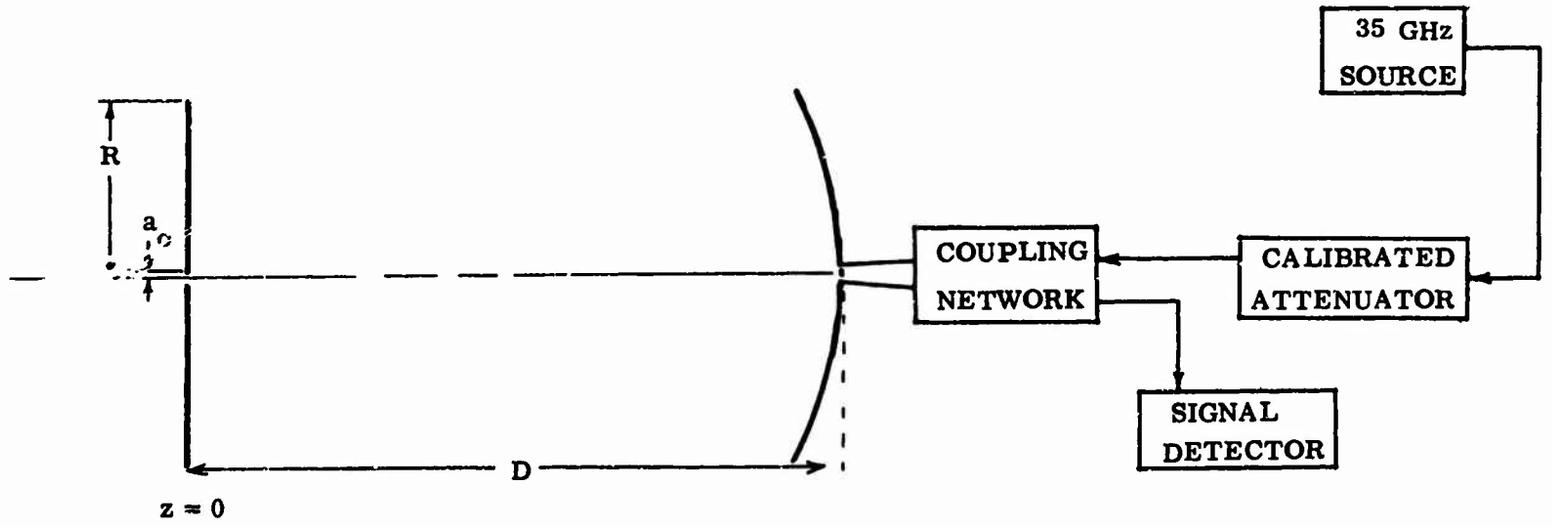

FIG. A-5
BLOCK DIAGRAM OF EQUIPMENT
FOR BEAM WAVEQUIDE RESONATOR RESPONSE MEASUREMENTS

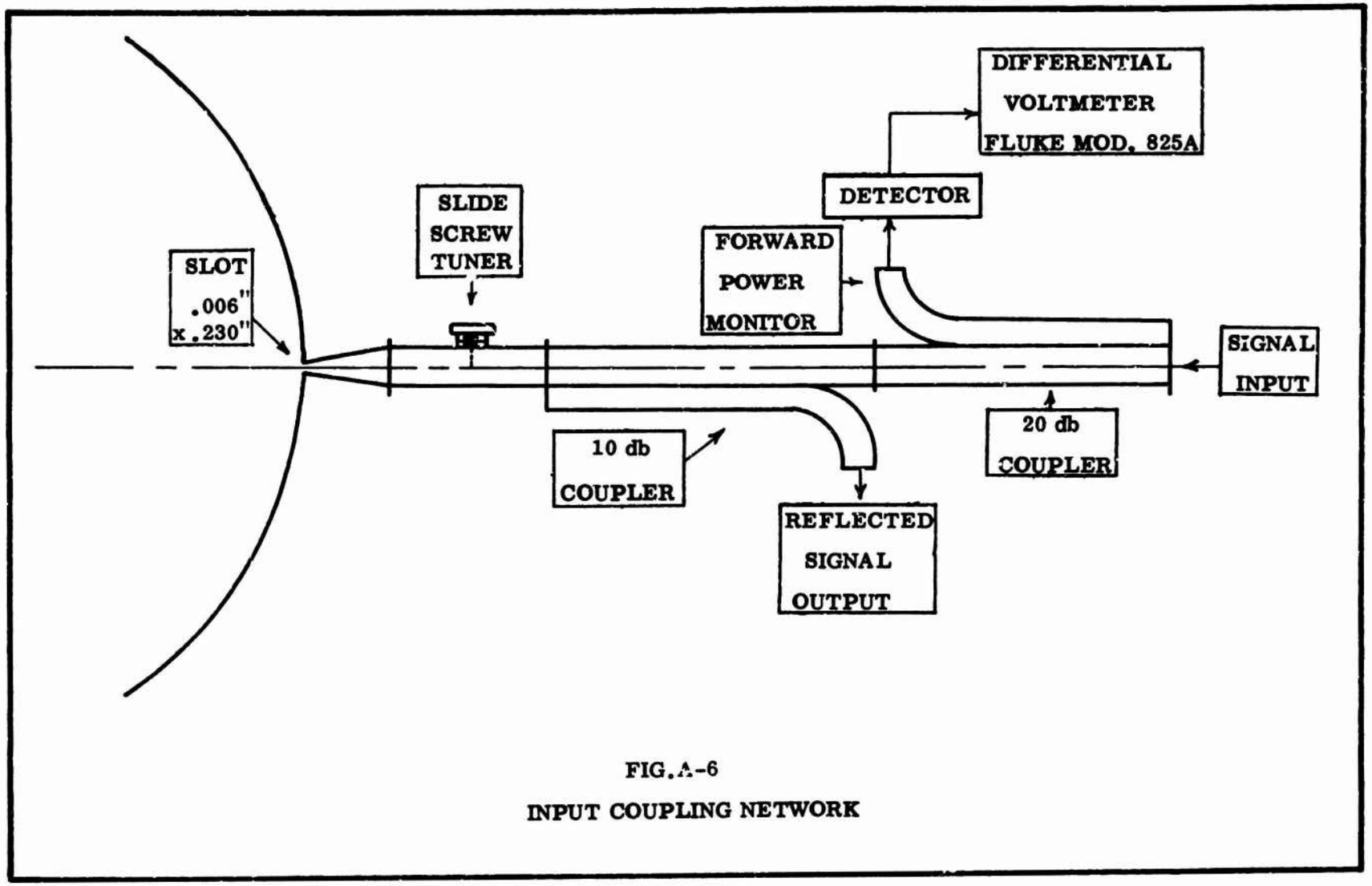

FIG. A-6

INPUT COUPLING NETWORK

The waveguide feeding the resonator tapers gradually to the dimensions of the narrow slot shown. For the coupling network of Fig. A-6, the variable attenuator for determining relative power would be located between the resonator and the receiver in order that the forward power monitor could be used to insure constant source power as a function of time and frequency.

A photograph of a typical confocal half resonator for testing is shown in Fig. A-7. The three support rods are steel, with the flat frame pieces made of 3/8 inch aluminum. The reflectors are mounted at four points to the frame upright plates. Compressible bushings between the reflectors and the frame allow reflector alignment. The center section shown in Fig. A-7 contains one of the reflectors. This section mounted on three ball bushings, is movable and permits the reflector separation to be adjusted. A micrometer control, part of which is visible at the far right of Fig. A-7, allows fine positioning of the reflector over a 2.5 cm range.

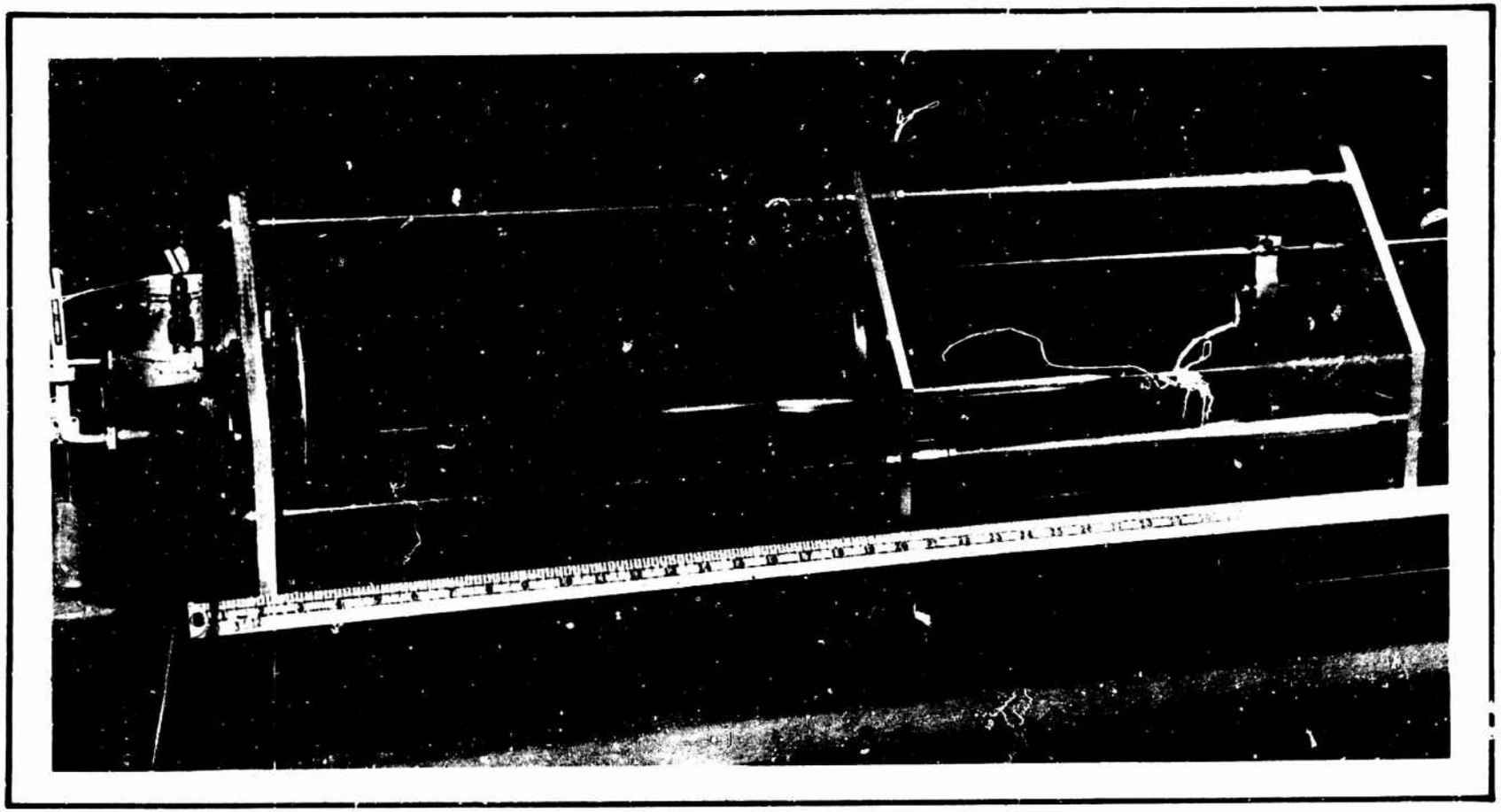

FIG. A-7

35 Gc BEAM WAVEGUIDE RESONATOR

IX. APPENDIX B

DISCUSSION OF Q

The quality factor or 'Q' of a device, circuit, or medium may in the most general sense be defined as the ratio of energy stored to the rate of energy dissipated. In the case where the energy stored is in harmonically time varying electromagnetic fields, Q is defined by

$$Q = 2\pi \frac{\text{Energy stored}}{\text{Energy dissipated per cycle}}$$

or

$$Q = 2\pi f \frac{W}{P}.$$

where f is the frequency

W = stored energy

P = the power loss, or energy dissipation per second.

For a lumped element resonant circuit or a closed cavity resonator, the Q is normally specified at $\omega = \omega_0$, defined as the resonant angular frequency, at which the stored energy is a maximum.

The concept of 'Q' is not limited to resonant systems. It may also be applied to a transmission medium in which case it is a measure of the rate of dissipation of energy from a traveling wave. Consider a wave expressed by

$$E = E_0(x,y) \exp[-(\alpha+j\beta)z]$$

Where α and β are both real, β is the propagation constant in radians per unit length, and α is the attenuation constant in nepers per unit length. The energy density is given by

$$w = 1/2\varepsilon EE^*$$

$$w = 1/2\varepsilon E_0^2 e^{-2\alpha z}$$

and the time rate of decrease of the energy density is

$$\frac{dw}{dt} = \frac{dw}{dz}\frac{dz}{dt} = 1/2v\varepsilon E_0^2(-2\alpha) e^{-2\alpha z}$$

and from the expression for Q

$$Q = 2\pi f \frac{w}{dw/dt} = 2\pi f \left(\frac{1}{v(2\alpha)}\right)$$

when v is the velocity of propagation.

The power loss in an interval of length D is given by

$$L_{db} = 4.43 \ln(1-2\alpha D) = 8.68\alpha D$$

for $\alpha << 1$. And since $f/v = 1/\lambda$

$$Q = \frac{8.68\alpha D}{\lambda L_{db}} \qquad \text{(B-1)}$$

This expression for the Q is the most useful form for use with open resonators and expresses the losses as a percentage over a given interval or iteration. Care must be used, however, in the choice of the interval D over which the losses are calculated. Every interval of length D irrespective of the locations of the end points must have the same total loss. Thus, if the losses are the same at each reflector of the resonator, the Q may be defined in terms of the losses over the interval D where D is the separation between the reflectors. If, however, the losses are different at the two reflectors, the Q must be defined in terms of a length 2D and the total loss when expressed in db, is the sum of the losses at each reflector.

With the aid of the information given in section IV, the theoretical unloaded Q of an open resonator may be determined from a knowledge of the reflector separation and the diffraction and resistive losses for the reflectors. For circuit applications and experimental studies, the Q must be expressible in terms of the measurable quantities such as frequency and relative power.

A general equivalent circuit for an open resonator is given in Fig. B-1. The T networks at the input and output are general representations of coupling networks. If an ideal transformer is to be included in the representation of the coupling network, all elements shown may be considered as transformed to

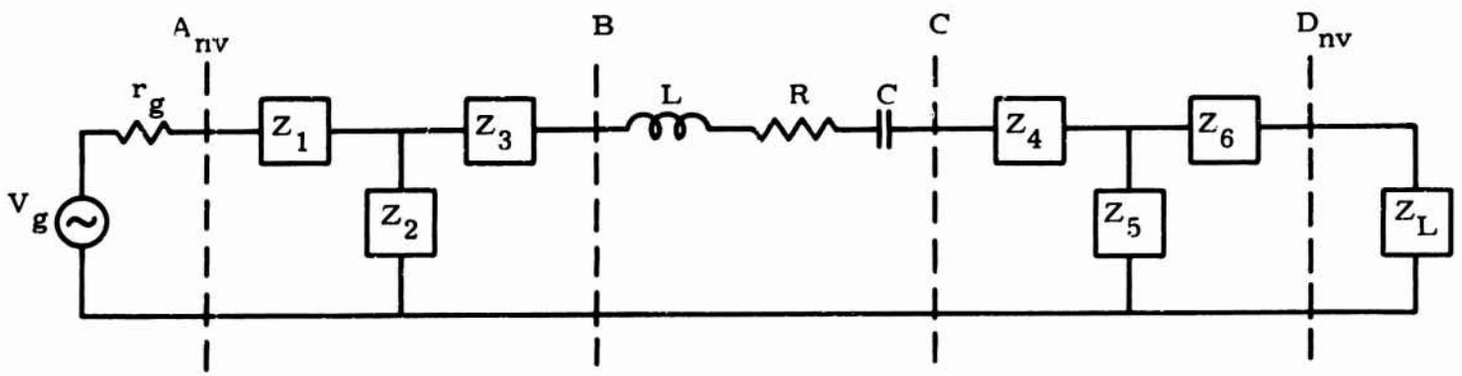

FIG. B - 1

OPEN RESONATOR
GENERAL EQUIVALENT CIRCUIT

the resonator side of the transformers. For a shunt rather than a series representation of the resonator, a quarter wave length of transmission line may be included in Z_3 and Z_4. The reason for this is that for a cavity to appear as a short circuit or an open circuit at resonance and to appear the opposite off resonance depends upon the choice of the reference plane. The theoretical unloaded and uncoupled Q discussed above may be defined in terms of R, L, and C by the relation

$$Q_{00} = \frac{\omega_o L}{R} \tag{B-2}$$

where $$\omega_o = 2\pi f_o = (LC)^{-1/2} \tag{B-3}$$

Due to the multiple mode resonance properties of open resonators, each mode may have a different Q value, resonant frequency, and coupling coefficient, and therefore a resonant circuit together with a coupling network will be required for each mode. These circuits may be considered connected in parallel between the source and the load. For the circuit of Fig. B-1, the scattering matrix is the best representation at microwave frequencies, since the reflection coefficients at the terminals and the transmission coefficient are easily measurable.

The method used here was to divide the circuit into three sections which are shown between the reference planes of Fig. B-1. The ABCD matrix was calculated for each section and the ABCD matrix for the overall circuit was obtained by multiplying the individual matrices together. The ABCD matrix was then converted to the scattering matrix.

The ABCD matrix is defined as follows:

$$[ABCD] = [u] = \begin{bmatrix} u_{11} & u_{12} \\ u_{21} & u_{22} \end{bmatrix} \tag{B-4}$$

Now for the network of Fig. B-1

$$[u] = \begin{bmatrix} 1+\frac{Z_1}{Z_2} & \frac{Z_1}{Z_2} \\ \frac{1}{Z_2} & 1+\frac{Z_3}{Z_2} \end{bmatrix} \times \begin{bmatrix} 1 & Z_0 \\ 0 & 1 \end{bmatrix} \times \begin{bmatrix} 1+\frac{Z_4}{Z_5} & \frac{Z_2}{Z_5} \\ \frac{1}{Z_5} & 1+\frac{Z_6}{Z_5} \end{bmatrix} \tag{B-5}$$

and hence the u_{ij} elements for the overall matrix become

$$u_{11} = \frac{1}{Z_2 Z_5}\left[(Z_2+Z_1)(Z_5+Z_4+Z_0) + |Z|_1\right] \tag{B-6}$$

$$u_{12} = \frac{1}{Z_2 Z_5}\left[(Z_2+Z_1)|Z|_2 + Z_0(Z_2+Z_1)(Z_5+Z_6) \right.$$

$$\left. |Z|_1 \quad (Z_5+Z_6)\right] \tag{B-7}$$

$$u_{21} = \frac{1}{Z_2 Z_5}\left[Z_0+Z_4+Z_5+Z_2+Z_3\right] \tag{B-8}$$

$$u_{22} = \frac{1}{Z_2 Z_5}\left[|Z|_2 + (Z_2+Z_3+Z_0)(Z_5+Z_6)\right] \tag{B-9}$$

where $|Z|_1 = Z_1Z_2 + Z_2Z_3 + Z_1Z_3$

and $|Z|_2 = Z_4Z_5 + Z_5Z_6 + Z_4Z_6$

The conversion from the ABCD matrix to the scattering matrix may be found in the literature, and including normalization with respect to the input and output line impedances may be written in the form

$$S = \begin{bmatrix} S_{11} & S_{12} \\ S_{21} & S_{22} \end{bmatrix} \tag{B-10}$$

where

$$S_{11} = \frac{Z_{20}U_{11} + U_{12} - Z_{10}Z_{20}U_{21} - Z_{10}U_{22}}{Z_{20}U_{11} + U_{12} + Z_{10}Z_{20}U_{21} + Z_{10}U_{22}} \tag{B-11}$$

$$S_{12} = \frac{2(Z_{10}Z_{20})^{1/2}(U_{11}U_{22} - U_{12}U_{21})}{Z_{20}U_{11} + U_{12} + Z_{10}Z_{20}U_{21} + Z_{10}U_{22}} \tag{B-12}$$

$$S_{21} = \frac{2(Z_{10}Z_{20})^{1/2}}{Z_{20}U_{11} + U_{12} + Z_{10}Z_{20}U_{21} + Z_{10}U_{22}} \tag{B-13}$$

$$S_{22} = \frac{Z_{20}U_{11} - U_{12} + Z_{10}Z_{20}U_{21} - Z_{10}U_{22}}{Z_{20}U_{11} - U_{12} + Z_{10}Z_{20}U_{21} - Z_{10}U_{22}} \tag{B-14}$$

For the scattering matrix, S_{11} would be the input reflection coefficient assuming a load which has no reflection. When the load is mismatched such that it has a reflection coefficient Γ', then the input reflection coefficient to the network is given by[33]

$$\Gamma = S_{11} + \frac{(S_{12})^2\Gamma'}{1 - S_{22}\Gamma'} \tag{B-15}$$

The matrix element S_{12} is the transmission coefficient from the source to the load under conditions of matched load. For the network of Fig. B-1 it can be shown that $u_{11}u_{22} - u_{21}u_{12} = 1$. Then by definition the network will be reciprocal in that $S_{11} = S_{12}$.

Many of the measurements made in this study were performed on a single-ended resonator; i.e., there was only one coupling port. This requires that $Z_{20} = 0$ in Eq. B-11. Then

$$S_{11} = \frac{u_{12} - Z_{10}u_{22}}{u_{12} + Z_{10}u_{22}}$$

Furthermore $Z_4 = Z_5 = 0$ in Eqs. B-7 and B-9 in order to obtain the single port circuit and hence

$$S_{11} = \frac{-Z_{10}[Z_2 + Z_3 + Z_0] + [|Z|_1 + Z_0(Z_2 + Z_1)]}{Z_{10}[Z_2 + Z_3 + Z_0] + [|Z|_1 + Z_0(Z_2 + Z_1)]} \tag{B-16}$$

A similar result may be obtained by the more direct but less general method of calculating the input reflection coefficient of a T-network terminated in a load Z_0.

---

33. J.L. Altman, Microwave Circuits, D. Van Nostrand Co., Inc., Princeton, N.J., 1964, p. 402.

Solutions relating the measurable dependence of S_{11} on frequency to the Q of the circuit represented by Z_0 have been worked out for the cases of loop and probe coupling to closed cavities.[34] Loop coupling may be represented by the shunt circuit of Fig. B-2, and probe coupling may be represented by the series circuit. The external circuit losses are represented by R_g, R_s represents losses in the coupling network, and n represents the degree of coupling between the external circuits and the cavity. In order to characterize these circuits, three Q values are defined such that

$$Q_L = 2\pi \frac{\text{Energy stored}}{\text{total energy dissipated per cycle}} \tag{B-17}$$

$$Q_0 = 2\pi \frac{\text{Energy stored}}{\text{(Energy dissipated per cycle in R and in the elements of the coupling network)}} \tag{B-18}$$

$$Q_{00} = 2\pi \frac{\text{Energy stored}}{\text{Energy dissipated per cycle in R}} \tag{B-19}$$

where R represents the internal losses of the resonator.

The Q factor measurable at the input terminals to the circuit is Q_L. The reflected response of either circuit of Fig. B-2 is shown in Fig. B-3 in terms of the square of the input reflection coefficient as a function of frequency. From Sucher and Fox, the loaded Q is given by[35]

$$Q_L = \alpha \frac{f_o}{2\delta f} \tag{B-20}$$

where

$$\alpha = \left[\frac{|\rho|^2 - |\rho_o|^2}{|\rho_1|^2 - |\rho|^2}\right]^{1/2} \tag{B-21}$$

and ρ = reflection coefficient at any frequency f

ρ_o = reflection coefficient at resonance

ρ_1 = reflection coefficient far off resonance.

---

34. D.D. King, Measurements at Centimeter Wavelengths, D. Van Nostrand Co., Inc., New York, 1952, pp. 129-137.
35. M. Sucher, J. Fox, Handbook of Microwave Measurements, 3rd Ed., Vol. II, Polytechnic Press, New York, 1963, p. 425.

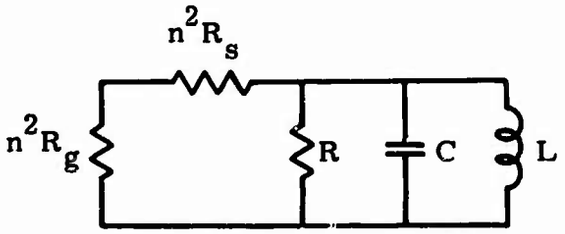

A. SHUNT CIRCUIT
(LOOP COUPLING)

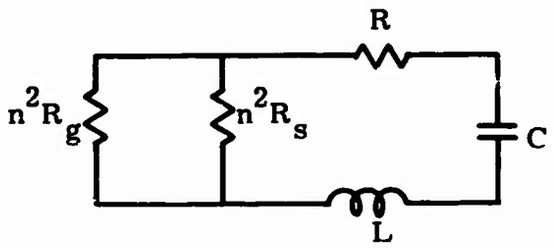

B. SERIES CIRCUIT
(PROBE COUPLING)

FIG. B - 2

COUPLED CAVITY
EQUIVALENT CIRCUITS

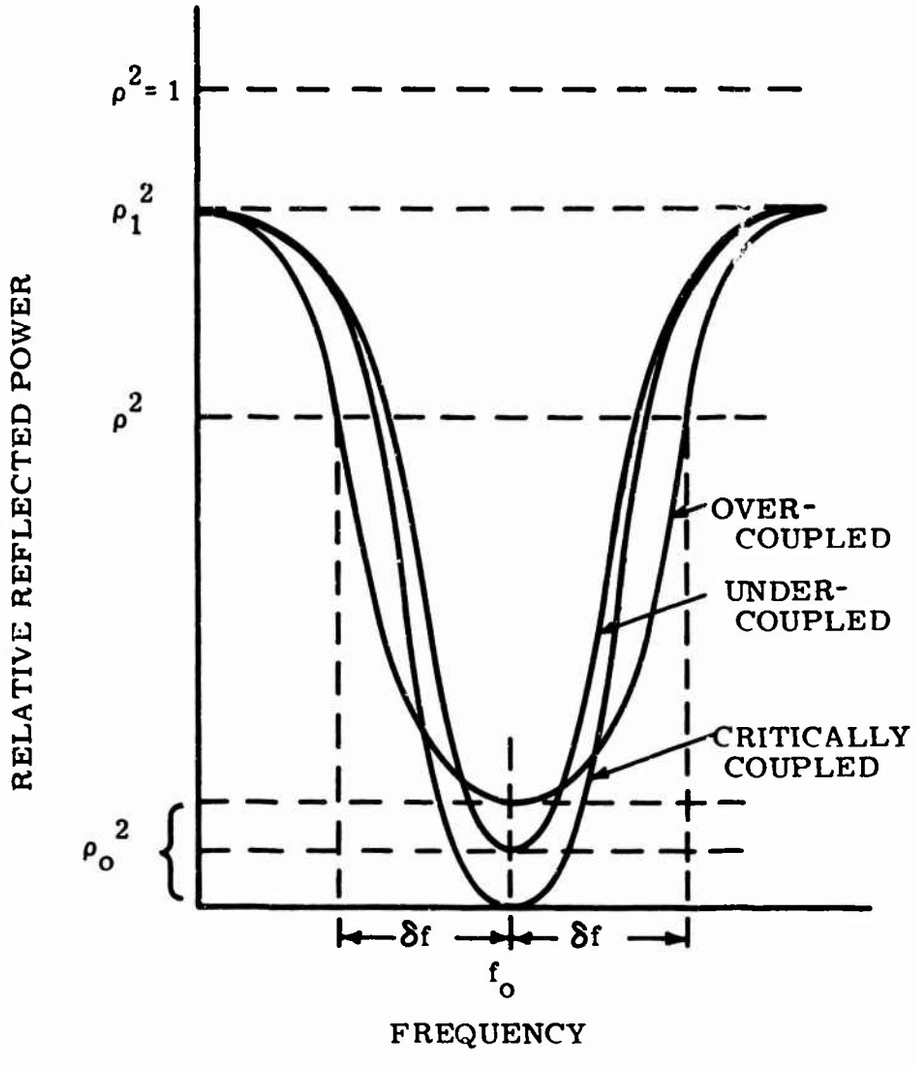

FIG. B - 3

REFLECTED RESPONSE
OF A TUNED CIRCUIT

and $2\delta f$ is the frequency difference between the two points where the relative reflected power is given by ρ^2. If $2\delta f$ is measured at the reflected power level where

$$\rho^2=(\rho_1^2 + \rho_o^2)/2$$

then $\alpha = 1$ and $Q_L = f_o/2\delta f$.

Also from Sucher and Fox, in terms of the square of the input reflection coefficients

$$\frac{Q_0}{Q_L} = \frac{2}{2 - |\rho_o| - |\rho_1|} \tag{B-22}$$

$$\frac{Q_{00}}{Q_L} = \frac{1 + |\rho_1|}{1 - |\rho_o|} \tag{B-23}$$

if the resonator is overcoupled,

and

$$\frac{Q_0}{Q_L} = \frac{2}{2 + |\rho_o| - |\rho_1|} \tag{B-24}$$

$$\frac{Q_{00}}{Q_L} = \frac{1 + |\rho_1|}{1 + |\rho_o|} \tag{B-25}$$

if the resonator is undercoupled.

Whether a particular resonator is overcoupled or undercoupled at resonance can be determined from a knowledge of the behavior of the phase of the reflection coefficient as the resonator is tuned through resonance. For a method of determining the degree of coupling without phase information about the reflection coefficient, consider Eq. B-16 and the series circuit of Fig. B-2. Let $Z_1 = Z_3 = 0$ in Eq. B-16, then $|Z|_1 = 0$, and

$$-S_{11} = \frac{Z_{10}Z_2 - Z_0Z_2 + Z_0Z_{10}}{Z_{10}Z_2 + Z_0Z_2 + Z_0Z_{10}}$$

Letting $Z_2 = n^2R_s$ and $Z_0 = R + j\omega L - j(1/\omega C) = R$ at resonance with the assumption that the source is matched to the transmission line such that $Z_{10} = n^2R_s$, then,

$$S_{11} = \frac{\frac{n^2 R_s R}{n^2 R_s + R} - n^2 R_g}{\frac{n^2 R_s R}{n^2 R_s + R} + n^2 R_g} \tag{B-26}$$

By definition, the circuit is undercoupled when

$$\frac{n^2 R_s R}{n^2 R_s + R} > n^2 R_g \tag{B-27}$$

and the circuit is overcoupled when

$$\frac{n^2 R_s R}{n^2 R_s + R} < n^2 R_g \tag{B-28}$$

When

$$\frac{n^2 R_s R}{n^2 R_s + R} = n^2 R_g$$

then $S_{11} = 0$ and the circuit may be considered critically coupled. If by some means R is increased, S_{11} and thus $|\rho_o|^2$ will increase for the undercoupled case. When the circuit is overcoupled and R is increased, S_{11} and $|\rho_o|^2$ decrease in magnitude, or approach zero. With beam waveguide resonators, R may easily be momentarily increased by inserting the hand into the edge of the resonator fields. Observation of the increase or decrease of $|\rho_o|^2$ then indicates whether the circuit is overcoupled or undercoupled. The choice of which of Eqs. B-22 through B-25 are to be used in calculating the unloaded and uncoupled Q values from the measured reflection coefficient magnitudes both on and off resonance and the measured loaded Q can then be made.

X. APPENDIX C

MULTIPLE MODE OPERATION OF CONFOCAL RESONATORS

In order for energy to be coupled from one mode to another due to a perturbation such as a coupling aperture in a resonator end plate requires that both modes be resonant simultaneously if there is to be a large energy transfer, or that the response curves for the resonances of the two modes overlap to a considerable degree. An attempt to show that it is possible for two modes to exist simultaneously in a beam waveguide resonator will be the object of this section. The electric fields of the modes for a beam waveguide are given by Eq. 4-24, thus

$$E_{xnv} = A_{nv}(1+u^2)^{-1/2} \left(\frac{\rho}{\rho_z}\right)^v L_n^v \left(\frac{\rho}{\rho_z}\right)^2 \qquad \text{(C-1)}$$

$$\cdot \exp\left[-\frac{1}{2}\left(\frac{\rho}{\rho_z}\right)^2 - j\,\psi\right] \begin{matrix}\cos v\phi \\ \sin v\phi\end{matrix}$$

where

$\psi = kz - (2n + v + 1)\tan^{-1}u + \frac{1}{2}(\rho/\rho_z)^2$

$n = 0, 1, 2, \ldots; v = 0, 1, 2, \ldots$

L_n^v = Laguerre polynomial of degree n and order v

ϕ = polar angle

$u = z/k\rho_o^2$

$k = 2\pi/\lambda$

λ = free-space wavelength

ρ = radial coordinate $\sqrt{x^2+y^2}$

$\rho_z^2 = \rho_o^2(1+u^2)$

and ρ_o is a mode set parameter determined by the focal length of the lenses and their separation, and may be expressed as follows:

$$\rho_o^2 = \frac{\sqrt{(2 - D/f)\ Df}}{k} \qquad \text{(C-2)}$$

where f = focal length of paraboloidal phase corrector

and D = distance from z = 0 to the lens or curved reflecting plate; (see Fig. A-5).

Note that D here is defined as the distance between reflectors of a confocal half resonator.*

Now each mode, as determined by n and v, has a plane phase surface at z = 0 i.e., the phase $\psi = 0$ for all ρ. The phase shift which is dependent on the mode but independent of ρ is of interest in setting up the resonance condition for a beam waveguide resonator. Thus

$$\psi = kz - (2n+v+1)\ \tan^{-1} u \qquad \text{(C-3)}$$

where u = 0 at z = 0.

Now for a confocal half resonator

$$D = f$$

$$\rho_o^2 = D/k$$

and $u = z/D$

The change in phase that takes place in traversing a distance D from z =0 to z = D is from Eq. C-3,

$$\Delta\psi = kD - (2n+v+1)\ \tan^{-1}\left(\frac{D}{D}\right)$$

$$\Delta\psi = kD - (2n+v+1)\ \frac{\pi}{4} \qquad \text{(C-4)}$$

*In the previous sections of this report D represented the length of the full confocal resonator.

The condition for resonance is that the phase shift in going from z = o to z = D be multiples of π radians. Thus

$$kD - (2n+v+1)\frac{\pi}{4} = m\pi \qquad \text{(C-5)}$$

If a confocal half resonator is to resonate at the lowest loss mode, i.e. n = v = 0, Eq. C-5 becomes

$$kD - \frac{\pi}{4} = m\pi \qquad \text{(C-6)}$$

Now $kD - \frac{\pi}{4}$ must remain constant if other modes are to resonate simultaneously with the L_o^o mode. That is, since m can change by integer values only, the term

$$(2n+v+1) = b$$

must be such that multiple values of π occur. Thus

$$kD - b\frac{\pi}{4} = m\pi \qquad \text{(C-7)}$$

where by inspection it can be seen that b can only take on values

$$b = 1, 5, 9, \text{ etc.}$$

For example if v=0, then n must be an even number to get resonance, i.e. n=0, 2, 4, etc., which yields modes L_o^o, L_2^o, L_4^o, etc. On the other hand if n=0 then only every fourth value of v can appear, i.e., v=0, 4, 8, etc., corresponding to the L_o^o, L_o^4, L_o^8, etc., modes. Table C-I lists values of n and v for b through 6 and the corresponding modes L_n^v.

If the resonator was adjusted to resonate the second lowest loss mode, i.e., the L_o^1 mode, then since n=0, and v=1 Eq. C-5 would become

$$kD - 2\left(\frac{\pi}{4}\right) = m\pi$$

b	n	v	L_n^v
1	0	0	L_o^o
2	0	1	L_o^1
3	0	2	L_o^2
	1	0	L_1^o
4	0	3	L_o^3
	1	1	L_1^1
5	0	4	L_o^4
	1	2	L_1^2
	2	0	L_2^o
6	0	5	L_o^5
	1	3	L_1^3
	2	1	L_2^1

Table C-I - Values of b, n, v and L_n^v

In this case $kD - \frac{\pi}{2}$ must remain constant if other modes are to resonate simultaneously with the L_o^1 mode. Note also that the resonator length is now different by $\pi/4$ radians from the length required to resonate the fundamental or L_o^o mode. Now

$$kD - b\left(\frac{\pi}{4}\right) = n\pi \qquad \text{(C-8)}$$

requires that

$$b = (2n+v+1) = 2, 6, 10, \text{etc.},$$

thus v must always be odd and n can be any integer including zero. Therefore, as can be seen from Table C-I, the

$$L_o^1, L_2^1, L_o^5, L_1^3, \text{etc.},$$

modes can resonate simultaneously for the same resonator length.

To summarize, the confocal half resonator adjusted to resonate the fundamental or lowest loss mode (L_o^o) will permit other modes to resonate simultaneously if

$$b = 1, 5, 9, \text{etc.},$$

which from Table C-I corresponds to the

$$L_o^o, L_1^2, L_2^o, L_o^4, L_4^o, L_o^8, \text{etc.},$$

modes.

The confocal half resonator adjusted to resonate the next to the lowest loss mode (L_o^1) will permit other modes to resonate simultaneously if

$$b = 2, 6, 10, \text{etc.},$$

which from Table C-I corresponds to the

$$L_o^1, L_2^1, L_o^5, L_1^3, \text{etc.},$$

modes. The resonator length for this latter condition differs from the first by $\pi/4$ radians.

This analysis can be extended to obtain resonance for next higher mode which according to Fig. 4-7 is the L_o^2 mode. Then

$$kD - 3(\tfrac{\pi}{4}) = m\pi$$

and $b = (2n+v+1) = 3, 7, 11,$ etc.

which from Table C-I corresponds to the

$$L_o^2, L_1^o, L_1^4, L_o^6, \text{ etc.},$$

modes. The resonator length in this case differs from the length for resonating the fundamental mode by $2(\frac{\pi}{4})$ radians. This resonator spacing also permits the L_1^o mode to resonate which is the fourth mode to appear in a beam waveguide.

Finally if the fifth mode, namely the L_1^1 mode, is to resonate then

$$kD - 4(\tfrac{\pi}{4}) = m\pi$$

and $b = (2n+v+1) = 4, 8, 12,$ etc.,

which from Table C-I corresponds to the

$$L_1^1, L_o^3, L_3^1, L_o^7, \text{ etc.},$$

modes. The resonator length in this case differs from the length required for resonating the fundamental L_o^o mode by $3(\frac{\pi}{4})$ radians.

An analysis similar to that made for the confocal half resonator can be made for the full confocal resonator. For the full resonator Eq. C-5 becomes

$$2kD - (2n+v+1)\ 2\ \frac{\pi}{4} = m\pi$$

or

$$2kD - (2n+v+1)\frac{\pi}{2} = m\pi \qquad \text{(C-9)}$$

Thus the full resonator adjusted to resonate the L_o^o low loss mode will permit other modes to resonate simultaneously if

$$b = 1, 3, 5, 7, \text{ etc.},$$

which from Table C-I corresponds to the

$$L_o^o, L_o^2, L_1^o, L_1^2, L_o^4, L_2^o, \text{ etc.},$$

modes.

The full resonator adjusted to resonate the second or L_o^1 mode will permit other modes to reeonate simultaneously if

$$b = 2, 4, 6, 8, \text{ etc.},$$

which, from Table C-I corresponds to the

$$L_o^1, L_1^1, L_o^3, L_2^1, L_1^3, L_o^5, \text{ etc.},$$

modes. The resonator length for this latter condition differs from the first by π/2 radians. The full confocal reeonator has twice as many modes resonant for e given length as the confocal half resonator does.

Thus, it requires only two different resonator lengths to resonete all possible modes when using the full confocal resonator. Four different resonator lengths are required to resonate all possible modes when using the confocal half resonator. These resonance conditions are summarized in Table C-2.

The order of the beam modes, arranged according to their diffrection loss, starting with the loweet loee mode is from Fig. 4-7,

$$L_o^o, L_o^1, L_o^2, L_1^o, L_1^1, L_1^2, L_2^o, L_2^1, \text{ etc.}$$

Of the modes listed above only the

Resonance Condition	$b = (2n+v+1)$	L_n^v
Half Resonator Adjusted for		
L_o^o mode	1,5,9,———	L_o^o, L_1^2, L_2^o, L_o^4, ---
L_o^1 mode	2,6,10,———	L_o^1, L_2^1, L_o^5, L_1^3, ---
L_o^2 mode	3,7,11,———	L_o^2, L_1^o, L_1^4, L_o^6, ---
L_1^1 mode	4,8,12,———	L_1^1, L_o^3, L_3^1, L_o^7, ---
Full Resonator Adjusted for		
L_o^o mode	1,3,5,7,---	L_o^o, L_o^2, L_1^o, L_1^2, ---
L_o^1 mode	2,4,6,8,---	L_o^1, L_1^1, L_o^3, L_2^1, ---

TABLE C-2

Resonance Conditions for Confocal Full and Half Resonators

L_0^0, L_1^0, and L_2^0

modes have a maximum field on the axis of the resonator. All the other modes have zero field on the resonator axis.

PART 2

XI. CUTOFF-COUPLED MICROWAVE FILTERS

Introduction

The characteristics, advantages, and limitations of waveguide filters using sections of guide operating in the cutoff region as coupling elements were determined. These filters consist of a dielectric filled section of waveguide, which forms the resonator, preceded and followed by short lengths of air filled waveguide operating in the evanescent mode. Special means for coupling energy into and out of such filters may have to be provided depending upon the kind of system they are intended to operate with.

The cutoff-coupled dielectric resonator was found to have many characteristics in common with the usual metal walled resonator and thus it can be used to form a waveguide filter. The band pass configuration was used to investigate the characteristics and behavior of cutoff coupled microwave filters. The expressions for the resonant frequency, Q and mid-band insertion loss were derived. These expressions were then used to design a typical band pass filter with a center frequency near 3 GHz. The model filter was constructed and measurements were made on it to verify the theoretical design.

A. Characteristics of Waveguides

A very brief review of some of the properties of waveguides appears desirable before details of the filter design are presented. The characteristics of guides operating in the propagating region are well known but some of the properties of guides operating in the evanescent or cutoff mode are less well known.

The TE mode will be the only propagating mode considered in the present study. Wave motion in the z-direction will be assumed so that the z variation of the fields in the waveguide are expressed by $e^{-\gamma z}$ where γ is the propagation constant in the guide. In general,

$$\gamma = \sqrt{\left(\frac{m\pi}{a}\right)^2 + \left(\frac{n\pi}{b}\right)^2 - \omega^2 \mu_o \epsilon} \qquad (11\text{-}1)$$

and

$$\gamma = j\beta \qquad \text{if } \left(\frac{m\pi}{a}\right)^2 + \left(\frac{n\pi}{b}\right)^2 < \omega^2\mu_o\epsilon$$

or

$$\gamma = \alpha \qquad \text{if } \left(\frac{m\pi}{a}\right)^2 + \left(\frac{n\pi}{b}\right)^2 > \omega^2\mu_o\epsilon$$

where β is the phase constant

α is the attenuation constant

ω is the applied angular frequency

ϵ is the permittivity of the medium in the guide

a and b are the usual cross-sectional dimensions of the waveguide

and m and n are integers including zero (note: m and n are not to be zero simultaneously).

Now when $\gamma = j\beta$, normal wave propagation in the guide takes place. When $\gamma = \alpha$, the waveguide is said to be cutoff and no wave propagation in the usual sense can take place. Fields do exist within the cutoff section of waveguide but they are highly attenuated with distance in the z-direction. The frequency at which γ becomes zero, i.e., the transition between propagation and no propagation, is called the cutoff frequency.

The components of the field within a rectangular waveguide operating in the TE_{10} mode can be written as follows:

$$\begin{aligned} H_z &= A \cos(\pi x/a)\, e^{-j\beta z} \\ H_x &= j\beta(a/\pi)\, A \sin(\pi x/a)\, e^{-j\beta z} \\ E_y &= -(\omega/\beta)\sqrt{\mu\epsilon}\, ZH_x = -j\omega(a/\pi)\sqrt{\mu\epsilon}\, Z\, A \sin(\pi x/a)\, e^{-j\beta z} \\ E_x &= E_z = H_y = 0 \end{aligned} \qquad (11\text{-}2)$$

where A is an amplitude constant

and $Z = \sqrt{\mu/\epsilon}$ is the intrinsic impedance of the medium (wave impedance for unbounded medium).

When the waveguide is non-propagating or cutoff the field components are the same as above except $j\beta$ is replaced by α.

Thus,

$$H_z = A \cos(\pi x/a)\, e^{-\alpha z}$$

$$H_x = \alpha(a/\pi)\, A \sin(\pi x/a)\, e^{-\alpha z}$$

$$E_y = -j(\omega/\alpha)\sqrt{\mu\varepsilon}\, ZH_x = -j\omega(a/\pi)\sqrt{\mu\varepsilon}\, ZA \sin(\pi x/a)\, e^{-\alpha z} \quad (11\text{-}3)$$

$$E_x = E_z = H_y = 0$$

1. Reflection and Transmission Coefficients at a Junction of Propagating and Cutoff Waveguide

Insight into the properties of the fields in a cutoff section of waveguide may be obtained by investigating the behavior of the fields of a propagating wave in a dielectric-filled guide when the wave encounters an abrupt transition to a cutoff section of waveguide. This problem will help to formulate or establish a useful transmission line analogy of a cutoff waveguide.

In Fig. 11-1 are shown the various transverse components of the fields involved on both sides of the junction for a TE mode in the propagating waveguide section. Now the tangential components of the $\bar{E}$ field must be equal on both sides of the junction between the two sections of waveguide and hence the relation between the incident E_i, the reflected E_r and the transmitted E_t fields is determined. The tangential compoents of the $\bar{H}$ field are similarly related.

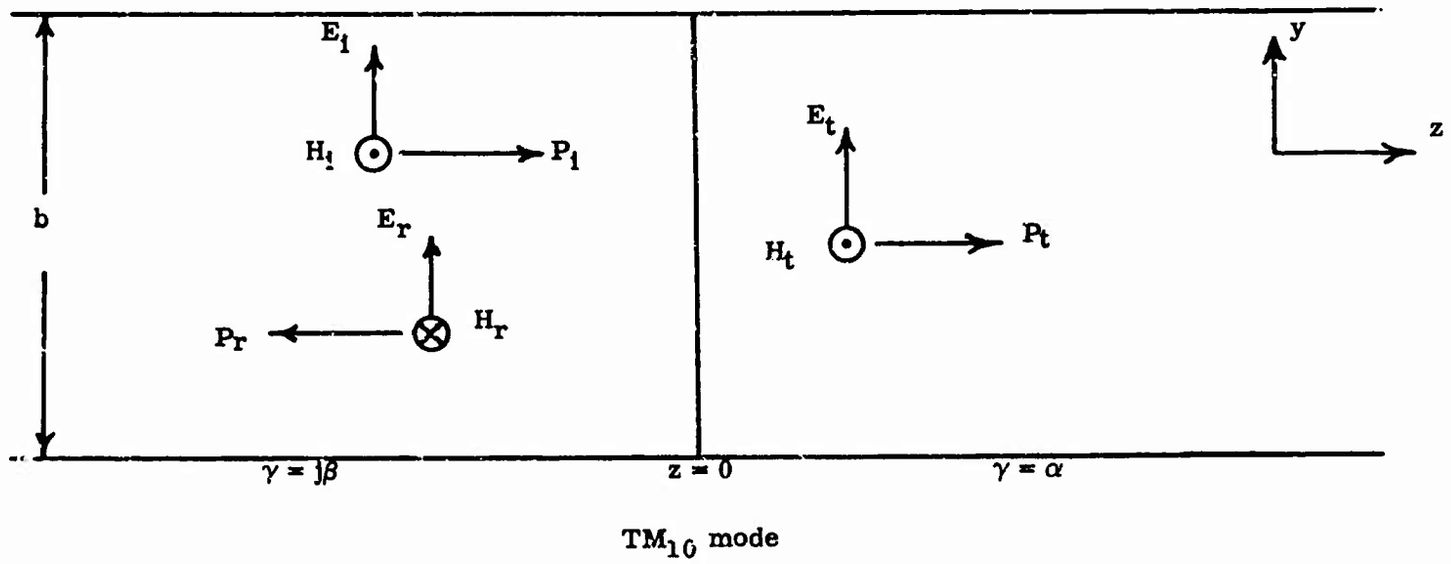

FIG. 11-1 JUNCTION OF PROPAGATING AND CUTOFF SECTION OF WAVEGUIDE

Using Eqs. 11-2 and 11-3, the E_y components at z=0 are equated as follows:

$$-j\omega\sqrt{\mu_o\varepsilon_o}\sqrt{\mu_o/\varepsilon_o}A_i \sin(\pi x/a) - j\omega\sqrt{\mu_o\varepsilon_o}\sqrt{\mu_o/\varepsilon_o}A_r \sin(\pi x/a)$$

$$= -j\omega\sqrt{\mu_o\varepsilon}\sqrt{\mu_o/\varepsilon}\ A_t \sin(\pi x/a)$$

or

$$A_i + A_r = A_t \tag{11-4}$$

Similarly the relation between the H components is obtained from the H_x component in Eqs. 11-2 and 11-3 as follows,

$$-j\beta(a/\pi)\ A_i \sin(\pi x/a) - j\beta(a/\pi)\ A_r \sin(\pi x/a) = \alpha\ (a/\pi)\ A_t \sin(\pi x/a)$$

or

$$j\beta A_i - j\beta A_r = \alpha A_t \tag{11-5}$$

Using Eqs. 11-4 and 11-5 the reflection coefficient is

$$\rho_\beta = A_r/A_i = (j\beta-\alpha)/(j\beta+\alpha) \tag{11-6}$$

and the transmission coefficient is

$$\tau_\alpha = A_t/A_i = j2\beta/(\alpha+j\beta) \tag{11-7}$$

Now for the case in which the fields exist in the cutoff section and emerge into a propagating section i.e., moving from right to left in Fig. 1-11 Eqs. 11-4 and 11-5 become

$$A_i + A_r = A_t \tag{11-8}$$

$$\alpha A_i - \alpha A_r = j\beta A_t \tag{11-9}$$

and the reflection coefficient is

$$\rho_\alpha = A_r/A_i = (\alpha - j\beta)/(\alpha + j\beta) \tag{11-10}$$

and the transmission coefficient is

$$\tau_\beta = A_t/A_i = 2\alpha/(\alpha - j\beta) \tag{11-11}$$

2. Transmission Line Analogy of Propagating and Cutoff Waveguides

a. Wave Impedance

In the case of the two-wire and coaxial transmission line the power carried by the line is usually associated with a voltage and a current. In a waveguide, on the other hand, the idea of a voltage and a current in the usual circuit sense is almost meaningless, and the power must be associated with the fields inside the guide. However, for the purpose of establishing a limited but very useful analogy between a waveguide and an ordinary transmission line, a voltage and current related to the fields in the guide can be defined. The definitions used here are not the only ones that could have been used.

The equivalent voltage associated with the TE_{10} mode in a rectangular waveguide is here defined as some constant times the peak electric field in the center of an infinitely long guide.

$$V = k\, E_{oy} \tag{11-12}$$

Similarly the equivalent current is defined as being proportional to the peak magnetic field at the center of the waveguide.

$$I = -\, k\, H_{ox} \tag{11-13}$$

Now the ratio of the transverse components of the fields in a waveguide has the dimensions of an impedance. Thus from Eq.11-2,

$$-E_y/H_x = (\omega/\beta)\sqrt{\mu\epsilon}\ \sqrt{\mu/\epsilon} = \omega\mu/\beta$$

The ratio of V to I from Eqs. 11-12 and 11-13 is

$$V/I = -\, E_{oy}/H_{ox} = \omega\mu/\beta$$

Now the ratio of V/I for an infinitely long transmission line is called the characteristic impedance. The analogous impedance in a waveguide is called the wave impedance, thus

$$Z_{TE} = \omega\mu/\beta \tag{11-14}$$

When this impedance ratio is determined for a waveguide operating below cutoff Z_{TE} using Eq. 11-3 becomes

$$Z_{TE} = j(\omega/\alpha)\sqrt{\mu\epsilon}\ \sqrt{\mu/\epsilon} = j\omega\mu/\alpha \tag{11-15}$$

Thus the wave impedance for a waveguide operating in the cutoff region is a reactance. The wave impedance changes from the resistive value given by Eq. 11-14 to the reactive value given by Eq. 11-15 at the cutoff frequency.

The transmission line definitions for the reflection and transmission coefficients are as follows,

$$\rho = V_{ref}/V_{inc} = (Z_L - Z_0)/(Z_L + Z_0)$$

and

$$\tau = V_{trans}/V_{inc} = 2Z_L/(Z_L + Z_0)$$

If the case of a propagating TE_{10} wave incident in a cutoff section of waveguide is considered then $Z_L = j\omega\mu/\alpha$ and $Z_0 = \omega\mu/\beta$.

Thus

$$\rho = (j\omega\mu/\alpha - \omega\mu/\beta)/(j\omega\mu/\alpha + \omega\mu/\beta)$$

$$\rho = (j\beta - \alpha)/(j\beta + \alpha)$$

and

$$\tau = (j2\omega\mu/\alpha)/(j\omega\mu/\alpha + \omega\mu/\beta)$$

$$\tau = j2\beta/(\alpha + j\beta)$$

These expressions for ρ and τ are identical with Eqs. 11-6 and 11-7 obtained from field theory and show the validity of the transmission line analogy in this instance. A result identical to Eqs. 11-10 and 11-11 is obtained when the above procedure is applied to the case of a cutoff section of guide terminated with a propagating section of waveguide. Thus a section of waveguide can be represented by a transmission line with a characteristic impedance equal to $j\omega\mu/\gamma$, where γ is equal to $j\beta$ if the guide is propagating a single mode and it is equal to α if the guide is operated in the cutoff region. The analogies verified above are shown in Fig. 11-2.

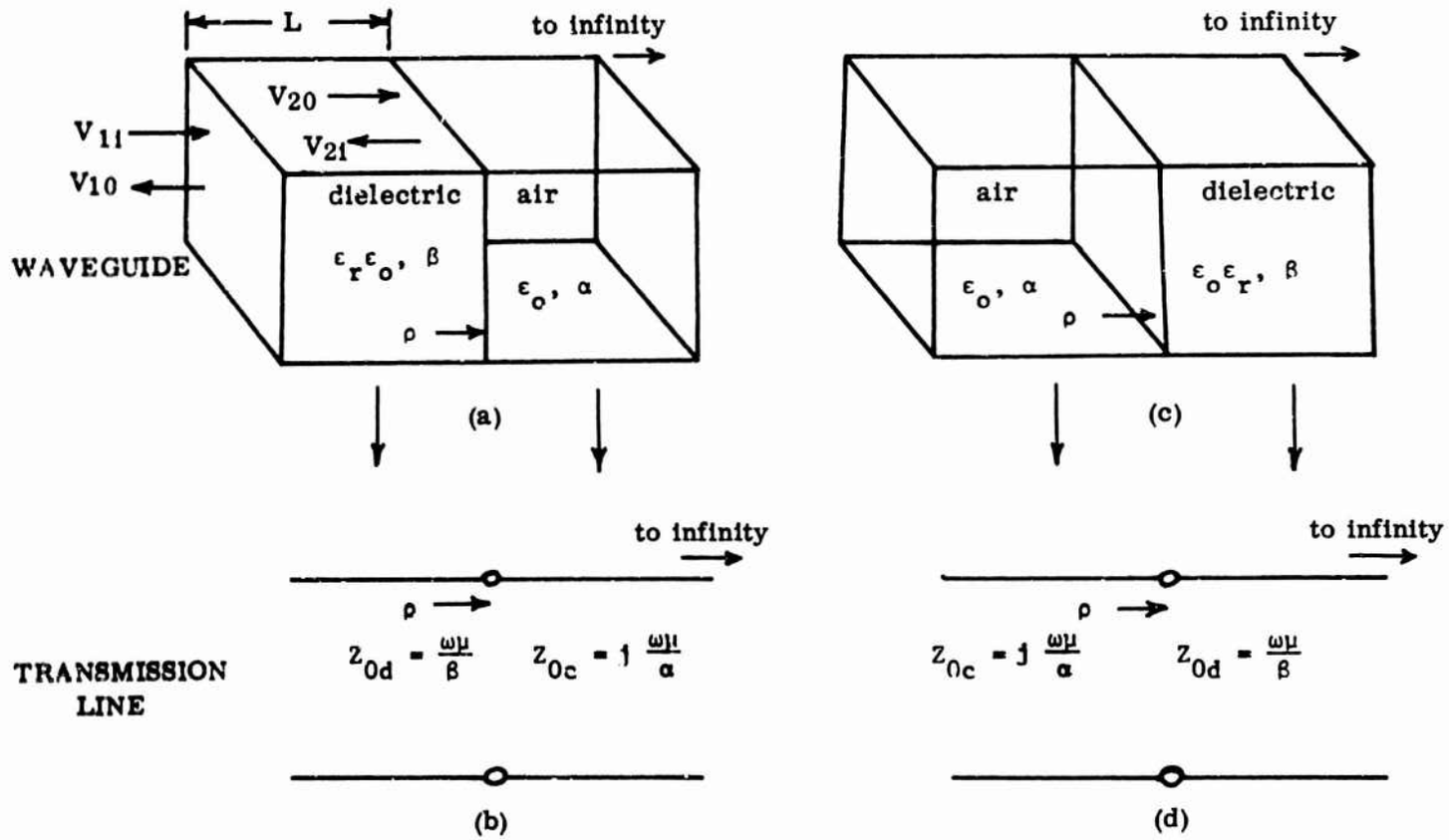

FIG. 11-2 ANALOGY OF WAVEGUIDE TO TRANSMISSION LINE

b. Power Flow in Cutoff Waveguide

The power flow into and out of a waveguide operating in the cutoff region can be determined with the aid of the transmission line analogy. Since the wave impedance and hence the input impedance of an infinitely long section of waveguide in the cutoff region is reactive i.e., $Z_{TE} = j\omega\mu/\alpha$, no power is accepted by the cutoff waveguide.

A finite length of waveguide operated in the cutoff region and terminated in a general load characterized by an impedance Z_L has an input impedance given by the usual transmission line equation

$$Z_{in} = Z_0(1+\rho e^{-2\gamma d})/(1-\rho e^{-2\gamma d}) \tag{11-16}$$

where d is length of waveguide section

Z_0 is the characteristic impedance or in the present case the wave impedance of the waveguide

γ is the propagation constant

and ρ is the reflection coefficient of the load.

Now for a waveguide beyond cutoff

$$Z_{in} = \frac{j\omega\mu}{\alpha} \frac{1 + \frac{Z_L-(j\omega\mu/\alpha)}{Z_L+(j\omega\mu/\alpha)} e^{-2\alpha d}}{1 - \frac{Z_L-(j\omega\mu/\alpha)}{Z_L+(j\omega\mu/\alpha)} e^{-2\alpha d}} \tag{11-17}$$

In general the input impedance given by Eq. 11-17 will have both a real and reactive component. The real part of this input impedance will account for some power entering the input part of the cutoff section of waveguide.

It appears that there is no reason why a cutoff section of waveguide cannot be considered lossless and hence the output power should be equal to the input power. On the other hand the fields in a cutoff section of guide are attenuated by the factor $e^{-\alpha d}$ and hence it appears at first glance

that the input power will be reduced by the factor $e^{-2\alpha d}$ by the time it reaches the output port. The best way to settle this apparent contradiction is to calculate and compare the input and output power associated with a section of waveguide operating in the cutoff region.

The power at any point on a transmission line can be determined from the expression

$$P = \frac{1}{2} V I^* \tag{11-18}$$

where V and I are peak values of the total voltage and total current

When Eq. 11-18 is applied to a section to waveguide viewed as a four terminal network the input and output powers are (see Fig. 11-2).

$$P_{in} = \frac{1}{2} (V_{10} + V_{11}) (I_{10} + I_{11})^* \tag{11-19}$$

$$P_{out} = \frac{1}{2} (V_{20} + V_{21}) (I_{20} + I_{21})^* \tag{11-20}$$

where V and I are the equivalent voltages and currents defined previously in Eqs. 11-12 and 11-13.

Subscripts 1 and 2 refer to the input and output ports respectively and i and 0 refer to the incoming and outgoing voltages and currents Furthermore in transmission line analysis the ratio of the incident voltage to the incident current is the characteristic impedance Z_0, and this same ratio for the reflected components of voltage and current is $-Z_0$. Thus since the wave impedance of a cutoff section of guide is reactive Eqs. 11-19 and 11-20 become,

$$P_{in} = \frac{1}{2} (V_{10} + V_{11}) (V_{11}/jX_o - V_{10}/jX_o)^* \tag{11-21}$$

$$P_{out} = \frac{1}{2} (V_{20} + V_{21}) (V_{20}/jX_o - V_{21}/jX_o)^* \tag{11-22}$$

Now expanding the expression for P_{in} and P_{out} and keeping track of the real (RE) and imaginary (IM) components in Eqs. 11-21 and 11-22

$$P_{in} = \frac{1}{2X_o}\left[j(V_{11IM}^2 + V_{11RE}^2 - V_{10RE}^2 - V_{10IM}^2)\right. \\ \left. + (2V_{10RE}V_{11IM} - 2V_{10IM}V_{11RE})\right] \tag{11-23}$$

$$P_{out} = \frac{1}{2X_o}\left[j(V_{20RE}^2 + V_{20IM}^2 - V_{21RE}^2 - V_{21IM}^2)\right. \\ \left. + (2V_{21RE}V_{20IM} - 2V_{21IM}V_{20RE})\right] \tag{11-24}$$

Equations 11-23 and 11-24 have both real and imaginary parts. The real parts account for real input and output powers. Furthermore since the input quantities are related to the output quantities by

$$V_{10} = V_{21}\, e^{-\alpha L} \text{ and } V_{11} = V_{20}\, e^{+\alpha L}$$

the real part of Eq. 11-23 can be transformed to

$$(P_{INRE})_{AT\ OUTPUT} = \frac{1}{2X_o}(2V_{21RE}V_{20IM} - 2V_{21IM}V_{20RE})$$

However this is the same as the real power at the output given by Eq. 11-24 Thus power is conserved in the cutoff section of waveguide.

B. Cutoff-Coupled Dielectric Resonator

1. Fundamental Concepts

An electromagnetic resonator is formed by placing short circuits at both ends of a section of transmission line. The transmission line can be

a two-wire line, a coaxial line or a section of waveguide. The short circuits at each end (assumed lossless) have a reflection coefficient of unity and hence reflect all the energy incident on them. The standing wave pattern set up along the length of the line must have a zero field at each end plate. When these boundary conditions are met, the short circuited transmission line or waveguide section is said to be in resonance. A transmission line section is resonant at certain discrete frequencies which correspond to the number of half wavelengths contained in the standing wave pattern. Thus the voltage or field at the mid-point between the two reflecting end plates is always either a maximum or zero. A line section terminated in an open circuit at each end will also form a resonantor since an infinite impedance representing the open circuit also yields a reflection coefficient of unity. The characteristics ascribed to the short circuited resonator above apply also to the open circuited resonator.

When a dielectric filled section of waveguide is terminated in an infinitely long cutoff section of waveguide, the magnitude of the reflection coefficient at the junction viewed from the propagating side is

$$|\rho_\beta| = \sqrt{\beta^2+\alpha^2}\Big/\sqrt{\beta^2+\alpha^2} = 1$$

Thus it is possible to set up a resonator using a dielectric-filled propagating section of waveguide terminated at each end by infinitely long cutoff sections of waveguide.

In a practical filter energy must be coupled into and out of the resonator. In a metal walled resonator this coupling of energy is usually done by means of small holes or irises in the resonator end plates. In the cutoff-coupled dielectric resonator energy can be fed into and removed from

the filter by using finite lengths of cutoff coupling sections. The amount or degree of coupling, measured in terms of the fraction of the incident wave entering the dielectric resonator, can be controlled by the choice of the length of the cutoff coupling section used. A quantitive measure of the coupling can be obtained by using a coupling factor K defined by

$$K = \tau e^{-\alpha L} \tag{11-25}$$

where τ is the transmission coefficient given by Eq. 11-7 or 11-11,

α is the attenuation per unit length of the cutoff waveguide section

and L is the length of the cutoff coupling section

A simple band-pass filter made up of waveguide sections all having the same size cross-section would consist of a dielectric-filled resonator section which has air filled sections at each end which serve as the cutoff coupling sections. In order that energy can be fed to and removed from the filter, some means of coupling to the cutoff sections must be provided. One such means would be to use dielectric-filled propagating sections of waveguide to couple into and out of the cutoff coupling sections. Such an arrangement along with the cutoff-coupled band pass filter is shown in Fig. 11-3 Probe antennas extending into the cutoff coupling waveguide sections could also be used to couple energy into and out of the filter system.

Having described the fundamental ideas upon which the cutoff-coupled dielectric resonator band pass filter is based, the remainder of this section will be devoted to deriving quantitative design equations. Determining the resonance conditions, the relations for the various Q factors

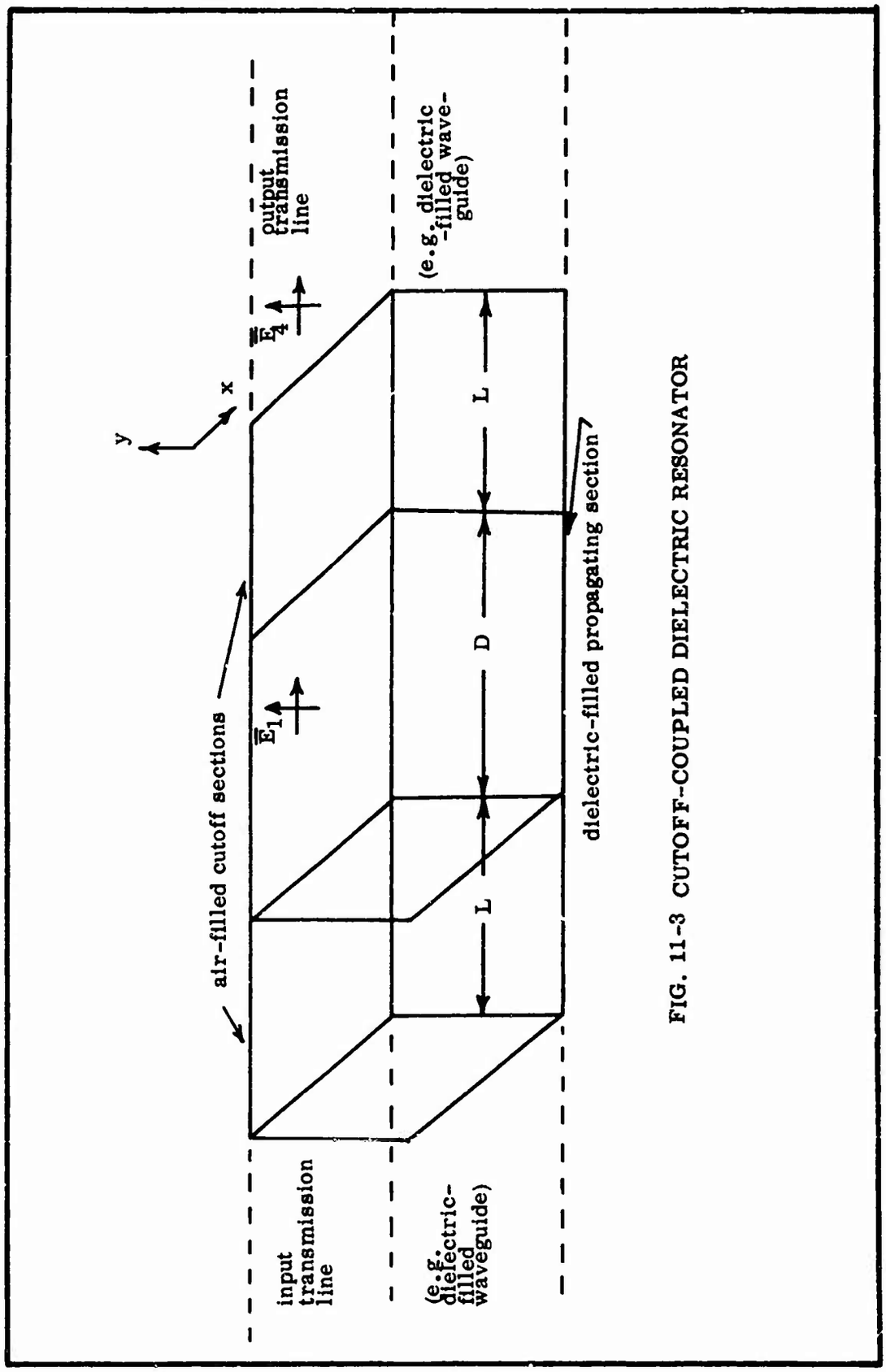

FIG. 11-3 CUTOFF-COUPLED DIELECTRIC RESONATOR

of a dielectric resonator and the insertion loss at resonance comprises the important design information that will be developed.

2. Resonance of Dielectric Filled Waveguide Bounded by Cutoff Sections

The resonant frequencies of a completely enclosed metal walled resonator are usually obtained by solving Maxwell's equations subject to the proper boundary conditions. A dielectric-filled waveguide section with infinitely long cutoff coupling sections at each end corresponds to the completely enclosed metal resonator. When small coupling holes are used in the metal walled resonator or when relatively long but finite length cutoff sections are used with the dielectric resonator, the resonant frequencies will be changed only slightly in most cases.

The dielectric filled resonator to be analyzed is shown in Fig. 11-4 Three different approaches for determining the resonant frequencies will be discussed briefly.

a. Field Approach

The electric field of the TF mode in the waveguide resonator which will be assumed to be in the y-direction, will be made up of two traveling waves propagating in opposite directions. Now $\overline{E}_1$ is shown traveling in the -z direction and $\overline{E}_2$ in the +z direction in Fig. 11-3. Thus

$$E_y = E_1 \sin(m\pi x/a) \cos(n\pi y/b) e^{j\beta z} + E_2 \sin(m\pi x/a) \cos(n\pi y/b) e^{-j\beta z} \qquad (11-26)$$

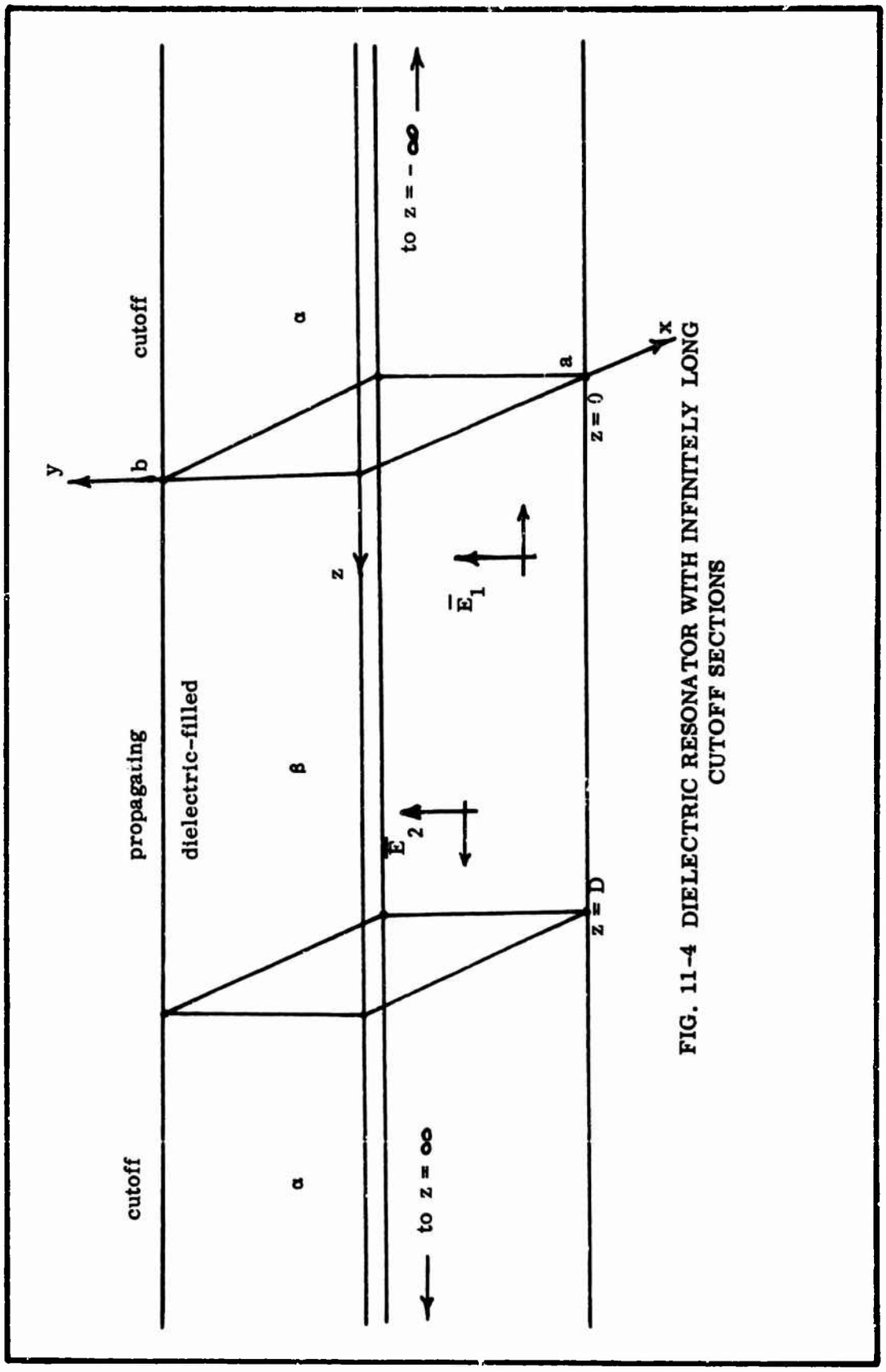

FIG. 11-4 DIELECTRIC RESONATOR WITH INFINITELY LONG CUTOFF SECTIONS

The boundary conditions at z = 0 and z = D require that the total E_y field take on values determined by the reflection coefficients at the junction between the resonator and the cutoff waveguide section. The only variable in the equation for E_y is β and its value, which is dependent on frequency, will make it possible to meet the boundary conditions. The frequencies for which the boundary conditions are satisfied are the resonant frequencies of the dielectric-filled resonator.

At z = 0

$$E_{y|z=o} = E_1 \sin(m\pi x/a)\cos(n\pi y/b)(1+[j\beta-\alpha]/[j\beta+\alpha]) \qquad (11\text{-}27)$$

where $E_2 = E_1(j\beta-\alpha)/(j\beta+\alpha)$

since from Eq. 6

$$\rho_\beta = (j\beta-\alpha)/(j\beta+\alpha)$$

and E_1 is viewed as the incident wave at the z = o interface.

Now at z = D

$$E_{y|z=D} = E_1 \sin(m\pi x/a)\cos(n\pi y/b)e^{j\beta D}+E_2 \sin(m\pi x/a)\cos(n\pi y/b)e^{-j\beta D} \qquad (11\text{-}28)$$

$$= \sin(m\pi x/a)\cos(n\pi y/b)(E_1 e^{j\beta D}+E_2 e^{-j\beta D})$$

where in this case E_2 must be treated as the incident wave

Hence,

$$\rho_\beta = \frac{E_1 e^{j\beta D}}{E_2 e^{-j\beta D}} = \frac{E_1 \cos\beta D + jE_1 \sin\beta D}{E_2 \cos\beta D - jE_2 \sin\beta D} = \frac{j\beta - \alpha}{j\beta + \alpha}$$

After some algebraic manipulation the following is obtained

$$\tan \beta D = \frac{2\alpha\beta}{\beta^2 - \alpha^2} \tag{11-29}$$

or

$$\tan \beta D + \frac{2\alpha\beta}{\alpha^2 - \beta^2} = 0$$

Taking the arctangent of both sides

$$\beta D + \arctan \left(\frac{2\alpha\beta}{\alpha^2 - \beta^2}\right) = \arctan (0) = p\pi \tag{11-30}$$

where p is an integer including zero

Both Eqs. 11-29 and 11-30 are transcendental and β which determines the resonant frequencies of the dielectric resonator, must be found by trial. Thus no equation which expresses the resonant frequency f_r explicitly can be written. An f_r is first assumed and α and β determined from Eq. 11-1. These values must in turn satisfy Eq. 11-30 for a given D.

b. Phase Shift Approach

As mentioned earlier, at resonance the electric field E or the voltage V is either a maximum or zero at the center or midpoint along the length of the resonator. This behavior, which is the basis of the phase shift method for determining the resonance condition, is due to the assumed identical boundaries at each end of the resonator. Furthermore, the reflection at each end must be lossless and the resonator itself must be lossless if the standing wave resulting from the interference of oppositely traveling waves is to go to zero instead of to a minimum at the midpoint of the resonator.

To have either a maximum or zero of the standing wave pattern at the midpoint of the resonator requires that the total phase shift the traveling wave experiences in going from the center to one end of the resonator and then back to the center again must be $p\pi$. Now p, called the mode number, must be either zero or a positive integer.

Applying the criterion that the phase shift must equal $p\pi$ for resonance, to the cutoff-coupled dielectric resonator, there results, (see Fig. 11-2a, in which L is length from the center to one end of the resonator and L = (1/2)D where D is total resonator length).

$$V_{2i} = \rho V_{20}$$

$$V_{20} = V_{1i} e^{-j\beta L}$$

$$V_{10} = V_{2i} e^{-j\beta L}$$

Thus
$$V_{10} = \rho V_{20} e^{-j\beta L} = \rho V_{1i} e^{-2j\beta L}$$

or
$$\frac{V_{10}}{V_{1i}} = \rho e^{-2j\beta L} = e^{-j\beta D}$$

However, from Eq. 11-6

$$\rho = \frac{j\beta-\alpha}{j\beta+\alpha}$$

which can be written, assuming perfect reflection

$$\rho = \frac{j\beta-\alpha}{j\beta+\alpha}\,\frac{\alpha-j\beta}{\alpha-j\beta} = \frac{-\alpha^2+j\alpha\beta+\beta^2}{\alpha^2+\beta^2} = 1e^{j\phi}$$

where ϕ is the phase shift produced on reflection

$$\phi = \arctan \frac{IM}{RE} = \arctan \frac{2\alpha\beta}{\beta^2-\alpha^2} = - \arctan \frac{2\alpha\beta}{\alpha^2-\beta^2}$$

Thus

$$\frac{V_{10}}{V_{11}} = \rho e^{-j\beta D} = e^{j\phi} e^{-j\beta D} = e^{-j(\beta D + \arctan \frac{2\alpha\beta}{\alpha^2-\beta^2})}$$

But for resonance the total phase shift must be equal to $p\pi$. Thus

$$\beta D + \arctan \left(\frac{2\alpha\beta}{\alpha^2-\beta^2}\right) = p\pi$$

which is identical to Eq. 11-30 obtained by the field approach.

When Eq. 11-30 is solved for D, recalling that

$$\beta = \frac{2\pi}{\lambda}$$

$$D = \frac{\lambda}{2\pi} \left(p\pi - \arctan \frac{2\alpha\beta}{\alpha^2-\beta^2}\right)$$

$$D = \frac{p\lambda}{2} - \frac{\lambda}{2\pi} \arctan \frac{2\alpha\beta}{\alpha^2-\beta^2} \qquad (11\text{-}31)$$

or

$$D = \frac{p\lambda}{2} + s$$

where $\quad -\lambda/4 \leq s \leq +\frac{\lambda}{4}$

Thus the length D of the cutoff-coupled dielectric resonator is equal to p half wavelengths plus or minus a length $|s|$ which is determined by the phase shift of the reflection from the junction between the dielectric filled section and the cutoff section of waveguide.

The standing wave patterns in the dielectric filled section of a cutoff-coupled dielectric resonator for p = 0, 1 and 2 are shown in Fig. 11-5. These standing wave patterns have either a maximum or zero field at the resonator midpoint. The correct standing wave pattern of the two (one solid and the other dotted) shown for each value of p is determined by calculating the value of the field or the reflection coefficient at the ends of the resonator. The magnitude of field strength at the ends of the resonator is, with the aid of Eq. 11-6 given by

$$E = \left|1 + \frac{j\beta - c}{j\beta + \alpha}\right| E_1$$

$$E = \left|1 + 1 \angle \arctan \frac{2\alpha\beta}{\beta^2 - \alpha^2}\right| \qquad (11\text{-}33)$$

An expression for the magnitude of the field strength versus distance in the dielectric-filled resonator may be obtained by generalizing Eq. 11-33 as follows

$$E = \left|e^{-j\beta z} + e^{j\beta z}\, e^{j\beta \arctan\left(\frac{2\alpha\beta}{\beta^2 - \alpha^2}\right)}\right| E_1 \qquad (11\text{-}34)$$

Thus specifying p alone is not sufficient for sketching the standing wave pattern inside this resonator. The value of α and β must be known as indicated in Eq. 11-34.

c. ABCD Matrix Method

Another method for deriving the condition for resonance expressed by Eq. 11-29 involves the use of the network chain matrix. This matrix is also called the ABCD matrix and is discussed in books on network theory.

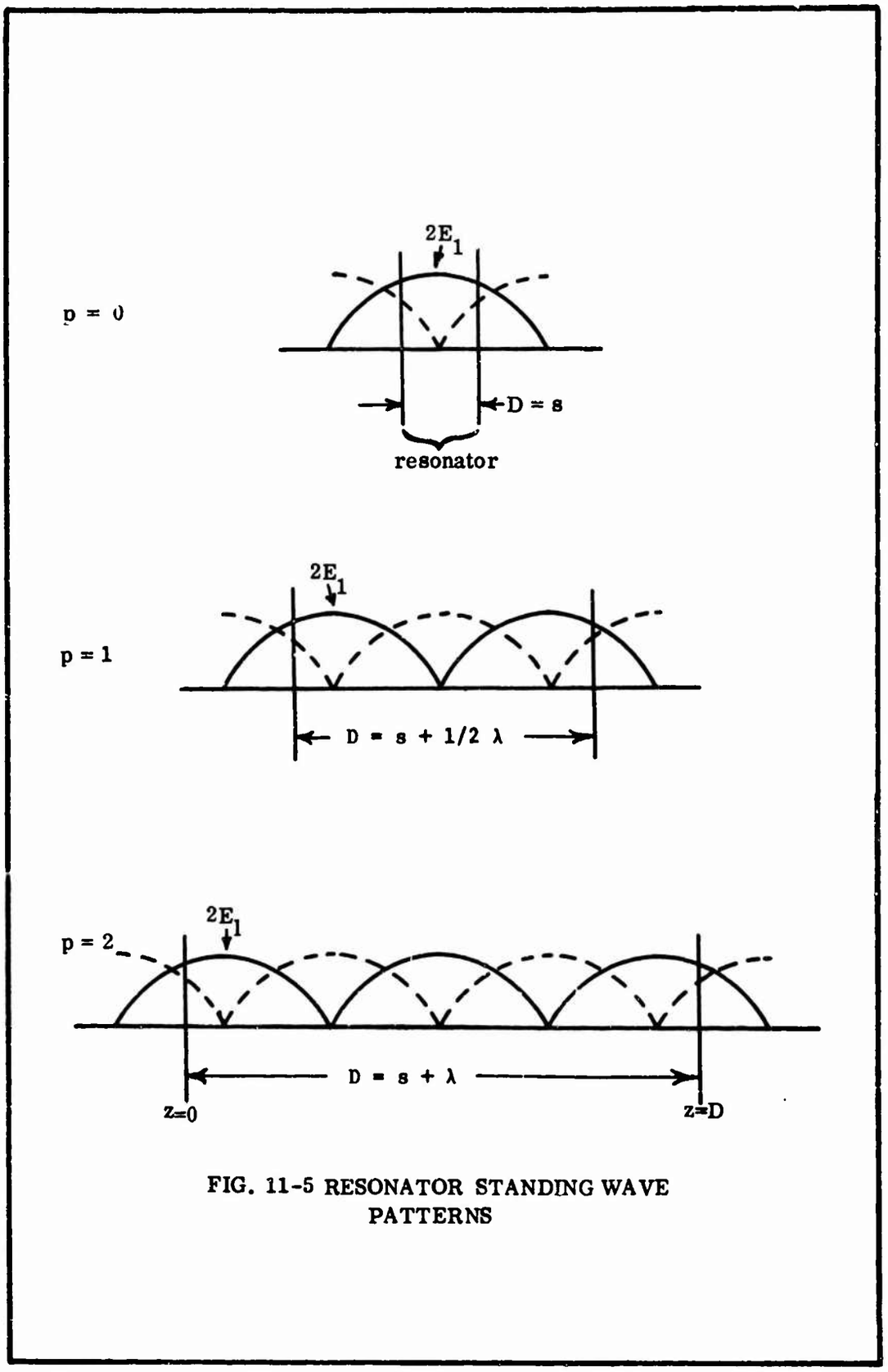

FIG. 11-5 RESONATOR STANDING WAVE PATTERNS

The first step in this method for determining the resonance condition is to use the ABCD matrix to find the input impedance Z_i of a length of propagating wave guide when it is terminated by an infinitely long cutoff section. The impedance of this terminating section is the wave impedance of the cutoff waveguide, $Z_L = j\omega\mu/\alpha$. Next it must be proved that the quarter wave transformer relation $Z_o^2 = Z_i Z_L$ applies in this case in order to show that a maximum or minimum in the standing wave pattern occurs at the midpoint of the resonator. Finally the equation must be reduced to the form of Eq. 11-29.

This method has been carried out and does yield the desired result. The details of the procedure are not presented here, first because it involves a great deal of algebraic manipulation, and second, the method makes use of the fact that the total phase shift experienced by a wave going from the center of the resonator to the cutoff section and back to the center is an integral multiple of 180°. This latter condition however is the basis for the phase shift method just discussed and therefore the matrix method is not an entirely different method.

The scatter-chain matrix could be used instead of the ABCD matrix to arrive at the desired results. However, the equations become even more involved than for the ABCD matrix because in this case two matrices instead of one are necessary at the junction between the propagating and cutoff sections.

C. Cutoff-Coupled Dielectric Resonator Band Pass Filter

1. Resonator Quality Factors

The relations necessary to design a cutoff-coupled dielectric resonator to be used as a two port band pass filter are to be derived. The actual filter

under consideration using finite lengths of cutoff coupling sections and connected between two propagating transmission lines is shown in Fig. 11-3.

The quantitative relations sought can be obtained with the aid of one of the well developed equivalent circuit techniques used for ordinary metal-walled microwave resonator design. The equivalence of the lumped parameter circuit used in this technique is in the similarity of the frequency response near resonance of the circuit to that of a microwave resonator.

The lumped parameter parallel R-L-C circuit representing a resonator is shown in Fig. 11-6(a). The ideal transformers in the circuit represent the coupling of the resonator to the source and load. The source and its resistance and the load resistance are also shown in Fig. 11-6(a). The circuit is said to be in resonance when the inductive susceptance cancels the capacitive susceptance leaving just a conductance. This resonance condition, for which the input voltage and current are in phase, occurs at a frequency called the resonant frequency f_r. The response or relative output power versus frequency near resonance is shown in Fig. 11-6(b). The reference level of 0 db shown in Fig. 11-6(b) is for the resonator removed from the circuit and the curve thus displays the insertion loss of the resonator versus frequency.

The selectivity or resonance curve shown in Fig. 11-6(b) is the same as that obtained for a microwave resonator near the resonant frequency, and hence the definition of the quality factor or Q of the lumped constant equivalent circuit applies also to microwave resonators. The general definition of the Q is

$$Q = \omega \frac{W_s}{P_L} \tag{11-35}$$

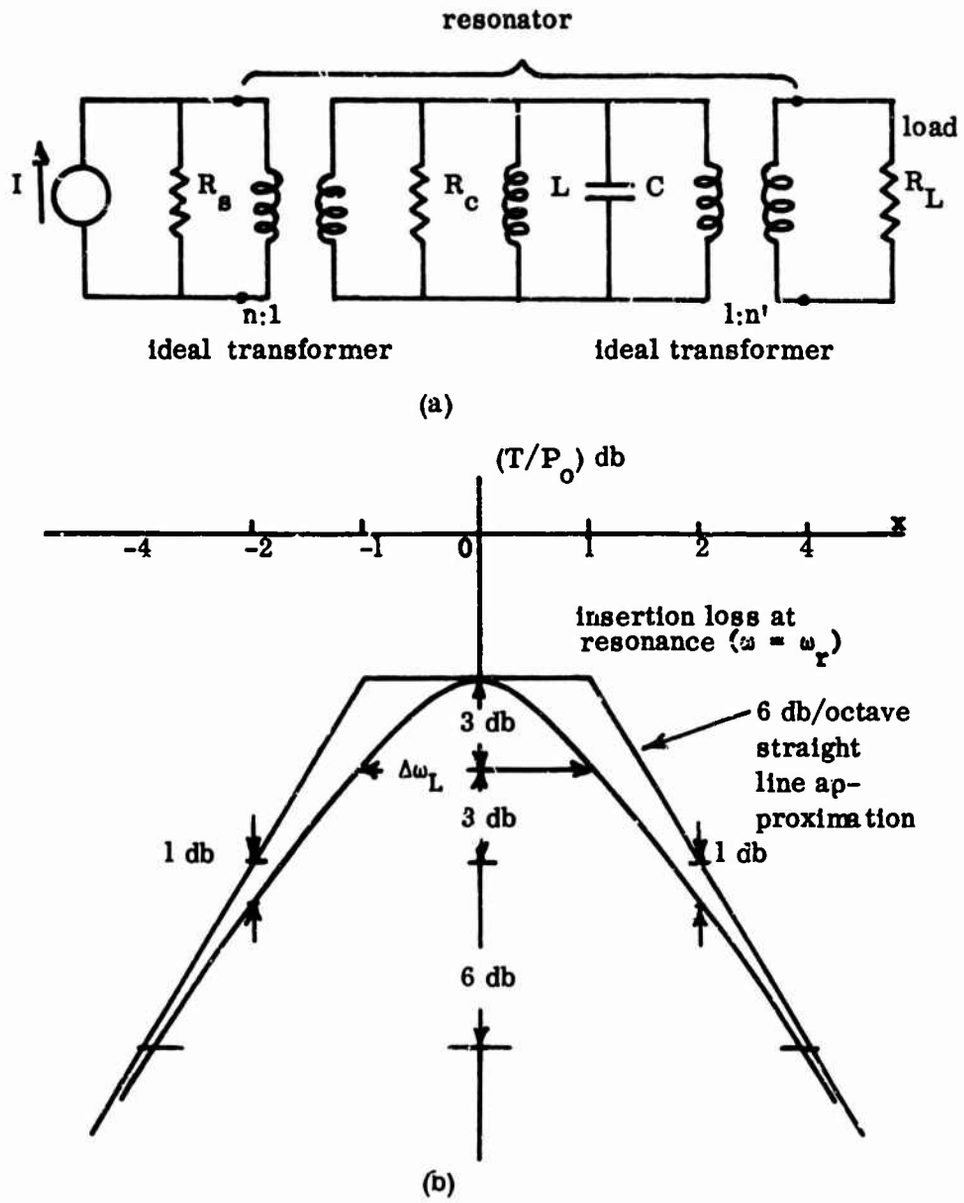

$x = 2(\omega-\omega_r)/\ell\omega_L)$

T = load power with resonator in circuit

P_o = load power with resonator removed

FIG. 11-6 EQUIVALENT CIRCUIT AND INSERTION LOSS CURVE OF A RESONATOR

where Q is a ratio or dimensionless quantity

W_s is the total energy stored in the resonator at resonance

and P_L is the time average power loss or the time rate of dissipation of energy due to losses

Various Q's can be defined and will differ from each other depending on how the time average power loss is determined. The loaded quality factor Q_L is defined by Eq. 11-35 but the time average power loss includes all the energy dissipating elements shown in Fig. 11-6(a), i.e., the load R_L, the resonator itself R_c and the source R_s. The unloaded quality factor Q_u is also defined by Eq. 11-35 but for this case the only energy dissipating element considered is R_c and hence Q_u does not include energy lost in the circuit external to the resonator. Finally two external quality factors are each also defined by Eq. 11-35 except that for Q_{E1} only the source resistance R_s is used in determining the power loss whereas for Q_{E2} only the load resistance R_L is used. If Q_u, Q_{E1} and Q_{E2} of a resonator are known then Q_L can be found from[36]

$$Q_L = \frac{1}{\frac{1}{Q_u} + \frac{1}{Q_{E1}} + \frac{1}{Q_{E2}}} \tag{11-36}$$

Also the equation for the selectivity curve of Fig. 11-6(b) in terms of the Q's is

$$\frac{T}{P_o} = \frac{4Q_L^2}{Q_{E1}Q_{E2}} \frac{1}{\{1+Q_L^2[2(\omega-\omega_r)/\omega_r]^2\}} \tag{11-37}$$

---

36. Jerome L. Altman, Microwave Circuits, D. Van Nostrand Co., New York, 1964 p. 219-228, 239.

where T is the power in the load R_L with resonator in the circuit

and P_o is power in the load R_L with resonator removed from the circuit

The value of Q_L can be determined from the selectivity curve with the aid of the following equation,

$$Q_L = \frac{\omega_r}{\Delta\omega_L} \tag{11-38}$$

where $\Delta\omega_L$ is the 3db bandwidth.

2. Calculation of Q's for Cutoff-Coupled Dielectric Resonator

The peak energy stored in a cavity is determined from a knowledge of the field distribution within the resonator. The general expression for the energy stored is[37]

$$W_s = \frac{1}{2}\epsilon \int_v E_y^2 (x,y,z)\, dV \tag{11-39}$$

where E_y is the peak value of the electric field in the resonator

For a $TE_{1,0,p}$ mode

$$E_y (x,y,z) = (2E_1 \sin \pi x/a) f(z) \tag{11-40}$$

where f(z) is the variation of E_y with z as shown in Fig. 11-5.

---

37. A. B. Bronwell and R. E. Beam, Theory and Application of Microwaves, McGraw-Hill Book Co., New York, 1947, p. 372.

Thus

$$W_s = \frac{1}{2} \epsilon \, b \, 4 \, E_1^2 \, (a/2) \int_{z=o}^{D} f^2(z) \, dz \qquad (11\text{-}41)$$

When the specific field distribution in the z direction is known the integral can be evaluated.

a. Unloaded Q

The unloaded Q of a dielectric filled cavity can be calculated when the energy dissipated within the resonator is known. One part of the energy lost is due to the energy dissipated in the dielectric material filling the cavity and the other part is due to energy dissipated in the metal walls. These losses within the resonator can be considered separately so that a Q based on dielectric losses only and a Q based on conduction losses only can be calculated separately. These separate Q's can then be used to find the unloaded Q_u. It will be assumed that no energy is lost in the cutoff coupling sections.

The $Q_{u(D)}$ accounting for dielectric losses only can be calculated once the time average power lost in the dielectric is determined, since W_s has already been determined by Eq. 11-39. The time average power loss is [38]

$$P_{(D)} = \frac{1}{2} \omega \int_v \epsilon'' E_y^2 \, dV + \frac{1}{2} \sigma \int_v E_y^2 \, dV$$

where ϵ'' is the imaginary part of the permitivity which accounts for the polarization damping loss

and σ is the conductivity of the dielectric

Thus the Q from Eq. 11-35 is

---

38. Robert Plonsey and Robert E. Collin, Principles and Applications of Electromagnetic Fields, McGraw-Hill Book Co., New York, 1961, p. 316.

$$Q_{u(D)} = \omega_r \frac{\frac{1}{2}\varepsilon \int_v E_y^2 \, dV}{\frac{1}{2}\omega_r \int_v \varepsilon'' E_y^2 \, dV + \frac{1}{2}\sigma \int_v E_y^2 \, dV}$$

$$Q_{u(D)} = \frac{\omega_r \varepsilon}{\omega_r \varepsilon'' + \sigma}$$

But the loss tangent of a dielectric is defined as

$$\tan \delta_L = \frac{\omega\varepsilon'' + \sigma}{\omega\varepsilon}$$

Thus

$$Q_{u(D)} = \frac{1}{\tan \delta_L} \tag{11-42}$$

The Q associated with the cavity wall losses is best obtained from[39]

$$Q_{u(w)} = \frac{2}{\delta} \frac{\int_v H^2 \, dV}{\int_A H_t^2 \, dA} \tag{11-43}$$

where H_t is the magnetic field tangent to the 4 metal walls of the cavity

and δ is the skin depth

The integral in the numerator is a measure of the energy stored and the integral in the denominator is a measure of the energy lost in the cavity. Now for the cutoff-coupled resonator

$$H_x = \frac{E_y}{\omega\mu/\beta} = \frac{2\beta E_1}{\omega\mu} \sin(\pi x/a) f(z)$$

---

39. H. A. Atwater, Introduction to Microwave Theory. McGraw-Hill Book Co., New York, 1962, p. 145.

with E_y given by Eq. 11-40. Note also that the H_x and H_z fields have their maximums a quarter wavelength apart along the z coordinate. Thus with the aid of Eq. 11-2, H_z can be written as

$$H_z = \left|\frac{H_x}{j\beta e/\pi}\right| \cos(\pi x/a)\, f(z-\lambda/4)$$

The integrals in Eq. 11-43 for $Q_{u(w)}$ are difficult to evaluate when the above expressions for H_x and H_z are used.

A good approximate value for $Q_{u(w)}$ can be obtained by solving Eq. 11-43 for a resonator exactly one half wavelength long. In such a case f(z) and $f(z-\lambda/4)$ are sine and cosine functions and $D = p\pi$ thus the integrals are easily evaluated to give[40]

$$Q_{u(w)TE_{1,0,1}} = \frac{ab\,\frac{\lambda}{2}\,[a^2+(\lambda/2)^2]\sqrt{\pi f\mu\sigma}}{a^3(\lambda/2)+a(\lambda/2)^3+2(\lambda/2)^3 b} \qquad (11\text{-}44)$$

The $Q_{u(w)}$ of a resonator is approximately proportional to the ratio of its volume to metal suface area. For the cutoff-coupled dielectric resonator this ratio is essentially constant regardless of its length D, since the volume is abD and its metal surface area is D(2a+2b). Thus the value of $Q_{u(w)}$ should not differ greatly from that given by Eq. 11-44.

The actual unloaded Q_u of the cutoff-coupled dielectric resonator will be

$$Q_u = \frac{1}{\frac{1}{Q_{u(D)}} + \frac{1}{Q_{u(w)}}} \qquad (11\text{-}45)$$

---

40. Atwater, p. 145.

However as will be shown later $Q_{u(w)\ TE_{1,0,1}}$ will be very much larger than $Q_{u(D)}$ and hence the approximate value of $Q_{u(w)}$ given by Eq. 11-44 will be sufficiently accurate to calculate Q_u using Eq. 11-45.

b. External Q

When the external Q is calculated the time average power loss in the load at either the input or output port of the resonator must be known. In order to calculate this power loss it will be convenient to assume matched conditions at the input and output of the resonator. In general matched conditions can be met in practice especially now that isolators are available. Thus the power flowing along a matched waveguide (perhaps in this case a dielectric filled waveguide to make it propagating) is given by

$$P_T = \frac{1}{2} \text{Re} \int_0^b \int_0^a E_y H_x^* \, dx \, dy$$

where for the TE_{10} mode

$$E_y = E_4 \sin(\pi x/a)$$

$$H_x = H_4 \sin(\pi x/a)$$

and E_4 and H_4 are amplitude factors in the input or output waveguides

Then

$$P_T = \int_0^b \int_0^a \frac{1}{2} E_4 \sin(\pi x/a) \frac{E_4}{R_o} \sin(\pi x/a) \, dx \, dy$$

or

$$P_T = P_{LOAD} = \frac{1}{2} \frac{E_4^2 \, ab}{R_o} \qquad (11\text{-}46)$$

where $R_o = -E_4/H_4 = \omega\mu_o/\beta$ is the wave impedance

It would be very desirable to have Eq. 11-46 expressed in terms of the field amplitude E_1 in the resonator, since then Q_E could be calculated using Eq. 11-35 because W_s is already known in terms of E_1. Now from Fig. 11-3 it can be seen that a portion of E_1 is transmitted into the cutoff-section, attenuated in passing through the cutoff-section and finally transmitted into the propagating output waveguide as E_4. Thus

$$E_4 = E_1 \tau_\alpha \tau_\beta e^{-\alpha L}$$

where τ_α and τ_β are given by Eqs. 11-7 and 11-11 respectively

and L is the length of the cutoff-section

The expression for τ_α is for an infinitely long cutoff-section; however, in a practical filter even though this section is not infinitely long, it is long enough so that any reflected wave from the output would be sufficiently attenuated in traveling back to the resonator that it can be neglected. Thus

$$E_4 = E_1 \frac{j2\beta}{\alpha+j\beta} \frac{2\alpha}{\alpha+j\beta} e^{-\alpha L}$$

or

$$|E_4| = \frac{4\alpha\beta e^{-\alpha L}}{\alpha^2+\beta^2} E_1$$

and

$$P_T = P_{LOAD} = \frac{1}{4} \frac{ab(16\alpha^2\beta^2 e^{-2\alpha L})}{R_o(\alpha^2+\beta^2)^2} E_1^2$$

Now R_o is equal to $\omega\mu_o/\beta$ and assuming the input and output propagating waveguide sections are filled with the same dielectric as the resonator then the β's are the same and

$$P_{LOAD} = \frac{4ab\alpha^2\beta^2 e^{-2\alpha L}}{\omega\mu_o(\alpha^2+\beta^2)^2} E_1^2 \tag{11-47}$$

Then Q_{E1} or Q_{E2} can be calculated using Eqs. 11-41 and 11-47 in Eq. 11-35.

$$Q_{E1} = Q_{E2} = \frac{\omega_r^2 \varepsilon_r \varepsilon_o (\alpha^2+\beta^2)^2 \int_o^D f^2(z)\, dz}{4\alpha^2\beta^3 e^{-2\alpha L}} \tag{11-48}$$

Finally Q_L can now be calculated with the aid of Eq. 11-36 since Q_{E1}, Q_{E2} and Q_u are known.

3. Insertion Loss at Resonance

The fraction of the incident power P_o transmitted by a resonator at resonance is from Eq. 11-37

$$\left.\frac{T}{P_o}\right|_{res} = \frac{4Q_L^2}{Q_{E1}Q_{E2}} \tag{11-49}$$

Now Q_L can be determined from Eq. 11-36 and since in most cases $Q_{E1} = Q_{E2} = Q_E$

$$Q_L = \frac{1}{\frac{1}{Q_u} + \frac{2}{Q_E}} = \frac{Q_E}{[Q_E/Q_u+2]} \tag{11-50}$$

Hence

$$\left.\frac{T}{P_o}\right|_{res} = \frac{4}{[Q_E/Q_u+2]^2}$$

or the inverse

$$\left.\frac{P_o}{T}\right|_{res} = \frac{[Q_E/Q_u+2]^2}{4} \tag{11-51}$$

Thus the insertion loss $P_o/T|_{res}$ increases as Q_E increases and approaches infinity as Q_E approaches infinity. This means very little energy is coupled into and out of the resonator. On the other hand as Q_E approaches zero the insertion loss also approaches zero. But since Q_L is never larger than Q_E the design of symmetrical filters of this type results in a compromise between low insertion loss and high Q_L.

D. Cascaded Resonator

It is well known that when two identical tuned circuits or resonators are connected in series or cascade, the overall selectivity will be increased over that of one tuned circuit alone. Another way of stating this is that the bandwidth is reduced or that the Q of the combination is higher than the Q of a single unit.

In practice two kinds or types of cascaded resonators or multistage filters are recognized. The division is based on the type of coupling used to connect the resonators together. The two types are direct coupled filters, in which the output of one resonator is coupled directly into the input of the next resonator and quarter-wave coupled filters, in which a quarter-wave transmission line is used to couple the resonators together. Thus far only the case corresponding to the direct coupled filter has been tried with cascaded cutoff-coupled resonators.

In direct coupled metal-walled resonators one can show that for identical resonators the resonant frequency is the same as it was for just one of the resonators, regardless of how tight the coupling is. The reason for this can be seen from the sketches of the standing wave patterns shown in Fig. 11-7. In Fig. 11-7(a) the pattern for a single resonator at resonance is shown. In Fig. 11-7(b is shown the standing wave pattern for two identical resonators in cascade and direct coupled. Note that this pattern is always the same, no matter how

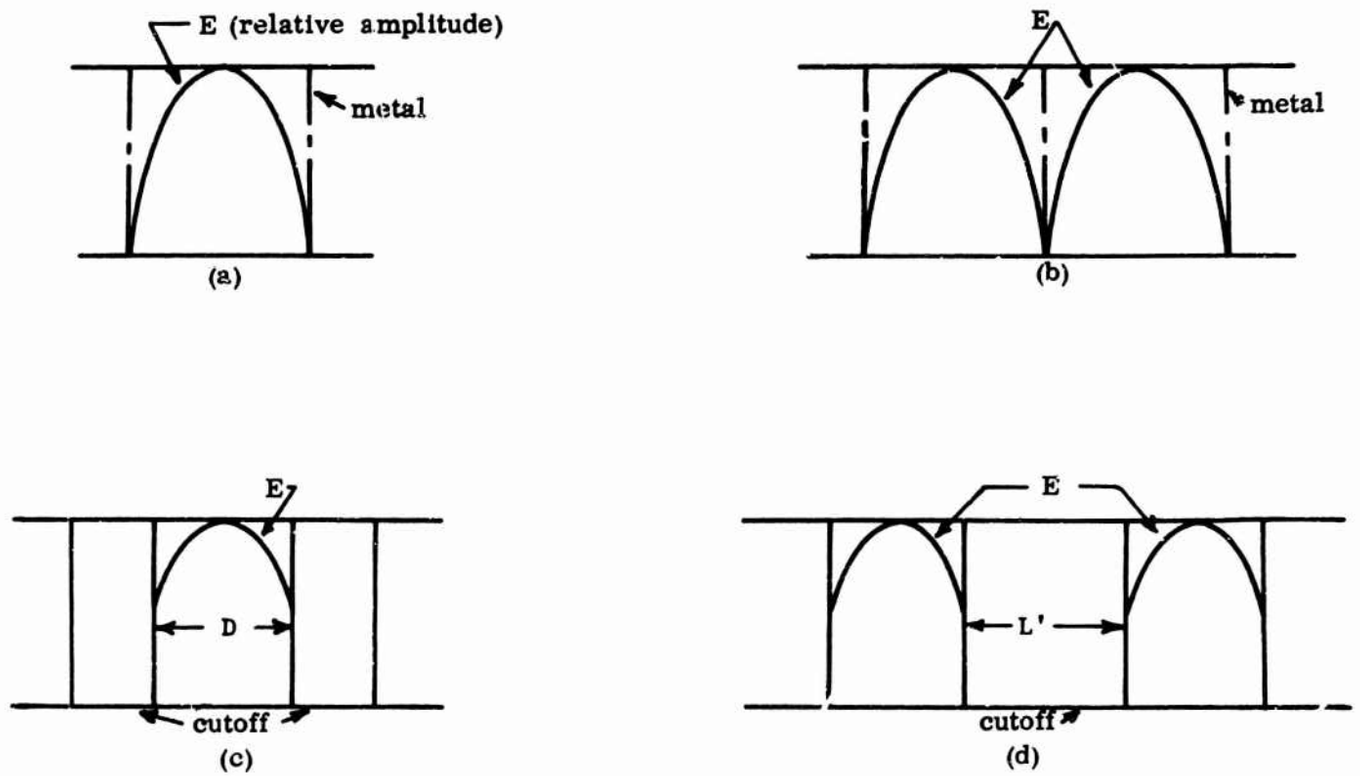

FIG. 11-7 STANDING WAVE PATTERNS IN CASCADED RESONATORS

tightly coupled the resonators are. In the extreme case, when the wall dividing the resonators is removed, the combination can still resonate at the original frequency since the new single resonator would still contain an integral number of the original half-wavelengths.

The standing wave pattern for a single resonator cutoff-coupled filter is shown in Fig. 11-7(c). Note that because of the reactive but finite impedance at each end of the dielectric filled resonator, the standing wave pattern does not go to zero at the ends. The case corresponding to direct coupling between two cutoff-coupled dielectric resonators is shown in Fig. 11-7(d). If in this latter case, it was desired to obtain maximum coupling by reducing the length L' of the cutoff-coupling section to zero, a single resonator of length 2D would be formed. However for the original applied frequency there can not be a zero or maximum field at the midpoint of the resonator as required for resonance. In order to obtain a zero field at the midpoint of the new larger single resonator, and hence be in resonance, would require that the applied frequency be increased. This would correspond to the case of p = 1 in Eq. 11-30. Thus the new single resonator cannot resonate at the same frequency as the two lossly coupled resonators do.

Some characteristics of cascaded cutoff-coupled dielectric resonators differ somewhat from those of metal-walled resonators. As with metal walled resonators the cutoff-coupled filter will have a Q curve or selectivity curve as shown in Fig. 11-6 with an increased value of Q_L and in general an increased insertion loss at resonance compared with a single resonator filter. However, the resonant frequency of the cascaded cutoff-coupled filter will in general be changed from that of a single resonator filter. As the length of the cutoff-section between the dielectric filled resonator approaches zero, f_r must either approach the resonant frequency of a single resonator of length

2D or it must increase above that for a single resonator in order to obtain a zero field at the midpoint of a resonator of length 2D. As the length of the cutoff section between the dielectric filled resonators is increased, the resonant frequency approaches that of the individual resonators making up the cascade. Quantitative formulation of this behavior has not yet been attempted.

In practice it is virtually impossible to fabricate two identical resonators that can be used in cascade. The resonator with the lower resonant frequency could be shortened slightly in an attempt to make it coincide with the second resonator. A better way however is to make use of a small perturbation such as a screw inserted into the volume of the resonator where the field amplitude is large. Such a perturbation can be shown to be equivalent to a capacitance shunting the resonator and hance results in increasing the C in the equivalent circuit of Fig. 11-6. Thus the resonant frequency can be shifted an amount determined by the depth of penetration of the screw into the dielectric filled resonator. The details of construction of such a tunable resonator as well as the fabrication and experimental measurements made on cutoff-coupling dielectric resonators will be given next.

E. Fabrication and Measurement Technique

1. Construction of the Filters

Rectangular waveguide normally used at X-band was chosen as the most suitable for making up the experimental filters. This waveguide size (0.9 x 0.4 inches) is cut-off for the intended operating frequency of 3.0 GHz but can be made

propagating by filling the guide with a high dielectric constant material. The normal cut-off frequency of air-filled X-band waveguide is 6.57 GHz but this cut-off frequency can be reduced to a value well below 3.0 GHz by filling the guide with a commercial dielectric called "Stycast Hi K", which has a dielectric constant of 10.[41] This material is a hard white plastic that can be machined quite easily. It is however somewhat brittle and hence is easily broken or chipped.

The resonators were made by cutting a section of the X-band waveguide to the length required for a dielectric-filled section. Then a piece of the dielectric was machined and force-fitted inside the waveguide so that it filled the waveguide as completely as possible. A number of pieces of waveguide (air-filled), cut to convenient lengths (such as 1", 1/2", 1/4", 1/8"), were made complete with flanges. These pieces formed the cutoff coupling sections. When these pieces were joined to both ends of the dielectric-filled section, a complete cutoff-coupled dielectric resonator resulted. A photograph of such a resonator is shown in Fig. 11-8.

A possible drawback to this method of construction is that the dielectric material is force-fitted into the waveguide. It is generally impossible to have the dielectric touching the waveguide in all places, and hence there will always be a few small air spaces between the faces of the dielectric block and the waveguide walls. Such small air spaces or minor flaws can introduce large susceptances into the guide. A technique suggested by Goodwin and Moss to eliminate air gaps is to electroform with silver or copper onto the dielectric filling the guide.[42]

---

41. "Stycast Hi K", is manufactured by Emerson & Cuming, Inc. Canton, Massachusetts.

42. F. E. Goodwin and G. E. Moss, "Broad-Band Impedance Matching into Dielectric-Filled Waveguides," IEEE Transactions on Microwave Theory and Techniques, Vol. MTT-11, No. 1, January 1963, p. 37.

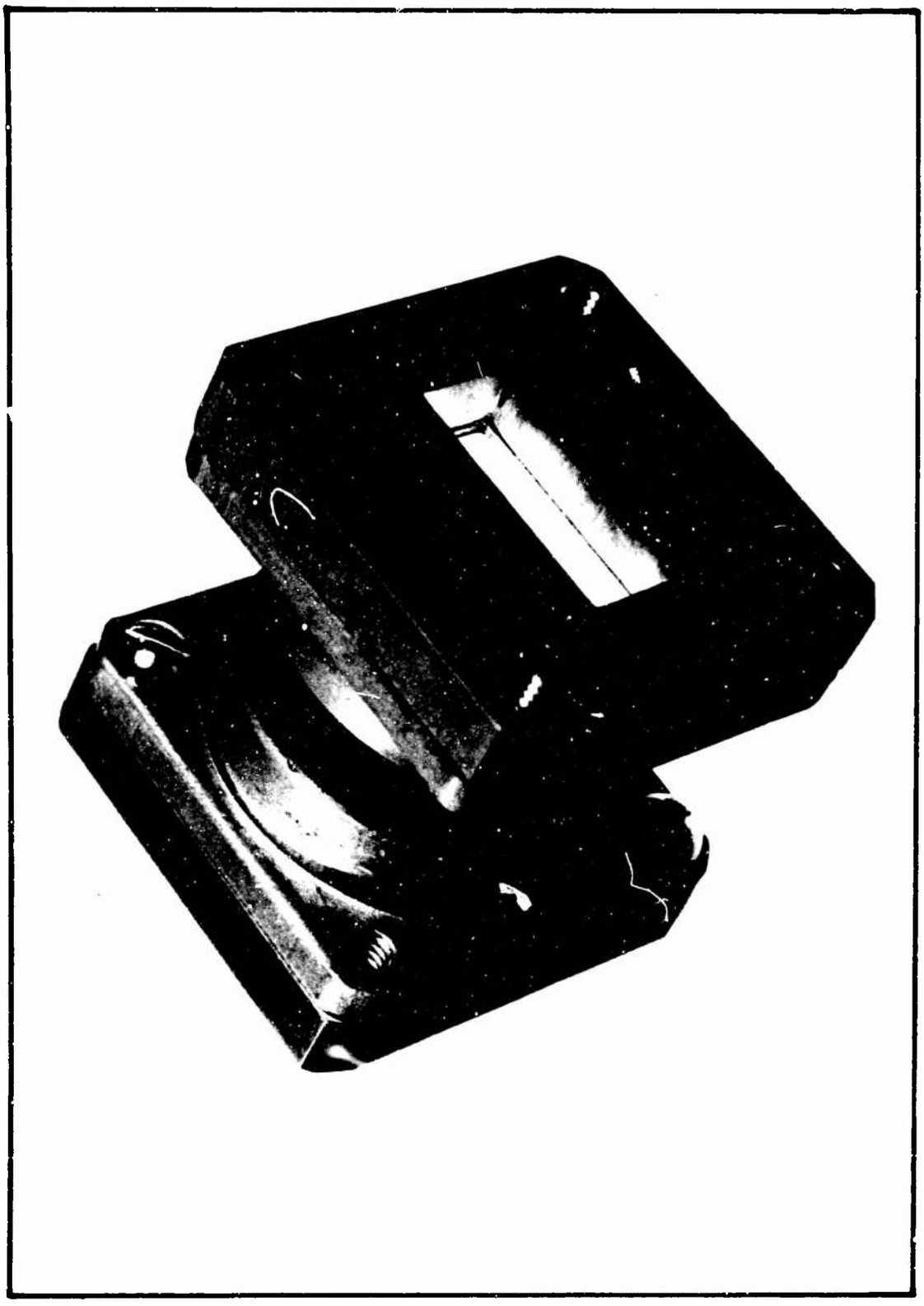

FIG. 11-8 CUTOFF-COUPLED DIELECTRIC RESONATOR FILTER

A resonator whose resonant frequency was adjustable was also constructed. A resonator that has a standing wave pattern with a maximum field at the midpoint between the two end flanges was selected for this. It was made tunable by drilling a hole at the standing wave pattern maximum 1/8" deep into the dielectric filling the resonator. A nut for a No. 8 screw was soldered on the top outside of the waveguide in order that the depth or penetration of the screw into the hole in the dielectric could be adjusted. This adjustable susceptance is equivalent to changing the effective length of the dielectric filling the resonator. A tunable resonator is shown in the photograph of Fig. 11-9.

2. Coupling into Dielectric-Filled Waveguide

It appeared that a propagating dielectric-filled waveguide of the same cross-sectional size as the resonator would be desirable at both resonator ports to carry energy into and out of the filter. Furthermore, if the dielectric constant of the filled waveguide sections is the same as that of the resonator, then the equation for Q_E would be simplified. It was therefore decided to use X-band waveguide filled with Stycast Hi K dielectric material with an ε_r=10 to couple into and out of the filters. A suitable means of coupling these dielectric-filled waveguides to the source and load must now be decided on.

The 3 GHz or S-band source available was a 726B klystron and had a coaxial output. A suitable load which would also serve to measure the output power of the filter would be either a crystal or a thermistor. Both of these devices were available in coaxial form. Thus coupling to the dielectric-filled waveguides using regular X-band coax-to-waveguide junctions (with adjustable plungers for tuning) filled with dielectric was considered. However, when two of these dielectric-filled junctions were tried out by joining their flanges together and connecting one junction to the source and the other to a crystal by coaxial

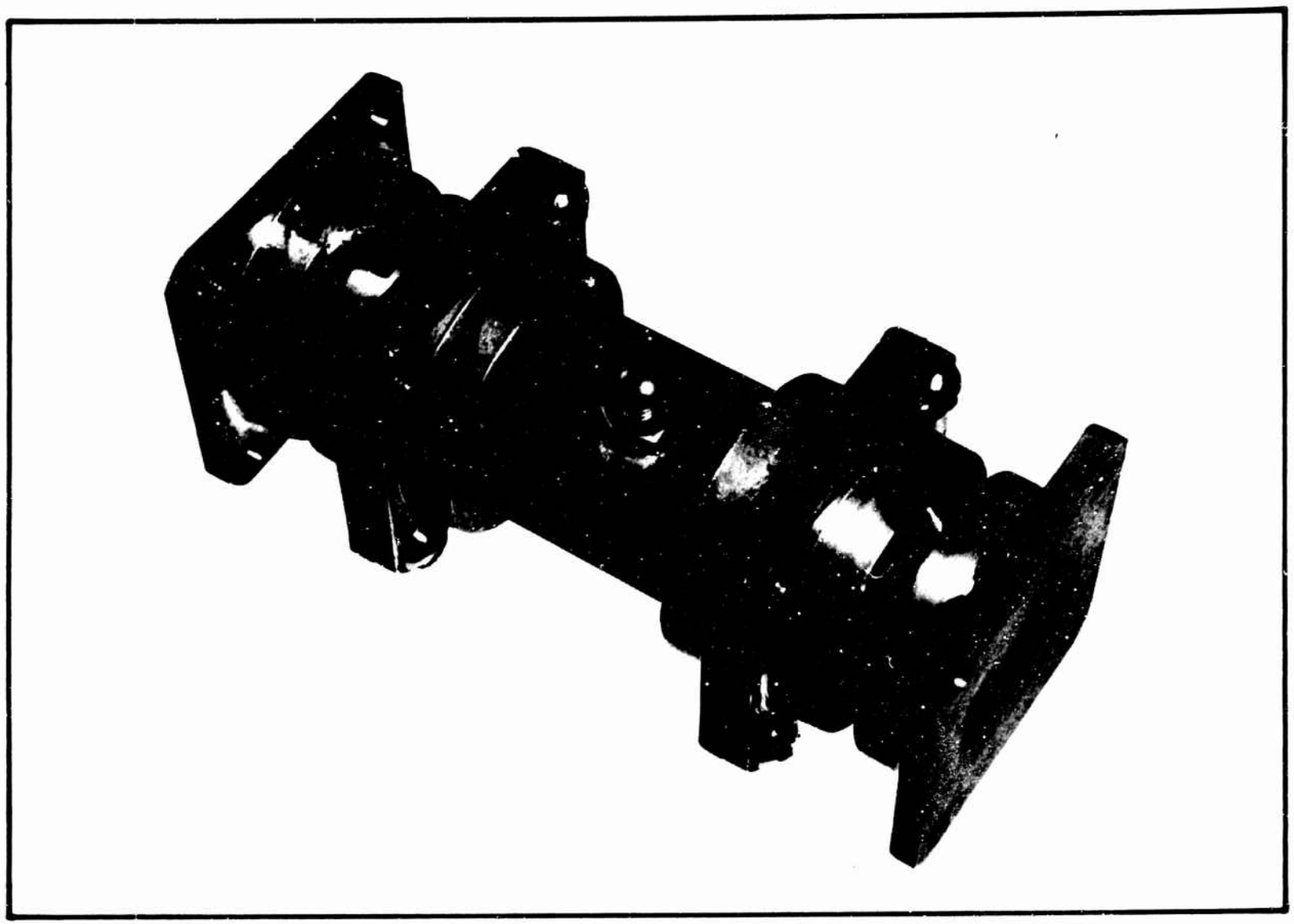

FIG .11-9 TUNABLE CUTOFF-COUPLED DIELECTRIC RESONATOR FILTER

cables, it was observed that the crystal output current varied considerably with frequency. This variation might be due to several factors. First, the junctions were designed for use at X-band rather than at S-band. Secondly, the junction cannot be tuned with its metal plunger since the dielectric can extend only up to the adjustable plunger. Thus it appeared that the dielectric-filled junctions were not suitable for coupling from a coaxial cable to the dielectric-filled waveguide.

An alternative means of coupling into the dielectric-filled waveguide is to go from a coaxial cable to an S-band (air-filled) waveguide using the conventional S-band junction, and then use a transition from the S-band waveguide to the dielectric-filled X-band waveguide. This waveguide transition might be either a straight line taper or a step taper. Because of ease of fabrication the straight taper section was used.

This straight line transition consists of a tapered waveguide with a dielectric insert having a reverse taper. Such waveguide taper sections can be seen in the photograph of Fig. 11-10. Note that the waveguide walls in both E and H planes are tapered along straight lines from S-band size to X-band size. Not observable in the photograph is the tapered dielectric insert which is inside each waveguide taper. The tapered dielectric piece begins as a point at the S-band end of the transition and in the center of the cross-section of the waveguide. As the metal waveguide walls taper down to X-band size, the dielectric insert tapers up along straight lines in both planes until it becomes X-band size at the same point that the metal waveguide walls become X-band size. Thus a gradual transition is made from air-filled S-band to dielectric-filled X-band waveguide. As long as the length of the tapered section is much greater than a wavelength, such a transition will transmit power with negligible reflections.

The tapers constructed were 3" in length and used Stycast Hi K, which had a dielectric constant of 10, for the insert. To test the performance of these tapers, their X-band flanges were connected together and a 726B klystron was

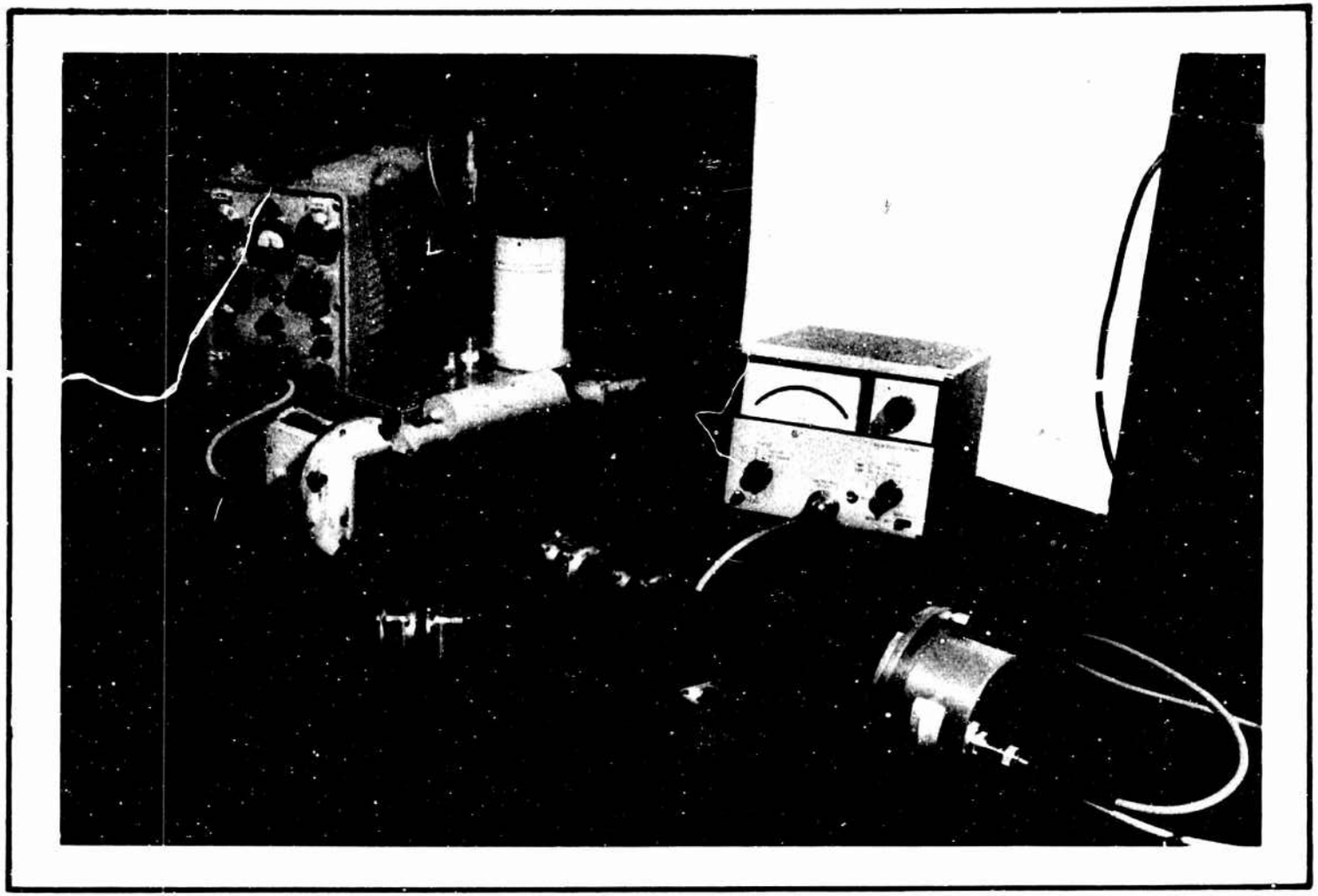

FIG.11-10 SYSTEM FOR POINT-BY-POINT FREQUENCY RESPONSE MEASUREMENT

used to feed power through a coaxial cable to the S-band waveguide. An S-band thermistor was used to monitor the output power. The output power was constant within ± 2 db from 2.90 GHz to 3.45 GHz.

3. Swept-Frequency Method

The basic circuit used for the insertion loss versus frequency measurements made on the filters is shown in Fig. 11-10. A coaxial cable was connected from the output of a 726B klystron through an attenuator, an H-P 536 wavemeter, and a Sperry 04452 ferrite isolator to an S-band (air-filled) waveguide. The purpose of the isolator was to ensure that the resonator saw a matched waveguide impedance at its input port, so that Eq. 11-48 for Q_E is valid. A taper was used to feed the power from the S-band guide to the dielectric-filled X-band guide. From the X-band guide the power was fed into the input cutoff section, the dielectric-filled section, and the output cutoff section of the cutoff-coupled dielectric resonator. Finally, power was led from the resonator through another section of dielectric-filled X-band guide, and then through a taper to an S-band guide where a load served as a detector.

In Fig. 11-10 the load is shown as a thermistor; however the photograph shows the point-by-point measuring set-up rather than the swept-frequency method. In the swept-frequency method the thermistor was replaced by a crystal detector, the output of which was connected to one of the vertical inputs of a dual trace oscilloscope. In addition a coaxial cable and crystal was connected from a second output of the klystron to the second vertical input of the oscilloscope, and a cable was connected from the sawtooth terminal of the oscilloscope to the modulation input terminal of the klystron power supply. Thus the frequency of the klystron was swept (modulated) and the direct output of the klystron and the output of the resonator were monitored on the oscilloscope as a function of frequency.

The swept-frequency method was used to obtain an approximate value of the resonant frequency, and the insertion loss at resonance of the resonator. In addition the swept-frequency method of measurement permitted a check for power transmitted by the resonator at frequencies other than those near resonance. In order to determine accurately the response of the filter, that is, insertion loss versus frequency, a point-by-point method of measurement was used.

4. The Point-by-Point Method

The point-by-point method of measurement uses the circuit and equipment shown in Fig. 11-10. The output power was measured with an H-P S486A thermistor and associated H-P 431B power meter. The remainder of the equipment has already been described. The particular combination of thermistor and power meter used gave very accurate power readings. The accuracy is rated at $\pm 5\%$ of full scale and thus the power readings were usually accurate to within a few tenths of a decibel.

The technique used to measure the insertion loss versus frequency was as follows. First, with the circuit identical to that shown in Fig. 11-10 (no modulation of the klystron), the frequency and output power were read and recorded. The second step consisted of removing the entire filter from the circuit and joining together the two X-band flanges of the tapers. The new reading on the power meter was noted, and in addition the frequency was checked with the wavemeter to make sure no frequency drift had occurred. Thus the insertion loss at a particular frequency was obtained by subtracting the two power readings obtained in manner just described. Other points on the Q curve were found by changing the klystron frequency and repeating the above procedure.

The insertion loss at resonance was found with a slight change in procedure. Near resonance the power output meter reading was observed while the repeller

voltage of the klystron was varied (and thereby varying the frequency). The frequency for which the maximum power reading obtained determined resonance. The insertion loss at this frequency was then measured.

F. Theoretical Design and Experimental Results

1. Single Stage Filters

a. Design

The design of single stage curoff-coupled band pass filters can be accomplished by using the theory presented in the previous section. The waveguide size, the relative dielectric constant to be used in the propagating sections, and the resonant frequency of the filter must be decided upon first. The air-filled waveguide must be of such dimensions that it is cutoff at resonance but can be made propagating when it is filled with the dielectric material. The experimental filters described in the previous section use X-band waveguide and a material with a dielectric constant of 10 for a chosen resonant frequency of 3.10 GHz. The only parameters that remain to be determined are the lengths of the propagating and cutoff sections.

The length D of the propagating section is determined by Eq. 11-29 or 11-30.

$$\tan \beta D = \frac{2\alpha\beta}{\beta^2 - \alpha^2} \qquad (11\text{-}29)$$

or

$$\tan \beta D + \frac{2\alpha\beta}{\alpha^2 - \beta^2} = 0$$

Taking the arctangent of both sides

$$\beta D + \arctan\left(\frac{2\alpha\beta}{\alpha^2-\beta^2}\right) = \arctan(0) = p\pi \qquad (11\text{-}30)$$

where p is an integer including zero

α is the attenuation constant of cutoff section

and β is the phase constant of propagating section

Since the resonant frequency has been specified, α and β of the cutoff and propagating sections respectively can be found by substituting ω_r and the proper value of ε in Eq. 11-1 with m=1 and n=o since the TE_{10} mode is being considered.

$$\gamma = \sqrt{\left(\frac{m\pi}{a}\right)^2 + \left(\frac{n\pi}{b}\right)^2 - \omega^2\mu_o\varepsilon} \qquad (11\text{-}1)$$

where ε is the permittivity of the medium in the guide

a and b are the usual cross-sectional dimensions of the waveguide

and m and n are integers including zero (note: m and n are not to be zero simultaneously).

Thus the only unknowns in Eq. 11-30 are the length D and the mode number p. Now from the relation between D and p expressed by Eq. 11-31.

$$D = \frac{p}{2} - \frac{\lambda}{2\pi}\arctan\frac{2\alpha\beta}{\alpha^2-\beta^2} \qquad (11\text{-}31)$$

or

$$D = \frac{p\lambda}{2} + s$$

where

$$-\lambda/4 \leq s \leq +\frac{\lambda}{4}$$

it is clear that the shortest possible resonator length corresponds to p=o. As p takes on increasing integral values (1,2,3,$\cdots$) the length D increases. Any integral value may be chosen, however, in order to make the resonator as compact as possible values of p = 0, 1, or 2 should be used. Once p has been chosen the value of D can be calculated from Eq. 11-30.

The values of α and β, determined by using the f_r, ϵ_r and the waveguide size chosen here, are

$$\alpha = 120.6 \text{ nepers/m}$$

$$\beta = 153.0 \text{ radians/m}$$

Then for p=0; D=0.875 cm = 0.344",

for p=1; D=2.92 cm = 1.15",

and for p=2; D=4.98 cm = 1.96".

The lengths of the cutoff sections of waveguide have a considerable influence on the loaded Q_L of the resonator filter. The length L of a cutoff section has a direct bearing on the external Q_{E1} as shown by Eq. 11-48.

$$Q_{E1} = Q_{E2} = \frac{\omega_r^2 \epsilon_r \epsilon_o (\alpha^2+\beta^2)^2 \int_0^D f^2(z)\, dz}{4\alpha^2\beta^3 e^{-2\alpha L}} \qquad (11\text{-}48)$$

In turn Q_{E1} influences Q_L according to Eq. 11-50, where for simplicity Q_{E2} is assumed to be equal to Q_{E1}.

$$Q_L = \frac{1}{\frac{1}{Q_u} + \frac{2}{Q_E}} = \frac{Q_E}{[Q_E/Q_u+2]} \qquad (11\text{-}50)$$

Thus, if the design calls for equal length cutoff sections at both ends of the resonator, i.e., $Q_{E1} = Q_{E2}$, then Eqs.11-48 and 11-50 specify Q_L.

In order to calculate Q_{E1} from Eq. 11-48 the value of

$$\int_{z=0}^{z=D} f^2(z)\, dz$$

must first be determined. To do this f(z) must be plotted using Eq. 11-34.

$$E = e^{-j\beta z} + e^{j\beta z}\, e^{j\beta \arctan\left(\frac{2\alpha\beta}{\beta^2-\alpha^2}\right)}\, E_1 \qquad (11\text{-}34)$$

Now f(z) is the amplitude of the standing wave pattern relative to the incident field E_1 in the propagating section. Thus

$$f(z) = \frac{|E \text{ from Eq. } 11\text{-}34|}{E_1}$$

Typical curves of f(z) were shown in Fig. 11-5 of a previous section. Now the square of f(z) must be integrated along the length of the propagating section of waveguide. The value of this integral is then substituted into Eq. 11-48 along with ω_r, α, β and L to determine Q_{E1}.

In order to determine the value of Q_L from Eq. 11-50 the value of $Q_E = Q_{E1} = Q_{E2}$ and Q_u the unloaded Q must be known. Now Q_u depends on $Q_{u(w)}$ the unloaded Q accounting for waveguide wall losses and $Q_{u(D)}$ the unloaded Q accounting for dielectric losses. The value of $Q_{u(w)}$, though only approximate, is given by Eq. 11-44.

$$Q_{u(w)\ TE_{1,0,1}} = \frac{ab\,\frac{\lambda}{2}\,[a^2+(\lambda/2)^2]\,\sqrt{\pi f\mu\sigma}}{a^3(\lambda/2) + a(\lambda/2)^3 + 2(\lambda/2)^3\, b} \qquad (11\text{-}44)$$

the value of $Q_{u(D)}$ is given by the reciprocal of the loss tangent of the dielectric filling the resonator, thus

$$Q_{u(D)} = \frac{1}{\tan \delta_L} \tag{11-42}$$

Therefore to make $Q_{u(w)}$ and $Q_{u(D)}$ high, the metal of the waveguide walls should have high conductivity and the loss tangent of the dielectric filling the resonator should be small. With $Q_{u(w)}$ and $Q_{u(D)}$ known the value of Q_u can be determined from Eq. 11-45.

$$Q_u = \frac{1}{\frac{1}{Q_{u(D)}} + \frac{1}{Q_{u(w)}}} \tag{11-45}$$

Finally the value of Q_L can now be determined from Eq. 11-50.

It can be seen from the above procedure that the value of Q_L can be controlled by varying such factors as L and D. Increasing L increases Q_E, and increasing D also increases Q_E since then the integral of the square of f(z) over the length D increases. Now Q_L can approach the value of Q_u if Q_E is made large enough. On the other hand, as Q_E approaches zero so does Q_L.

It is almost obvious that if a high Q_L is desired then a high insertion loss at resonance must be accepted. The relationship is given by the ratio of the transmitted power T to the incident power P_o. This ratio is according to Eq. 11-51.

$$\left.\frac{T}{P_o}\right|_{res} = \frac{4}{[Q_E/Q_u+2]^2} \tag{11-51}$$

Using the procedures and equations just presented it is possible to predict the behavior of the filter. Once f_r, Q_L and the insertion loss at resonance are known, the frequency response of the filter can be calculated. This can be done by the equation and information given in Fig. 11-6.

The values of the various Q's associated with filters which have specific resonator lengths D equal to 0.344", 1.15" and 1.96" were calculated. The function f(z) required for these calculations is shown in Fig. 11-11.
The integration of $f^2(z)$ is carried out as follows:

$$\int_o^D f^2(z)\,dz = (p+1)\int_o^{\lambda/2} \sin^2\left(\frac{\pi z}{\lambda/2}\right) dz - 2\int_o^{0.227"} \sin^2(\pi z/\lambda/2))\,dz$$

But $\lambda = 2\pi/\beta = 4.1$ cm = 1.615", 0.227" = 0.577×10^{-2} m, and the two integrals are evaluated as:

$$\int_o^D f^2(z)\,dz = (p+1)\,(\lambda/2\cdot 1/2) - 2(z/2 - 1/4(\lambda/(2\pi))\sin(4\pi z/\lambda))\Big|_o^{0.577\times10^{-2}}$$

$$= (p+1)(1.025 \times 10^{-2}) - (.577 - .163\sin 76.6^{\circ})\times 10^{-2}$$

$$= ((p+1)(1.025) - .418) \times 10^{-2}$$

So for p = 0 (D=.344"): $\int_o^D f^2(z)\,dz = .607$

for p = 1 (D = 1.15"): $\int_o^D f^2(z)\,dz = 1.632$

for p = 2 (D = 1.96"): $\int_o^D f^2(z)\,dz = 2.657$

Q_{El} can be put in the form:

$$Q_{El} = 2.93\left(\int_o^D f^2(z)\,dz\right)\varepsilon^{2\cdot 120.6\,L}$$

This equation was evaluated for typical values of L and p:

p	L	Q_{El}
2	3/4"=1.9×10^{-2}m	770
	1"	3510
	1 1/8"	7620
	1 1/4"	16000
1	1.036"	2790
0	1.015"	910

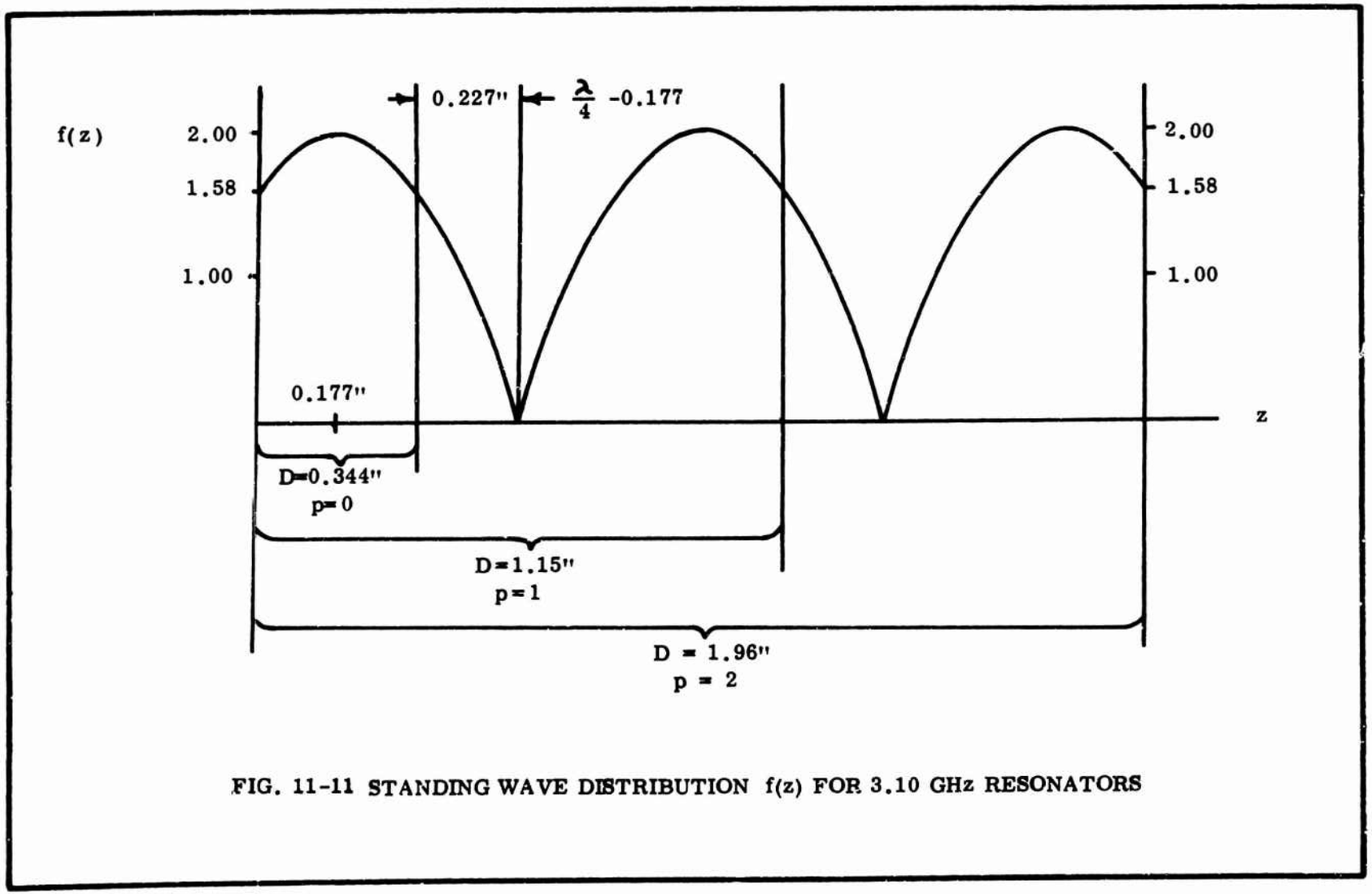

FIG. 11-11 STANDING WAVE DISTRIBUTION f(z) FOR 3.10 GHz RESONATORS

The loss tangent of the dielectric material used in these resonators is given by the manufacturer as 0.0007, therefore $1/Q_{u(D)} = 0.0007$. The value of $Q_{u(w)}$ using Eq. 44 is 6,130 for copper waveguide walls. Thus $1/Q_{u(w)} \cong 0.000163$ and hence from Eq. 50 $1/Q_u \cong 0.000863$.

With the above values of Q_{El} and Q_u known, Q_L and the insertion loss at resonance were calculated and have the values shown in Table 11-I.

b. Experimental Results

A typical measured curve of insertion loss versus frequency is shown in Fig. 11-12. The measured insertion loss at resonance and the measured Q_L obtained from the response curves for the six single stage filters constructed are shown in Table 11-I. A comparison between the experimental and predicted values of insertion loss and Q_L listed in Table 11-I shows good agreement.

The measured resonant frequencies for the four filters with D = 1.96" were very close to the predicted value of 3.100 GHz. A resonator with D = 1.15" resonanted at 3.014 GHz. This deviation of f_r from the predicted value could have been caused by a deviation in the value of ϵ_r of the dielectric from its nominal value of 10 or by a loose fit in the waveguide, creating a susceptance across the guide. The dielectric slab was sanded down to a length of 1.007". The results for this case are given in Table 11-I and shows how f_r can be increased by reducing the length of the dielectric section. A resonator with a D = 0.344" resonated at 2.984 GHz. This dielectric slab was also sanded down to a length of D = 0.314". The resonant frequency was raised to 3.088 GHz as shown in Table 11-I. An attempt to raise the frequency further resulted in the accidental breaking of the dielectric slab.

A characteristic noted in all measured response curves was an unsymmetry about the center frequency. The response curve shown in Fig. 11-12 is typical of the unsymmetry observed. An ideal symmetrical Q curve is shown dotted in Fig. 11-12.

TABLE 11-I

COMPARISON OF THEORETICAL AND EXPERIMENTAL RESULTS

I. D = 1.96"			
Outoff section length L	Parameter	Theoretical Value for Q_u = 1155	Value observed experimentally
3/4"	f_r	3.100 GHz	3.10 GHZ
	Q_L	289	260
	Ins.Loss$\|_{res.}$	2.47 db	1.60 db
1"	f_r	3.100 GHz	3.10 GHz
	Q_L	698	620
	I.L.$\|_{res.}$	8.14 db	5.6 db
1 1/8"	f_r	3.100 GHz	3.102 GHz
	Q_L	890	700
	I.L.$\|_{res.}$	12.61 db	13.2 db
1 1/4"	f_r	3.100 GHz	3.10 GHz
	Q_L	1,010	780
	I.L.$\|_{res.}$	17.9 db	17.8 db
II. D = 1.077"			
Cutoff section length L	Parameter	Theoretical Value for Q_u = 1155 (D = 1.15")	Value observed experimentally
1.036"	f_r	3.100 GHz	3.102
	Q_L	634	450
	I.L.$\|_{res.}$	6.83 db	5.4 db
III. D = .314"			
Cutoff section length L	Parameter	Theoretical Value for Q_u = 1155 (D = 0.344")	Value observed experimentally
1.015"	f_r	3.100 GHz	3.088 GHz
	Q_L	327	310
	I.L.$\|_{res.}$	2.90 db	4.3 db

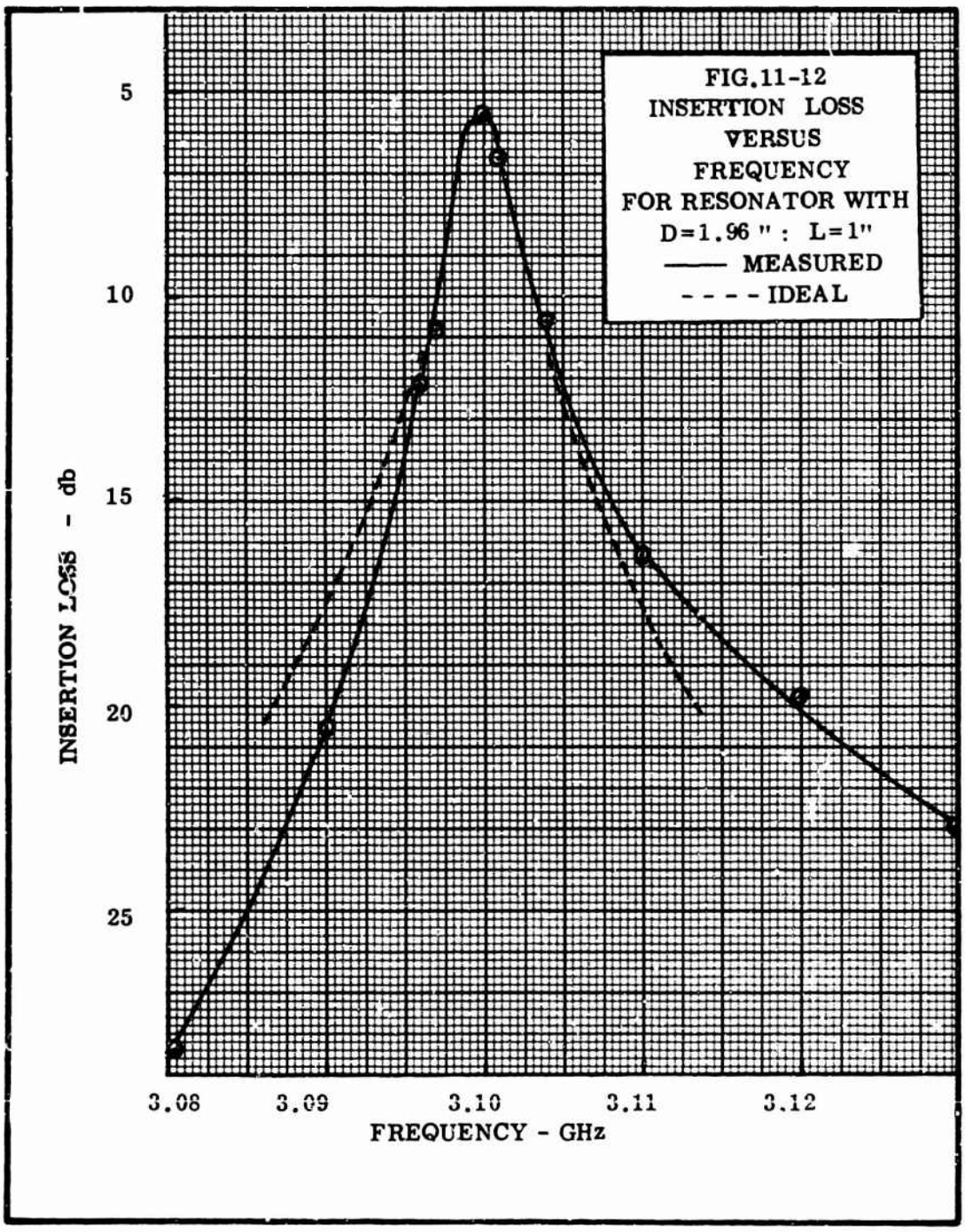
FIG.11-12
INSERTION LOSS
VERSUS
FREQUENCY
FOR RESONATOR WITH
D=1.96" : L=1"
—— MEASURED
- - - - IDEAL
INSERTION LOSS - db
5
10
15
20
25
3.08
3.09
3.10
3.11
3.12
FREQUENCY - GHz

A comparison between the two curves reveals that the measured insertion loss is larger at frequencies below resonance and smaller at frequencies above resonance than would be obtained for a symmetrical response curve. This effect might be due to some imperfection in the measuring system; however, the effect can also be explained, in part at least, by examining the theory developed for the cutoff-coupled dielectric filter.

It will be recalled that the resonance condition for this type of filter is

$$\tan \beta D = \frac{2\alpha\beta}{\beta^2-\alpha^2} \qquad (11\text{-}29)$$

However for conventional metal-walled resonators (all of which theoretically have perfectly symmetrical Q curves) the length D must be an integral number of half-wavelengths. That is:

$$\tan \beta D = 0 \qquad (11\text{-}29a)$$

where β is a function of frequency and can be said to be proportional to frequency over a fairly large range. The value of β versus frequency is shown in Fig. 11-13.

As the frequency is changed from the resonance condition of the above equations, the equations become inequalities. The difference between the right hand side and the left hand side of this inequality increases as the frequency deviation from resonance increases. This difference influences the response curve and hence the insertion loss of the resonator. Note that in Eq. 11-29a only the left side varies with frequency while in Eq. 11-29 the right side also varies with frequency. For the cutoff-coupled resonators tested here, α and β vary with frequency as shown in Fig. 11-13. It can be seen, from Fig. 11-13, that near 3.10 GHz, β is only slightly greater than α. Thus the product $\alpha\beta$ will be fairly constant with frequency while the difference $(\beta^2-\alpha^2)$ will be fairly small and will vary greatly with frequency near 3.10 GHz. For example, at 3.05 GHz, $(\beta^2-\alpha^2) = 7{,}600$, while at

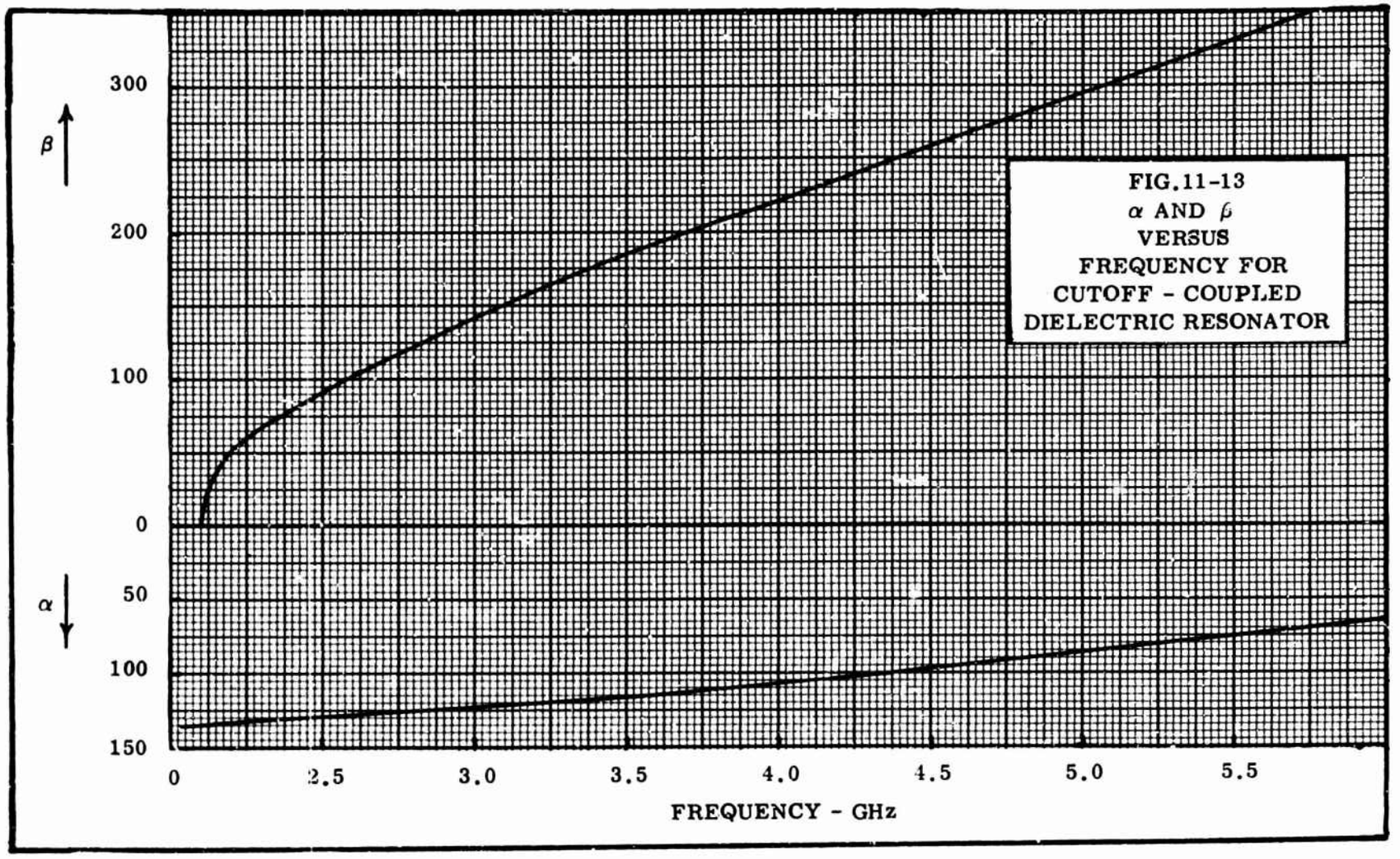

FIG. 11-13
α AND β
VERSUS
FREQUENCY FOR
CUTOFF - COUPLED
DIELECTRIC RESONATOR

3.15 GHz it is equal to 10,400. As the frequency f increases, β increases and α decreases. Thus, while the left side of Eq. 11-29 is increasing, the right side is decreasing. On the other hand as f decreases, α increases and β decreases and hence the left side of Eq. 11-29 decreases and the right side increases. Now since β is only slightly greater than α, the departure from the resonance condition of Eq. 11-29 occurs at a rate faster for decreasing values of f than it does for increasing values of f. This conclusion arrived at from Eq. 11-29 is borne out by the results of the measurements; that is, all measured response curves were unsymmetrical as predicted here.

2. Cascaded Resonator Filters

The theory of cascaded cutoff-coupled dielectric resonator filters presented in an earlier section was practically all qualitative. Thus it is not possible to design a cascaded resonator filter in as precise a manner as was done for the single stage filters.

In making up a cascaded resonator filter it is first necessary to fabricate two resonators with identical resonant frequencies. One of the resonators chosen for this was the resonator with D = 1.96" and L = 3/4". The other resonator used was tunable and had a D = 1.93" and L = 3/4". The construction of such a tunable resonator was described earlier.

Actually two such adjustable resonators were constructed originally, both with D = 1.96", and although they were constructed to be as nearly identical as possible, each behaved quite differently. One resonated at 3.076 GHz while the other resonated at 3.047 GHz (both measurements taken with the tuning screw turned all the way in). This behavior tends to confirm the previously stated suspicion that either the dielectric constant of the material used varies slightly from piece to piece or that small air gaps between the dielectric and the waveguide walls are sometimes present. To circumvent this uncertainty in f_r, the dielectric

pieces can be made somewhat longer than the calculated value of L and then sanded down in steps (checking f_r after each step) until f_r has increased to the desired value. For example, the adjustable resonator with f_r = 3.076 GHz was sanded down to 1.930". Then with its tuning screw turned all the way in f_r was 3.095 GHz, and with the screw all the way out f_r was 3.104 GHz.

The adjustable resonator and the fixed resonator with D = 1.96" and L = 3/4" were cascaded. That is, a cascaded filter was made up which consisted of a 3/4" cutoff section at the input, followed by the 1.93" propagating section with the adjustable tuning screw, followed by 1 1/2" of cutoff waveguide (3/4" from each of the two single stage filters), followed by the second fixed tuned 1.96" propagating section, and finally terminated by a 3/4" cutoff section at the output. The response curve of this cascaded filter was measured and is shown in Fig. 11-14.

While not changing anything else in this cascaded filter, the cutoff length L' between the two propagating resonant sections was decreased in steps from the 1 1/2" value. The measured response curve for L' = 0 is shown in Fig. 11-15. For all the values of L' tried the resulting values of f_r were recorded. These values of f_r versus L' are plotted in Fig. 11-16.

The experimental results obtained agree with the qualitative predictions made earlier. One of the more important predictions verified by the measurements was that f_r does vary with the cutoff length L' between the propagating resonant sections. For large L', f_r approaches the resonant frequency of the individual resonators. As L' is made smaller and approaches zero, f_r approaches the value for a single resonator whose propagating section has a length D equal to the sum of the two propagating section lengths making up in the cascaded filter. The resonator used in these measurements had an f_r = 3.305 GHz for L' = 0. If the α and β which correspond to this frequency (118.0 and 170.1

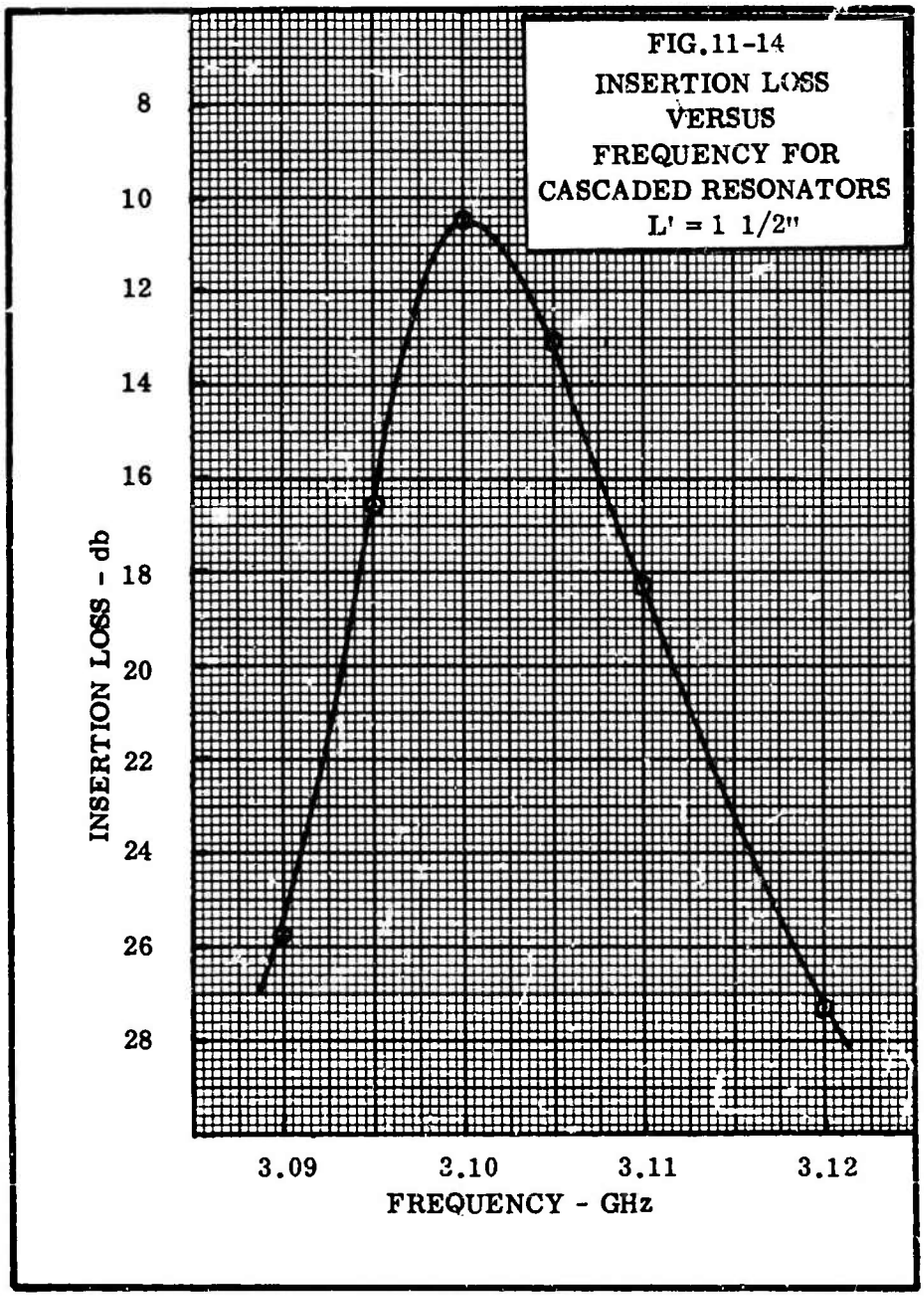
FIG.11-14
INSERTION LOSS
VERSUS
FREQUENCY FOR
CASCADED RESONATORS
L' = 1 1/2"
8
10
12
14
16
18
20
22
24
26
28
INSERTION LOSS - db
3.09
3.10
3.11
3.12
FREQUENCY - GHz

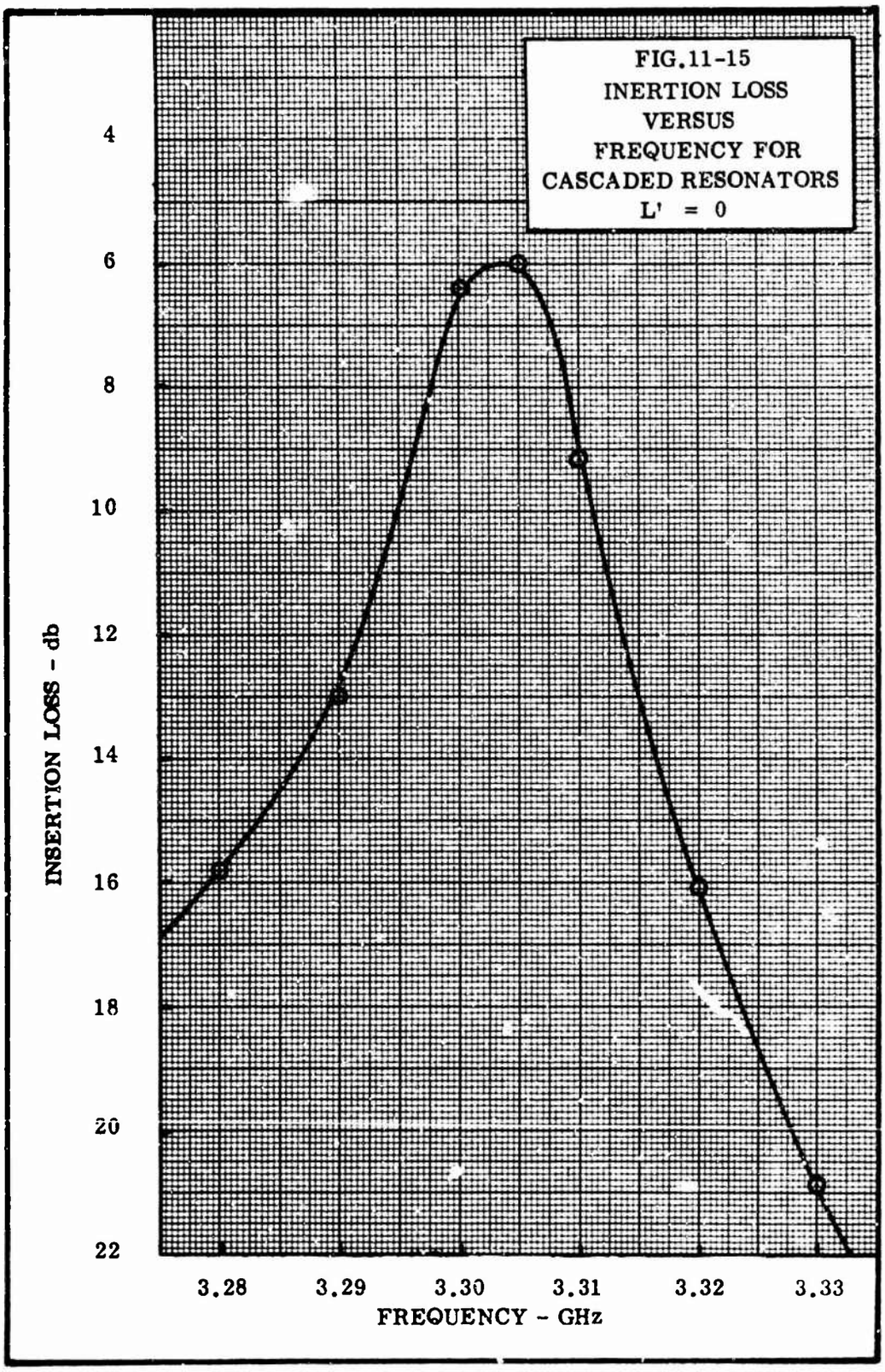
FIG.11-15
INERTION LOSS
VERSUS
FREQUENCY FOR
CASCADED RESONATORS
L' = 0
INSERTION LOSS - db
4
6
8
10
12
14
16
18
20
22
3.28
3.29
3.30
3.31
3.32
3.33
FREQUENCY - GHz

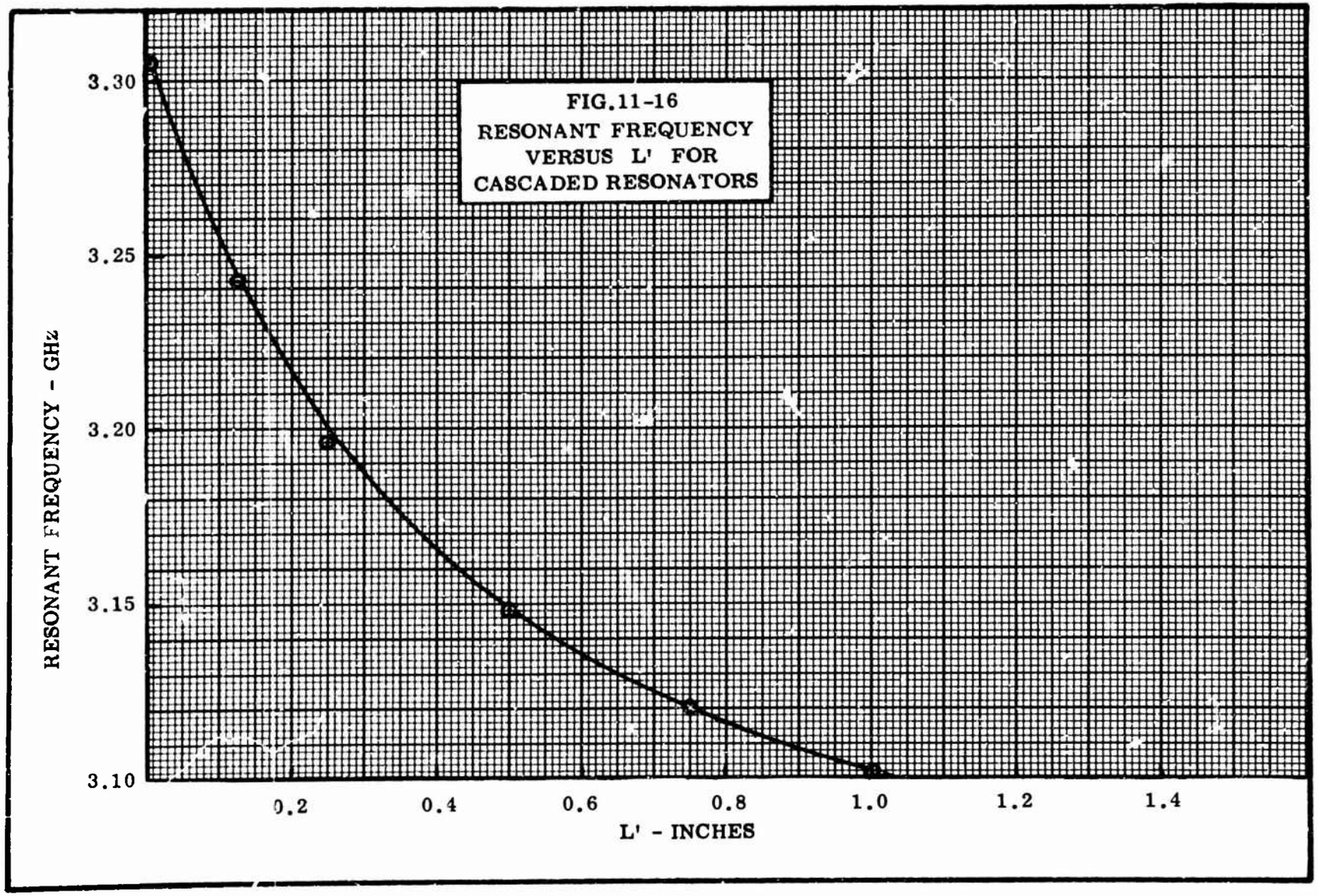
FIG.11-16
RESONANT FREQUENCY
VERSUS L' FOR
CASCADED RESONATORS
RESONANT FREQUENCY - GHz
3.30
3.25
3.20
3.15
3.10
0.2
0.4
0.6
0.8
1.0
1.2
1.4
L' - INCHES

respectively) and the total length D which is equal to 3.92" = 9.96 x 10^{-2} m are used in Eq. 11-29 the resonance condition is found to be satisfied. It is interesting to note that the relation between f_r and L' appears to be an exponential (Fig. 11-16). The relation can be expressed as:

$$f_r = 3.10 + 0.20\ \varepsilon^{-L'/0.34"}$$

where L' is in inches and f_r is in GHz. The values of f_r given by this empirical relation are almost identical to those plotted in Fig. 11-16.

The measurements made on the cascaded filter also verify the prediction that cascading results in an increase in Q_L. This behavior is not unlike that obtained for conventional filters. The Q_L of the cascaded filter calculated from Fig. 11-14 is 345. The Q_L of the adjustable resonator was found to be 258 while that of the fixed resonator was found earlier and is listed in Table 11-I as 260. Thus cascading these two resonators did result in a filter with a significantly higher Q_L.

Although cascading did increase Q_L, it could also have been increased by using a single stage filter with a longer cutoff section. The question arises as to whether a single stage filter can be made to have both a higher Q_L and a lower insertion loss at resonance than the cascaded filter. The cascaded filter used in these measurements had an insertion loss at resonance of 10.6 db (Fig. 11-14) and a Q_L of 345. However, the fixed resonator which was used in the cascade has a Q_L of 780 when used with cutoff sections 1 1/4" long (see Table 11-I). Furthermore, when the cutoff sections of the single stage filter were reduced to 1" a value of Q_L = 620 was obtained for an insertion loss at resonance of only 5.6 db. Thus it is possible for the single stage resonator to have a higher Q_L and a lower insertion loss at resonance than a filter made of two cascaded resonators.

XII. CONCLUSIONS AND RECOMMENDATIONS

The cutoff-coupled dielectric resonator can be used as a two port band pass filter. Its insertion loss varies with frequency in much the same manner as the insertion loss of a lumped parameter filter or of a conventional metal-walled microwave resonator.

The theory presented in this part of the report predicts the resonant frequency, the loaded Q_L, and the insertion loss at resonance of the cutoff-coupled dielectric resonator band pass filter. It was found that the cutoff-coupled resonator has a standing wave pattern at resonance which consists in general of a non-integral number of half wavelengths. This fact makes the calculation of the resonant frequency, the loaded Q_L, and the insertion loss at resonance somewhat more difficult than in the case of the conventional metal-walled microwave resonator.

Various cutoff-coupled bandpass filters were constructed for use at S-band. These filters were built with X-band waveguide, and ranged in length from about 2" to 5". A dielectric material with $\varepsilon_r = 10$ and a loss tangent = 0.0007 was used to fill the resonators. Measurements on these filters showed values of Q_L as high as 780. However, to obtain insertion losses at resonance of less than 2 db the Q_L had to be decreased to about 250 by shortening the lengths of the cutoff sections. The measured values of Q_L, f_r, and insertion loss at resonance agreed quite well with the values obtained by calculation using the theory. The measured response curves were however, always somewhat unsymmetrical about the resonant frequency. The unsymmetry is due at least in part to the variation of the propagation and attenuation constants with frequency.

Cascading of two cutoff-coupled dielectric resonator band pass filters was investigated. The theory and measurements show that the resonant frequency of the cascaded filter varies greatly with the length of the cutoff section between

the two propagating resonant sections. Prediction of the exact behavior of the cascaded cutoff-coupled filter was not fully accomplished due to the complexity of the problem.

The use of a cutoff-coupled dielectric resonator band pass filter instead of a conventional metal-walled filter may be advantageous in two ways. First, the cutoff-coupled filter is small in size. Secondly, it is highly compatible for use with dielectric-filled waveguide systems.

Further investigations in this area might include studies of other types of cutoff-coupled microwave filters, such as band rejection filters and branching filters. Also, some of the more difficult theoretical problems encountered in the present study might be investigated further, perhaps using computer techniques.

XIII. SELECTED BIBLIOGRAPHY

BOOKS:

Altman, Jerome L., Microwave Circuits. Princeton: D. Van Nostrand Company, 1964.
1964.

Atwater, H.A., Introduction to Microwave Theory. New York: McGraw-Hill Book Company, 1960.

Moore, Richard K., Traveling-Wave Engineering. New York: McGraw-Hill Book Company, 1960.

Plonsey, Robert and Collin, Robert E., Principles and Applications of Electromagnetic Fields. New York: McGraw-Hill Book Company, 1961.

PERIODICALS:

Goodwin, F.E. and Moss, G.E., "Broad-Band Impedance Matching into Dielectric-Filled Waveguides," IEEE Transactions on Microwave Theory and Techniques, Vol. MTT-11, No. 1, January 1963, pp. 36-39.

Part 3

RECTANGULAR BEAM WAVEGUIDE RESONATOR AND ANTENNA

Introduction

The study carried out during this phase of the research dealt with two general applications of the beam waveguide of rectangular symmetry. These were the rectangular beam waveguide resonator and the rectangular beam waveguide antenna formed from the resonator.

The field configurations inside the resonator were determined as were also the resonant frequencies. Design criteria, fabrication techniques, and methods of coupling to the resonator were devised. The predicted characteristics of the resonator developed from the resonator theory were verified experimentally.

The theory of the rectangular beam waveguide antenna was developed and an equivalent circuit of the cavity backed antenna was derived. Both slot and hole coupling were studied analytically and experimentally. Designs for exciting both the n=o and n=1 modes were worked out and the use of both of these modes for a monopulse radar antenna was investigated.

XIV. THEORY OF THE RECTANGULAR BEAM WAVEGUIDE RESONATOR

A. Beam Waveguide of Rectangular Symmetry

The beam waveguide of rectangular symmetry has been investigated theoretically by Schwering.[43] His investigation is based on the principle that the general solution for the fields in a source free region of free space can be obtained by a superposition of plane waves travelling in all directions. Restricting the direction of propagation of the plane waves to lie within a small

43. F. Schwering, "Reiterative Wave Beams of Rectangular Symmetry," Archiv der Elecktrischen Uebertragung, vol. 15, 1961, pp. 555-564.

angle around the beam axis permits an approximation to be made that results in the separation of the total field into two partial fields. One partial field has only E_x and H_y for transverse components:

$$E_x = \sum_{n,m=o}^{\infty} E^{(1)}_{n,m}(x,y,z)e^{-jkz}$$

$$H_y = \sqrt{\varepsilon_o/\mu_o}\ E_x \qquad (14\text{-}1)$$

where k = propagation constant in free space

μ_o = permeability of free space

ε_o = permittivity of free space

n and m are non-negative integers called mode numbers

The other partial field has only E_y and H_x for transverse components:

$$E_y = \sum_{n,m=o}^{\infty} E^{(2)}_{n,m}(x,y,z)e^{-jkz}$$

$$H_x = -\sqrt{\varepsilon_o/\mu_o}\ E_y \qquad (14\text{-}2)$$

To find an expression for the beam modes $E^{(1,2)}_{n,m}(x,y,z)$, the phase correction ψ made by each phase transformer shown in Fig. 14-1 is written as

$$\psi(x,y) = -\psi_o + \psi_x x^2 + \psi_y y^2 \qquad (14\text{-}3)$$

where ψ_o, ψ_x, ψ_y are constants

The special case $\psi_x = \psi_y$ corresponds to a beam waveguide of cylindrical symmetry. The values of ψ_x and ψ_y differ from each other for a beam waveguide of rectangular symmetry. It can be shown that the orthogonal beam modes of rectangular symmetry are described over the range $|z| \leq z_o$ by:

$$E^{(1,2)}_{n,m}(x,y,z) = \alpha^{(1,2)}_{n,m}\ \{[1 + (2u_o^2 z/k)^2]\ [1 + (2v_o^2 z/k)^2]\}^{-1/4} \cdot$$

$$He_n\left(\frac{2u_o x}{\sqrt{1+(2u_o^2 z/k)^2}}\right) \cdot He_m\left(\frac{2v_o y}{\sqrt{1+(2v_o^2 z/k)^2}}\right) \cdot$$

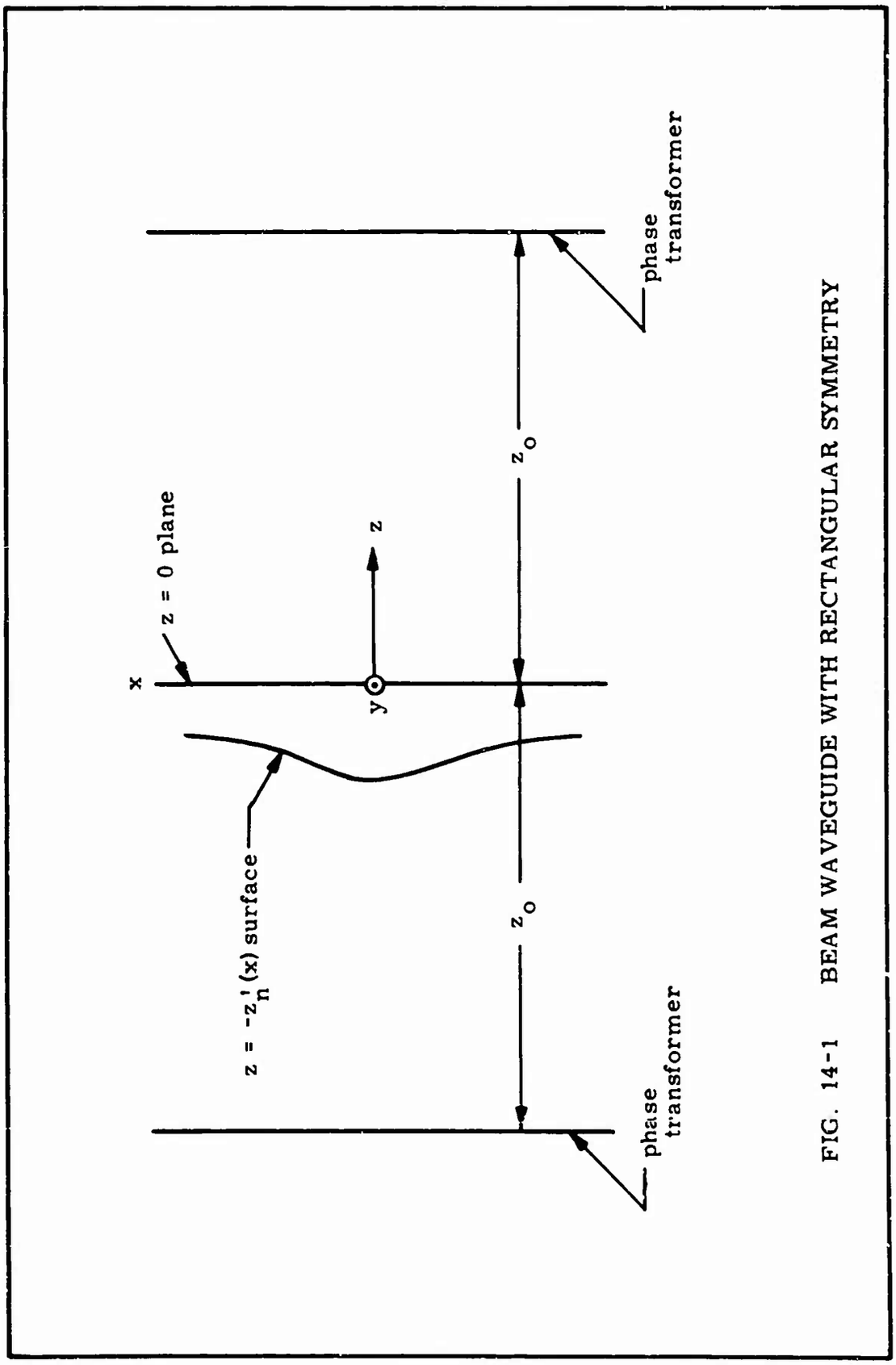

FIG. 14-1 BEAM WAVEGUIDE WITH RECTANGULAR SYMMETRY

$$\exp\left\{-\frac{u_o^2x^2}{1+(2u_o^2z/k)^2}-\frac{v_o^2y^2}{1+(2v_o^2z/k)^2}\right\}\cdot$$

$$\exp\left\{-j\left[\frac{2u_o^4zx^2/k}{1+(2u_o^2z/k)^2}+\frac{2v_o^4zy^2/k}{1+(2v_o^2z/k)^2}-(n+1/2)\arctan(2u_o^2z/k)-(m+1/2)\arctan(2v_o^2z/k)\right]\right\} \tag{14.4}$$

where u_o = parameter determining field variation along the x direction

v_o = parameter determining field variation along the y direction

He_n = Hermite polynomial of degree n

$\alpha_{n,m}$ = a constant amplitude factor depending in value on excitation method and shape of phase transformers

The total field is the superposition of all the beam modes with non-zero values of $\alpha_{n,m}$.

A useful dimensionless parameter w_o can be defined by

$$w_o = 2u_o^2z_o/k \tag{14-5}$$

A special case of a beam waveguide of rectangular symmetry occurs when v_o is set equal to zero. Equation 14-4 is then simplified substantially, and becomes

$$E_n^{(1,2)}(x,z) = \alpha_n^{(1,2)}\left[1+(2u_o^2z/k)^2\right]^{-1/4} He_n\left(\frac{2u_ox}{\sqrt{1+(2u_o^2z/k)^2}}\right)\cdot$$

$$\exp\left\{-\frac{u_o^2x^2}{1+(2u_o^2z/k)^2}-j\left[\frac{2u_o^4zx^2/k}{1+(2u_o^2z/k)^2}-(n+1/2)\arctan(2u_o^2z/k)\right]\right\} \tag{14-6}$$

Note that now the beam modes are independent of y. This y independence can be brought about by constructing the waveguide to be independent of y, that is, by letting the ψ_y of the phase transformers be zero.

B. Forming a Closed Resonator

Any waveguide may be formed into a resonator by placing short circuits along two phase fronts that are separated at resonance by $p\pi$ radians of phase

shift, where p is an integer. Phase fronts of the beam waveguide of rectangular symmetry are found using the equations of the previous section.

The case of a beam waveguide with $v_o = 0$ is the only one that will be treated in this report. Such a waveguide has the transverse electric field components of the nth mode given by Eqs. 14-1, 14-2, and 14-6 as:

$$E_{x,y} = \alpha_n^{(1,2)} [1+(2u_o^2 z/k)^2]^{-1/4} He_n\left(\frac{2u_o x}{\sqrt{1+(2u_o^2 z/k)^2}}\right) \exp\left\{-\frac{u_o^2 x^2}{1+(2u_o^2 z/k)^2}\right\}$$

$$\exp\left\{-j\left[\frac{2u_o^4 z x^2/k}{1+(2u_o^2 z/k)^2} - (n+1/2)\arctan(2u_o^2 z/k)\right]\right\}\exp(-jkz) \qquad (14\text{-}7)$$

The phase shift ϕ_n is thus

$$\phi_n = kz + \frac{2u_o^4 z x^2/k}{1+(2u_o^2 z/k)^2} - (n+1/2)\arctan(2u_o^2 z/k) \qquad (14\text{-}8)$$

Hence $\phi_{n\ z=0} = 0$. So the $z = 0$ plane is a surface of constant phase. This plane is chosen as the convenient position of one of the short circuits of the resonator. Then the other short circuit needed to make a resonator must lie along a phase front which at resonance has $\phi_n = p\pi$. Here the integer p is set equal to unity for the sake of making the resonator of small size. The surface with $\phi_n = \pi$ is denoted as the surface $z = -z_n'(x)$ shown in Fig. 14-1.

To find $z_n'(x)$ the following equation must be solved:

$$\pi = kz_n' + \frac{2u_o^4 z_n' x^2/k}{1+(2u_o^2 z/k)^2} - (n+1/2)\arctan(2u_o^2 z/k) \qquad (14\text{-}9)$$

Replacing u_o by w_o using Eq. 14-5 gives

$$\pi = kz_n' + \frac{kw_o^2 x^2 z_n'/2z_o^2}{1+w_o^2(z_n'/z_o)^2} - (n+1/2)\arctan(w_o z_n'/z_o) \qquad (14\text{-}10)$$

Generally z_o is many wavelengths long. Typically, z_o is at least 50λ, where λ is the wavelength. Now z_n' corresponds to π radians of phase shift, and so z_n' is approximated by $\lambda/2$. Thus if w_o is ten or less the maximum value of $(w_o z_n'/z_o)$ is about $(10(\lambda/2)/50\lambda) = 0.10$. Then

$$\arctan(w_o z_n'/z_o) \approx w_o z_n'/z_o$$

and $$1 + (w_o z_n'/z_o)^2 \leq 1.01 \simeq 1$$

hence $$\phi = \pi \simeq z_n' \left[k + k \frac{w_o^2 x^2}{2z_o^2} - (n+1/2) \frac{w_o}{z_o}\right] \tag{14-11}$$

Solving for the phase front surface $z_n'(x)$, the surface at which the short circuit must be placed, yields

$$z_n'(x) = \frac{\pi}{k \left[1 + \frac{w_o^2 x^2}{2z_o^2} - (n+1/2) \frac{w_o}{kz_o}\right]} \tag{14-12}$$

Using $k = 2\pi/\lambda$ gives

$$z_n'(x) = \frac{\lambda/2}{1 - (n+1/2)\frac{w_o}{kz_o} + \frac{w_o^2 x^2}{2z_o^2}} \tag{14-13}$$

Thus once w_o, n, z_o, and k are chosen, Eq. 14-12 may be used to determine $z_n'(x)$ for the resonator.

The positions of the two short circuits required for a resonator have now been established at $z = 0$ and $z = -z_n'(x)$, as sketched in Fig. 14-1. In practice these short circuits would consist of metal walls that approximate perfect conductors. The y independence of the resonator, because $v_o = 0$, dictates that both short circuits must extend to $y = +\infty$ and $y = -\infty$. This infinite extension is impractical, so some way is sought to confine the resonator to small y space while still having $v_o = 0$.

The method devised for limiting the y extension of the resonator is to place metal walls approximating perfect conductors at two constant y planes, $y = -h/2$ and $y = +h/2$. Figure 14-2 shows the rectangular beam waveguide resonator thus formed.

The boundary conditions at perfect conductors are well known,

$$\begin{aligned} \bar{n} \times \bar{E} &= 0 \\ \bar{n} \times \bar{H} &= \bar{J}_s \end{aligned} \tag{14-14}$$

where $\bar{n}$ is the unit vector normal to the conducting surface

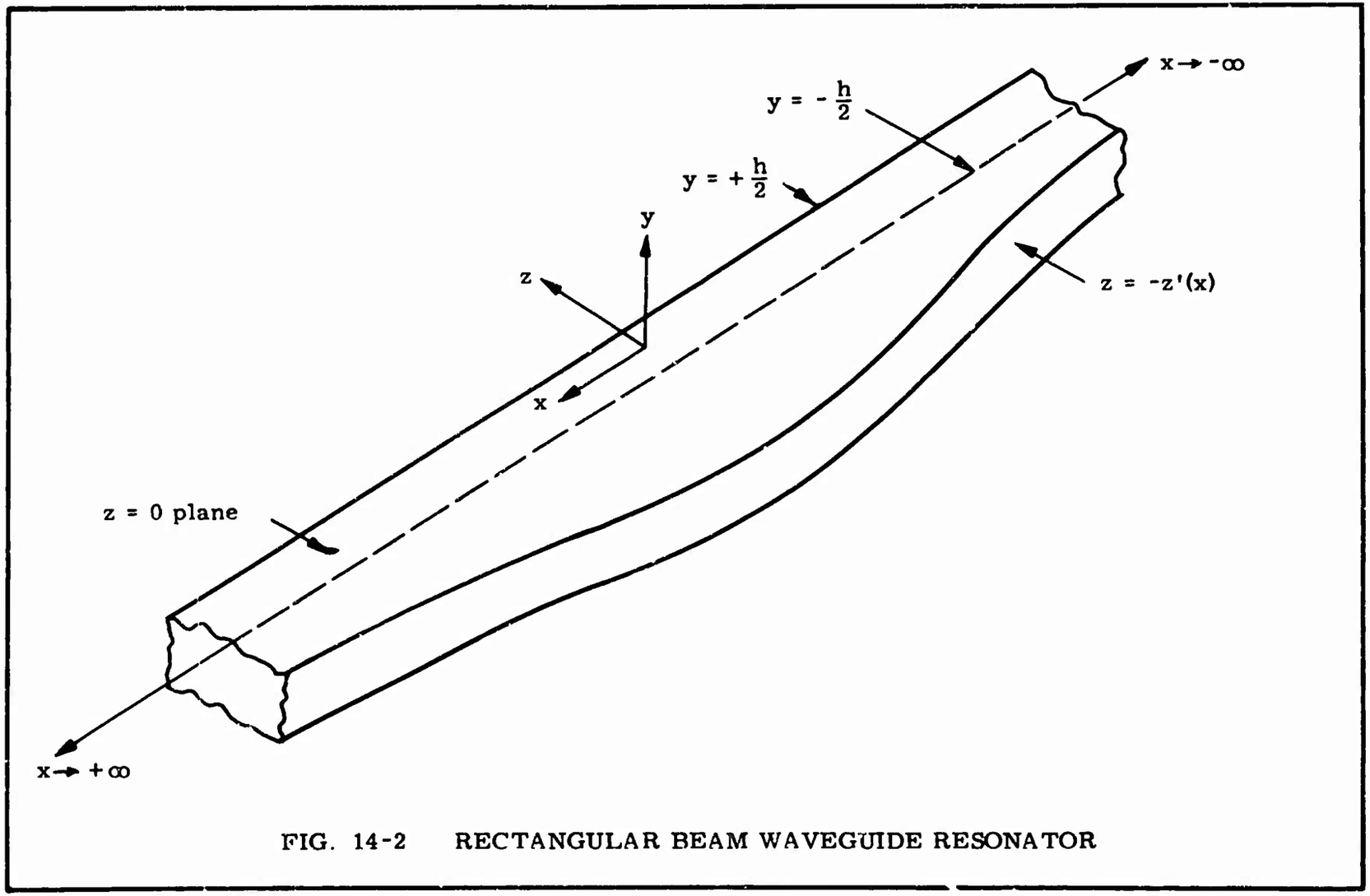

FIG. 14-2 RECTANGULAR BEAM WAVEGUIDE RESONATOR

and $\bar{J}_s$ is the surface current density in the conductor

Applying the first condition to the resonator walls at $y = + h/2, - h/2$ gives $E_x = E_z = 0$ at these two constant y planes. But since $v_o = 0$, the resonator fields are invariant with y, and thus E_x and E_z must be zero everywhere within the resonator. Then the partial field relation in Eq. 14-1 gives $H_y = 0$. The other transverse partial field consists of E_y and H_x as given by Eq. 14-2 and can exist in the resonator.

The only possible complication due to the introduction of the conducting planes at $y = + h/2, - h/2$. is the possibility of resonance between these parallel planes. Plane waves with $\bar{H} = H_o \bar{u}_x$ and $\bar{E} = E_o \bar{u}_z$ travelling in the $\pm y$ directions shown in Fig. 14-2 would resonate if $h = \lambda/2$ Note that H_o and E_o are constants. Such a resonance is not a rectangular wave beam resonance but is similar to an ordinary parallel-plane resonance. To avoid this spurious resonance, h must be restricted to $h < \lambda/2$ throughout the frequency range of interest.

C. Determination of Resonant Frequencies

The resonant frequencies of the rectangular beam waveguide resonator can be derived from Eq. 14-12 for $z_n'(x)$ in terms of k. Rearranging the equation gives k in terms of $z_n'(x)$:

$$k_n = \frac{\frac{\pi}{z_n'(x)} + (n + \frac{1}{2}) \frac{w_o}{z_o}}{1 + \frac{w_o^2 x^2}{2z_o^2}} \qquad (14\text{-}15)$$

Using $k = 2\pi f/c$,

$$f_n = \left[\frac{cz_o^2}{2\pi z_o^2 + \pi w_o^2 x^2}\right] \left[\frac{\pi}{z_n'(x)} + (n + \frac{1}{2}) \frac{w_o}{z_o}\right] \qquad (14\text{-}16)$$

Equation 14-16 can be put in a more convenient form by letting $x = 0$, thus

$$f_n = \frac{c}{2z_n'(0)} + (n + \frac{1}{2}) \frac{w_o c}{2 z_o} \tag{14-17}$$

The above expressions for the resonant frequencies raise the question as to whether a given resonator with a short circuit at $z_n'(x) = z_r'(x)$ has only a single resonant frequency denoted by f_r or whether there are also other resonant frequencies. For a mode to be in resonance the position $z_n''(x)$ of its phase front must coincide with the fixed reflecting surface $z'(x)$. If it is assumed that the reflecting surface $z'(x)$ has been calculated to be equal to the phase front of the $n = 0$ mode, then all n modes will be resonant in the resonator only if

$$z_n''(x) = z_o''(x)$$

Substituting in Eq. 14-17 gives

$$\frac{\pi}{k_n - (n + \frac{1}{2}) \frac{w_{on}}{z_o} + k_n \frac{w_{on}^2 x^2}{2z_o^2}} = \frac{\pi}{k_o - \frac{1}{2} \frac{w_{oo}}{z_o} + k_o \frac{w_{oo}^2 x^2}{2z_o^2}} \tag{14-18}$$

Let $\frac{w_{on}}{z_o}$ be denoted by p_n. The above equation is true for all x only if two conditions hold,

$$k_n - (n + \frac{1}{2}) p_n = k_o - \frac{1}{2} p_o \tag{14-19}$$

and

$$k_n p_n^2 = k_o p_o^2 \tag{14-20}$$

Substituting Eq. 14-20 in Eq. 14-19

$$k_n - (n + \frac{1}{2}) p_o \sqrt{k_o/k_n} = k_o - \frac{1}{2} p_o \tag{14-21}$$

Letting $k_n = k_o + \Delta k_n$,

$$\Delta k_n - (n + \tfrac{1}{2})\, p_o \sqrt{\frac{k_o}{k_o + k_n}} = -\tfrac{1}{2}\, p_o \qquad (14\text{-}22)$$

But for Δk_n small, which is true for small n, results in

$$\sqrt{\frac{k_o}{k_o + k_n}} \cong \sqrt{\frac{k_o - k_n}{k_o}} = \sqrt{1 - \frac{\Delta k_n}{k_o}} \cong 1\, \frac{\Delta k_n}{2k_o}$$

So Eq. 14-22 becomes

$$\Delta k_n - (n + \tfrac{1}{2})\, (1 - \frac{\Delta k_n}{2k_o})\, p_o = -\tfrac{1}{2}\, p_o$$

Thus

$$\Delta k_n - (n + \tfrac{1}{2})\, p_o + (n + \tfrac{1}{2})\, \frac{\Delta k_n}{2k_o}\, p_o = -\tfrac{1}{2}\, p_o$$

$$\Delta k_n + (n + \tfrac{1}{2})\, \frac{\Delta k_n}{2k_o}\, p_o = np_o$$

Finally, using $k = 2\pi f/c$,

$$\Delta f_n = \frac{np_o}{1 + (n + \frac{1}{2})\, \frac{p_o}{2k_o}} \cdot \frac{c}{2\pi} \qquad (14\text{-}23)$$

$$\text{where } \Delta f_n = f_n - f_o$$

Thus the resonant frequency f_n for any mode n is known in terms of f_o. All modes can resonate in the resonator with the fixed short circuits. Each mode however resonates at a different frequency f_n.

A simplified expression for Δf_n may be found for small n. Recall that z_o is at least 50λ and w_o is less than 10. Then for k_o corresponding to some microwave frequency and for n=10 or less

$$(n+1/2)\, \frac{p_o}{2k_o} << 1$$

Hence

$$\Delta f_n = \frac{cnw_o/z_o}{2\pi}$$

or if the quantity Δf is set equal to $f_{n+1}-f_n$, thus

$$\Delta f = \frac{cw_o}{2\pi z_o} \tag{14-24}$$

which is compatible with Eq. 14-17. Hence Eq. 14-17 is valid for f_n for n = 0 to at least 10 in a resonator built with a short circuit position at $z_n'(x) = z_o'(x)$.

There is another way of showing that Eq. 14-17 is valid for small values of n. From Eq. 14-20 it is obvious that w_{on} varies with f_n as,

$$w_{on} = D/\sqrt{f_n} \tag{14-25}$$

where D is a constant

Thus for a small frequency range, for example from 9.0 to 9.5 GHz, which corresponds to small values of n, w_{on} will be approximately the constant w_o. Then Eq. 14-19 gives once again that $\Delta f = cw_o/(2\pi z_o)$. In conclusion, Eq. 14-17 correctly gives the resonant frequencies of the rectangular beam waveguide resonator.

D. Resonator Field Configurations

Since it has been assumed that field variations in the y direction do not exist the only field variations that do exist are those in the x direction and those in the z direction. The z variation of the fields in the resonator is quite simple since it is known that the field near the plane z = 0 of Fig. 14-1 is approximately a plane wave of E_y and H_x travelling in the z direction, and that the phase shift the wave undergoes in travelling to the short circuit at $z'(x)$ is π radians. Thus the E_y and H_x field variations with z are sin $(\pi z/z')$ and cos $(\pi z/z')$ respectively.

The x variation of the fields is given by the equation for the beam modes of rectangular symmetry as ,

$$g(u_o x) = He_n \left[\frac{2u_o x}{\sqrt{1 + (2u_o^2 \frac{z}{k})^2}} \right] \varepsilon^{-\frac{u_o^2 x^2}{1 + (2u_o^2 \frac{z}{k})^2}} \varepsilon^{-j \frac{2u_o^4 \frac{z}{k} x^2}{1 + (2u_o^2 \frac{z}{k})^2}} \qquad (14\text{-}26)$$

where the He_n are Hermite polynomials of degree n.

It is important to note that there are at least two different types of Hermite polynomials in widespread use. The Hermite polynomials used for the rectangular beam waveguide for orders up to n=7 are,[44]

$$He_o(x) = 1,\ He_1(x) = x,\ He_2(x) = x^2 - 1$$
$$He_3(x) = x^3 - 3x,\ He_4(x) = x^4 - 6x^2 + 3$$
$$He_5(x) = x^5 - 10x^3 + 15x$$
$$He_6(x) = x^6 - 15x^4 + 45x^2 - 15$$
$$He_7(x) = x^7 - 21x^5 + 105x^3 - 105x$$

Since u_o^2/k is usually much grater than z', Eq. 14-26 may be written as,

$$|g(u_o x)| \cong He_n[2(u_o x)]e^{-(u_o x)^2} = g_n(u_o x) \qquad (14\text{-}27)$$

The function $g_n(u_o x)$ influences the coupling to each resonant mode and also determines the performance of the resonator as an antenna. Thus a plot of $g_n(u_o x)$ for various modes is of interest. An IBM 1620 computer was used to calculate $g_n(u_o x)$ for values of n = 0 to n = 7. The functions are plotted versus $u_o x$ for $x > 0$ in Figs. 14-3 through 14-10. The Hermite polynomials $He_n(2u_o x)$ are odd functions for n odd and even for n even, therefore

$$g(-u_o x) = g(u_o x) \text{ for n even}$$
$$\text{and } g(-u_o x) = -g(u_o x) \text{ for n odd.}$$

The graphs are not normalized since the various possible normalizations that could be made are all equally logical.

---

44. F. Schwering, "Reiterative Wave Beams of Rectangular Symmetry", Archiv der Elektrischen Uebertragung, vol. 15, 1961, pp. 557 and 564. W. Magnus and F. Oberhettinger, Functions of Mathematical Physics, Chelsea Publishing Co., Toronto, 1949, pp. 80-82.

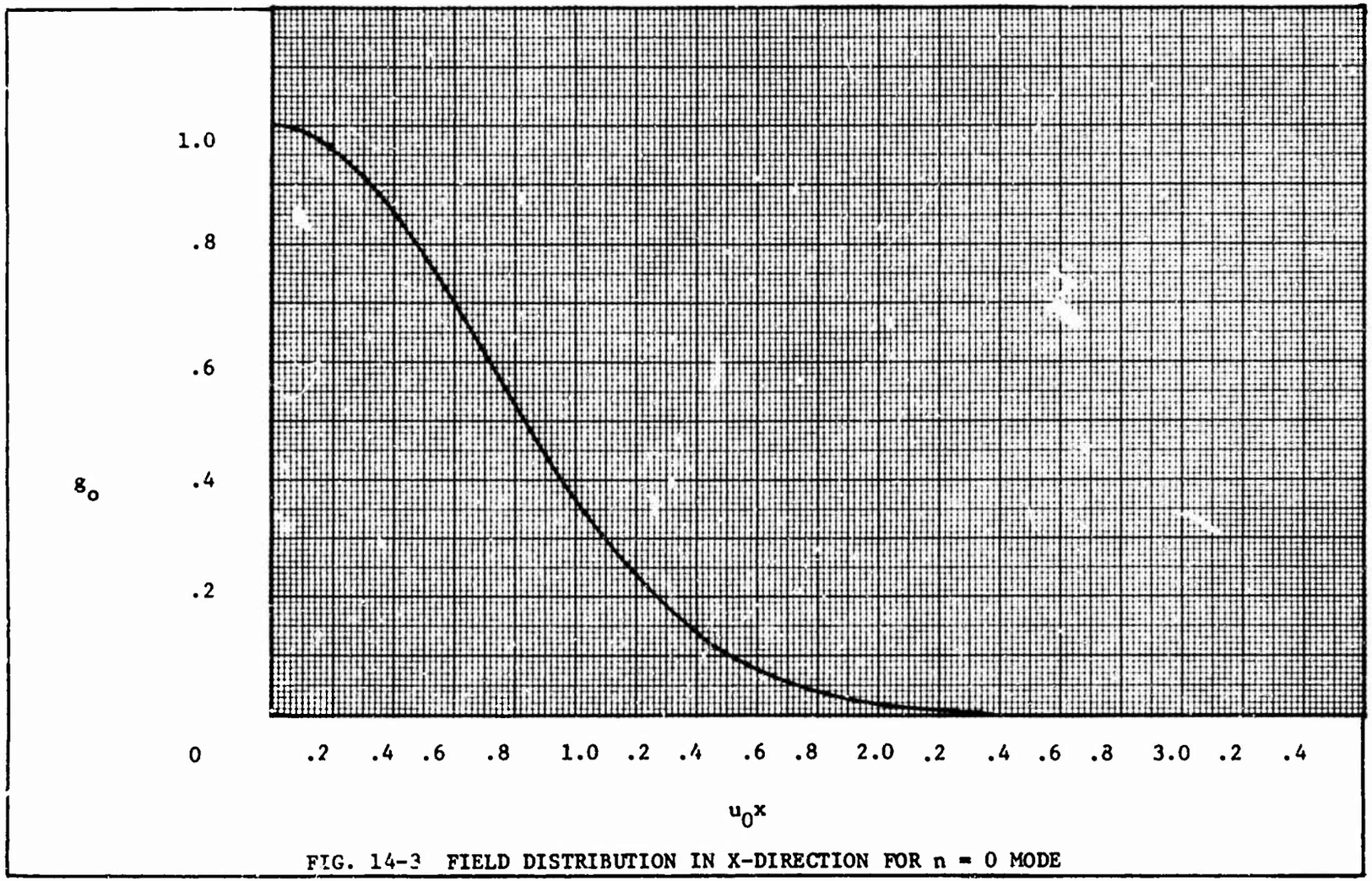

FIG. 14-3 FIELD DISTRIBUTION IN X-DIRECTION FOR n = 0 MODE

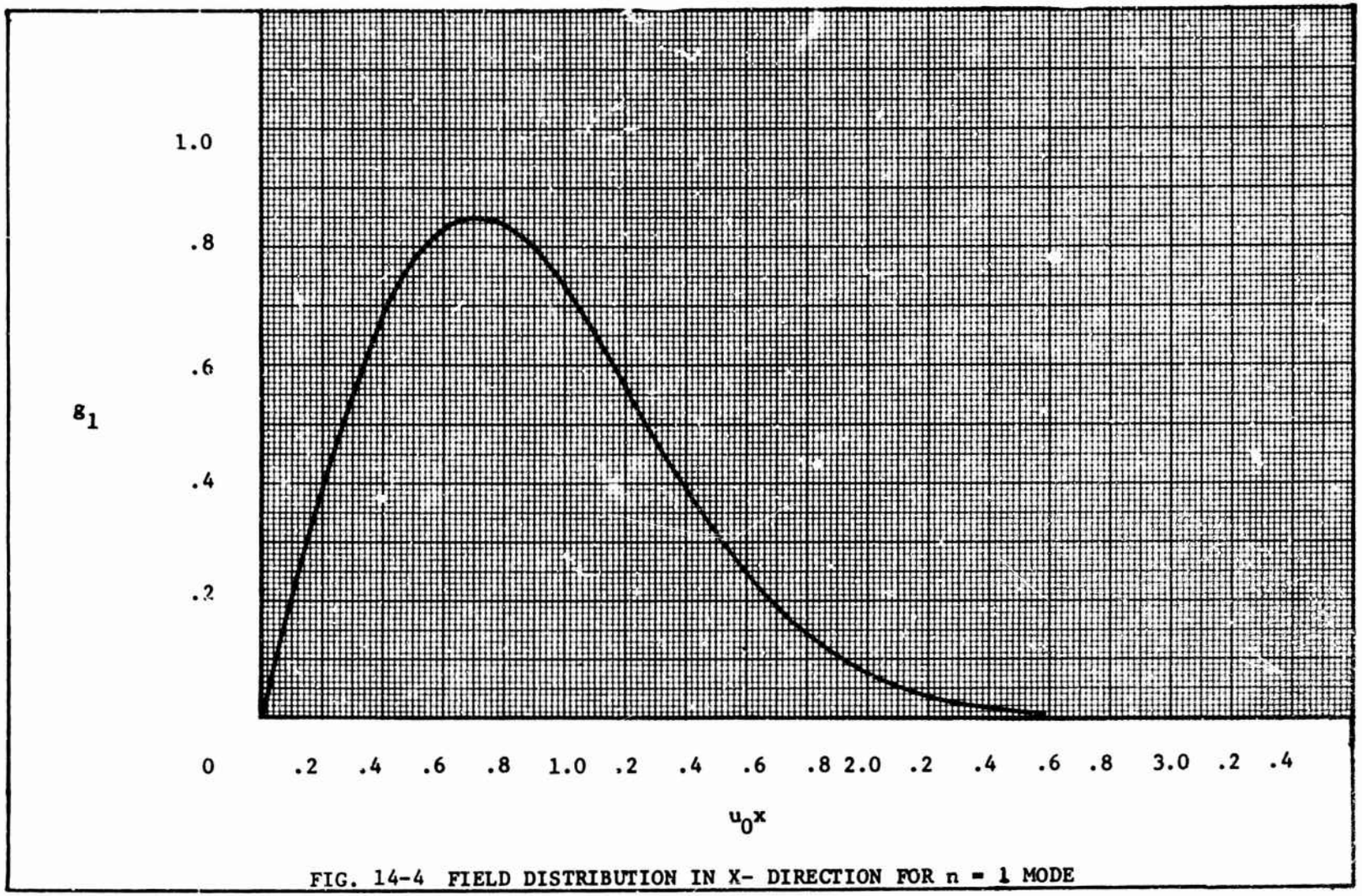

FIG. 14-4 FIELD DISTRIBUTION IN X- DIRECTION FOR n = 1 MODE

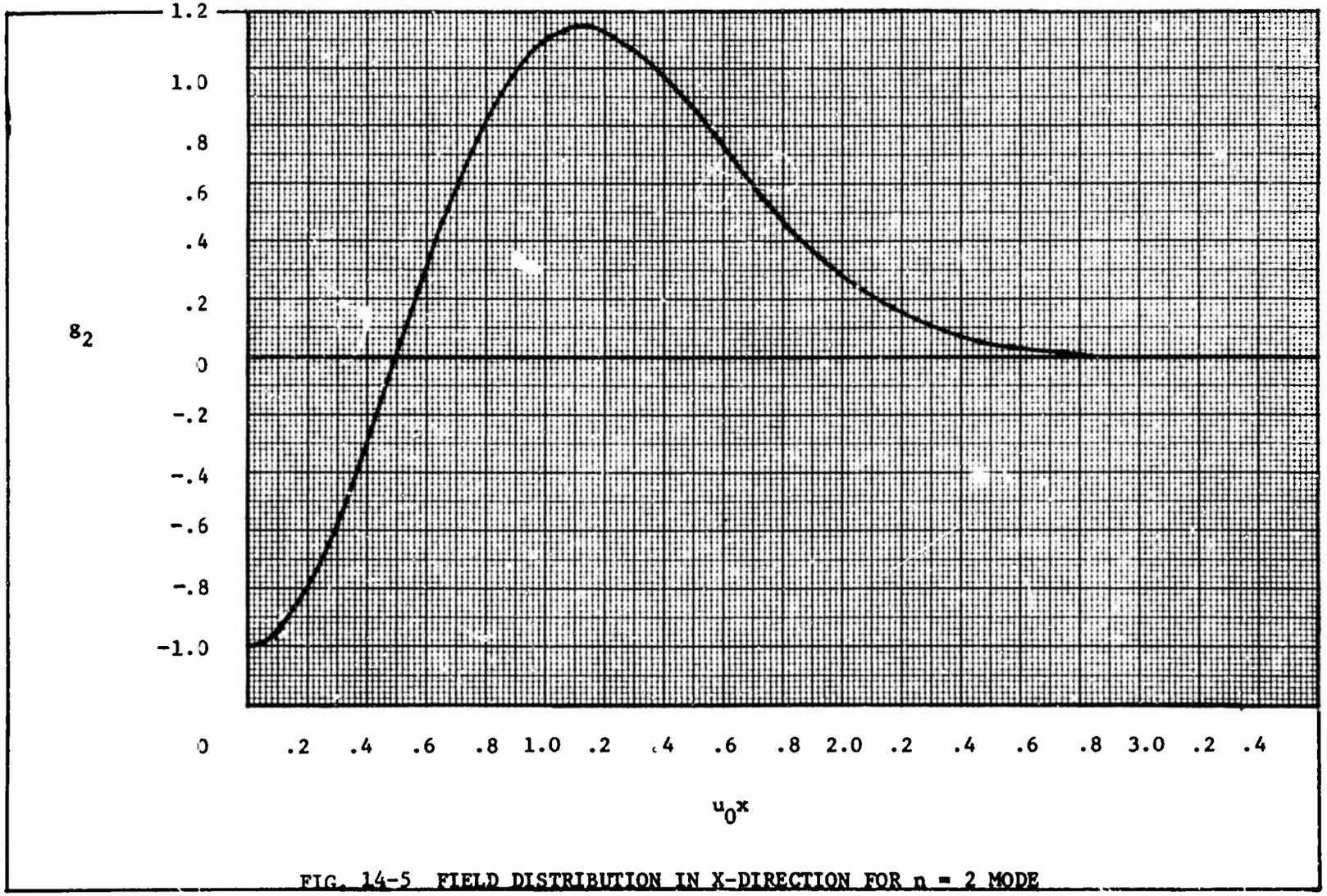

FIG. 14-5 FIELD DISTRIBUTION IN X-DIRECTION FOR n = 2 MODE

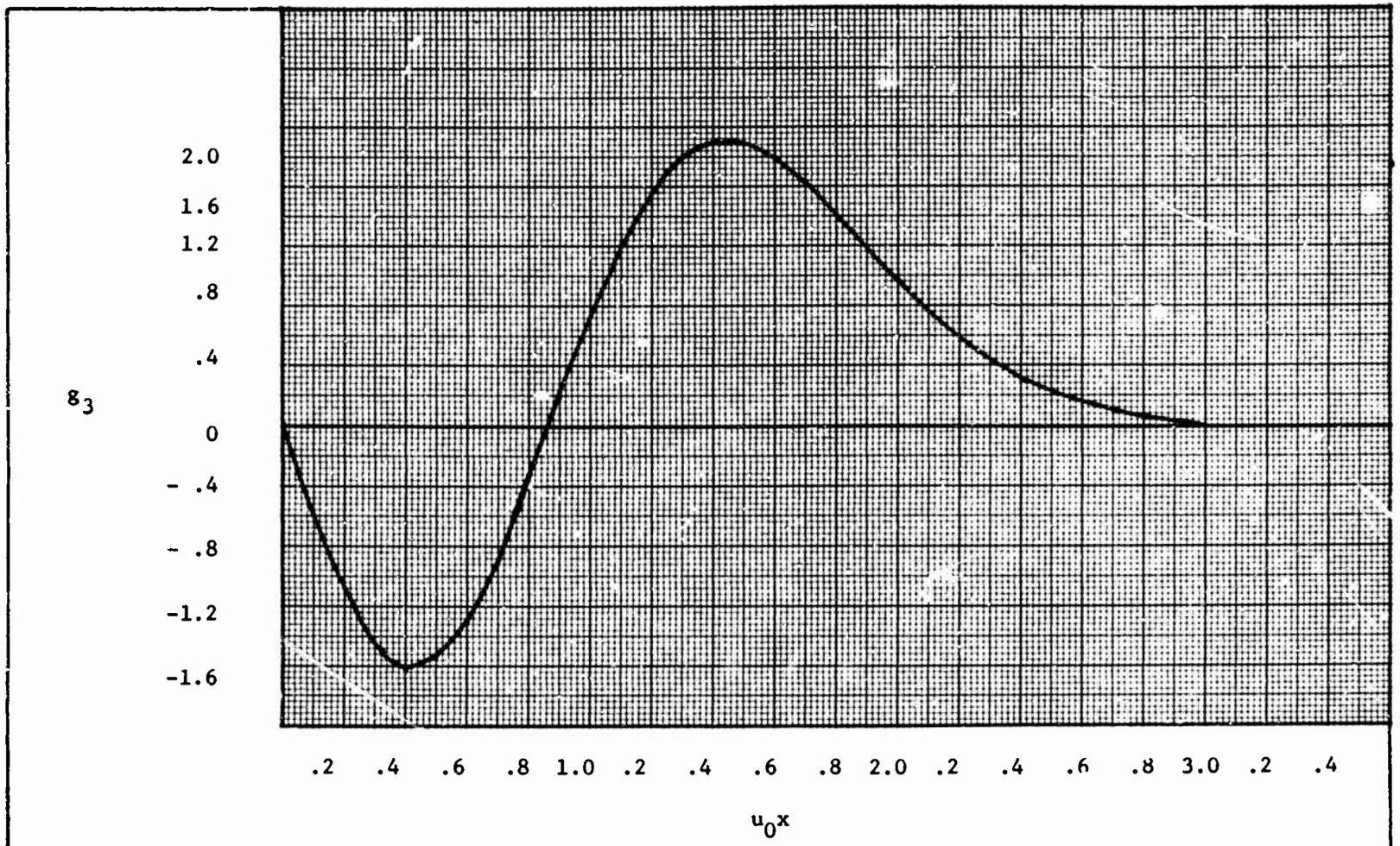

FIG. 14-6 FIELD DISTRIBUTION IN X-DIRECTION FOR n = 3 MODE

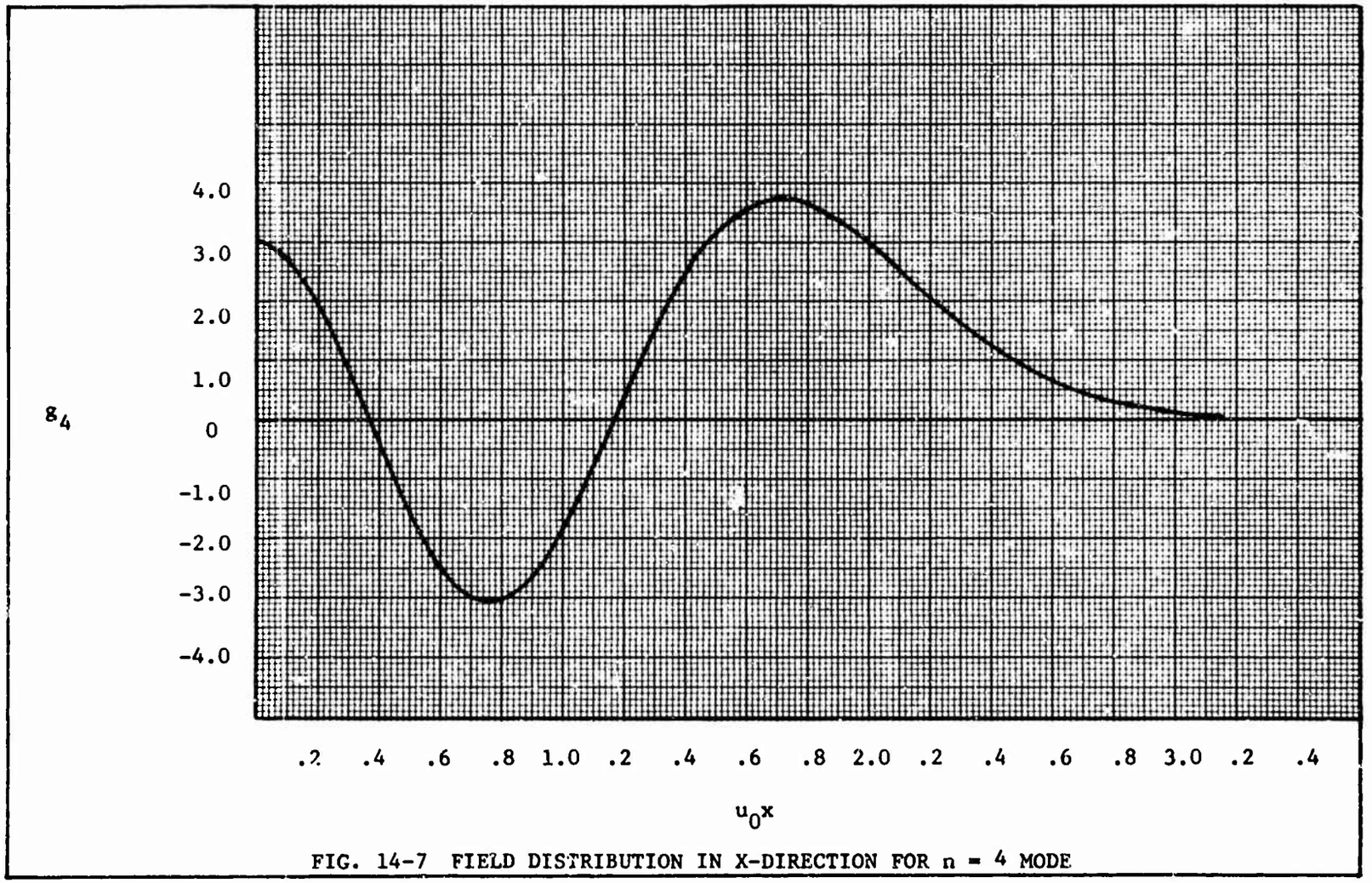

FIG. 14-7 FIELD DISTRIBUTION IN X-DIRECTION FOR n = 4 MODE

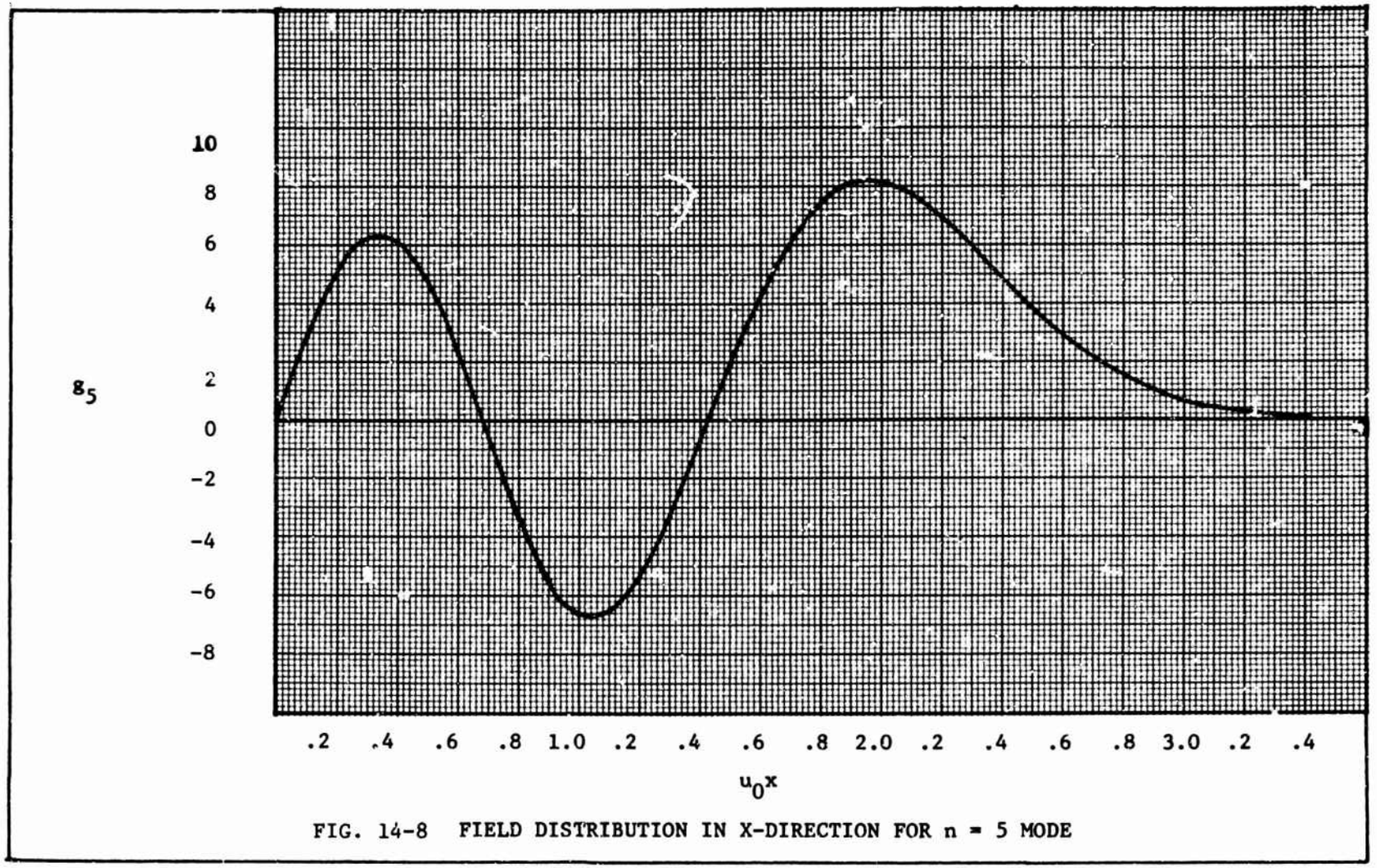

FIG. 14-8 FIELD DISTRIBUTION IN X-DIRECTION FOR n = 5 MODE

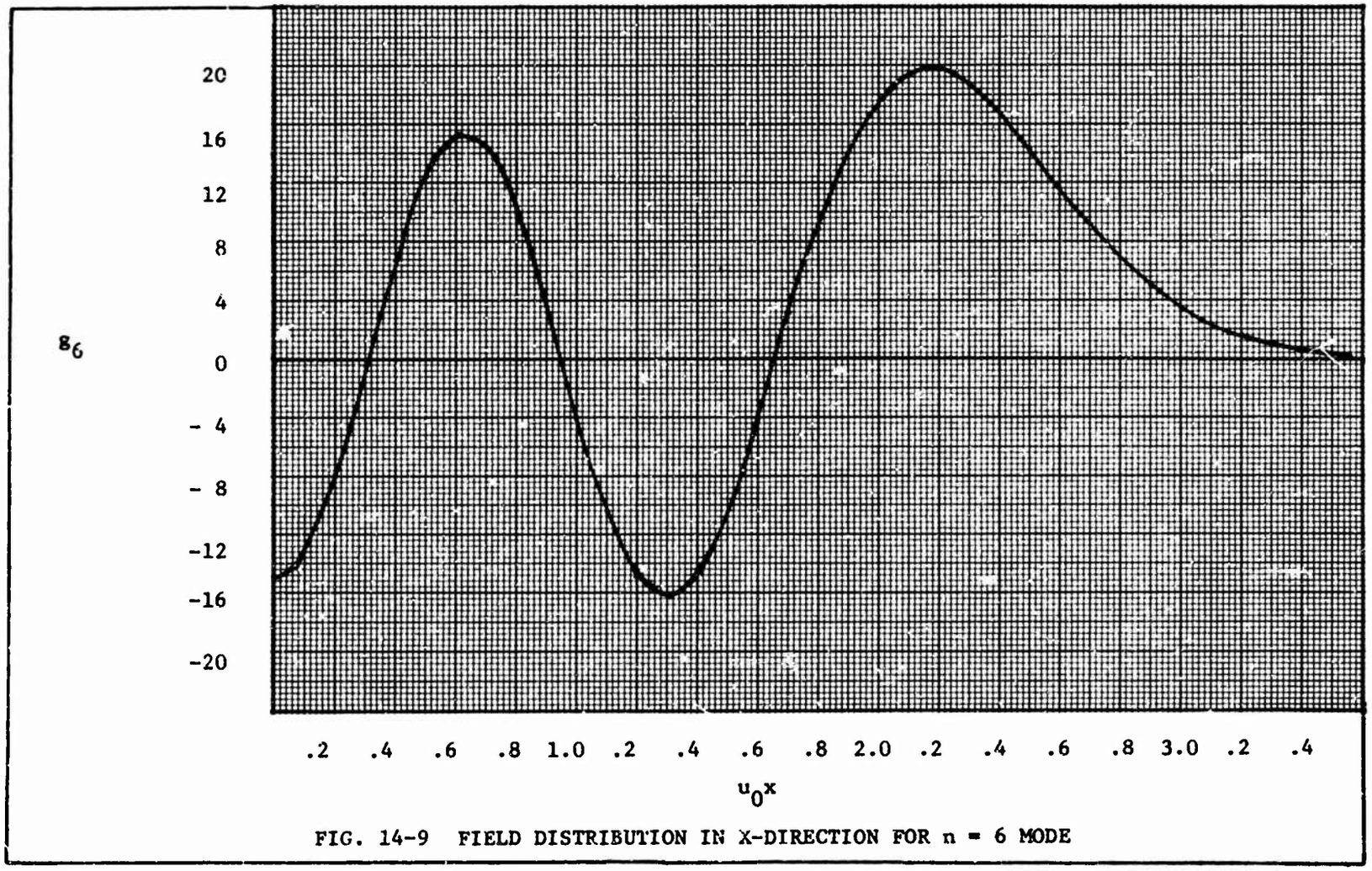

FIG. 14-9 FIELD DISTRIBUTION IN X-DIRECTION FOR n = 6 MODE

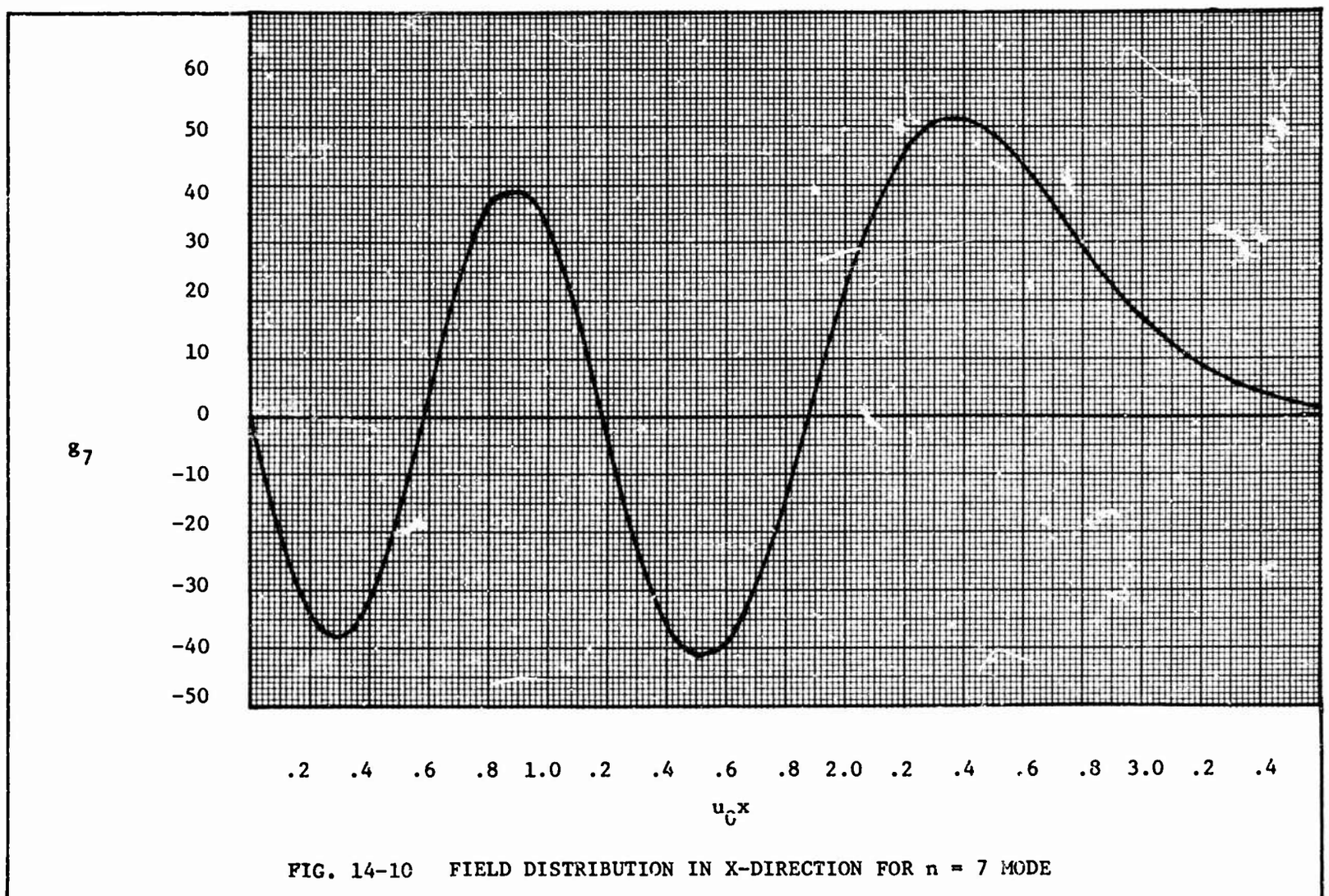

FIG. 14-10 FIELD DISTRIBUTION IN X-DIRECTION FOR n = 7 MODE

E. Theoretical Expression for Unloaded Q

The unloaded Q of a resonator is given by the well known expression

$$Q_{oo} = \omega_r \frac{W_s}{P_c} \tag{14-28}$$

where ω_r = resonant angular frequency

W_s = energy stored in resonator at resonance

P_c = power dissipated in resonator at resonance.

In an open resonator and particularly in a beam waveguide resonator three types of power dissipation may take place. They are diffraction loss, radiation loss due to the coupling structure and conduction loss in the resonator end plates. In the type of beam waveguide resonator being considered in the present study no radiation loss can take place. This will be true even if the resonator shown in Fig. 14-2 is of finite length in the $\pm$ x-direction. The length in a properly designed resonator is such that the openings at the ends are cutoff to waves in the $\pm$ x-direction. Some diffraction could take place; however the design is such that this loss is negligibly small. Thus the principal loss that must be accounted for is the copper loss in the four sides of the resonator. Equation 14-28 then can be written[45]

$$Q_{oo} = \omega_r \frac{\mu_o \int_V H^2 \, dV}{\int_S R \, H_{tan}^2 dS} \tag{14-29}$$

where V = volume of resonator

μ_o = permeability of air filling resonator

H_{tan} = tangential component of H at surface S

S = surface of all the metal walls that make up the resonator

$R = \sqrt{\frac{\omega_r \mu_o}{2\sigma}}$ = surface resistivity of metal walls where σ is the conductivity

45. H.A. Atwater, Introduction to Microwave Theory, McGraw-Hill Book Co., New York, New York, 1962, p. 145.

Now since the resonator fields do not vary in the y-direction

$$\int H^2 \, dV = h \int H^2 \, dx \, dz \tag{14-30}$$

If it is assumed that the walls in the planes y = constant have a surface with resistance R_1 and area S_1 and that the other walls have a surface with resistance R_2 and area S_2 then

$$\int_S R H_{tan}^2 \, dS = R_1 \int_{S_1} H_{tan}^2 \, dS_1 + R_2 h \int_s H_{tan}^2 \, dx \tag{14-31}$$

The energy stored and power lost calculated on the assumption of the existence in the resonator of plane waves very closely approximates the actual conditions in the rectangular beam waveguide resonator. Thus the H is

$$H = H_x = H_o \cos \frac{2\pi}{\lambda_o} z \; g(x) \tag{14-32}$$

where $H_o g(x)$ is the H field distribution along the plane z = 0

When this value for H is substituted in Eqs. 14-29, 30 and 31 the value for Q_{oo} is

$$Q_{oo} = \frac{\omega_r \mu_o h \int_x \int_{z=o}^{\lambda_o/2} H_o^2 \cos^2 \frac{2\pi}{\lambda_o} z \; g^2(x) \, dx \, dz}{2 R_1 \int_{z=o}^{\lambda_o/2} \int_x H_o^2 \cos^2 \frac{2\pi}{\lambda_o} z \; g^2(x) \, dx \, dz + 2 R_2 h \int_x H_o^2 \cos^2 \frac{2\pi}{\lambda_o} z \Big| g^2(x) dz \Big|_{z=o, \frac{\lambda_o}{2}}} \tag{14-33}$$

Now $H_o^2 \int_x g^2(x) \, dx$ is a common term and may be cancelled. Also

$$\int_o^{\lambda_o/2} \cos^2 \frac{2\pi}{\lambda_o} dz = \frac{\lambda_o}{4}$$

Thus Eq. 14-33 reduces to

$$Q_{oo} = \frac{\omega_r \mu_o \; h \frac{\lambda_o}{4}}{2R_1 \frac{\lambda_o}{4} + 2 R_2 h} \tag{14-34}$$

If $R_1 = R_2 = R$ then Q_u becomes

$$Q_{oo} = \frac{\omega_r \mu_o \; h \frac{\lambda_o}{2}}{R(\lambda_o + 4h)} \tag{14-35}$$

Note that Q_{oo} is independent of the mode number since g(x) does not appear in the equation.

F. Probe Coupling to Various Modes

The theory of a probe-coupled microwave resonator has been developed.[46] The equivalent lumped-parameter circuit is shown in Fig. 14-11 and the values of R, L, and C near the resonant frequency f_n of the nth mode are given by

$$R_n = \frac{Q_{oo}}{\omega_o}\left(\frac{a_n}{I}\right)^2 ; \quad L_n = \left(\frac{a_n}{I\omega_o}\right)^2 ; \quad C_n = \left(\frac{I}{a_n}\right)^2 \tag{14-36}$$

where $a_n = \int \bar{e}_n \cdot \bar{J} \cdot dV$ (14-37)

$\bar{e}_n$ = normalized electric field of n^{th} resonator mode

$\bar{J}$ = assumed current distribution on probe

I = input current to probe

V = volume of resonator

Now $\bar{e}_n$ must satisfy the orthogonality relationship,

$$\int \epsilon \, \bar{e}_n \cdot \bar{e}_m^* \, dV = \delta_{nm} = \begin{cases} 0 \text{ for } n \neq m \\ 1 \text{ for } n = m \end{cases} \tag{14-38}$$

It was shown in section D of this report that for the rectangular beam waveguide resonator the electric field is of the form,

$$\bar{e}_n = \bar{u}_y \, N_n \, He_n(2u_o x) \, e^{-u_o^2 x^2} \sin \frac{2\pi z}{\lambda_o} \tag{14-39}$$

where N_n is the normalizing constant.

Now $\bar{e}_n$ given by Eq. 14-39 must satisfy Eq. 14-38. To do this the integral of Eq. 14-38 must be evaluated.

$$\int_{z=o}^{z'(x)} \int_{y=-\frac{h}{2}}^{\frac{h}{2}} \int_{x=-\infty}^{\infty} N_n \, He_n(2u_o x) e^{-u_o^2 x^2} \; N_m \, He_m(2u_o x) e^{-u_o^2 x^2} \cdot \sin^2 \frac{2\pi z}{\lambda_o} \, dx \, dy \, dz$$

---

46. R.F. Harrington, Time-Harmonic Electromagnetic Fields, McGraw-Hill Book Company, New York, New York, 1961, pp. 431-436.

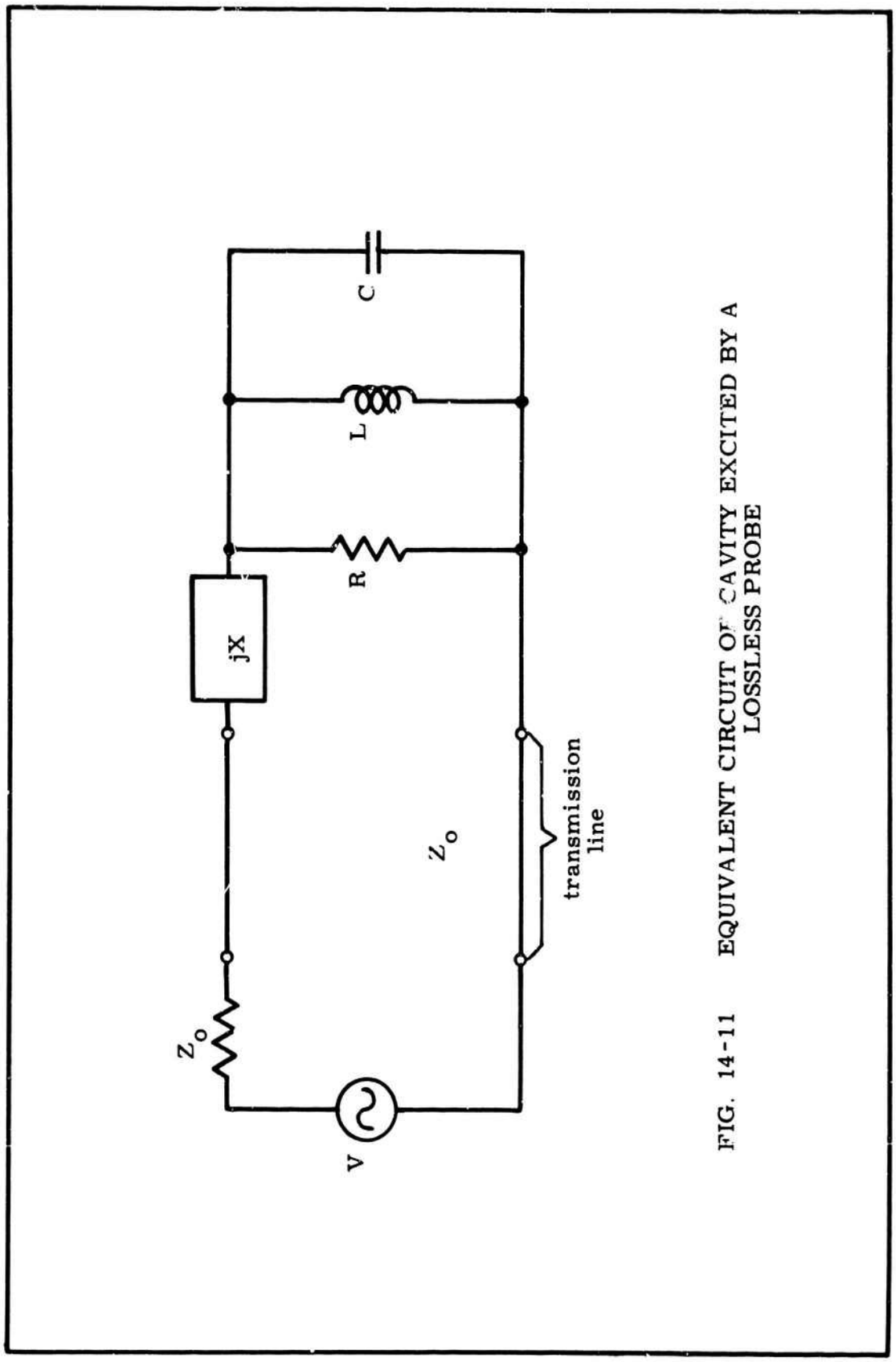

FIG. 14-11 EQUIVALENT CIRCUIT OF CAVITY EXCITED BY A LOSSLESS PROBE

When the approximation is made that z ranges from zero to $-z'(x) = -\lambda_o/2$ then

$$N_n N_m \epsilon h \int_{-\infty}^{\infty} He_n(2u_o x)\, He_m(2u_o x)\, e^{-2u_o^2 x^2}\, dx \int_{z=o}^{\lambda_o/2} \sin^2 \frac{2\pi}{\lambda_o} z\, dz \qquad (14\text{-}40)$$

Now [47]

$$\int_{-\infty}^{\infty} He_n(v)\, He_m(v)\, e^{-\frac{v^2}{2}}\, dv = n!\sqrt{2\pi}\,\delta_{nm}$$

Therefore

$$\int_{-\infty}^{\infty} He_n(2u_o x)\, He_m(2u_o x)\, e^{-2u_o^2 x^2}\, dx = \frac{n!}{u_o}\sqrt{\frac{\pi}{2}}\,\delta_{nm} \qquad (14\text{-}41)$$

Thus Eqs. 14-38 through 14-40 are valid for $n \neq m$. Equation 14-40 may be solved for N_n when $n=m$ thus

$$N_n^2\, \epsilon h \frac{\lambda_o}{4} \int_{-\infty}^{\infty} He_n^2(2u_o x)\, e^{-2u_o^2 x^2}\, dx = 1$$

or

$$N_n = \frac{1}{\sqrt{\epsilon h \frac{\lambda_o}{4} \int_{-\infty}^{\infty} He_n^2(2u_o x)\, e^{-2u_o^2 x^2}\, dx}}$$

$$N_n = \frac{1}{\sqrt{\epsilon h \frac{\lambda_o}{4} \frac{n!\sqrt{\pi}}{u_o\sqrt{2}}}} \qquad (14\text{-}42)$$

Now that $\bar{e}_n$ has been shown to satisfy the orthogonality relationship there remains the choice of a current distribution along the probe. A reasonable assumption appears to be that a standing wave of current of sinusoidal form exists along the probe.

$$\bar{J} = J_y \bar{u}_y = \begin{cases} I_n \dfrac{\sin k\,(y - \frac{h}{2} + d)}{\sin kd}\, \delta(x)\, \delta(z + \frac{\lambda_o}{4}) & \text{for } y > \frac{h}{2} - d \\ 0 & \text{for } y < \frac{h}{2} - d \end{cases} \qquad (14\text{-}43)$$

47. Second reference in footnote 44, p. 82.

where d is the probe depth, that is the extension of the probe from the wall at $y = +\frac{h}{2}$ to the length $y = +\frac{h}{2} - d$. It is also important to note that the probe is assumed to have a delta function dependence in the x and z directions in Eq. 14-43. This assumption makes the required integration much simpler but will affect the accuracy of the solution, since the probe does have a finite radius. Substituting Eqs. 14-39 and 14-43 into Eq. 14-37 gives,

$$a_n = \int_{z=0}^{\frac{\lambda_o}{2}} \int_{y=\frac{h}{2}-d}^{\frac{h}{2}} \int_{x=-\infty}^{\infty} \frac{He_n(2u_o x)\, e^{-u_o^2 x^2} \sin\frac{2\pi}{\lambda_o} z\, I_n \sin k(y - \frac{h}{2} + d)}{\sqrt{ch\,\frac{\lambda_o}{4}\int_{-\infty}^{\infty} He_n^2(2u_o x)\, e^{-2u_o^2 x^2}\, dx}\ \sin kd}$$

$$\cdot\delta(x)\ \delta(z + \frac{\lambda_o}{4})\ dx\ dy\ dz \qquad (14\text{-}44)$$

$$\frac{a_n}{I_n} = \frac{He_n(0)}{\sqrt{ch\,\frac{\lambda_o}{4}\int_{-\infty}^{\infty} He_n^2(2u_o x)\, e^{-2u_o^2 x^2}\, dx}} \int_0^{\frac{\lambda_o}{2}} \sin\frac{2\pi}{\lambda_o} z \cdot\delta\,(z - \frac{\lambda_o}{4})$$

$$\cdot\int_{\frac{h}{2}-d}^{\frac{h}{2}} \frac{\sin k(y - \frac{h}{2} + d)}{\sin kd}\ dy \qquad (14\text{-}45)$$

Now

$$\int_0^{\frac{\lambda_o}{2}} (\sin\frac{2\pi}{\lambda_o} z)\ \cdot\delta(z - \frac{\lambda_o}{4})\ dz = \sin\frac{\pi}{2} = 1$$

and

$$\int_{\frac{h}{2}-d}^{\frac{h}{2}} \frac{\sin k\left(y-\frac{h}{2}+d\right)}{\sin kd}\,dy = \int_0^{kd} \frac{\sin u}{\sin kd}\,\frac{du}{k} \tag{14-46}$$

$$= -\frac{(1-\cos kd)}{k \sin kd}$$

$$= -\frac{1}{k}\tan\frac{kd}{2}$$

Therefore

$$\frac{a_n}{I_n} = \frac{-He_n(0)\tan\frac{kd}{2}}{k\sqrt{\epsilon h\,\frac{\lambda_o}{4}\int_{-\infty}^{\infty} He_n^2(2u_o x)\,e^{-2u_o^2x^2}\,dx}} \tag{14-47}$$

Substituting this result into Eq. 14-36 for R_n yields

$$R_n = \frac{Q_{oo}}{\omega_o}\left(\frac{He_n^2(0)\tan^2\frac{kd}{2}}{k^2\epsilon h\,\frac{\lambda_o}{4}\int_{-\infty}^{\infty} He_n^2(2u_o x)\,e^{-2u_o^2x^2}\,dx}\right) \tag{14-48}$$

Using Eq. 14-41 gives

$$R_n = \frac{Q_{oo}}{\omega_n}\,\frac{He_n^2(0)\tan^2(kd/2)}{k^2\epsilon h(\lambda_o/4)\,\frac{n!}{u_o}\sqrt{\pi/2}} \tag{14-49}$$

At a resonant frequency f_n the net reactance of the L-C combination in the equivalent circuit is zero. Thus the equivalent circuit of the rectangular beam waveguide resonator at resonance is simply the resistor R_n of value given by Eq. 14-49. For a transmission line of characteristic impedance Z_o feeding the probe, the reflection coefficient at f_n is thus

$$\rho_o\Big|_n = (R_n - Z_o)/(R_n + Z_o) \tag{14-50}$$

Critical coupling, for which $\rho_o = 0$, will then occur at a different probe depth for each mode. Critical coupling to the nth mode means that

$$Z_o = \frac{Q_{oo}}{\omega_o}\left[\frac{He_n^2(0)\,\tan^2\frac{kd}{2}}{k^2\varepsilon h\,\frac{\lambda_o}{4}\int_{-\infty}^{\infty} He_n^2(2u_o x)\,e^{-2u_o^2x^2}\,dx}\right] \tag{14-51}$$

or

$$\frac{Z_o\omega_o k^2\varepsilon h\,\frac{\lambda_o}{4}}{Q_{oo}} = \text{constant} = \left[\frac{He_n^2(0)}{\int_{-\infty}^{\infty} He_n^2(2u_o x)\,e^{-2u_o^2x^2}\,dx}\right]\tan^2\frac{kd}{2} \tag{14-52}$$

The terms on the left hand side of Eq. 14-52 are approximately constant at least for the first 8 modes. Equation 14-52 reveals that as the probe depth d is increased from zero the first mode to become critically coupled is the one which yields the largest value of

$$\frac{He_n^2(0)}{\int_{-\infty}^{\infty} He_n^2(2u_o x)\,e^{-2u_o^2x^2}\,dx} = \frac{\text{energy density at probe}}{\text{integral of energy density (x-direction)}}$$

$$= \frac{He_n^2(0)}{\frac{n!}{u_o}\sqrt{\frac{\pi}{2}}}$$

$$= \text{normalized energy density at probe}$$

$$= u_{pn} \tag{14-53}$$

The next mode that would change from undercoupling to critical coupling would be the mode with the second largest value of normalized energy density at the probe. Thus, it may be concluded that as the probe penetrates into the resonator the modes become critically coupled in sequence n=n', n'', n''', ..., where $u_{pn'} > u_{pn''} > u_{pn'''} > \ldots$. This observation bears out what would be expected from physical considerations namely, that the mode which has its

energy concentrated in the vicinity of the probe would become critically coupled at a smaller probe depth than a mode which has its energy concentration more remote from the probe.

In general the equivalent circuit of Fig. 14-11 has a probe reactance jX inserted as shown. Thus near each resonant frequency the equivalent circuit consists of R_n in series with jX. The result is a detuning effect due to the reactance and a slight altering of the resonant frequency. At resonance however, the input impedance at the probe is just R_n.

XV. MEASUREMENTS MADE ON A BEAM WAVEGUIDE RESONATOR

A. Design

The theory developed for the beam waveguide resonator was to be verified. To do this a rectangular beam waveguide resonator was designed and fabricated which had a resonant frequency for the n=o mode near 9.0 GHz.

The most important parameter in the design of the resonator is the ratio (w_o/z_o). This ratio determines both the frequency spacing between modes and the spread (standard deviation) of the Gaussian field amplitude distribution in the x-direction for the n=o mode. The value for z_o was chosen equal to 100λ which at a frequency of 9.0 GHz results in $z_o = 3.33$ meters. A value for $w_o = 5$ was chosen since this resulted in a reasonable value for Δf of 72 MHz as determined from Eq. 14-22. The amplitude of the field as a function of x for the n=o mode is

$$g_o(x) = \epsilon^{-\frac{kw_o}{2z_o}x^2} \tag{15-1}$$

Thus the amplitude will be only $1/\epsilon$ of its maximum value at a distance $x(1/\epsilon) = 0.084$ meters from the center of resonator shown in Fig. 14-2. At a distance of x=15 inches or 0.381 meters

$$f(x) = \epsilon^{-(0.381)^2/(0.084)^2} = \epsilon^{-20.6} = 10^{-11}$$

The larger the value chosen for the ratio (w_o/z_o) the larger Δf will be and the smaller $x(1/\epsilon)$ will be. The value of (w_o/z_o) cannot be made too large without violating one of the conditions assumed in the solution for the beam modes. The beam modes for the confocal case for which $w_o = 1$ were derived on the condition that z_o be of the order of $50/\lambda$ so that (w_o/z_o) has a maximum value of about $(1/50\lambda)$. Since $w_o=5$ and $z_o=100\lambda$, which are the values chosen for the present design, result in a value for (w_o/z_o) of $(1/20\lambda)$ the question of the validity of the mode solution arises. It will be assumed for the present that the value of $(1/20\lambda)$ is a reasonable upper bound for (w_o/z_o). Thus the corresponding value of $\Delta f = 72$ MHz for $f = 9.0$ GHz will also be considered an upper bound.

The equation for the curved surface $z'(x)$ of the resonator must be known so that this surface can be machined. The curve for the n=o mode can be calculated by substituting $(w_o/z_o) = (1/20\lambda)$ and $f = 9.0$ GHz into Eq. 14-12,

$$z'(x) = \frac{0.66}{1+7.42\times10^{-4}x^2} \qquad (15\text{-}2)$$

where $z'(x)$ and x are in inches for convenience of the machinist

Several factors must be taken into consideration when deciding on the distance the resonator is to extend in the x-direction. A previous calculation showed that at x=15 inches the amplitude of the field was only 10^{-11} of the amplitude at the center of the resonator. Thus if the resonator was made 15 inches on each side of center the total length of 30 inches would still be a convenient size for machining. Finally, the value $z_n'(x=L/2=15")$ is 0.565".

The corresponding cutoff frequency $f_c = c/(2z'_n(L/2)) = 10.50$ GHz, which is sufficiently high to prevent any waves of interest from escaping out the ends. Hence L was chosen to be 30".

The value chosen for the resonator height h was 3/8". This dimension is considerably smaller than $\lambda/2$ anywhere in the X band range and thus parallel-plate resonances should be impossible. The height is still large enough to give the resonator reasonable volume.

B. Fabrication

The resonator was made out of a 1 1/8" x 3" x 30" piece of brass stock and a 1 1/2" x 1/4" x 30" brass strip. The large piece of brass had a trough milled into it thus forming the three surfaces z'(x), y = + 3/16" and y = - 3/16". The trough was milled using a 3/8" x 1" diameter side cutter. The depth of cut was determined from values calculated with the aid of Eq. 15-2. The curve z'(x) is so gradual that z'(x) was approximated by cutting steps spaced one inch apart. The steps were rounded off because of the size of the milling cutter and a very smooth curve resulted all the way from z'(0") where the depth of cut was 0.66 inches to z'(15") were the depth of cut was 0.565 inches. The brass strip which formed the fourth wall of the resonator at the plane z=o was attached with screws spaced every 3/4" in the x-direction and in two rows y = $\pm$ 3/8". The resonator was made with care since dimensions were to be held to within one or two thousands of an inch. The resonator was also designed to be rigid enough to resist warping and is the reason that, although the maximum depth of the trough is only 0.66 inches, the dimension of the brass block along the z-axis was 3 inches. The photograph of the completed resonator is shown in Fig. 15-1.

The coupling arrangement to the x-band waveguide is also shown in Fig. 15-1. The coaxial to waveguide junction has its type N plug converted to a

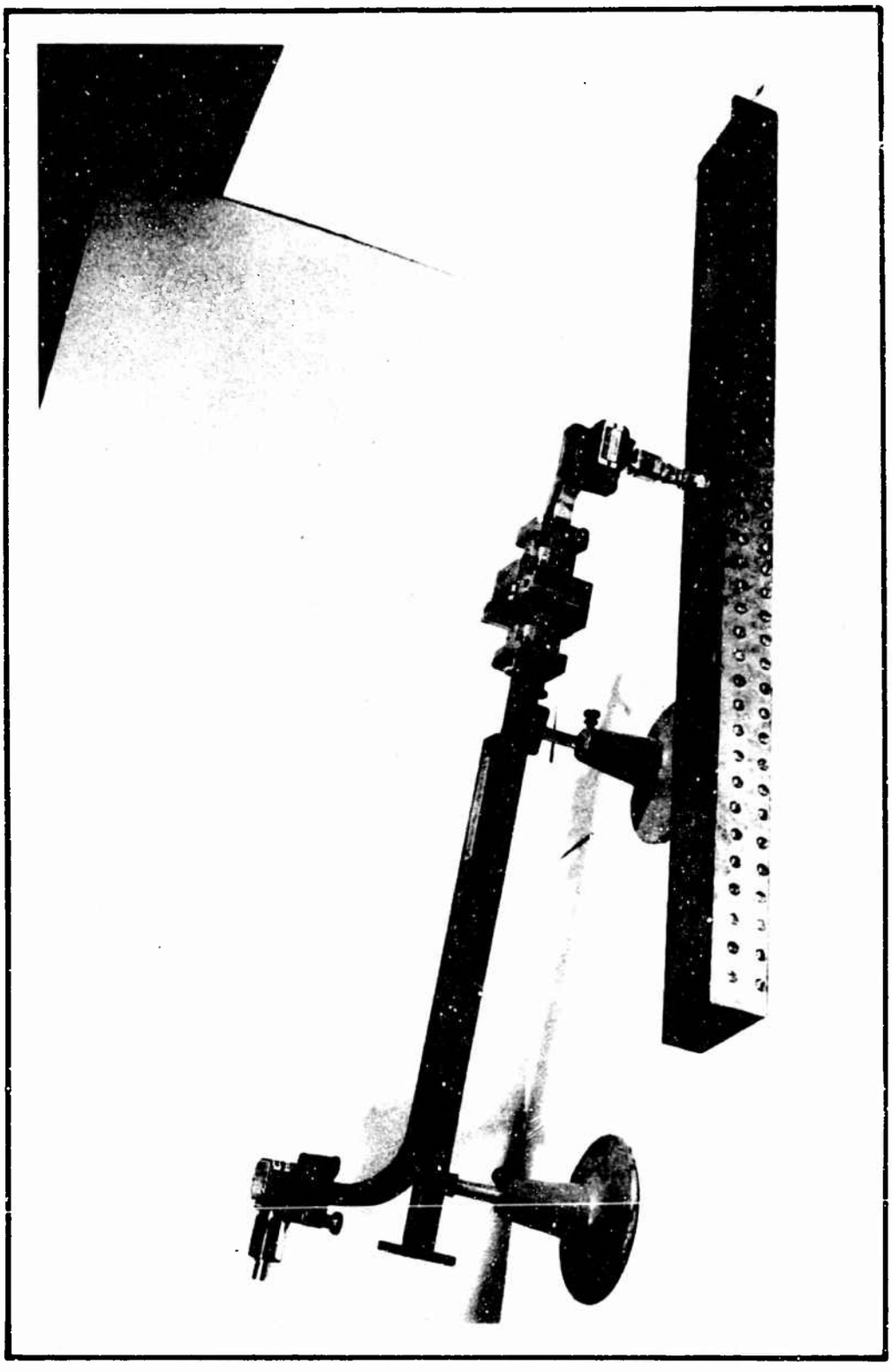

FIG. 15-1. EXPERIMENTAL RECTANGULAR BEAM WAVEGUIDE RESONATOR

type BNC jack by means of a N to BNC adapter. The BNC jack connects to a small rigid coaxiable cable which was inserted through a thread sleeve or bolt. The center conductor of this coaxial cable extends about 1/8 inch beyond the end of the threaded sleeve and acts as a small antenna or coupling probe when projected into the resonator. The vertical direction in Fig. 15-1 corresponds to the y-direction in Fig. 14-2. Since the E field is in the y-direction, and for the n=o mode has its maximum ampliutde at x=o, $z = \frac{z'(0)}{2}$, a tapped hole to receive the coupling probe was inserted in the resonator at this point. The probe coupling can be adjusted by turning the threaded sleeve in or out as desired. Since the end of the threaded sleeve is flush with the upper inner wall of the resonator at only one setting of the probe depth, a small perturbation will be introduced for all other probe depth settings. However, since the sleeve is only 3/16 inches in diameter the distortion of the fields is expected to be small.

C. Measurement Techniques

Measurements of the parameters of the rectangular beam waveguide resonator were made using reflectometer apparatus. Figure 15-2 is a block diagram of the apparatus. The apparatus displays two patterns on the oscilloscope. One pattern is the reflected power along the vertical scope axis versus frequency f along the horizontal axis. The other pattern is incident power versus frequency.

The system was calibrated as follows. With the waveguide switch closed and the incident power variable attenuator set at zero db the reflected power variable attenuator was adjusted to make the outputs of both of the coupler crystal detectors equal when monitored by the oscilloscope. Since the crystals used were a matched pair, variations in the power output of the oscillator

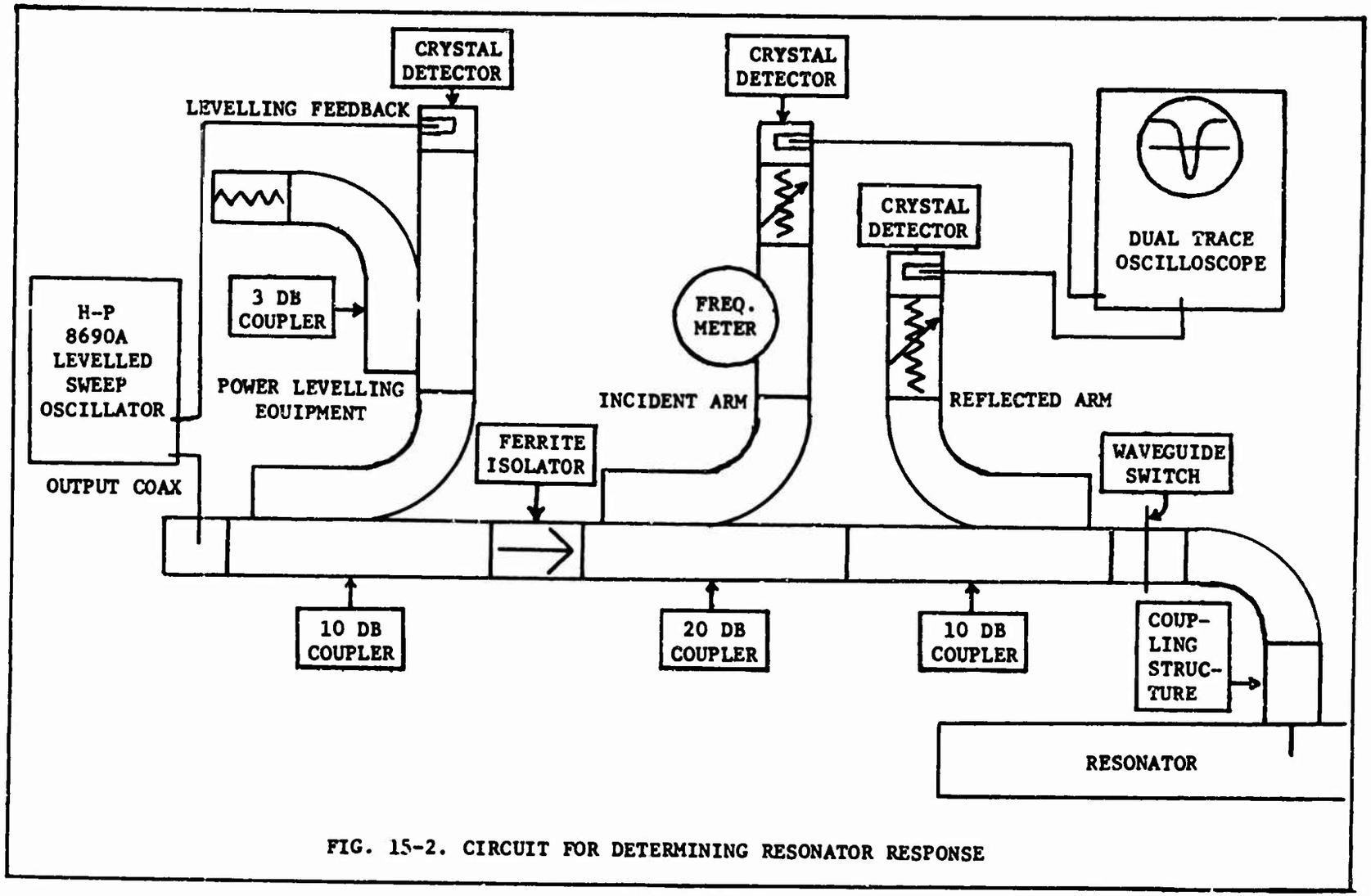

FIG. 15-2. CIRCUIT FOR DETERMINING RESONATOR RESPONSE

did not unbalance the crystal output readings. When the waveguide switch was opened the incident power to and the power reflected by the resonator were displayed on the scope. The displayed incident power was quite constant with frequency, varying by only $\pm$ 0.3 db over the entire X band. The constancy was due to the action of the levelling feedback and to the very flat frequency response of the precision multi-hole directional couplers.

The observed variations of the reflected power, denoted by P_r, with frequency can be used to obtain the values of all the important resonator parameters. In order to be certain that the response or Q curve obtained for a resonator is not being influenced by the method of measurement or some other external factors, a comparison of the measured and theoretical responses of the resonator is usually made. The theoretical frequency response of a one port closed resonator is of the form[48]

$$\frac{P_c}{P_o} = \frac{4Q_L^2}{Q_{ex}Q_{oo}} \left[\frac{1}{1 + 4\,Q_L^2 \left(\frac{f-f_r}{f_r}\right)^2} \right] \qquad (15\text{-}3)$$

where P_c = power absorbed by one-port resonator

P_o = incident power

Q_L = loaded Q

Q_{ex} = external Q

Q_{oo} = unloaded Q

f_r = resonator frequency

f = any frequency near resonance

---

48. J. Altman, Microwave Circuits, D. Van Nostrand Co., Inc., Princeton, N.J., 1964, p. 227.

This equation is valid for a high Q cavity with negligibly small coupling losses.

Now if at $f = f_r$, $P_c = P_o$ then no power is reflected by the resonator at reasonance and the resonator is said to be critically coupled. Thus,

$$\left.\frac{P_c}{P_o}\right|_{f=f_r,\ c.c.} = 1 = \frac{4Q_L^2}{Q_E Q_{oo}} \tag{15-4}$$

and hence

$$\left.\frac{P_c}{P_o}\right|_{c.c.} = \frac{1}{1 + 4Q_L^2\left(\frac{f-f_r}{f_r}\right)^2} \tag{15-5}$$

It will be convenient to rearrange this equation in order to arrive at a straight line relationship between frequency and resonator response.

$$1 + 4Q_L^2\left(\frac{f-f_r}{f_r}\right)^2 = \left.\frac{P_o}{P_c}\right|_{c.c.}$$

$$(f-f_r)^2 = \frac{f_r^2}{4Q_L^2}\left[\left.\frac{P_o}{P_c}\right|_{c.c.} - 1\right]$$

$$|f-f_r| = \frac{f_r}{2Q_L}\sqrt{\left.\frac{P_o}{P_c}\right|_{c.c.} - 1} \tag{15-6}$$

Now $P_o = P_r + P_c$

where P_r = reflected power

Therefore

$$\frac{P_c}{P_o} = 1 - \frac{P_r}{P_o} \tag{15-7}$$

and Eq. 15-6 becomes

$$|f-f_r| = \frac{f_r}{2Q_L}\sqrt{\frac{\frac{1}{\frac{P_r}{P_o}}\Big|_{c.c.} - 1}{1 - \frac{P_r}{P_o}\Big|_{c.c.}}}$$

or

$$|f-f_r| = \frac{f_r}{2Q_L\sqrt{\frac{P_o}{P_r}\Big|_{c.c} - 1}} \qquad (15\text{-}8)$$

Since f_r and Q_L are not a function of frequency a plot of $|f-f_r|$ versus $\left[\frac{P_o}{P_r}\Big|_{c.c.} - 1\right]^{-1/2}$ should be a straight line.

The reflectometer apparatus shown in Fig. 15-2 was used to measure the dependence of $\frac{P_o}{P_r}\Big|_{c.c.}$ on frequency. The frequency over which the oscillator was swept was a small range around the n=o resonance. When the waveguide switch was opened the incident power to and the reflected power by the resonator was displayed on the scope. Readings of $P_o/P_r|_{c.c.}$ in db versus f were taken. The data was taken by leaving the reflected power variable attenuator set at its initial value and setting the incident power variable attenuator at some value, say x db. The two frequencies at which the reflected response curve crossed the straight line incident poer curve were determined by moving the wavemeter pip which was visible on the scope, to the two intersection points. At these two points, $\frac{P_o}{P_r}\Big|_{c.c.}$ = xdb. Additional data of $\frac{P_o}{P_r}\Big|_{c.c.}$ versus f was obtained by changing the setting of the incident power variable attenuator and noting the two new corresponding frequencies.

The data so obtained at critical coupling is then used to plot $\left[\frac{P_o}{P_r}\Big|_{c.c.} - 1\right]^{-1/2}$ versus f. If a straight line is obtained then the response observed is a true resonance.

Measurements can next be made of all the pertinent quality factors. The pertinent Q's are: Q_{oo}, Q_o, and Q_L. The definitions of these are,

$$Q_{oo} = \omega_r \frac{W_s}{P_c} \text{ ; unloaded and uncoupled Q} \tag{15-9}$$

$$Q_o = \omega_r \frac{W_s}{P_c + P_{co}} \text{ ; unloaded but coupled Q} \tag{15-10}$$

and

$$Q_L = \omega_r \frac{W_s}{P_c + P_{co} + P_{ex}} \text{ ; loaded Q} \tag{15-11}$$

where W_s = energy stored in resonator

P_c = power absorbed by one port resonator

P_{co} = power lost in coupling network

P_{ex} = power lost in external circuit

The actual values of the Q's were determined from the magnitudes of three measured reflection coefficients. They are

$$|\rho_o| = \sqrt{\frac{P_r}{P_o}\Big|_{f=f_r}} \tag{15-12}$$

$$|\rho_1| = \sqrt{\frac{P_r}{P_o}\Big|_{f}} \quad \text{where f is far from } f_r \tag{15-13}$$

$$|\rho| = \sqrt{\frac{P_r}{P_o}\Big|_{f}} \quad \text{where f is any f near } f_r \tag{15-14}$$

These reflection coefficient magnitudes are the square roots of three values of the power ratio P_r/P_o which was just discussed.

The equivalent circuit shown in Fig. 15-3 may be used to arrive at the expression for Q_L in terms of ρ_o, ρ_1 and ρ.[49] The circuit is valid for a probe coupled resonator viewed from a position on the transmission line leading to the probe which is called the detuned open position. The resistor R_1 accounts for the power loss in the coupling and R accounts for the power absorbed by the resonator. It can be shown that

49. M. Sucher and J. Fox, Handbook of Microwave Measurements, 3rd Ed., Vol. II, Polytechnic Press of the Polytechnic Inst. of Brooklyn, New York, N.Y., 1963, pp. 425-427, 451-455, 484-485.

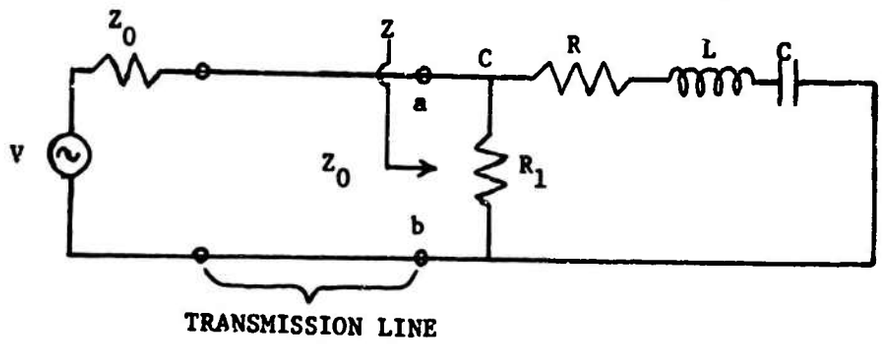

(a)

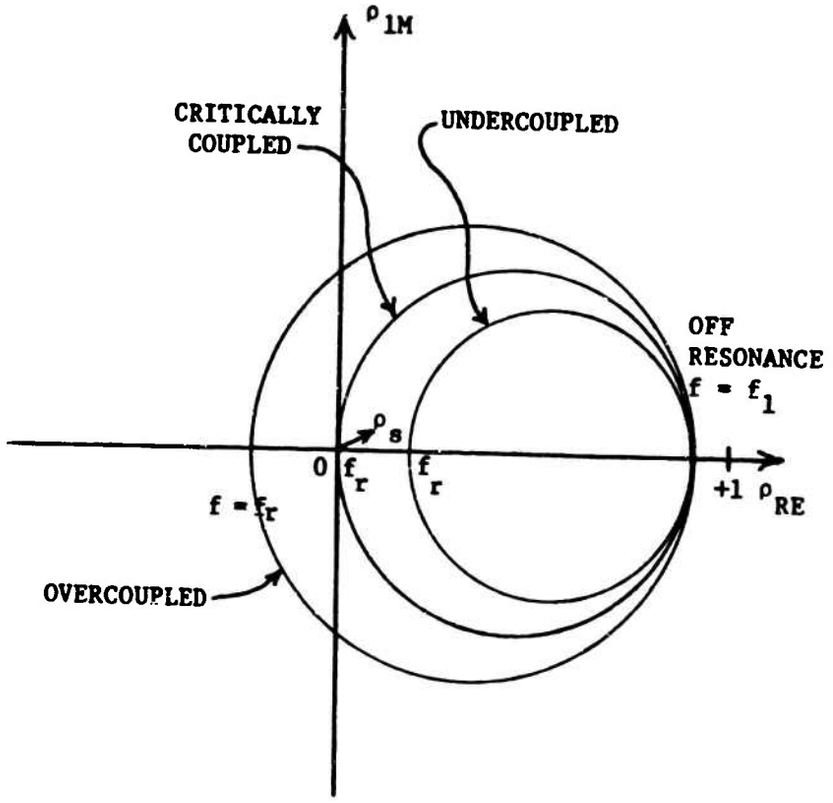

(b)

FIG. 15-3. EQUIVALENT CIRCUIT AND LOCI OF REFLECTION COEFFICIENT FOR PROBE-COUPLED RESONATOR

$$Q_L = \alpha \frac{f_r}{f} \tag{15-15}$$

where

$$\alpha = \sqrt{\frac{|\rho|^2 - |\rho_o|^2}{|\rho_1|^2 - |\rho|^2}} \tag{15-16}$$

and f is the difference between the two frequencies at which $|\rho|^2$ is measured.

When the probe-coupled resonator is overcoupled then

$$\frac{Q_o}{Q_L} = \frac{2}{2 - |\rho_o| - |\rho|} \tag{15-17}$$

and

$$\frac{Q_{oo}}{Q_L} = \frac{1 + |\rho_1|}{1 - |\rho_o|} \tag{15-18}$$

When the resonator is undercoupled then

$$\frac{Q_o}{Q_L} = \frac{2}{2 + |\rho_o| - |\rho_1|} \tag{15-19}$$

and

$$\frac{Q_{oo}}{Q_L} = \frac{1 + |\rho_1|}{1 + |\rho_o|} \tag{15-20}$$

The overcoupled condition exists where $\rho_o > 0$, and the undercoupled condition when $\rho_o < 0$.

The validity of Eqs. 15-18 and 15-20 can be shown using the equivalent circuit of Fig. 15-3. The reflection coefficient for a wave incident on the resonator at terminals a-b is

$$\rho = \frac{Z - Z_o}{Z + Z_o}$$

Since terminals a-b are at a detuned open position ahead of the probe, R_1 must be greater than Z_o so that

$$|\rho_1| = \frac{R_1 - Z_o}{R_1 + Z_o}$$

At resonance Z is equal to

$$Z = \frac{R_1 R}{R_1 + R}$$

and hence

$$\rho_o = \frac{\frac{R_1 R}{R_1+R} - Z_o}{\frac{R_1 R}{R_1+R} + Z_o} = \frac{R_1 R - Z_o(R_1+R)}{R_i R + Z(R_1+R)}$$

As indicated in Fig. 15-3, for the undercoupled resonator $\rho_o > 0$, $|\rho_o| = \rho_o$ since R_1 in parallel with R is larger than Z_o. Physically this means that the probe extends into the resonator only a small distance and hence is only lightly coupled to the resonance mode, and therefore the impedance seen at the terminals a-b is larger than Z_o. On the other hand if the resonator is over-coupled then $\rho_o < 0$ so that $|\rho_o| = -\rho_o$. Thus both Eq. 15-18 and Eq. 15-20 can be rearranged and written as

$$\frac{Q_{oo}}{Q_L} = \frac{1 + \frac{R_1 - Z_0}{R_1+Z_0}}{1 + \frac{R_1 R - Z_0(R_1+R)}{R_1 R + Z_0(R_1+R)}} \qquad (15\text{-}21)$$

Now Q_{oo} and Q_L can be expressed in terms of the elements of the equivalent circuit. Thus $Q = \omega_r L/R_{EQ}$ where R_{EQ} is the total equivalent resistance seen from the L-C terminals and hence

$$Q_L = \frac{\omega_r L}{R + \frac{R_1 Z_0}{R_1+Z_0}}$$

and

$$Q_{oo} = \frac{\omega_r L}{R}$$

Therefore

$$\frac{Q_{oo}}{Q_L} = \frac{R + \frac{R_1 Z_0}{R_1+Z_0}}{R} = \frac{R_1 R + Z_0 R + R_1 Z_0}{R_1 R + Z_0 R} \qquad (15\text{-}22)$$

Substituting Eq. 15-22 into Eq. 15-21 the following relation is obtained.

$$\frac{R_1R+Z_0R+R_1Z_0}{R_1R+Z_CR} = \frac{1+\dfrac{R_1-Z_0}{R_1+Z_0}}{1+\dfrac{R_1R-Z_0(R_1+R)}{R_1R+Z_0(R_1+R)}} \qquad (15\text{-}23)$$

It is easy to show that the left hand side of Eq. 15-23 is indeed equal to the right hand side and hence the validity of Eqs. 15-18 and 15-20 has been shown.

However, before Eqs. 15-18 and 15-20 or Eqs. 15-17 and 15-19 can be used to determine Q_{oc} and Q_o, the coupling condition of the resonator, that is whether overcoupled or undercoupled, must be known. The coupling condition for each resonant mode can be determined experimentally by making one simple measurement. There are at least three different measurement techniques that can be used to determine the coupling condition. The one used here consists of substituting a slide screw tuner for the waveguide switch shown in Fig. 15-2. The tuner adds a shunt susceptance across terminals a-b of Fig. 15-3 and produces a reflection at this point. This reflection coefficient may be denoted by ρ_s. To make the measurement, the tuning screw is extended far enough into the waveguide to alter the reflected power pattern on the oscilloscope. The reflected power and hence its trace on the scope is dependent on the vector sum of the reflection coefficient ρ_s and the reflection coefficient of the resonator. The two reflection coefficients are shown in Fig. 15-3.

Now if the minimum power point on the oscilloscope pattern describes a circle in the clockwise direction when the tuning screw of the slide screw tuner is moved along the waveguide and away from the resonator, then the resonator is overcoupled.[50] If on the other hand the minimum power point describes a circle in the counter-clockwise direction the resonator is undercoupled. When the resonator is critically coupled the minimum power point on the scope

---

50. Sucher and Fox, pp. 450-451.

has no circular motion when the slide screw tuner is moved. With the coupling condition known the values Q_{oo} and Q_o can be calculated from the measured reflection coefficients.

D. Comparison of Experimental and Theoretical Results

The reflectometer apparatus shown in Fig. 15-2 was used to display the power reflected by the resonator versus frequency in the X band range. Sharp resonant dips were observed. The frequencies of the observed resonant minimums are listed in Table 15-I. The first eight resonant frequencies which appeared as the frequency was swept from 8.0 GHz upwards are listed. Not all modes were observable for certain probe depths. When the threaded sleeve was turned in to get tighter coupling, the perturbation caused by the sleeve projecting into the resonator resulted in resonant frequency shifts of the order of 5 or 10 MHz maximum. The resonant frequencies listed in Table 15-I were all observed with the coupling probe in one fixed position except for the frequency of the n=o mode for which the probe depth had to be reduced.

Mode Number n	Measured Resonant Frequency GHz	Calculated Resonant Frequency GHz
0	8.975	8.975
1	9.055	9.047
2	9.115	9.119
3	9.196	9.191
4	9.259	9.263
5	9.337	9.335
6	9.407	9.407
7	9.483	9.479

TABLE 15-I

Resonant Frequencies of Rectangular Beam Waveguide Resonator

The measured resonant frequency of the n=o mode was not as close to the design value of 9.0 GHz as hoped for. The reason for the discrepancy is that the value of $z'(0)$, calculated from Eq. 14-12 or Eq. 15-2 was done with a slide rule.

When the value z'(0) = 0.660 inches and n=o are used in Eq. 14-17 an accurate calculation yields a resonant frequency of 8.983 GHz. However the tolerance on machining the resonator was $\pm$ 0.002 inches. If a maximum value of z'(0)=0.662 is used in Eq. 14-17 the resonant frequency could be shifted as much as 10 MHz. Thus the theoretical or calculated value of the resonant frequency for the n=o mode listed in Table 15-I could very well be 8.975 GHz. Using the 8.975 GHz as a starting point and adding 72 GHz successively, the seven resulting calculated resonant frequencies were obtained.

The theoretical or calculated resonant frequencies listed in Table 15-I depend on the value assigned to the ratio (w_o/z_o) at the desired resonant frequency for the n=o mode. In the present case w_o=5 at f=9.0 GHz was used and resulted in a frequency spacing between modes of Δf = 72 MHz. Now w_o does vary with frequency and by using w_o=5 and f=9.0 GHz in Eq. 14-23 the value of D obtained is 15.0 and when used with f=9.5 GHz the new value of $w_o = 15/\sqrt{9.5} = 4.87$. The change in w_o over the frequency range from 9.0 to 9.5 GHz is a negligible 2.6%. Thus the modes whose resonant frequencies lie in this range should be spaced by about 72 MHz. The eight measured values of the resonant frequencies listed in Table 15-I are very close to 72 GHz apart. The measured and calculated resonant frequencies compare favorably.

The reflectometer was next used to measure $[(P_o/P_r)\big|_{c.c} - 1]^{-1/2}$ at frequencies near the n=o mode. The measurements are plotted in Fig. 15-4. Since the points lie very nearly along a straight line, it can be concluded that true resonance was taking place. The resonator was evidently not being disturbed by the coupling scheme or by the measuring apparatus. The small deviations of some of the measured points from a straight line are probably due to some small measurement errors.

The coupling loss and quality factors of modes n=o through 7 were measured by the reflectometer technique discussed previously. The results are shown in

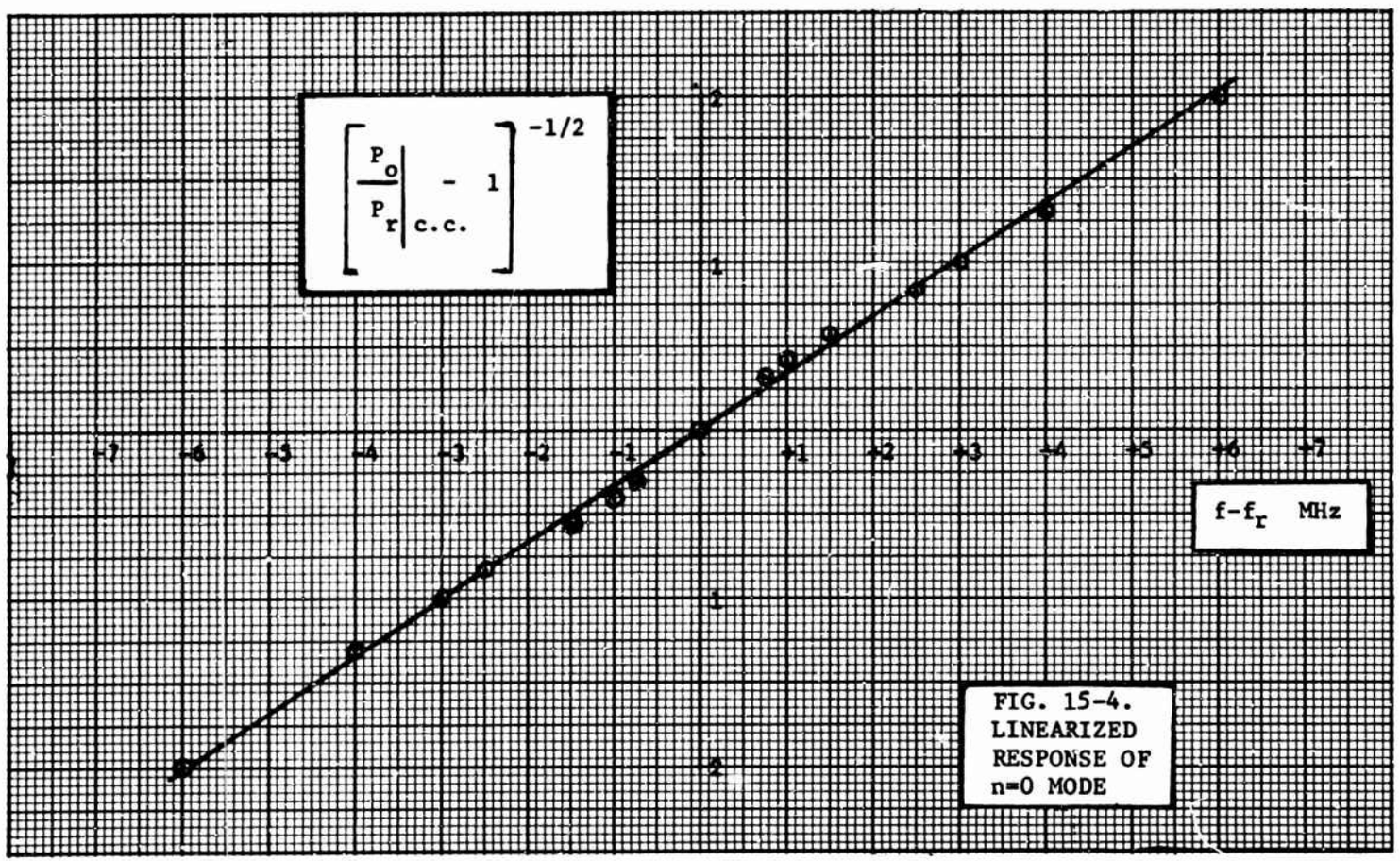

FIG. 15-4.
LINEARIZED
RESPONSE OF
n=0 MODE

Table 15-II. The first column of the table lists $|\rho_1|^2$, which is the coupling loss. The probe assembly with rigid coax was used when the measurements listed in this table were made. Using the probe assembly with flexible coax created an additional coupling loss of about 0.2 db. For example the n=o mode value of $|\rho_1|^2$ changed from -0.3 db to -0.5 db. Note also that the coupling loss increases somewhat at greater values of probe depth d, evidently due to currents in the probe. But all the listed values of $|\rho_1|^2$ indicate small loss. The coupling loss also may be inferred by comparing the measured values of Q_o and Q_{oo}. In all cases Q_o is only slightly less than Q_{oo}, indicating again that the probe coupling loss was small. The values of Q_{oo} are all very close to about 3300.

Recall that the theoretical Q_{oo} is given by Eq. 14-35. The values which must be substituted in the equation for the case of the resonator are: $\lambda_o = 3.33 \times 10^{-2}$m., σ = conductivity of brass = 16×10^6 mhos/m., $h = 0.98 \times 10^{-2}$ m. Calculations then give $Q_{oo} = 3350$. Thus the predicted Q_{oo} agrees very well with the nine measured values shown in Table 15-II.

The values of $|\rho_o|^2$ listed in Table 15-II are the measured power reflection coefficients at resonance. The theoretical values can be found using Eqs. 14-49 and 14-50. Since $He_n(0) = 0$ for n odd, Eq. 14-49 gives $R_n = 0$ for n odd. Therefore the theoretical value of $|\rho_o|^2$ is unity (-0.0 db) for n odd for all probe depths d. These modes can theoretically never reach the critical coupling condition $|\rho_o|^2 = 0$. But the table shows that experimentally $|\rho_o|^2$ can equal zero for n odd.

This disagreement is probably due to slight asymmetries which exist in the resonator due to fabrication tolerances. The probe is evidently not exactly at $x = 0$. Also, the curved surface $z = -z_n'(\sim)$ is evidently not perfectly symmetric about $x = 0$.

More satisfactory agreement between the coupling theory and experiment is found in the coupling to the even numbered modes. Equation 14-51 can be used

Relative Probe Depth	Mode No. n	$\|\rho_1\|^2$ db	$\|\rho_0\|^2$ db	$\|\rho\|^2$ db	Δf MHz	Q_L	Q_0	Q_{OC}	Coupling** Condition
	0	-0.3	-50	-3.0	6.0	1620	3120	3200	c
	1	-0.3	-1.6		could not be measured accurately				u
A*	2	-0.3	-7.2	-3.0	3.0	2570	3460	3500	u
	3	-0.4	-2.2		could not be measured accurately				u
	4	-0.4	-4.0		could not be measured accurately				u
	1	-0.55	-50	-3.0	6.0	1720	3240	3340	c
	2	-0.55	-4.1	-3.0	8.0	611	2800	3150	o
	3	-0.6	-50	-3.0	6.5	1650	3100	3200	c
B*	4	-0.7	-7.3	-3.0	8.5	1030	3180	3460	o
	5	-0.3	-6.0	-3.0	6.0	1670	3220	3300	c
	6	-0.55	-13	-3.0	8.0	1280	3050	3200	o
	7	-0.47	-50	-3.0	6.0	1770	3300	3400	c

*A - Probe extends about 1 mm into and beyond resonator top wall
B - Probe extends three mm into and beyond resonator top wall
**c - Critically coupled; o - overcoupled; u - undercoupled

TABLE 15-II

MEASURED VALUES OF Q FOR RECTANGULAR BEAM WAVEGUIDE RESONATOR

to predict the probe penetration, d, required for critical coupling of the even numbered modes. The value of Z_o, which is the characteristic impedance of the coaxial feed line, is approximately 50 ohms. The value of u_{pn} for the various modes can be obtained from Eq. 14-53. The values of $He_n(0)$ needed in Eq. 14-53 can be obtained from Figs. 14-3 through 14-10. The value of u_o for the resonator used in the measurements is 11.9/meter. Thus

$$u_{po} = 11.9\sqrt{2/\pi} = 9.50/\text{m}.$$

$$u_{p2} = (11.9/2)\sqrt{2/\pi} = 4.75/\text{m}.$$

$$u_{p4} = \frac{9(11.9)}{24}\sqrt{2/\pi} = 3.56/\text{m}.$$

$$u_{p6} = \frac{225(11.9)}{720}\sqrt{2/\pi} = 2.97/\text{m}.$$

$$u_{p8} = \frac{(105)^2(11.9)}{8\cdot 7\cdot 720}\sqrt{2/\pi} = 2.60/\text{m}.$$

The value of u_{po} plus the known values of the other variables when put in Eq. 14-51 yields a probe penetration d = 0.52 mm for critical coupling. This value is reasonably close to the experimental value of approximately one millimeter given in Table 15-II. No precise measurement of probe depth was warranted because of the perturbation introduced by the sleeve of the probe assembly.

The value of $|\rho_o|_n^2$ for the n=2 and n=4 modes when the n=o mode is critically coupled can be determined with the aid of Eq. 14-51 and the value of u_{po} for the n=o mode. Thus

$$50 = K\ (9.50)$$

where K is a constant and equal to 5.26. Now for other modes Eq. 14-48 yields

$$R_n = K\, u_{pn}$$

and hence

$$R_2 = 5.26\ (4.75) = 25$$

and $$R_4 = 5.26\ (3.56) = 18.75$$

The reflection coefficient ρ_o is

$$\rho_o = \frac{R_n - Z_o}{R_n + Z_o}$$

Thus $\rho_o^2\Big|_{n=2} = -9.5$ dB

and

$$\rho_o^2\Big|_{n=4} = -6.8 \text{ dB}$$

The measured values in Table 15-II are -7.2 dB and -4.0 dB respectively. While there is only fair agreement numerically for the values of ρ_o^2 and the error is probably due mostly to the assumption of an infinitely thin probe, the theory does correctly predict the order in which modes will critically couple. Increasing the probe depth from zero the theory predicts that the first five modes will become critically coupled in the order 0, 2, 4, with 1 and 3 simultaneously becoming critical last. Even for a fixed probe depth the value of ρ_o indicates the order in which critical coupling would take place. Table 15-II shows the order to be 0, 2, 4, 3 and 1. The fact that 3 is ahead of 1 is probably due in part to experimental error. In conclusion the experimental observations on the probe coupling are in good agreement with the theoretical predictions.

The only remaining topic is the reactance of the probe and its possible effect of shifting the resonant frequencies. Since the experimental resonant frequencies agree very well with those calculated by Eq. 14-17, the frequency shift due to probe reactance is negligible. Therefore the subject of probe reactance will not be dealt with in detail.

The study made of the rectangular beam waveguide resonator revealed that it behaves in a manner very similar to other waveguide resonators. The design of the rectangular beam waveguide resonator was straight-forward. The length of 15 inches on each side of center in the x-direction for the resonator is probably longer than necessary and in future designs it could be made considerably shorter. The actual fabrication of the resonator presented no serious mechanical problems.

The measured response curves for the resonator proved to be true Q curves. This means that the resonator was not being affected either by the method of measurement or by some other external factors. The reflectometer apparatus used for these measurements also served to measure all of the other important parameters of the rectangular beam waveguide resonator.

The conclusion to be drawn from this study is that the rectangular beam waveguide resonator behaves as predicted by the theory developed. The measured values of the resonant frequences, the Q's, and the various reflection coefficients agree closely with the theoretical values.

XVI. THEORY OF THE RECTANGULAR BEAM WAVEGUIDE ANTENNA

A. The Cavity-Backed Antenna

The fact that the n=o mode of the rectangular beam waveguide resonator has fields with the Gaussian distribution $\bar{E} = \bar{u}_y E_o e^{-u_o^2 x^2}$ suggests that it can be transformed into a narrow beam antenna. The transformation would consist of introducing an aperture along the x axis through the metal wall at z=o to couple the resonator fields to free space (see Fig. 14-2). The antenna so constructed is here given the name rectangular beam waveguide antenna.

Since the antenna aperture is backed by the resonator, the antenna is a type of "cavity-backed" antenna. In general the cavity-backed antenna must have an aperture which is large enough so that most of the input power to the cavity resonator is radiated into free space, yet not so large that the resonator field configuration is destroyed and hence also the desired antenna pattern. Such an antenna has reasonably high values of both radiation efficiency and Q. The bandwidth of the cavity-backed antenna is generally smaller than that of other types of antennas since its bandwidth is controlled by its Q_L. The familiar relation is that the bandwidth, $\Delta f = f_r/Q_L$.

A few types of cavity-backed antennas have been discussed in the literature. Jacobsen et al. have presented an antenna backed by a regular waveguide cavity.[51] The aperture in this case consists of many circular holes. The diameter and number of the holes determines the magnitude of the coupling to free space. Jacobsen et al. stress the point that any cavity-backed antenna has an advantage over other types of antennas because the phase of the aperture fields is constrained to be uniform by the cavity. The uniform phase eliminates phase error, thereby eliminating corresponding irregularities in the radiation pattern.

Instead of using holes, a slot can also serve as a coupling aperture, as in the cavity-backed antenna discussed by Adams.[52] Slot coupling in the rectangular beam waveguide antenna can be accomplished by cutting an opening in the z=o wall that extends from $y = -w/2$ to $+w/2$, with a slot width w of the order of a few thousandths of an inch, and from $x = -L_s/2$ to $+L_s/2$ where the slot length L_s is nearly equal to the length L of the resonator. Such a slot simulates a line source of fields along the x axis from $-L_s/2$ to $+L_s/2$ The radiated field from such a continuous line souce is proportional to its Fourier transform. Since the Fourier transform of a Gaussian source distribution is a Gaussian, the radiation pattern of the antenna excited in the n=o mode of the resonator can be shown to be a narrow beam Gaussian in the xz plane. The radiation pattern in the yz plane of the line source is a circle, that is, it is omnidirectional. The magnitude of the slot coupling from the resonator to free space will depend on the slot width w. The larger w is, the larger the coupling will be. The coupling will also be affected by the

---

51. S. Jacobsen, E. Andersen, and M. Gronlund, "An Antenna Illuminated by a Cavity Resonator", Proc. IEEE, vol. 51, November 1963, pp. 1431-1435.

52. A.T. Adams, "Flush Mounted Rectangular Waveguide Slot Antennas -- Theory and Design", IRE Trans. on Antennas and Propagation, vol. AP-15, May 1967, pp. 342-351.

thickness t of the metal wall in which the slot is cut.

An important effect of either the slot or the hole coupling in the cavity-backed antenna is an increase in the power loss above that of the one-port resonator. The power loss increases because power is now radiated into free space by the antenna aperture. Another effect of the aperture coupling is a possible change in the resonant frequency.

B. Equivalent Circuit of the Rectangular Beam Waveguide Antenna

The equivalent circuit of the rectangular beam waveguide resonator coupled to a source by a probe, was presented previously and is the circuit shown in Fig. 15-3. If the resonator is to form an antenna, then a second port through which the energy to be radiated can leave the resonator must be introduced. When a second coupling port is created which can be either a slot or holes used as an aperture then the equivalent circuit of the one port resonator must be modified.

When energy is coupled out of the resonator by a slot along the x-axis, the beam mode incident on the slot is approximately a plane wave with $\bar{E}$ in the y-direction. It can be shown that the impedance presented to a plane wave with its $\bar{E}$ field across the slot will be a resistance R_a in parallel with a capacitance C_a.[53] The capacitance implies that the coupling is of the electric-moment type which is the same type of coupling obtained with a probe. A resonator with input and output coupling of the electric type has been shown to have an equivalent circuit consisting of a series RLC resonant circuit in series with the coupling port impedances.[54] Thus the equivalent circuit for the slot coupled rectangular beam waveguide antenna is as shown in Fig. 16-1 where Z_a is a resistance R_a in parallel with a capacitive reactance $1/jB_a$.

---

53. R.F. Harrington, Time-Harmonic Electromagnetic Fields, McGraw-Hill Book Co., New York, N.Y., 1961, p. 183.

54. G. Goubau, Electromagnetic Waveguides and Cavities, Pergamon Press Inc., New York, N.Y., 1961, p. 514.

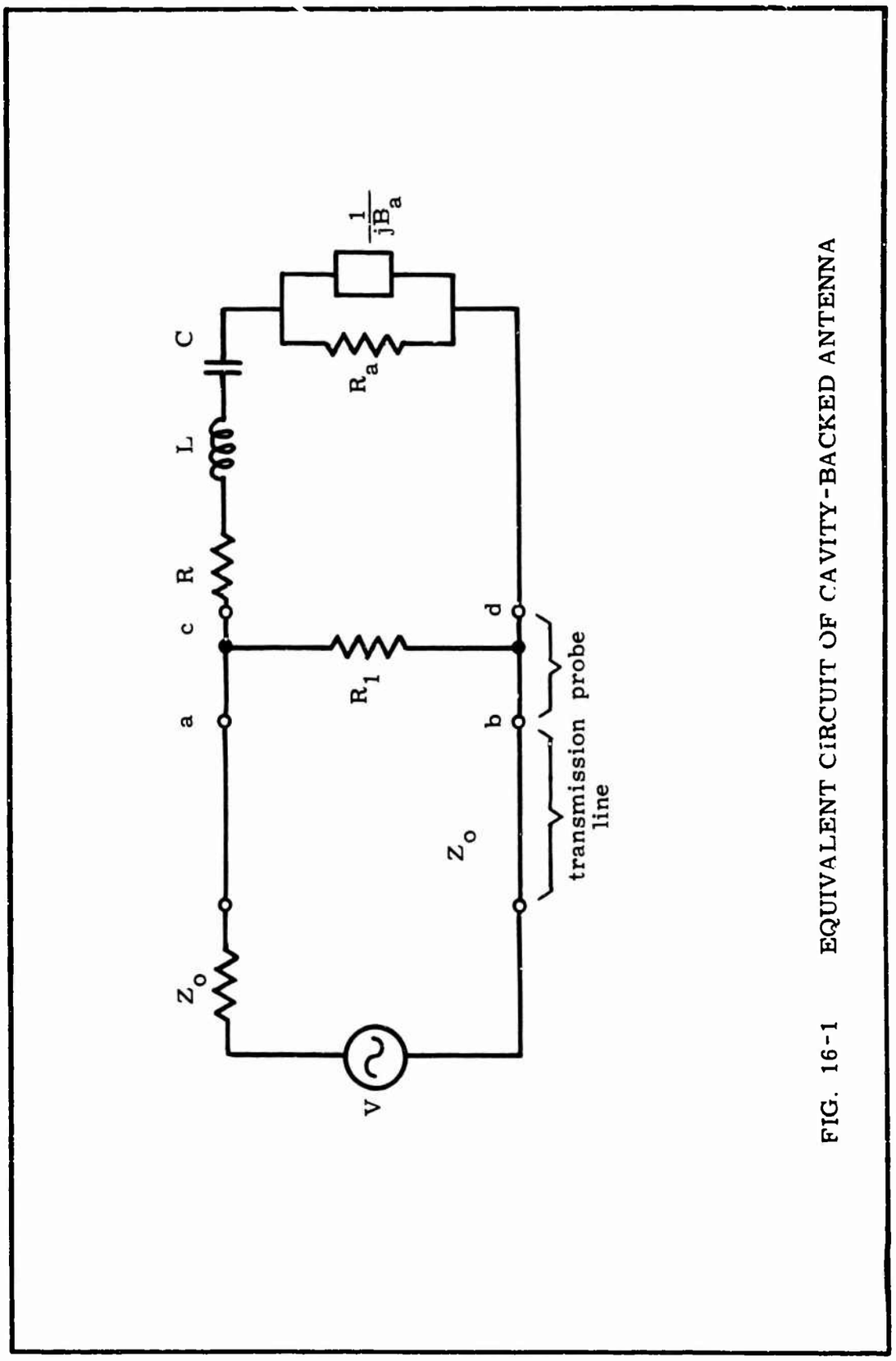

FIG. 16-1 EQUIVALENT CIRCUIT OF CAVITY-BACKED ANTENNA

When the output coupling impedance Z_a consists of a parallel combination of a resistance and capacitance, then the circuit of Fig. 16-1 is no longer a simple series or parallel resonant circuit of R, L and C. The impedance at the input coupling port, that is, at the probe indicated by the terminals a-b in Fig. 16-1 is

$$Z(\omega) = R+j\omega L - \frac{j}{\omega C} + \frac{(R_a)(-j/B_a)}{R_a - j/B_a} \tag{16-1}$$

$$Z(\omega) = R + \frac{R_a}{1 + (R_a B_a)^2} + j\left[\omega L - \frac{R_a^2 B_a}{1+(R_a B_a)} - \frac{1}{\omega C}\right] \tag{16-2}$$

or

$$Z(\omega) = R' + j\left[\omega L' - \frac{1}{\omega C}\right] \tag{16-3}$$

$$\text{where } R' = R + \frac{R_a}{1+(R_a B_a)^2}$$

$$\text{and } L' = L - \frac{R_a^2 B_a/\omega}{1+(R_a B_a)^2}$$

This impedance $Z(\omega)$ is of the same form as the $Z(\omega)$ of the original series circuit resonator (Eq. 16-2 with $R_a=0$) if R' and L' can be considered constant. Now for $R_a C_a$ not too much larger than $1/\omega$ or L/R_a, and for a range of ω from about 0.9ω to 1.1ω, L' and R' can be considered approximately constant and the slot coupled antenna should exhibit an input impedance very similar to that obtained for the one port resonator. The slot antenna will of course have a different input resistance R' at resonance and a different resonant frequency ω_r. The resonant frequency must satisfy the following condition.

$$\omega_r = \frac{1}{\sqrt{L'C}}$$

or

$$\omega_r = \frac{1}{\sqrt{LC - \dfrac{B_a C}{\omega_r(1/R_a^2+B_a^2)}}} \tag{16-4}$$

Thus Eq. 16-4 shows that the new resonant frequency is higher than the resonant frequency $\omega_r = 1/\sqrt{LC}$ of the original one port resonator. Solving for ω_r from either Eq. 16-2 or Eq. 16-4 gives,

$$\omega_r^2 LC - \omega_r \frac{B_a C}{(1/R_a^2+B_a^2)} - 1 = 0$$

or

$$\omega_r = \frac{B_a}{2L(1/R_a^2+B_a^2)} + \sqrt{\frac{B_a^2}{4L^2(1/R_a^2+B_a^2)} + \frac{1}{LC}} \qquad (16\text{-}5)$$

Under the stated assumptions the final equivalent circuit and the original equivalent circuit behave similarly except that the final circuit has new values of R and L. The Q's will be lower since power is being radiated from the coupling aperture. The Q's for the antenna are given by

$$Q_{oor} = \omega_r \frac{W_s}{P_{rad} + P_c} \qquad (16\text{-}6)$$

$$Q_{or} = \omega_r \frac{W_s}{P_{rad} + P_c + P_{co}}$$

$$Q_{Lr} = \omega_r \frac{W_s}{P_{rad} + P_c + P_{co} + P_{exl}}$$

where Q_{oor} = unloaded uncoupled Q with radiation

Q_{or} = unloaded Q with radiation

Q_{Lr} = loaded Q with radiation

W_s = energy stored in resonator

P_{rad} = power radiated

P_c = power dissipated in walls or absorbed by resonator

P_{co} = power lost in coupling probe

P_{ex1} = power lost in external input circuit

When these Q's are known, important parameters such as antenna efficiency Γ can be calculated. The antenna efficiency is defined as follows:

$$\Gamma = \frac{P_{rad}}{P_o} = \frac{P_{rad}}{P_{rad} + P_c + P_{co} + P_r} \tag{16-7}$$

where Γ is evaluated at resonance

P_o = power incident on resonator

P_r = power reflected by resonator

The value of Γ should be as near to one as possible. Thus the case of a critically coupled resonator is of interest since then $P_r = 0$ and

$$\Gamma\Big|_{c.c.} = \frac{P_{rad}}{P_{rad} + P_c + P_{co}} \tag{16-8}$$

If an external Q at port 2 (output port) is defined by

$$Q_{ex2} = \omega_r \frac{W_s}{P_{rad}} \tag{16-9}$$

then

$$\Gamma\Big|_{c.c.} = \frac{Q_{or}}{Q_{ex2}} \tag{16-10}$$

However the following is also true

$$\frac{1}{Q_{ex2}} = \frac{1}{Q_{oor}} - \frac{1}{Q_{oo}} \tag{16-11}$$

where $Q_{oo} = \omega_r \frac{W_s}{P_c}$ as previously measured.

Then

$$\Gamma\Big|_{c.c.} = Q_{or}\left(\frac{1}{Q_{oor}} - \frac{1}{Q_{oo}}\right) \tag{16-12}$$

Thus from the three measured Q's given in Eq. 16-12 the antenna efficiency can be determined.

The validity of Eq. 16-12 may be checked by assuming $P_{co} = 0$. Then $Q_{or} = Q_{oor}$ and

$$\Gamma\Big|_{c.c.} = Q_{oor}\left(\frac{1}{Q_{oor}} - \frac{1}{Q_{oo}}\right) \tag{16-13}$$

$$\Gamma\Big|_{c.c.} = 1 - \frac{Q_{oor}}{Q_{oo}} \tag{16-14}$$

$$\Gamma\Big|_{c.c.} = \frac{P_c + P_{rad} - P_c}{P_c + P_{rad}}$$

When the coupling is critical

$$R_a + \frac{R_a}{1 + (R_a B_a)^2} = Z_o \tag{16-15}$$

and hence

$$P_{rad} + P_c = P_{ex1}$$

thus

$$\Gamma\Big|_{c.c.} = \frac{P_{rad}}{P_{exl}} \tag{16-17}$$

$$\Gamma\Big|_{c.c.} = \frac{4P_{exl}P_{rad}}{(P_{exl}+P_{exl})^2} = \frac{4P_{exl}P_{rad}}{(P_{rad}+P_c+P_{exl})^2}$$

$$\Gamma\Big|_{c.c.} = \frac{4Q_L^2}{Q_{exl}Q_{ex}^2} \tag{16-18}$$

which is a familiar formula.[55]

Since critical coupling to the resonator is a desirable condition it may be of interest to calculate the probe depth required. A theory was presented in a previous section (Eq. 14-49) which predicts the required probe depth for critical coupling of a one port resonator. The formula was derived using several approximations, the most important of which was that the coupling loss P_{co} is negligibly small. The formula can be made valid for the case of the two-port resonator by simply changing Q_{oo} to Q_{oor}. Hence for critical coupling d, the probe depth, must satisfy

$$Z_o = \frac{Q_{oor}}{\omega_o} \frac{\tan^2 \frac{kd}{2}}{k^2 \epsilon h \frac{\lambda_o}{4}} \frac{He_n^2(0)}{\frac{n!}{u_o} \frac{\pi}{2}} \tag{16-19}$$

where d = depth of probe

n = mode number

h = height of resonator

k = wave number

λ_o = free space wavelength

He = Hermite polynomial

---

55. J. Altman, Microwave Circuits, D. Van Nostrand Co., Inc., Princeton, N.J. 1964, p. 240.

Since Q_{oor} is smaller than Q_{oo}, it is obvious that after port 2 has been introduced the probe depth d must be increased to maintain critical coupling.

C. The Slot Aperture

1. Radiation Field of Infinitely Long Slot Antenna

The equation for the radiation field produced by the n=o mode of a slot antenna will be derived. The slot of the rectangular beam waveguide antenna opening onto the z=o ground plane is shown in Fig. 16-2. The resonator is in back of the slot and extends from z=o to $z = - z_n'(x)$. The width of the slot is w and the length is L_s. This section of the report will consider the slot length L_s and the resonator length L is to be infinitely long.

The far field or radiation pattern of an aperture is generally determined by taking the Fourier transform of the field incident on the aperture.[56] Thus

$$\bar{E} = j(\bar{u}_\theta \sin\phi + \bar{u}_\phi \cos\theta\cos\phi) \frac{e^{-jkR}}{\lambda R} \cdot$$

$$\int_y \int_x E_y(x,y,o) e^{jk(\sin\theta\sin\phi y + \sin\theta\cos\phi x)} \, dxdy \qquad (16\text{-}20)$$

This equation is accurate provided the aperture extends at least several wavelengths in both the x and y directions. Only the n=o mode of the rectangular beam waveguide resonator, which has a travelling wave $\bar{E} = u_y E_o e^{-u_o^2 x^2}$ will be considered. Then Eq. 16-20 can be written as

$$\bar{E} = j(\bar{u}_\theta \sin\phi + \bar{u}_\phi \cos\theta\cos\phi) \frac{e^{-jkR}}{\lambda R} E_o I_y I_x \qquad (16\text{-}21)$$

---

56. J. Brown, "A Theoretical Analysis of Some Errors in Aerial Measurements", Proc. IEE, Vol. 105C, February 1958, pp. 343-344.

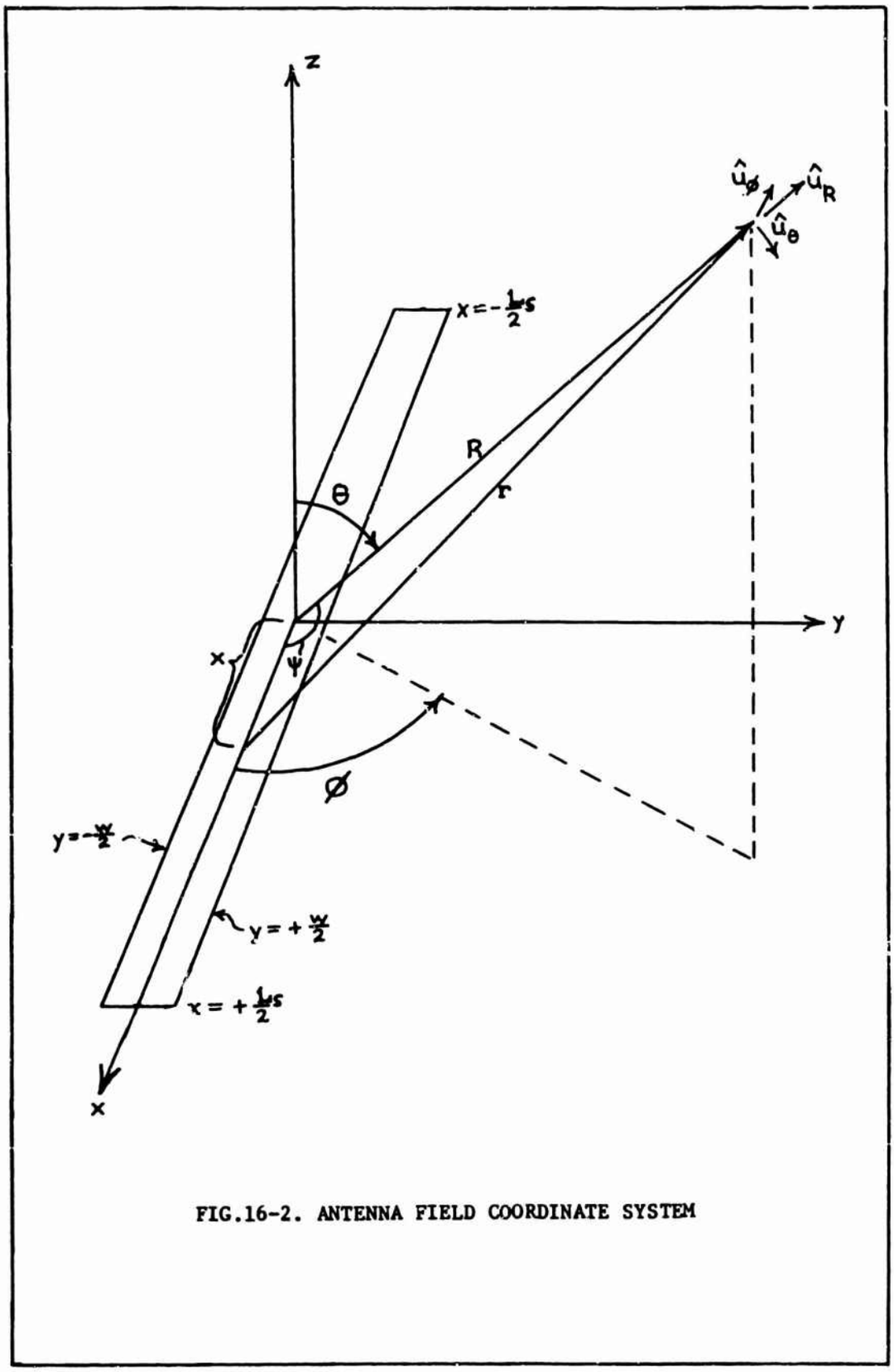

FIG.16-2. ANTENNA FIELD COORDINATE SYSTEM

$$\text{where } I_y = \int_{-\frac{w}{2}}^{\frac{w}{2}} e^{jk\sin\theta\sin\phi y}\, dy \tag{16-22}$$

$$\text{and } I_x = \int_{-\frac{L_s}{2}}^{\frac{L_s}{2}} e^{-u_o^2x^2+jk\sin\theta\cos\phi x}\, dx \tag{16-23}$$

The integral I_x can be evaluated by first completing the square in its exponent which yields

$$I_x = e^{-k^2\sin^2\theta\cos^2\phi/4u_o^2} \int_{-\frac{L_s}{2}}^{\frac{L_s}{2}} e^{-[u_o x - j(k\sin\theta\cos\phi/2u_o)]^2}\, dx \tag{16-24}$$

Now I_x is easily found since for the present case L_s is taken as infinite,[57]

$$I_x = \frac{\sqrt{\pi}}{u_o} e^{-k^2\sin^2\theta\cos^2\phi/4u_o^2} \tag{16-25}$$

The width w of the slot in the antenna under discussion is much smaller than the wavelength λ and hence the integral in Eq. 16-22 is not valid. Thus Eq. 16-21 becomes

$$\bar{E} = j(\bar{u}_\theta \sin\phi + \bar{u}_\phi \cos\theta\cos\phi)\, \frac{e^{-jkR}}{\lambda R} I_y \frac{\sqrt{\pi}}{u_o} e^{-k^2\sin^2\theta\cos^2\phi/4u_o^2} \tag{16-26}$$

where I_y is a function of w yet to be determined.

The power density S at a distance R from the antenna is found by taking the absolute value of the Poynting vector

$$\bar{S} = \bar{E} \times \bar{H}^*$$

where $H = (1/\eta)\, \bar{u}_R \times \bar{E}$ and $\eta = 377$ ohms.[58] Then

$$|\bar{S}| = \frac{E_o^2 I_y^2 \pi}{\lambda^2 R^2 u_o^2 \eta} (\sin^2\theta + \cos^2\theta\cos^2\phi)\, e^{-k^2\sin^2\theta\cos^2\phi/4u_o^2} \tag{16-27}$$

---

57. J. L. Powell and B. Crasemann, Quantum Mechanics, Addison-Wesley Publishing Company, Reading, Massachusetts, 1961, pp. 475-476.

58. Reference in footnote 56, page 344.

The functional dependence of S on θ and ϕ is apparent and results in the radiation pattern of the antenna at some constant distance R from the antenna.

The gain G of the antenna is given by the equation[59]

$$\lambda \frac{G}{4\left(\frac{L_s}{2}\right)} = \frac{\left| \int_{-\frac{1}{2}L_s}^{\frac{1}{2}L_s} E \, dx \right|^2}{L_s \int_{-\frac{1}{2}L_s}^{\frac{1}{2}L_s} |E|^2 \, dx} \qquad (16\text{-}28)$$

which applies for a line source radiating into all space. Since for the antenna under discussion radiation is into half space only the gain must be multiplied by 2 giving the following formula for the gain:

$$G = \frac{4}{\lambda} \frac{\left| \int_{-\frac{1}{2}L_s}^{\frac{1}{2}L_s} E(x) \, dx \right|^2}{\int_{-\frac{1}{2}L_s}^{\frac{1}{2}L_s} |E^2(x)| dx} \qquad (16\text{-}29)$$

Now for the n=o mode and $L_s \to \infty$

---

59. T. T. Taylor, "Design of Line-Source Antennas for Narrow Beamwidth and Low Side Lobes", IRE Trans. on Antennas and Propagation, Vol. AP-3, January, 1955, p. 24.

$$G = \frac{4}{\lambda} \frac{\left(\int_{-\infty}^{\infty} E_o e^{-u_o^2 x^2} \, dx \right)^2}{\int_{-\infty}^{\infty} E_o^2 e^{-2u_o^2 x^2} \, dx} \tag{16-30}$$

and

$$G = \frac{4}{\lambda u_o} \sqrt{2\pi} \tag{16-31}$$

The gain is related to the total power radiated, P_{rad}, and the maximum value S_{max}, of $S(\theta,\phi)$ of Eq. 16-27 in the following way.

$$G = \frac{4\pi R^2 S_{max}}{P_{rad}} \tag{16-32}$$

The value of P_{rad} can be obtained from

$$P_{rad} = P_{inc} T \tag{16-33}$$

where P_{inc} = power incident on slot

and T = transmission coefficient of slot and must be determined.

The value of P_{inc} for the antenna under discussion is

$$P_{inc} = \frac{1}{\eta} \int_{-\frac{w}{2}}^{\frac{w}{2}} \int_{-\infty}^{\infty} E_o^2 \, e^{-2u_o^2 x^2} \, dx \, dy \tag{16-34}$$

$$P_{inc} = \frac{w}{\eta} E_o^2 \frac{1}{u_o} \sqrt{\frac{\pi}{2}} \tag{16-35}$$

Thus P_{rad} is

$$P_{rad} = \frac{E_o^2}{\eta u_o} \sqrt{\frac{\pi}{2}} Tw \tag{16-36}$$

The transmission coefficient T as a function of slot width has been determined exactly for a capacitive ($\bar{E}$ transverse) slot in an infinitely thin perfectly conducting plane by Morse and Rubenstein.[60] Their determination, together with quite accurate variational approximations, has been used to plot the graph of Tw/λ versus w/λ shown in Fig. 16-3.[61]

An expression for I_y is now possible since the value of Tw is available from Fig. 16-3. Using Eqs. 16-31, 32 and 36 the value of S_{max} can be written

$$S_{max} = \frac{1}{4\pi R^2} \left(\frac{E_o^2}{u_o}\sqrt{\frac{\pi}{2}}\, Tw\right) \left(\frac{4}{u_o}\sqrt{2\pi}\right)$$

$$S_{max} = \frac{E_o^2\, Tw}{\eta\lambda u_o^2 R^2} \tag{16-37}$$

Comparing Eq. 16-37 with Eq. 16-27 it is evident that

$$I_y = \sqrt{Tw\lambda/\pi} \tag{16-38}$$

Thus the complete expressions for $\bar{E}$ and S are

$$\bar{E} = jE_o(\bar{u}_\theta \sin\phi + \bar{u}_\phi \cos\theta\cos\phi)\, \frac{e^{-jkR}}{u_o R}\sqrt{\frac{Tw}{\lambda}}\; e^{-k^2\sin^2\theta\cos^2\phi/4u_o^2} \tag{16-39}$$

and

$$S = \frac{E_o^2\, Tw}{\lambda R^2 u_o^2 \eta} (\sin^2\phi + \cos^2\theta\cos^2\phi)\; e^{-k^2\sin^2\theta\cos^2\phi/2u_o^2} \tag{16-40}$$

---

60. P. Morse and P. Rubenstein, "The Diffraction of Waves by Ribbons and Slits," Physical Review, Vol. 54, December 1, 1938, pp. 895-898.

61. J. N. Miles, "On the Diffraction of an Electromagnetic Wave through a Plane Screen," Journal of Appl. Phys., Vol. 20, August, 1949, pp. 767-768. See also R. F. Harrington, Time-Harmonic Electromagnetic Fields, McGraw-Hill Book Co., New York, N. Y., 1961, pp. 370-371.

where Tw/λ is obtained from Fig. 16-3. Equation 16-40 describes a radiation pattern shaped like a thin "pancake" lying in the yz plane with a maximum value at either $\theta=0$ or $\phi = \pm \pi/2$. The pattern in the xz plane, for which $\cos\phi = 1$, is proportional to $\cos^2\theta e^{-k^2\sin^2\theta/2u_o^2}$ and is essentially a Gaussian pattern. The polarization of the radiated field can be determined from Eq. 16-39. For example, for $\phi=0$, the field is polarized in the $\bar{u}_\phi$ or $\bar{u}_y$ direction.

The value of the Q of the rectangular beam waveguide resonator as a function of the radiated power can also be determined from the foregoing equations. Thus Eq. 16-36 which gives the total power radiated can be used to predict the value of Q_{oor} which is the unloaded uncoupled Q of the resonator. Recall that the external Q at the output or radiation port of the resonator is given by Eq. 16-9,

$$Q_{ex2} = \omega_r \frac{W_s}{P_{rad}}$$

and

$$W_s = \epsilon_o \int_v E^2 dV$$

where E is the r.m.s. value of the total electric field.

The value of E for the n^{th} mode is given by

$$E = |\bar{E}| = 2E_n He_n(2u_o x)e^{-u_o^2 x^2} \sin\left(\frac{2\pi}{\lambda} z\right) \qquad (16\text{-}41)$$

where E_n is the r.m.s. amplitude of the travelling wave of the n^{th} mode. Thus

$$Q_{ex2} = \omega_o \frac{\epsilon_o \int_{-\infty}^{\infty} (2E_n)^2 He_n(2u_o x)e^{-2u_o^2 x^2} dx \; h\frac{\lambda}{4}}{\frac{E_n^2}{\eta} Tw \int_{-\infty}^{\infty} He_n^2(2u_o x)e^{-2u_o^2 x^2} dx} \qquad (16\text{-}42)$$

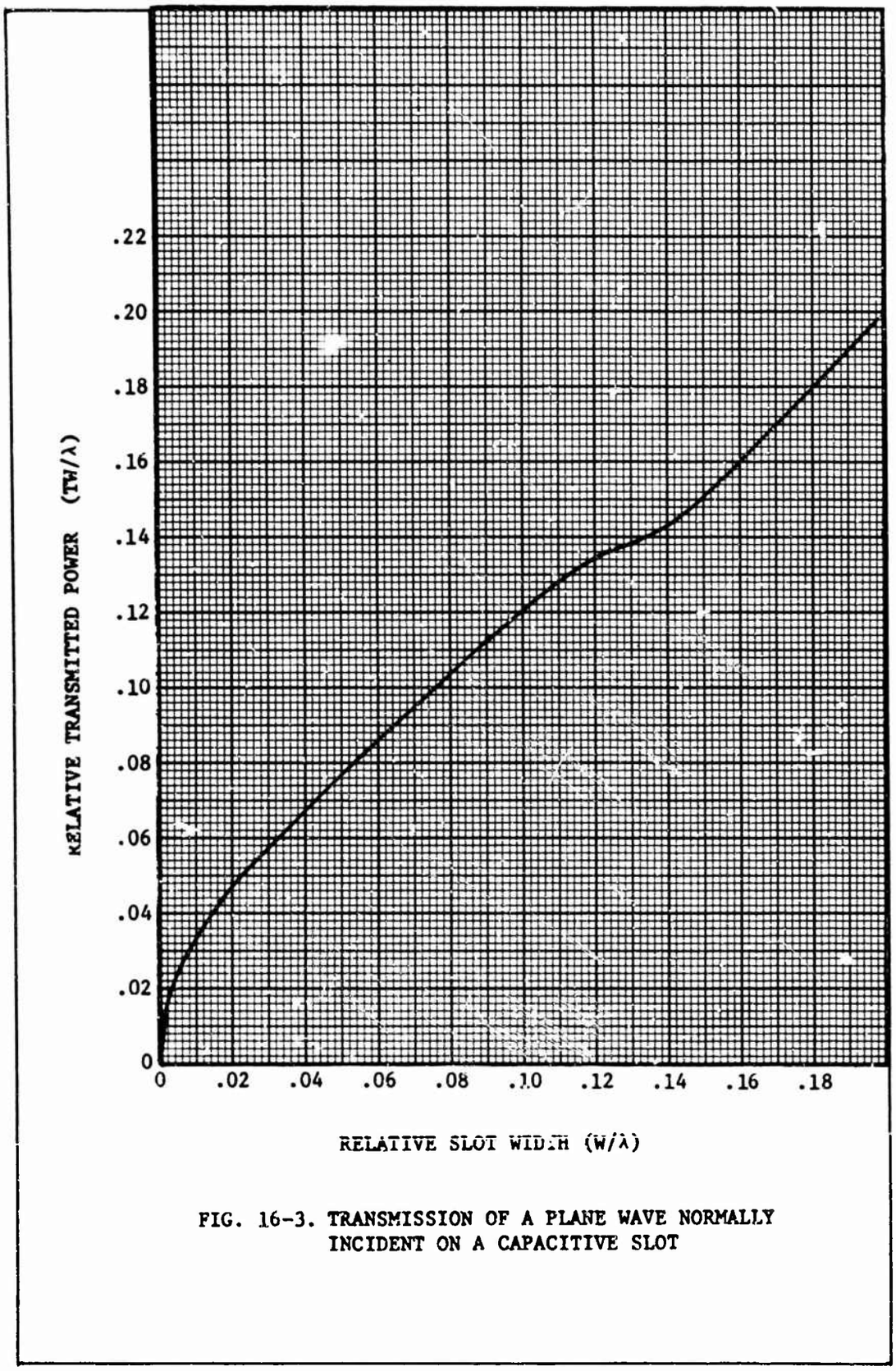

FIG. 16-3. TRANSMISSION OF A PLANE WAVE NORMALLY INCIDENT ON A CAPACITIVE SLOT

where h is the inside height of the resonator.

Simplifications yields

$$Q_{ex2} = \frac{kh}{Tw/\lambda} \tag{16-43}$$

where k is the wave number.

With the value of Q_{ex2} known the value of Q_{oor} can be determined from Eq. 16-11. Note that Q_{ex2} in Eq. 16-43 is independent of mode number.

2. Radiation Field of Finite Length Slot Antenna

A practical antenna will have a finite length. The slot length L_s in the x-direction will typically be such that $u_o L_s$ is between 3 and 10. If the integral I_x in Eq. 16-24 is evaluated for a finite slot length L_s a new value for S and hence a new radiation pattern will be obtained.

Transforming Eq. 16-24 by letting $\alpha = u_o x - jk\sin\theta\cos\phi/2u_o$,[62]

$$I_x = \frac{1}{u_o} e^{-X^2} \int_{-Y-jX}^{+Y-jX} e^{-\alpha^2} d\alpha \tag{16-44}$$

where $X = k\sin\theta\cos\phi/2u_o$ (16-45)

and $Y = u_o L_s/2$

Now from Cauchy's residue theorem of complex analysis, since $e^{-\alpha^2}$ has no singularities,

$$\oint_C e^{-\alpha^2} d\alpha = 0 \tag{16-46}$$

where C is any closed contour in the complex plane. Thus

$$\int_0^{-Y-jX} e^{-\alpha^2} d\alpha + \int_{-Y-jX}^{+Y-jX} e^{-\alpha^2} d\alpha + \int_{+Y-jX}^{0} e^{-\alpha^2} d\alpha = 0$$

62. This radiation pattern has very recently been mentioned in the literature. See T. C. Lee and J. D. Zook, "Light Beam Deflection with Electrooptic Prisms," IEEE Journal of Quantum Electronics, Vol. QE-4, July, 1968, pp. 442-454.

or

$$\int_{-Y-jX}^{+Y-jX} e^{-\alpha^2} d\alpha = -\int_{+Y-jX}^{o} e^{-\alpha^2} d\alpha - \int_{o}^{-Y-jX} e^{-\alpha^2} d\alpha \qquad (16\text{-}47)$$

Similarly

$$\int_{o}^{+Y-jX} e^{-\alpha^2} d\alpha + \int_{+Y-jX}^{o} e^{-\alpha^2} d\alpha = 0 \qquad (16\text{-}48)$$

$$\int_{o}^{+Y-jX} e^{-\alpha^2} d\alpha = -\int_{+Y-jX}^{o} e^{-\alpha^2} d\alpha \qquad (16\text{-}49)$$

Thus

$$\int_{-Y-jX}^{+Y-jX} e^{-\alpha^2} d\alpha = \int_{o}^{+Y-jX} e^{-\alpha^2} d\alpha - \int_{o}^{-Y-jX} e^{-\alpha^2} d\alpha \qquad (16\text{-}50)$$

To simplify further, let $\beta = \alpha/(Y-jX)$. Thus

$$\int_{o}^{Y-jX} e^{-\alpha^2} d\alpha = (Y-jX) \int_{o}^{1} e^{-(Y-jX)^2\beta^2} d\beta \qquad (16\text{-}51)$$

$$= Y \int_{o}^{1} e^{(-Y^2+X^2)\beta^2} e^{j2XY\beta^2} d\beta$$

$$- jX \int_{o}^{1} e^{(-Y^2+X^2)\beta^2} e^{j2XY\beta^2} d\beta$$

or

$$\int_{o}^{Y-jX} e^{-\alpha^2} d\alpha = Y \int_{o}^{1} e^{(-Y^2+X^2)\beta^2} \cos(2XY\beta^2) d\beta$$

$$+ X \int_{o}^{1} e^{(-Y^2+X^2)\beta^2} \sin(2XY\beta^2) d\beta$$

$$+ j\left[Y \int_{o}^{1} e^{(-Y^2+X^2)\beta^2} \sin(2XY\beta^2) d\beta - X \int_{o}^{1} e^{(-Y^2+X^2)\beta^2} \cos(2XY\beta^2) d\beta\right] \qquad (16\text{-}52)$$

Thus it is clear that changing the sign of Y will just change the sign of the real component of the integral on the left side of the equation. Changing the sign of X will just change the sign of the imaginary component of the integral. Thus

$$\int_o^{-Y-jX} e^{-\alpha^2} d\alpha = - \text{Re}\left[\int_o^{Y-jX} e^{-\alpha^2} d\alpha\right] + j\ \text{Im}\left[\int_o^{Y-jX} e^{-\alpha^2} d\alpha\right] \quad (16\text{-}53)$$

The expression for I_x in Eq. 16-44 becomes with Eqs. 16-50 and 53

$$I_x = \frac{1}{u_o} e^{-X^2} \text{Re}\left[2\int_o^{+Y-jX} e^{-\alpha^2} d\alpha\right] \quad (16\text{-}54)$$

Let $t = j\alpha$

$$I_x = \frac{1}{u_o} e^{-X^2} \text{Re}\left[-j2\int_o^{X+jY} e^{t^2} dt\right] \quad (16\text{-}55)$$

Further set $z = X+jY$

$$I_x = \frac{1}{u_o} e^{-X^2} \text{Re}\left[\frac{e^{-z^2} + \frac{j2}{\sqrt{\pi}} e^{-z^2}\int_o^z e^{t^2} dt}{-\frac{1}{\sqrt{\pi}} e^{-z^2}} + \sqrt{\pi}\right]$$

Tables are available that tabulate functions u and v that are defined by[63]

$$u+jv = e^{-z^2} + j\frac{2}{\sqrt{\pi}} e^{-z^2}\int_o^z e^{t^2} dt \quad (16\text{-}56)$$

Thus

$$I_x = \frac{\sqrt{\pi}}{u_o} e^{-X^2} \text{Re}[1-e^{z^2}(u+jv)] \quad (16\text{-}57)$$

but

$$e^{z^2} = e^{(X+jY)^2} = e^{X^2-Y^2}(\cos 2XY + j\sin 2XY) \quad (16\text{-}58)$$

---

63. V.N. Faddeyeva and N.M. Trent'ev, Tables of the Probability Integral for Complex Argument, Pergamon Press, New York, N.Y., 1961. See also M. Abramowitz and I. A. Stegun (Editors), Handbook of Mathematical Functions, National Bureau of Standards, U.S. Government Printing Office, Washington, D.C., 1965, pp. 297, 325-328.

Hence

$$I_x = \frac{\sqrt{\pi}}{u_o} e^{-X^2} \left\{1-\mathrm{Re}\left[e^{X^2-Y^2} (\cos 2XY+j\sin 2XY)(u+jv)\right]\right\} \qquad (16\text{-}59)$$

or

$$I_x = \frac{\sqrt{\pi}}{u_o} e^{-X^2} \left[1-e^{X^2-Y^2} (u\cos 2XY-v\sin 2XY)\right] \qquad (16\text{-}60)$$

Equation 16-60 is the final result for I_x. If $Y=u_o L_s/2$ is allowed to approach infinity then

$$I_x \xrightarrow[Y\to\infty]{} \frac{\sqrt{\pi}}{u_o} e^{-X^2} \left[1-e^{-\infty} (u\cos 2XY-v\sin 2XY)\right.$$

Tables of u and v indicate that they remain finite even for very large Y and thus

$$I_x \xrightarrow[Y\to\infty]{} \frac{\sqrt{\pi}}{u_o} e^{-X^2}$$

This agrees with Eq. 16-25 for the antenna with an infinitely long slit.

The value for I_x given by Eq. 16-60 will modify the expression for S given by Eq. 16-40. The new expression for S is

$$S = \frac{E_o^2 Tw}{\lambda R^2 u_o^2 \eta} (\sin^2\phi+\cos^2\theta\cos^2\phi)\, e^{-2X^2} \left[1-e^{X^2-Y^2} (u\cos 2XY-v\sin 2XY)\right]^2 \qquad (16\text{-}61)$$

Thus the radiation pattern is changed somewhat due to the finite length of the slot L_s. Other antenna characteristics are essentially unchanged. Equation 16-31 for G and Eq. 16-43 for θ_{ex2} are still accurate provided L_s is such that $u_o L_s$ ranges over typical values from 3 to 10.

3. Fresnel Field of Antenna

It is important, for purposes of measurements and tests, to know the distance from the antenna at which the radiation (far) field given by Eq. 16-21 begins. This distance can be estimated by examining the Fresnel field of the antenna. Instead of using the approximation implicit in Eq. 16-20, i.e.,

$$r\Big|_{y=0} \approx R - x\sin\theta\cos\phi \tag{16-62}$$

the more exact Fresnel approximation will be used. Thus from Fig. 16-2 it follows that

$$r^2\Big|_{y=0} = R^2+x^2-2Rx\cos\psi \tag{16-63}$$

$$\text{but } \cos\psi = (\text{x component of R})/\ R = R\sin\theta\cos\phi/R \tag{16-64}$$

$$\text{thus } r^2 = r^2+x^2-2Rx\sin\theta\cos\phi.$$

The Fresnel approximation is[64]

$$r=R-x\sin\theta\cos\phi + \frac{x^2}{2R}\,(1-\sin^2\theta\cos^2\phi) \tag{16-65}$$

and when squared is equal to r^2 except for negligible terms of the order of x^3R^{-1} and x^4R^{-2}.

Equation 16-21 can be modified to express the Fresnel field instead of the far field only, by adding the x^2 terms of Eq. 16-65 to the exponent, thus

$$\bar{E} = j(\bar{u}_\theta\sin\phi+\bar{u}_\phi\cos\theta\cos\phi)\,\frac{e^{-jkR}}{\lambda R}\,E_o\cdot$$

$$\int_{y=-\frac{w}{2}}^{\frac{w}{2}}\int_{x=-\frac{L_s}{2}}^{\frac{L_s}{2}} e^{-(u_o^2+j\,\frac{k}{2R}\,(1-\sin^2\theta\cos^2\phi))x^2}\,e^{jk(\sin\theta\cos\phi x+\sin\theta\sin\phi y)}\,dxdy \tag{16-66}$$

This can be rewritten as,

$$\bar{E} = j(\bar{u}_\theta\sin\phi+\bar{u}_\phi\cos\theta\cos\phi)\,\frac{e^{-jkR}}{R}\,E_o\sqrt{\frac{Tw}{\lambda\pi}}\,I_{xf} \tag{16-67}$$

where

$$I_{xf} = \int_{-\frac{L_s}{2}}^{\frac{L_s}{2}} e^{-(u_o^2+j\,\frac{k}{2R}\,(1-\sin^2\theta\cos^2\phi))x^2}\,e^{jk\sin\theta\cos\phi\,x}\,dx \tag{16-68}$$

---

64. R. C. Hanson, Microwave Scanning Antennas, Vol. 1, Academic Press, New York, N. Y., 1964, p. 26.

Now I_{xf} has been examined for $L_s = \infty$, in which case it has the value,[65]

$$I_{xf} = \frac{\sqrt{\pi}}{u_o\sqrt{1+jb}} e^{-k^2\sin^2\theta\cos^2\phi/(4u_o^2(1+jb))} \qquad (16\text{-}69)$$

where b = defocusing ratio = $k(1-\sin^2\theta\cos^2\phi)/2Ru_o^2$.

For $|\theta|$ less than about 20°, b is approximately constant and equal to $k/2Ru_o^2$. The Fresnel integral I_{xf} for $|\theta| < 20°$ is therefore a Gaussian function but with a greater standard deviation than the far field function I_x. However for b<0.1 the function I_{xf} has approximately the same standard deviation as I_x. Thus the distance $R=R_m$ for which b=0.1 may be taken as the border or edge of the far field. At a distance from the antenna smaller than R_m the power or field squared pattern, which is proportional to the square of I_{xf}, is broadened (defocused) but remains Gaussian.

D. Aperture of Closely Spaced Holes

1. Comparison with the Slot Aperture

An alternative to the slot aperture is an aperture consisting of a row of circular holes spaced along the x axis. This type of aperture coupling results in discrete sources rather than the continuous line source of the slot. Thus the radiation pattern of the holes is in general not found by taking a Fourier transform. Instead, assuming an infinitely thin wall in which the coupling holes are placed and an incident field that is uniform over a given hole, each hole can be treated as a magnetic dipole directed in the x-direction.[66] If there were no coupling between the holes, then the strength of each dipole would be proportional to the field incident on the hole from the resonator.

---

65. H. A. Wheeler, "Antenna Beam Patterns which Retain Shape with Defocusing," IRE Trans. on Antennas and Propagation, Vol. AP-10, September 1962, pp. 574-575.

66. H. A. Bethe, "Theory of Diffraction of Small Holes," Physical Review, vol. 66, nos. 7,8, October 1, 1944, pp. 165, 171.

In such a case the strength of the dipoles would follow a Gaussian distribution for the n=0 mode in the resonator. The radiation pattern of such an array of dipoles is easily calculated using antenna array theory. The appropriate formula is for an array of dipoles of constant phase positioned along the x axis:[67]

$$E_{rad}(\theta) \propto D_1 e^{jkx_1\cos\theta} + D_2 e^{jkx_2\cos\theta} + \ldots + D_N e^{jkx_N\cos\theta} \qquad (16\text{-}70)$$

where D_n = dipole strength of the n^{th} dipole

x_n = position of the n^{th} dipole on the x axis

$E_{rad}(\theta)$ = radiation field intensity as function of the angle θ in Fig. 16-2.

For example, for holes spaced every half wavelength from x = 0 to x = $\pm(1/2)L_s = \pm 14"$, the radiation pattern was calculated using Eq. 16-70 on an IBM 1620 digital computer. The pattern obtained is very similar to the Gaussian pattern obtained for slot coupling except that sidelobes appear which are approximately 60 db below the pattern maximum.

Coupling between the dipoles does exist, however, and will affect the power radiated by each dipole. Each dipole will radiate a power proportional to both the field strength inside the resonator and the field at the front of the hole produced by the other dipoles of the array. Thus it is difficult to say without further detailed analysis whether or not the power radiated by the dipoles still follows the Gaussian distribution which results in a narrow beam antenna. Since both the hole size and the number of holes used in the array can be changed, a large variation in the coupling is possible when hole coupling is used. This coupling variation will prove to be an important advantage over the slot aperture.

---

67. E. C. Jordan, Electromagnetic Waves and Radiating Systems, Prentice-Hall, Inc., Englewood Cliffs, N.J., 1950, p. 402.

A certain special case of hole aperture coupling can be analyzed without great difficulty. In this case the holes are all of constant diameter and are all spaced as close as possible alongside one another on the x axis. It is customary to calculate the radiation pattern in this case assuming the coupling to be uniform along the entire length of the holes. An example of such a calculation is given in the paper by Jacobsen et al.[68] Thus a row of closely spaced holes can be considered as a line source as far as the radiation pattern is concerned. Hence the radiation pattern and gain G calculated in the previous section for slot coupling apply also for the special case of hole coupling treated here.

Jacobsen also shows that the equivalent circuit of a cavity-backed antenna with hole apertures is of the form of Fig. 16-1. He also shows that B_a is negative, and thus Eq. 16-4 predicts a decrease in the resonant frequency rather than an increase as was the case for the slot. The values of B_a and R_a determine the transmission coefficient T for the hole apertures as derived in the next section.

2. Radiation Field of Hole Aperture

The transmission coefficient and the corresponding external Q of the closely spaced circular holes must be calculated before the radiation pattern of the antenna can be calculated. The transmission coefficient cannot be calculated by multiplying the transmission coefficient of a single hole by the number of holes. Bethe gives the transmission coefficient of a single isolated hole, but the presence of other holes causes the field on the outside of each hole to increase.[69] This mutual coupling increases the power radiated by each hole.

---

68. See reference in footnote 51.

69. See reference in footnote 66, p. 173.

Two valid methods of calculating the transmission coefficient and Q_{ex2} are presented here. The first method is based on calculations by Jacobsen et al.[70] and on the theory of artificial dielectrics. The second method involves expressing the holes as a line source of dipole moments.

Jacobsen's method of calculation consists of first finding the impedance Z_a of the holes in the aperture plate, then the corresponding power transmission coefficient T_p, and finally the corresponding Q_{ex2}. His calculations are carried out for the case of the infinite plane of holes shown partially in Fig. 16-4a. A TEM wave is assumed normally incident with E directed as shown. Conducting planes perpendicular to the plane of the holes and to the electric vector may be inserted without changing the field configuration. Such planes are indicated by the dotted lines in Fig. 16-4a. Thus parallel-plane waveguides are formed, each of which terminates in a row of holes, as shown in Fig. 16-4b. Collin shows that the impedance of the plate in Fig. 16-4b is the same as that of Fig. 16-4a.[71]

The rectangular beam waveguide antenna with an aperture of closely spaced holes is very similar to Fig. 16-4b. The resonator on the left side of the aperture feeds the row of holes through a parallel-plane waveguide as shown in Fig. 16-4b. On the right side of the aperture of holes, however, the situation differs from the parallel-plane waveguide. The antenna aperture must couple to free space and it will be assumed that it sees either a ground plane or flares. A ground plane is made by altering Fig. 16-4b so that the angle θ is 0° instead of 90°. Flares consist of altering Fig. 16-4b so that $0° < \theta < 90°$ and so that the metal plates are of finite length. Either of these alterations to Fig. 16-4b

---

70. See reference in footnote 51.

71. R. Collin, Field Theory of Guided Waves, McGraw-Hill Book Co., New York, N.Y., 1960, p.530.

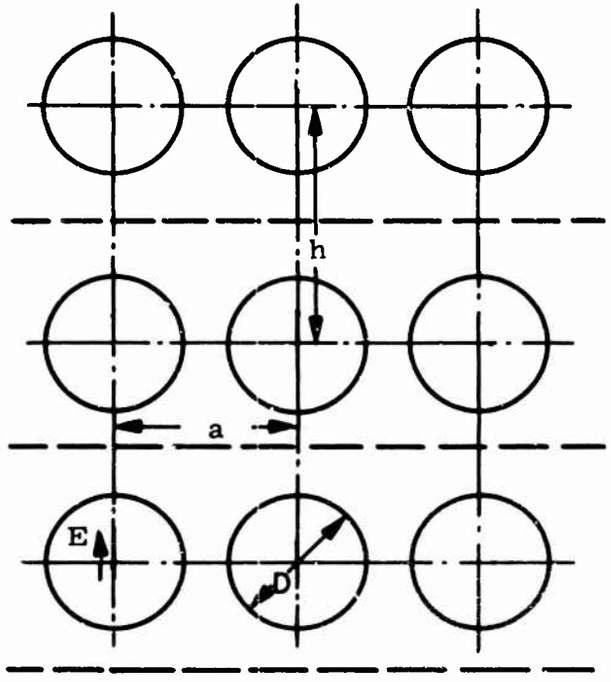

a) array in two dimensions

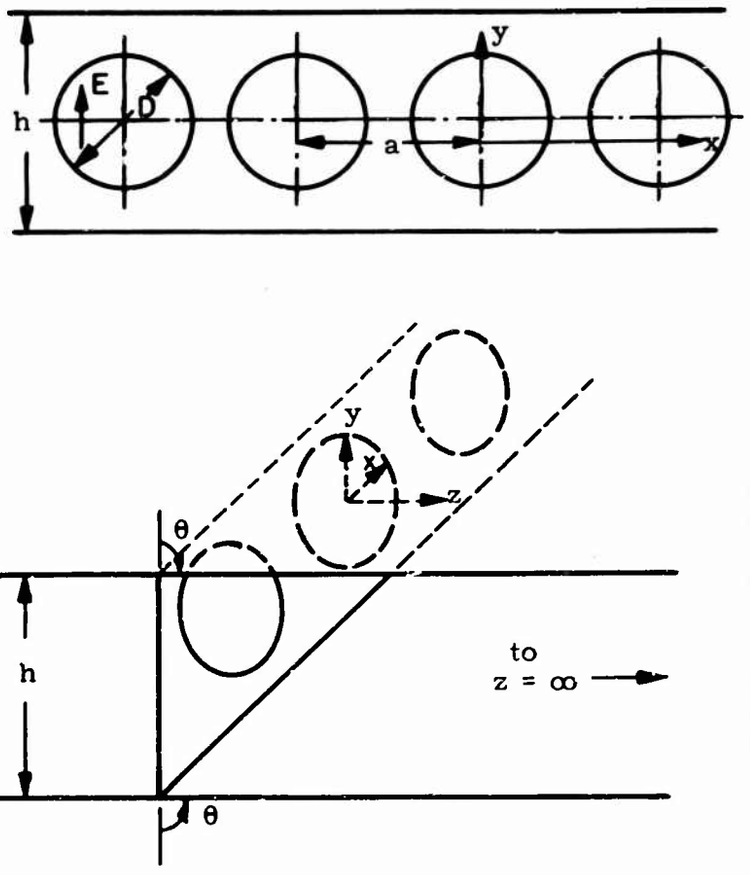

b) row of holes

FIG. 16-4 APERTURE OF CLOSELY SPACED HOLES

will alter the field configuration for z>0 and hence will alter the aperture inpedance Z_a and the corresnonding transmission coefficient somewhat. It is expected, however, that the impedance of the plate in Fig. 16-4a approximates the Z_a of the rectangular beam waveguide antenna with an aperture of closely spaced holes.

The equivalent circuit of a cavity-backed antenna with the hole aperture of Fig. 16-4b is the same as shown in Fig. 16-1 with the susceptance B_a in parallel with the resistance of free space.[72] Jacobsen gives the formula for the normalized susceptance $\tilde{B}_a = B_a Z_c$ for Fig. 16-4b with a = b as:

$$\tilde{B}_a = \underbrace{\left[-\frac{3\lambda a^2}{\pi D^3 \cos\theta}\right]}_{b_1}\underbrace{\left[1 - (\lambda_c/\lambda)^2\right]}_{b_2}\underbrace{\left[1 - \frac{2}{3}D^3 \cdot \frac{0.36}{a^3}\right]}_{b_3} \qquad (16\text{-}71)$$

where λ_c = cutoff wavelength for TE_{11} circular mode in circular waveguide of diameter d; $\lambda_c = 1.706D$

θ = angle of incidence of wave = 0° here

The factor b_1 is the basic normalized susceptance of a plate with circular holes and agrees with expressions found elsewhere such as in Collin.[73] The factors b_2 and b_3 are second order correction terms as explained by Jacobsen. The factor b_2 improves the accuracy of the $\tilde{B}_a$ expression for large values of diameter D. The factor b_3 improves the accuracy for very closely spaced holes. The assumption that $a<<\lambda$ was made in deriving b_3.

For the case of $a \neq b$, Eq. 16-71 must be modified. Examining Jacobsen's reference shows that (a^2) must be replaced by (ab) in the factor b_1, and that the factors b_2 and b_3 are unchanged.[74] This reference also shows that the factor 0.36 in the b_3 factor is actually 1.2/π, which equals 0.38. Hence the

---

72. See reference in footnote 51, p. 1432.

73. R. Collin, Foundations for Microwave Engineering, McGraw-Hill Book Co., New York, N.Y., p. 340.

74. See reference in footnote 71, pp. 522, 534-536.

susceptance expression becomes

$$B_a = -\frac{3\lambda ah}{\pi_p^3}[1-(\lambda_c/\lambda)^2][1-\frac{2}{3}\cdot 0.38(D/a)^3] \qquad (16\text{-}72)$$

The power transmission coefficient T_p is that of a normalized admittance $\tilde{Y}_a = 1+j\tilde{B}_a$ at the end of a transmission line. Thus

$$T_p = (1+\frac{1-\tilde{Y}_a}{1+\tilde{Y}_a})^2 = (1+\frac{1-1-j\tilde{B}_a}{1+1+j\tilde{B}_a})^2 = (\frac{2}{2+j\tilde{B}_a})^2 \qquad (16\text{-}73)$$

Typical values of $\tilde{B}_a$ will be much greater than two, so that

$$T_p \approx 4/(\tilde{B}_a^2) \qquad (16\text{-}74)$$

The external quality factor Q_{ex2} can be found directly in terms of T_p. By the previous definition $Q_{ex2} = \omega_r W_s/P_{rad}$. In the case of the rectangular beam waveguide resonator-antenna,

$$Q_{ex2} = \frac{2\pi f_r \varepsilon_o \int_v (2E_n(x)\sin(2\pi z/\lambda)^2\, dx\, dy\, dz}{T_p \int_{-\frac{1}{2}h}^{\frac{1}{2}h}\int_{-\infty}^{\infty} \frac{1}{\eta} E_n^2(x)\, dx\, dy} \qquad (16\text{-}75)$$

where E_n = incident electric field

$$Q_{ex2} = \frac{2\pi}{T_p}\frac{f\varepsilon\lambda}{1/\eta} \qquad (16\text{-}76)$$

But $\lambda = c/f = 1/(f\sqrt{\mu_o\varepsilon_o})$, thus

$$Q_{ex2} = 2\pi/T_p \qquad (16\text{-}77)$$

which agrees with an expression in Jacobsen for an ordinary waveguide cavity.[75]

Combining Eqs. 16-77, 74 and 72 gives the result

---

75. See reference in footnote 51, p. 1432.

$$Q_{ex2} = \frac{9\lambda^2 \; a^2h^2 \; (1-(\lambda_c/\lambda)^2) \; (1- \; (2/3)(D/a)^3 \cdot 0.38)^2}{2\pi D^6} \qquad (16\text{-}78)$$

This is an approximate expression for the Q_{ex2} of the antenna with an aperture of closely spaced holes. It is an approximation rather than an equality because the aperture does not open onto an infinitely long parallel-plane waveguide. With this Q now known approximately, the value of Q_{oor} may be calculated using Eq. 16-11.

The effect of the holes on the resonant frequency is easily seen by noting that B_a in Eq.16-72 is negative. Then according to Eq. 16-4 ω_r will be lowered because of the holes.

The second method of calculating Q_{ex2} will now be given. The first step is to find the expression for the line source of dipole moments which are produced by the closely spaced holes. Then the power radiated by this line source is found and finally Q_{ex2} is determined.

The strength of the line sound is related to the size and number of circular holes. Each hole has the magnetic dipole moment[76]

$$\bar{P}_m = \frac{1}{3} D^3 \bar{H}_o \qquad (16\text{-}79)$$

where $\bar{H}_o$ is the incident magnetic field. Now the electric field in the hole is related to the dipole moment per unit area, $\bar{p}_m$, by[77]

$$j\bar{E} = \omega\mu_o \bar{p}_m \times \bar{u}_z \qquad (16\text{-}80)$$

$$\text{where } \bar{p}_m = \bar{P}_m/A \qquad (16\text{-}81)$$

Usually the area A is that of the circular hole. However, assume

$$A = a\,w$$

where a is the hole separation as before and w is some unknown width in y

---

76. See reference in footnote 71, p. 301.

77. G. Goubau, unpublished notes.

over which the dipole moment is spread. Then there exists a line source of value

$$E_y(x,y,0) = \omega\mu_o \frac{D^3 H_o}{3aw} \qquad \text{for } |y| < \frac{1}{2}w$$

$$= 0 \qquad\qquad |y| > \frac{1}{2}w \tag{16-83}$$

Note the similarity to a slot. Since here the width w is of ambiguous value, a way is sought to eliminate it from the determination of Q_{ex2}. The elimination of w can be achieved if the approximation that E_y has a delta function dependence in y is assumed. Hence

$$E_y(x,y,0) = \omega\mu_o \frac{D^3 H_o}{3a} \delta(y) \tag{16-84}$$

This equation is the same as Eq. 16-83 for $w \to 0$; both equations have the same value of $\int_y E_y\, dy$ = voltage.

The power radiated by the line source of Eq. 16-84 can be calculated by the techniques used previously for the slot. The radiated field strength is given by Eq. 16-21:

$$\bar{E} = j(\bar{u}_o \sin\phi + \bar{u}_\phi \cos\theta\cos\phi) \frac{e^{-jkR}}{\lambda R} I_y I_x \tag{16-85}$$

$$\text{where } I_y = \int_{-\infty}^{\infty} \omega\mu_o \frac{D^3 H_o}{3a} \delta(y)\, e^{jk\sin\theta\sin\phi y}\, dy \tag{16-86}$$

$$I_x = \frac{\sqrt{\pi}}{u_o} e^{-k^2\sin^2\theta\cos^2\theta/4u_o^2} \tag{16-87}$$

Thus

$$I_y = \omega\mu_o D^3 H_o/(3a) \tag{16-88}$$

So

$$\bar{E} = j(\bar{u}_o \sin\phi + \bar{u}_\phi \cos\theta\cos\phi) \frac{D^3\sqrt{\epsilon_o/\mu_o}E_o}{3a} \frac{e^{-jkR}\omega\sqrt{\pi}}{\lambda R} e^{-k^2\sin^2\theta\cos^2\phi/4u_o^2} \tag{16-89}$$

where E_o is the incident electric field of the n=o mode. Equation 16-89

describes the same radiation pattern as that of the slot.

Now the maximum value of Eq. 16-89 is

$$E_{max} = \frac{e^{-jkR}}{\lambda R}\frac{\sqrt{\pi}}{u_o}\omega\frac{D^3\sqrt{\mu_o\varepsilon_o}}{3a}E_o \qquad (16\text{-}90)$$

Therefore

$$S_{max} = \left|E_{max}\right|^2/\eta = \frac{\varepsilon_o\pi\omega^2E_o^2\sqrt{\mu_o\varepsilon_o}\,D^6}{9u_o^2\lambda^2R^2a^2} \qquad (16\text{-}91)$$

From Eqs. 16-31 and 16-32,

$$G = \frac{4}{\lambda u_o}\sqrt{2\pi} = \frac{4\pi R^2 S_{max}}{P_{rad}}$$

Thus

$$P_{rad} = \frac{\pi^{3/2}\varepsilon_o\omega^2E_o^2D^6}{9\sqrt{2}\,cu_o\lambda a^2} \qquad (16\text{-}92)$$

Now $Q_{ex2} = \omega_r W_s/P_{rad}$, so

$$Q_{ex2} = \frac{\omega\varepsilon_o 4E_o^2(\lambda/4)h\sqrt{\pi/2}/u_o}{P_{rad}} \qquad (16\text{-}93)$$

Substituting Eq. 16-92 into Eq. 16-93 and simplifying gives the final result

$$Q_{ex2} = \frac{9\lambda^3 ha^2}{2\pi^2 D^6} \qquad (16\text{-}94)$$

It is interesting to compare Eq. 16-94 with the result of the other method, Eq. 16-78. Equation 16-78 contains more factors than does Eq. 16-94, but using the fact that closely spaced holes have $(D/a)\approx 1$, both equations give

$$Q_{ex2} = C_E a^2 D^{-6} \qquad (16\text{-}95)$$

where C_E is a function of λ and h

The factor D^{-6} agrees with Bethe's coupling hole theory which has the radiated power proportional to D^{6}.[78] The factor a^2 can be eliminated by noting that

78. See reference in footnote 66, p. 173.

the number of holes N in the line source of Length L is

$$N = L/a \tag{16-96}$$

Thus $a^2 = L^2/N^2$, so

$$Q_{ex2} = \frac{C_E L^2}{D^6 N^2}$$

Hence the power radiated is proportional to the square of the number of holes if all other parameters remain constant.

The factor C_E in Eq. 16-95 is expressed somewhat differently by Eqs. 16-94 and 78. This difference is not too surprising considering the different approximations made in each method. The next section will compare actual numerical values of Q_{ex2} calculated from these two equations. The values obtained by Eq. 16-94 should be slightly more accurate than those obtained using Eq. 16-78, since the second method assumed radiation into half space rather than into a waveguide.

XVII EXPERIMENTAL STUDY OF THE RECTANGULAR BEAM WAVEGUIDE ANTENNA

A. Measurement Apparatus and Techniques

Two measurement techniques were used to investigate the experimental cavity-backed antenna. The first was the reflectometer technique discussed previously in section XV. The second technique involved measuring the radiation pattern of the antenna.

The reflectometer technique is applicable because it was shown previously that the cavity-backed antenna with either the slot or the hole aperture has an equivalent circuit which is a resonant circuit. In section XV the technique was used to measure the Q_{oo} and Q_o of the closed resonator. For the cavity-backed antenna the same technique was used to measure Q_{oor} and Q_{or}.

These measurements were always made with the probe adjusted for critical coupling, unless otherwise stated.

The antenna radiation pattern measurements were made in a chamber which was about 2 meters wide, 4 meters high, and 8 meters long. The entire floor of the chamber, as well as the walls to a height of 2.2 meters, was covered with a microwave absorber. The rectangular beam waveguide antenna, with its xz plane horizontal, was placed on a 1 meter high turntable located at one end of the measuring chamber as shown in Fig. 17-1. To prevent reflections off of the front of the table, microwave absorber was placed over it. The antenna with the probe adjusted for critical coupling was fed by a klystron through an isolator.

A receiving horn was located at the other end of the measuring chamber some six meters from the transmitter. The horn was aimed at the transmitting antenna. A microwave superheterodyne receiver was used as a detector.

The antenna pattern was measured by using a precision waveguide attenuator located at the input of the receiver to maintain a constant receiver output while the rectangular beam waveguide antenna was rotated about its y axis. The angle rotated was the angle θ of Fig. 17-2, measured between the z axis and the line joining the transmitting and receiving antennas. The radiation pattern then is the plot of the measured attenuation at the receiver versus θ. The gain was measured by comparing the maximum attenuation required at the receiver for the beam waveguide antenna with the maximum attenuation required when the antenna was replaced with a standard gain horn. The measured gain thus included the effects of losses within the resonator.

The length of the chamber is believed to be adequate for radiation field measurements. This adequacy was determined by evaluating Eq. 16-69 for the

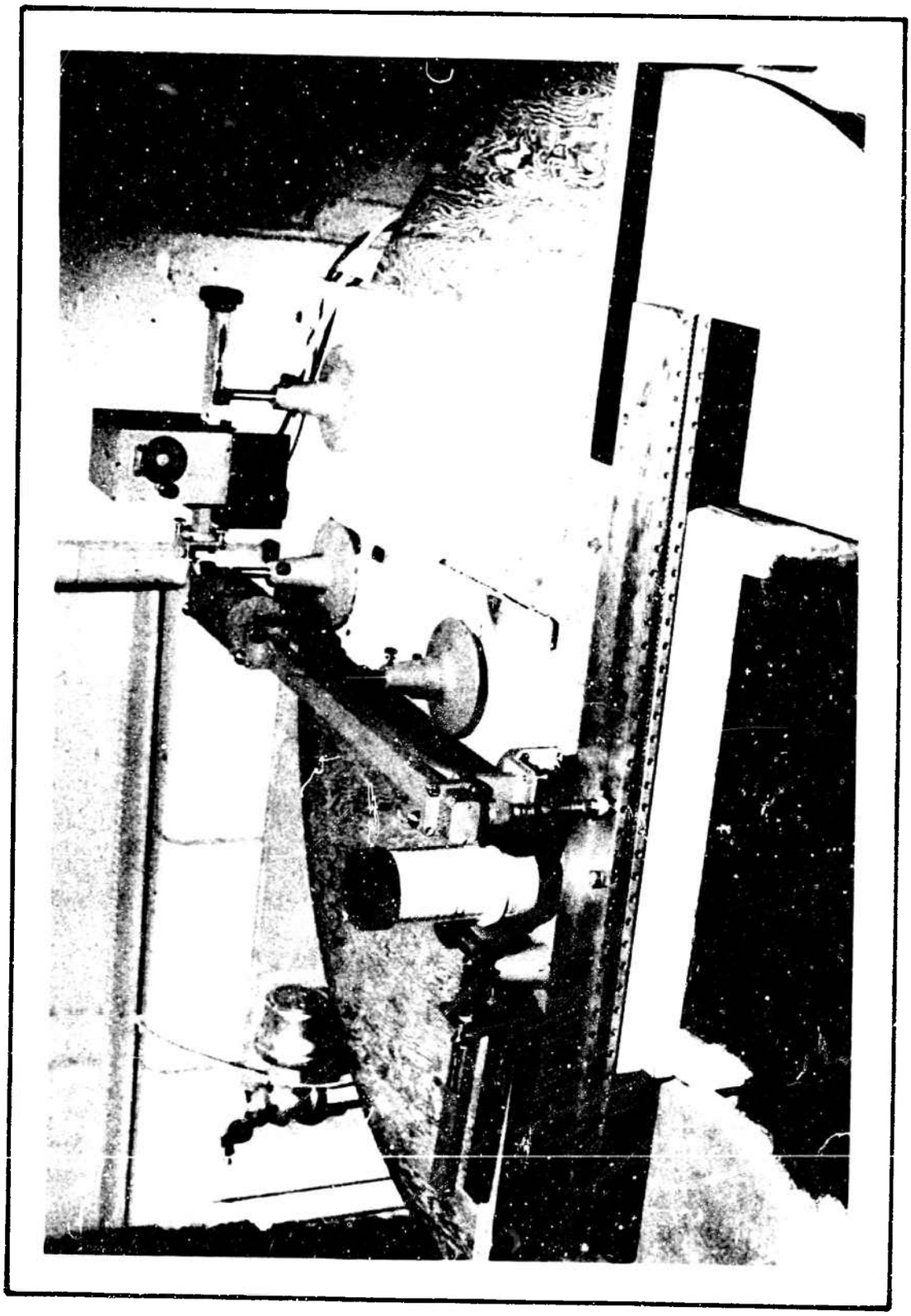

FIG. 17-1. ANTENNA AND TURNTABLE

Fresnel field. The distance $R = R_m$ at which the radiation or far field begins can be calculated from Eq. 16-69 with $\sin\theta\cos\phi = 0$. Thus

$$R_m = 5k/u_o^2 \tag{17-1}$$

For the experimental antenna $u_o^2 = 141\ m^{-2}$ so that $R_m = 6.68$ m. The field patterns measured in the chamber were made at a distance of six meters from the antenna. Although the measurements were made at a distance somewhat less than $R_m = 6.68$ m., the measured patterns should be very similar to the theoretical radiation field pattern.

Certain imperfections existed in the pattern measuring arrangement. These consisted mainly of reflections from the walls of the measuring chamber and leakage from the waveguide system. It appears that the measurements are reliable to levels of 35 or 40 db below the expected pattern maximums. A better chamber would be needed if greater accuracy were required.

B. Slot Aperture

1. Design and Fabrication

The fabrication of the rectangular beam waveguide antenna was achieved by modifying the experimental resonator of section XV. The original resonator was fabricated with a removable wall at the z = 0 plane. This wall or plate was a brass strip 1/4" x 1 1/8" x 30" and was held in place by 80 screws. To make the resonator into an antenna the solid wall had to be removed and replaced with a thinner brass strip with coupling apertures in it such as holes or a slot. The cross-section of this new wall in which the coupling apertures were placed as shown in Fig. 17-2. Also shown are brass flares which can be attached if desired. The flares extend in x from x = -12" to +12". The thickness of the z = 0 wall in the region where the slot or holes were cut was 0.025" and extended

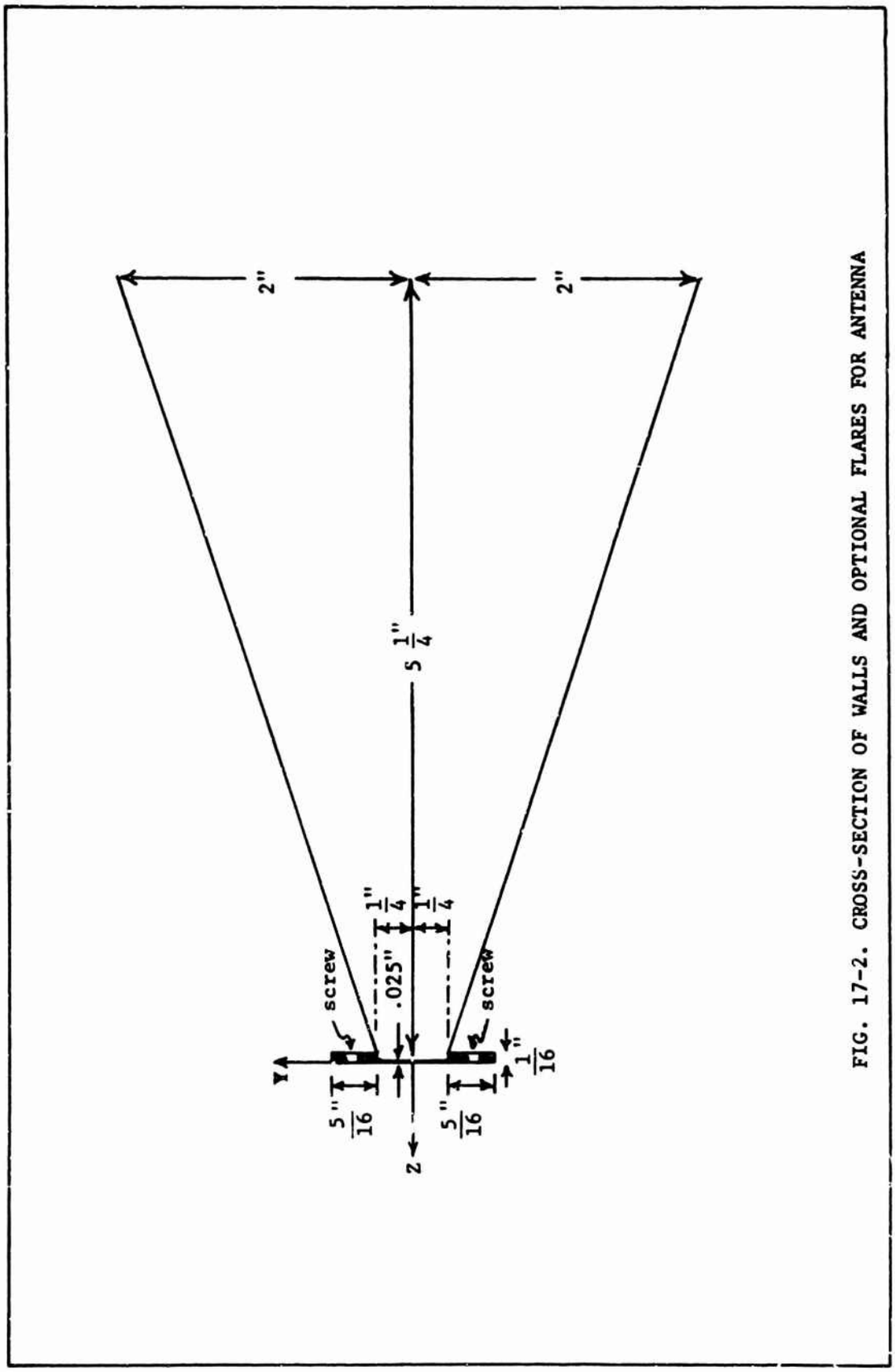

FIG. 17-2. CROSS-SECTION OF WALLS AND OPTIONAL FLARES FOR ANTENNA

the full length of the x axis of the resonator. It was hoped that the wall thickness of 0.025" would be thin enough to approximate the infinitely thin wall assumed in the previous section. The new wall was also held in place with 80 flat head screws extending from x = -15" to x = +15".

The first slot antenna was made by sawing a slot from x = -12" to x = +12" of nominal width w = 0.018". The sawing was done after the wall had been attached to the resonator with the 80 screws, since screwing down the wall after sawing the slot could result in stretching the slot width in places. All burrs were removed with a file while the wall was still attached with the screws. Ideally, the slot should then occupy the area from y = 0.009" to +0.009" and from x = -12" to +12". In fact, however, the y boundaries of the carefully machined slot were somewhat in error. This error was due to two causes. First, the saw wandered off the x axis as it cut, producing a very slightly crooked line which wanders a few thousandths of an inch off the x axis. Secondly, the width of the slot was not 0.018" but 0.018" $\pm$ 0.002". That is, the width was nonuniform, varying by as much as $\pm$ 0.002" along the length of the slot. This slight nonuniformity is undesirable since it could conceivably perturn the radiation pattern.

A second slot antenna was later made by removing the z = 0 wall of the first slot antenna and replacing it with a similar wall that had a slot cut in it which had a width of 0.010". The width of the 0.010" slot varied by $\pm$ 0.002" along its length. This is a variation of $\pm$ 20%, larger than that of the 0.018" slot. The two walls with the slots are shown in the photograph of Fig. 17-3. The 0.010" slot width was the smallest that could be machined, since narrower saws broke while sawing.

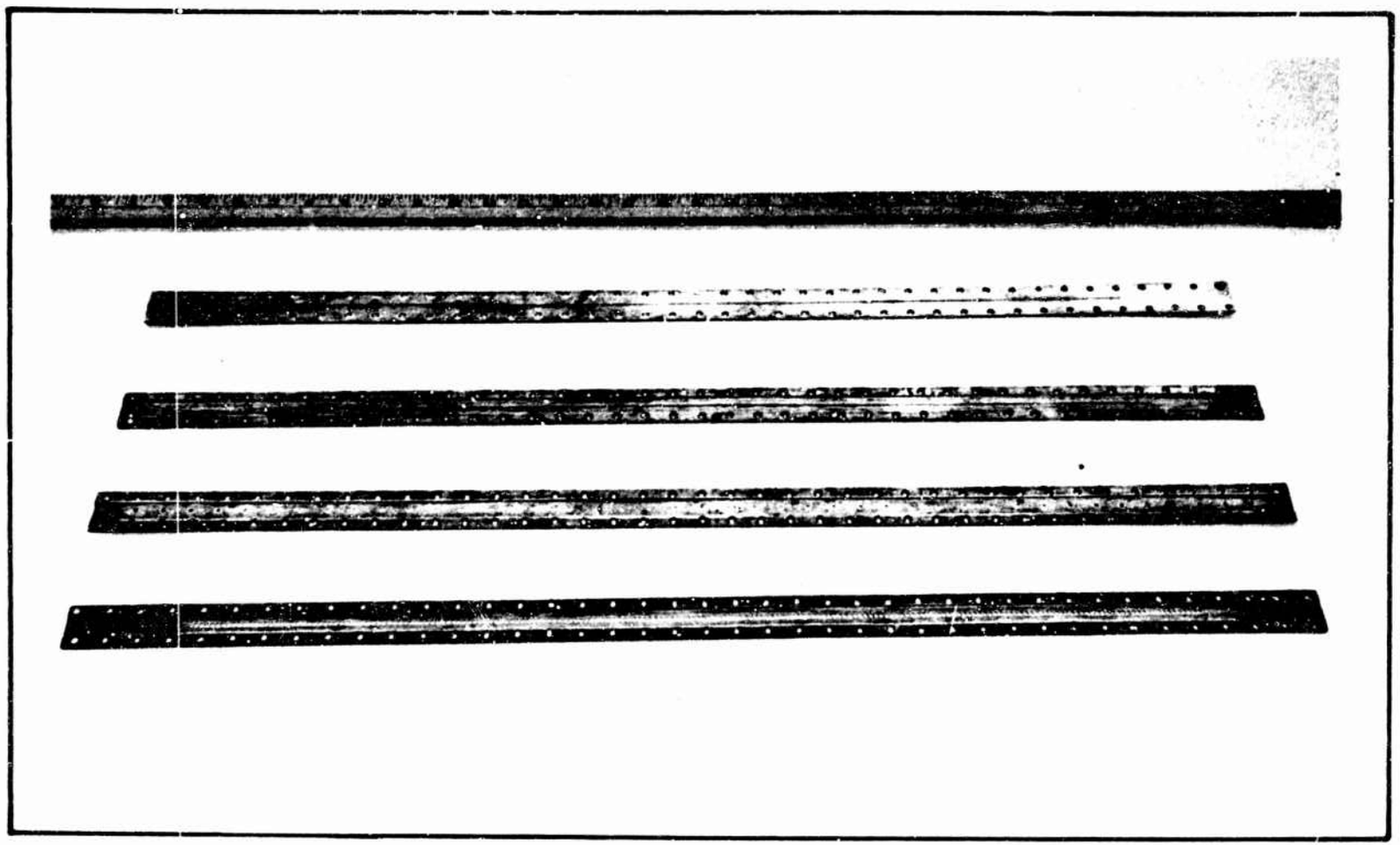

FIG. 17-3. WALLS WITH A SLOT OR HOLES

2. Results of Measurements

The slot antenna with w = 0.018" was the first to be tested. It was attached to the reflectometer apparatus and the probe depth was adjusted for critical coupling for the n = o mode. Then the quality factors listed in Table 17-1 were measured. Note that the use of the optional brass flares of Fig. 17-2 had little effect on the Q's. The purpose of the flares was to introduce directivity in the yz plane and thereby to raise the antenna gain.

The antenna gain and radiation pattern for the slot with w = 0.018" were measured at the resonant frequency of the n = o mode. The total measured gain was 14.0 db without the flares and 19.0 db with the optional flares in place. The radiation patterns are shown in Fig. 17-4.

The theoretical Q_{oor} of the antenna was previously calculated and resulted in a value of $Q_{oor} = 52$. The experimental values of 150 and 160 in the Table are about three times as large as the theoretical value. The antenna slot coupling wall was about 0.025" thick so that this dimension was even greater than the slot width w = 0.018". Thus the assumption used in the theory of having an infinitely thin slot wall is not valid for the experimental antenna. A thick slot wall would tend to increase Q_{oor} and this was borne out by the measurements.

The experimental radiation patterns of Fig. 17-4 do not agree with the theoretical Gaussian radiation pattern of the n=o mode. The dotted line in Fig. 17-4 shows the calculated or theoretical pattern. Note that there is agreement only over the range $|\theta| < 7°$. For $|\theta| > 7°$ the experimental patterns are poor. This is possibly due to the following reasons:

First, the antenna cavity may contain fields that have a small n=1 component in addition to the n=o mode. This multimoding stems from the overlap of the n=o

	One-Port Resonator	0.010" Slot with Flares	0.018" Slot No Flares	0.018" Slot With Flares
Resonant Frequency $f_{n=o}$, GHz	8.975	9.342	9.375	9.380
Loaded Q for critical coupling	1620	110*	80*	90*
Unloaded Uncoupled Q	3200	200*	160*	170*
Unloaded but Coupled Q	3120	190*	150*	160*
Probe depth for critical coupling	about 1 mm.	about 5 mm.	about 6 mm.	about 6 mm.

* Accuracy in doubt since Q's are so low that observed reflection pattern from antenna input has an n=o resonance so broad that it apparently overlaps somewhat into the n=1 resonance.

TABLE 17-I

MEASURED VALUES OF Q FOR THE SLOT ANTENNA

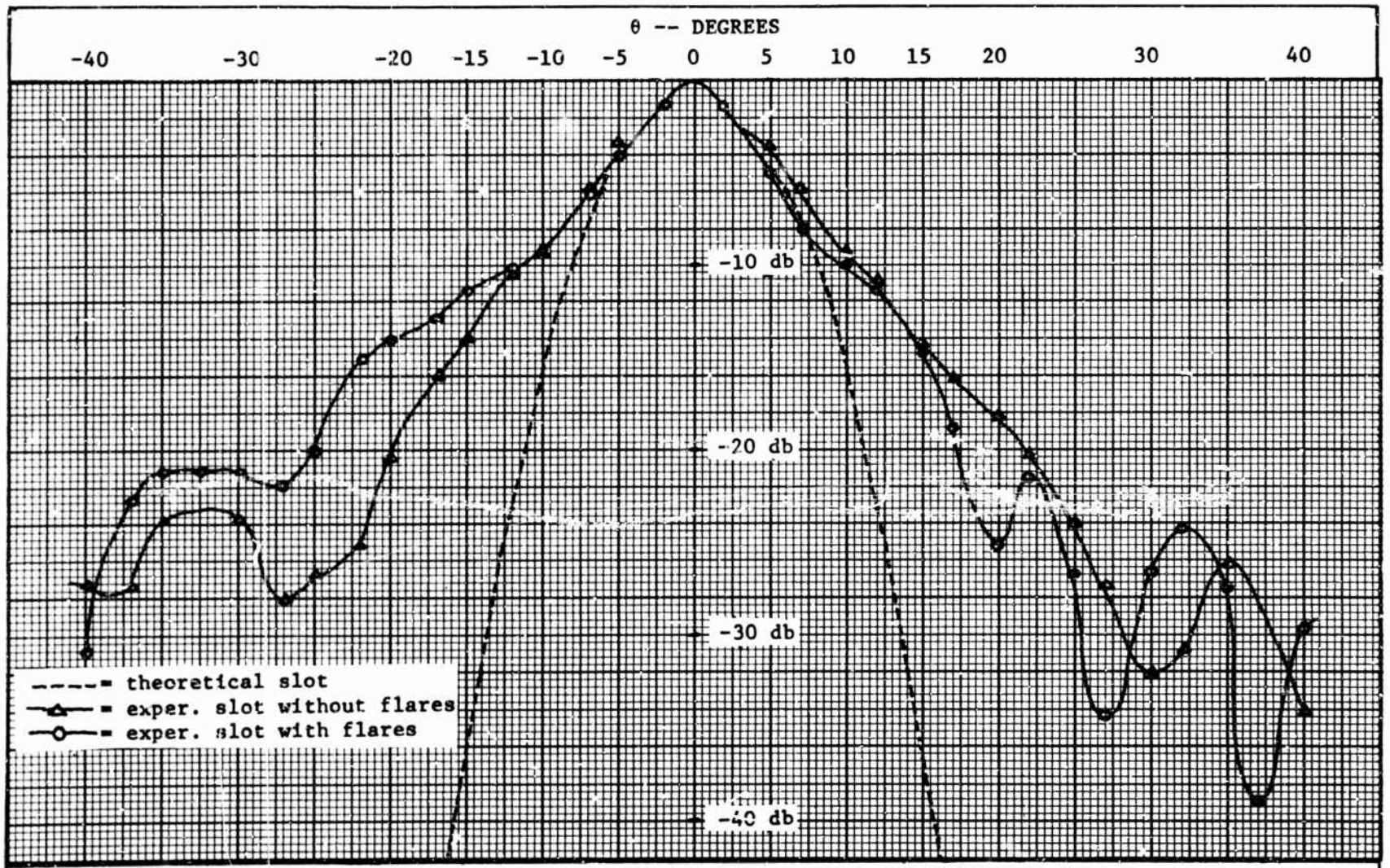

FIG.17-4. RADIATION PATTERNS OF THE SLOT ANTENNA

and n=1 resonance curves and is due to the low Q's listed in Table 17-1. Thus exciting the antenna at $f_{n=o}$ produces fields of the n=o mode with the addition of small amplitude fields of the n=1 mode. The exciting probe is at position x = 0 and should theoretically not excite the n=1 mode at any frequency. However in section XV it was shown that asymmetry in the machined resonator allowed some excitation of the n=1 mode. If the Q's of the antenna could somehow be raised, thereby lessening the mode overlap, this multimoding and the corresponding degradation of the radiation pattern would be eliminated.

Another reason for the poor radiation patterns may stem directly from the fact that the Q's were very much less than those of the closed resonator. The beam modes were originally derived for a resonator with enclosed walls of perfect conductors. The use of finite high conductivity walls should not perturb the fields very much, nor will the introduction of a small coupling probe. However, introducing slot coupling so large in magnitude that Q_{oor} is reduced to 160 may allow resonator fields other than beam modes to exist.

Since the slot width w = 0.018" produced low Q's and a poor radiation pattern, it was decided to test the slot antenna with w = 0.010". The measured Q's are listed in Table 17-1. Note that they are each slightly higher than those obtained with w = 0.018" and hence agree with theory.

The radiation pattern of the slot with w = 0.010" was not significantly changed from that of the slot with w = 0.018". The reason for the lack of improvement is evidently that the slight increase in the Q's was offset by the nonuniformity of $\pm$ 0.002" in the machined slot width.

In conclusion, the slot aperture has too large a transmission coefficient for the size slot widths that can be machined accurately. Only slots of width greater than about 0.018" can be machined accurately, however such widths transmit so much power that the Q of the resonator is drastically reduced. The

very low Q results in a poor radiation pattern. Hence another type of aperture coupling must be used that has a lower transmission coefficient. Therefore an aperture made up of circular holes was investigated experimentally.

C. Aperture of Closely Spaced Holes

1. Design and Fabrication

The design of the hole apertures consists of choosing a hole diameter which will result in reasonably high values of antenna efficiency and Q's. If the holes can be machined accurately then the aperture should yield a better antenna pattern than does the slot antenna.

The theory given in the previous section of this report predicts the external Q's for an antenna with holes of constant diameter closely spaced along the x axis. The value of Q_{ex2} is determined either by Eq. 16-78 or 16-94. Equation 16-94 is probably more accurate. Thus substituting h = 0.98 cm and λ = 3.33 cm in Eq. 16-94 results in

$$Q_{ex2} = (16.5 \times 10^{-8} \text{ meters}^4)\, a^2\, D^{-6} \qquad (17\text{-}2)$$

For example let D = 0.15" = 0.381×10^{-2} m. and a = 0.175" = 0.445×10^{-2} m. Such holes can be accurately drilled. Then Q_{ex2} from Eq. 17-2 is 1,090. This value is useful and reasonable. It is much greater than the 53 calculated for the slot and hence should produce a better radiation pattern than did the slot. Also, since it is much less than Q_{oo} = 3300 for the closed resonator, the antenna efficiency should not be too much less than unity. Hence the diameter D = 0.15" and spacing a = 0.175" were chosen for the antenna. The corresponding Q_{ex2} given by Eq. 16-78 is 70% of that given by Eq. 17-2, and this percentage holds for all antennas with the ratio (D/a) = 15/17.5 = 0.85. From now on the theoretical Q_{ex2} will be assumed to be that given by Eq. 17-2.

The fabrication of the antenna consists of drilling the holes along the x axis of a brass wall of the type shown previously in Fig. 17-2. The wall is

then attached to the experimental resonator using screws every half wavelength along the x direction. Since the aperture holes have diameter D = 0.150" and separation a = 0.175", the separation between the outer edges of the holes was 0.025". This separation was small enough to be considered close spacing yet large enough to prevent buckling or deformation of the metal between the holes when they were drilled. The first hole was drilled at x = 0 and then the other holes were drilled in both the +x and the -x directions along the 30 inch length of the aperture wall. Hence the centers of the holes were placed at x = 0, ± 0.175", ± 0.250",..., ± 14.875". All holes were carefully drilled and all burrs were carefully removed.

Two other similar antenna walls were also made. One had holes of diameter D = 0.10", the other D = 0.175". Both had 0.025" separation between the edges of the holes, so that a in Eq. 17-2 was 0.125" and 0.200" respectively. The wall with D = 0.10" was of the same outer dimensions as shown previously in Fig. 17-2. However, the wall with D = 0.175" was made out of a large sheet of brass in order to approximate a full ground plane. The brass sheet extended to y = + 2 1/2" and - 2 1/2" instead of the ± 9/16" of Fig. 17-2.

In addition to the above three walls with closely spaced holes, a few walls with smaller holes spaced relatively far apart were also made. No design of such apertures is possible since no theory for holes other than closely spaced ones has been devised. A wall with holes spaced closely and another with holes spaced far apart are shown in Fig. 17-3.

2. Results of Measurements

Measurements on the antenna with hole apertures consisted of determining the Q's and the radiation pattern. Data on apertures using three different diameter holes was obtained.

Table 17-II lists the Q's measured with the reflectometer for three antennas with closely spaced holes excited with the n=o mode. Also listed are the theoretical values of Q_{oor} calculated using Eqs. 17-2 and 16-11. The agreement between the theoretical and experimental values is good except for the case D = 0.100". This discrepancy may be due to possible increased ohmic losses around the holes and will be discussed at the end of this section.

Figure 17-5 shows the experimental radiation patterns for the cases D = 0.10" and D = 0.15". Note that the experimental data points all lie very close to the theoretical curve of Eq. 16-61. In addition the experimental patterns were very smooth between the data points, as was observed by rotating the antenna while watching the receiver output. Thus the experimental and theoretical curves coincide, at least down to about -30 db. Below this level the accuracy of the measurements is doubtful as was explained earlier. In summary, over the range of accurate measurement the measured and theoretical patterns are in excellent agreement.

The measured total gains, G_T, were 11.0 db for D = 0.150" and 7.6 db for D = 0.100". The theoretical gains are calculated by first finding the efficiency Γ from 16-12 using the measured Q values of Table 17-II. The calculations give Γ = -2.34 db for D = 0.10", and Γ -1.40 db for D = 0.15". Now G_T db = G db + Γ db. The value of G is 14.0 db according to Eq. 16-31, but this equation was derived under the assumption of an infinite ground plane. Experimentally only a partial ground plane was present. Hence some radiation could exist for z<0. Thus the theoretical or calculated value of G for this case must be less than 14.0 db by perhaps 1 or 2 db but not by as much as 3 db since this would imply equal radiated power in both half planes, i.e., in the z<0 as well as z>0 directions. If an estimated value of G = 12.5 db is used then G_T becomes 10.1 db for D = 0.10" and 11.1 db for D = 0.15".

The measured value of G_T = 11.0 db for D = 0.150" is in good agreement with the

Hole Diameter D inches	Measured $f_{n=o}$ GHz	Measured probe depth, crit. coupled	$Q_{L_{c.c.}}$ exper.	Q_{or} exper.	Q_{oor} exper.	Q_{oor} theor.	Measured Total Gain db.
0.100*	8.940	2 mm.	720	1360	1400	2130	7.6
0.150*	8.892	2.5 mm.	440	810	840	820	11.0
0.175#	8.878	3 mm.	318	600	620	480	13.4
0.150#	8.880	2.5 mm.	520	970	1000	820	12.0

*antenna has partial ground plane extending to y = ± 7/16"

#antenna has larger ground plane extending to y = ± 2 1/2"

TABLE 17-II

MEASURED VALUES OF Q FOR ANTENNAS WITH CLOSELY SPACED HOLES

spacing a = D+0.025"

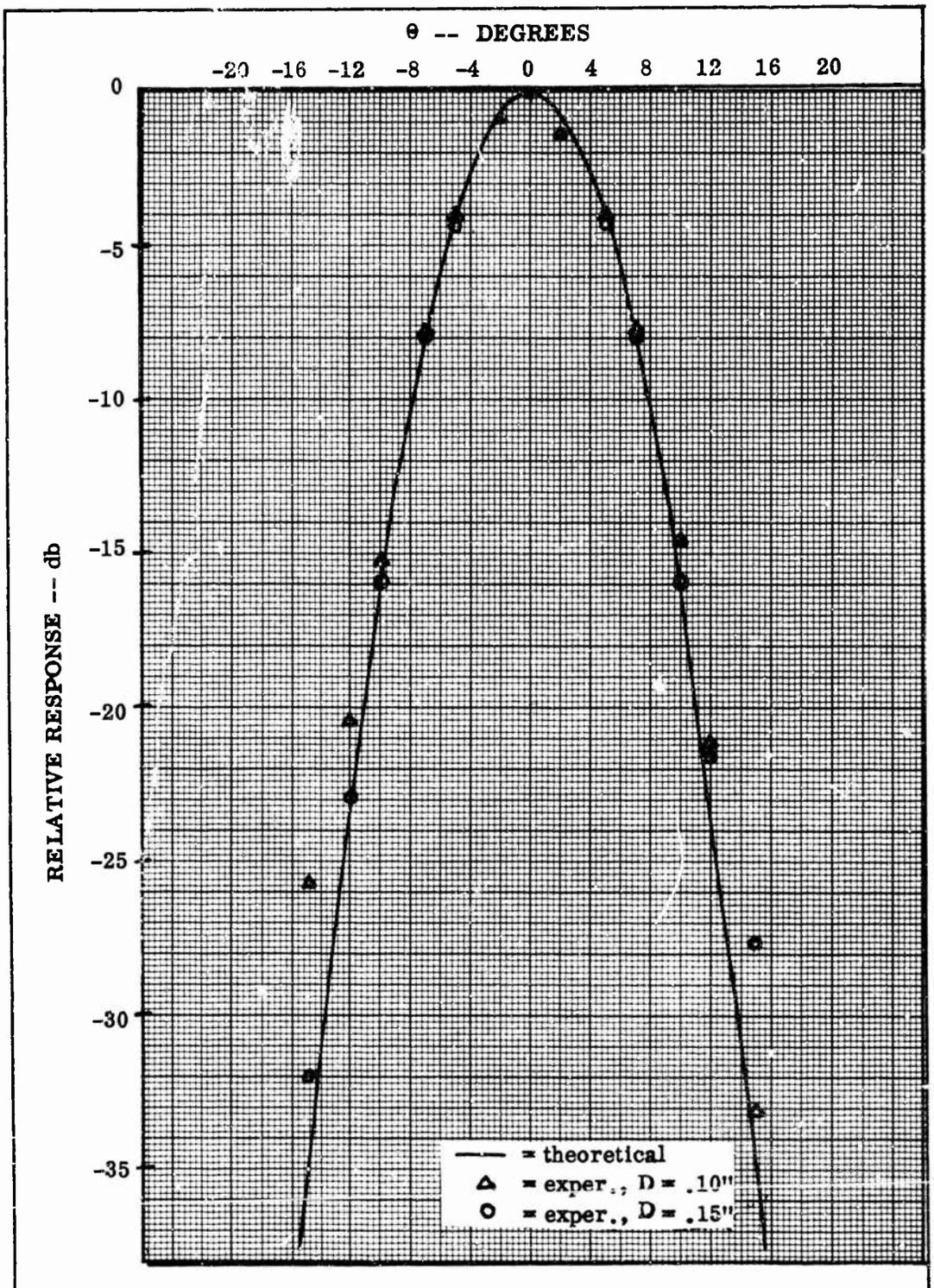

FIG. 17-5. RADIATION PATTERNS OF ANTENNAS WITH CLOSELY SPACED HOLES

theoretical value of 11.1 db. The measured value of G_T = 7.6 db for D = 0.100" is somewhat low compared to the theoretical value of 10.1 db.

A wall with hole diameters D = 0.150" was fabricated which extended to y = ± 2 1/2". Measurements for the resulting antenna with this larger ground plane are listed in Table 17-II. The Q's are slightly higher than those of the previous antenna with D = 0.150", perhaps due to better cleaning of the brass. As expected its radiation pattern was very similar to that of Fig. 17-5. Note, however, that the measured gain increased by 1.0 db because of the larger ground plane.

Figure 17-6 shows the experimental radiation pattern for the case D = 0.175". Note that for $|\theta|<9°$ the experimental values agree with the theoretical Gaussian pattern, but for $|\theta|>9°$ the experimental pattern does not drop off as rapidly as the Gaussian. According to Table 17-II, Q_{oor} = 620 and is evidently low enough to cause deterioration of the pattern.

The measured total gain G_T was 13.4 db. Since in this case the wall approximated a full ground plane by extending to y = ± 2 1/2", the theoretical total gain is G_T = 14.0 db + Γ db. The value of Γ is -1.0 db using the measured Q's of Table 17-II in Eq. 16-12. The resulting G_T is therefore 13.0 db, which agrees well with the measured value of 13.4 db.

In conclusion, the theoretical Gaussian pattern was successfully achieved with an antenna using closely spaced holes and which had a Q_{oor} > 800, corresponding to efficiency Γ = -1.4 or more decibels. The best value of Q_{oor} is about 800 since the Gaussian pattern is then produced with maximum efficiency.

Though the antenna of closely spaced holes performs successfully, a brief study of hole apertures which are not closely spaced was also made. The spacing chosen was a = 1/8", and hole diameters were varied from 0.022" to 0.100". It was found that the values of Q_{oor} and total gain G_T were in general too low to allow measurement of radiation patterns.

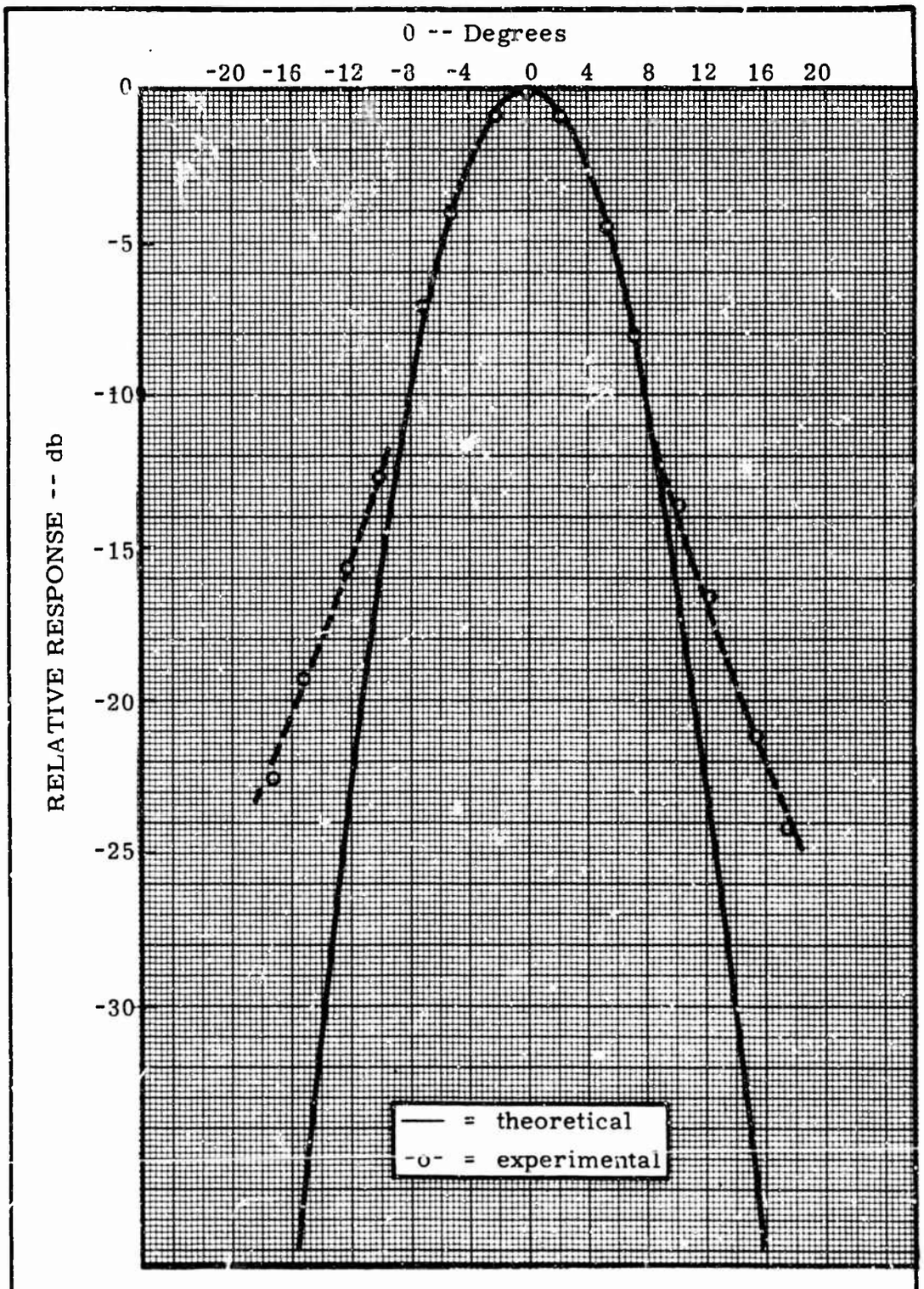

FIG. 17-6 RADIATION PATTERN OF ANTENNA WITH CLOSELY SPACED HOLES
D = 0.175"

A possible explanation for the low Q_{oor} at, for example, D = 0.0225" is that the ohmic losses around the holes are large. To investigate this explanation, another z = 0 wall was made, but instead of coupling holes indentations of depth 0.025" and diameter 0.0225" were drilled every 1/8" along the inside of the wall. The measured Q_{oo} was 2620, which indicates somewhat greater ohmic loss than for the closed resonator of section XV, which had a Q_{oo} = 3300. Thus the assumption that holes do not alter the ohmic loss is only approximately true.

Since the ohmic loss for D = 0.0225" is not large enough to explain the low value Q_{oor} = 1070, the radiated power must be large for this particular diameter. An experimental probing of the radiated field showed strong maxima along the +x and -x axes, indicating the presence of surface waves. Evidently these surface waves are produced by the widely spaced holes and couple strongly to the internal resonator field to give the low Q. Thus widely spaced holes do not give desirable results.

To summarize this section, it has been shown experimentally that closely spaced circular holes produce the Gaussian radiation pattern with good efficiency. The slot aperture was not as successful because a sufficiently narrow slot could not be machined. Therefore, a practical rectangular beam waveguide antenna can be constructed by drilling closely spaced circular holes along the x axis of the rectangular beam waveguide resonator.

XVIII. THE RECTANGULAR BEAM WAVEGUIDE MONOPULSE ANTENNA

A. Use of n=1 and n=o Modes for Monopulse Antenna

The n=1 and n=o modes of the rectangular beam waveguide antenna have possible application in monopulse radar and tracking systems. To investigate this application a brief description of the antenna requirements of monopulse radar will be helpful.

A monopulse radar antenna sends out a single pulse of radiation aimed in the vicinity of a target object. The pulse reflected by the object is then received by the monopulse antenna. The monopulse antenna performs the special function of indicating the range and angular position of the object on the basis of the single pulse.

A monopulse radar antenna can also be used in tracking a continuous signal source instead of a radar pulse. The antenna indicates the angle θ from which the received radiation is emanating. Hence monopulse antennas also have applications in radio astronomy and satellite communication.

The monopulse antenna as first developed consisted of a pair of identical regular waveguide horns aimed in slightly different directions. The horns were connected to two different ports of a hybrid tee junction and the remaining two ports of the junction then simultaneously contained microwave signals that were the sum and the difference of the horn signals. The sum pattern is an antenna field strength pattern which is a symmetric or even function of θ. The difference signal corresponds to an antisymmetric or odd field strength pattern.

Both symmetric and antisymmetric field strength patterns are required of any monopulse antenna. In 1962 Wheeler proposed two theoretical antenna field strength patterns as an ideal pair for monopulse radar.[79] The proposed symmetric field strength pattern was the Gaussian pattern produced by the Gaussian line source distribution $E_{ee} e^{-u_o^2 x^2}$. The antisymmetric field strength pattern proposed was the derivative of a Gaussian produced by the line source distribution $E_{ox} e^{-u_o^2 x^2}$. However, these two line source distributions have not been physically realizable up to now. Only sinusoidal approximations to these distributions[80]

---

79. H. A. Wheeler, "Antenna Beam Patterns which Retain Shape with Defocusing," I.R.E. Trans. on Ant. & Prop., vol. AP-10, Sept. 1962, pp. 573-580.

80. H. W. Redlien, "Monopulse Operation with Continously Variable Beamwidth by Antenna Defocusing," IEEE Trans. on Antennas and Propagation, vol. AP-16, July, 1968, pp. 415-423.

have been available.

The two proposed line source distributions are identical to those of the n=o and n=1 modes of the rectangular beam waveguide antenna. The n=o mode line source distribution $E \propto e^{-u_o^2 x^2}$ was shown in section XVI to produce the Gaussian symmetric field strength pattern $E(\theta) \cong \text{constant} \cdot e^{-k^2 \sin^2 \theta / 4u_o^2}$. The n=1 mode has the line source distribution $E \propto x\, e^{-u_o^2 x^2}$ and produces the antisymmetric field strength pattern.

To operate a monopulse system using the rectangular beam waveguide antenna, two such antennas would be needed. One antenna must have the resonant frequency of its n=o mode, $f_{n=o}$, equal to the desired operating frequency. The other antenna must have its $f_{n=1}$ equal to the same operating frequency f_{op}. The antennas must be oriented with both z = 0 aperture walls facing in the same direction. The distance between the two antennas should be small enough so that the angle θ measured from either of their z axes to any target object is approximately the same. But the two antennas should be spaced apart by perhaps a meter or so to minimize possible mutual coupling.

B. Theory of Antenna Excited in n=1 Mode

The derivation of the radiation pattern of the antenna excited in the n=1 mode will be similar to that used for the n=o mode and carried out in section XVI. The field incident on the aperture of the antenna for the n=1 mode is,

$$\bar{E} = \bar{u}_y E_1 \, He_1 (2u_o x)\, e^{-u_o^2 x^2} \tag{18-1}$$

but $He_1 (2u_o x) = 2u_o x$, giving

$$\bar{E} = \bar{u}_y E_1 2u_o x\, e^{-u_o^2 x^2} \tag{18-2}$$

Now using the Fourier transform technique, the radiated field strength for the

case of a slot aperture excited in the n=1 mode is,

$$\bar{E} = j(\bar{u}_0 \sin\phi + \bar{u}_\phi \cos\theta\cos\phi) \frac{e^{-jkR}}{\lambda R} E_1 I_y I_{x1} \tag{18-3}$$

where $I_y = \sqrt{Tw\lambda/\pi}$

$$I_{x1} = \int_{-\frac{L_s}{2}}^{+\frac{L_s}{2}} 2u_o x e^{-u_o^2 x^2 + jk\sin\theta\cos\phi x}\, dx \tag{18-4}$$

The coordinates and symbols are those used in the previous derivation. Now I_{x1} can be evaluated without difficulty when $L_s = \infty$.

Then

$$I_{x1} = 2u_o \int_{-\infty}^{+\infty} x e^{-u_o^2 x^2 + jk\sin\theta\cos\phi x}\, dx \tag{18-5}$$

From a table of Fourier transforms[81]

$$\int_{-\infty}^{+\infty} jf e^{-\pi\beta f^2} e^{j2\pi fg}\, df = -g\beta^{-3/2} e^{-\pi g^2/\beta} \tag{18-6}$$

Let $\pi\beta = u_o^2$, $f = x$, and $2\pi g = k\sin\theta\cos\phi$. Then

$$I_{x1} = \frac{2u_o}{j} \left[\frac{-k\sin\theta\cos\phi\,\pi^{3/2}}{2\pi u_o^3}\right] e^{-(k\sin\theta\cos\phi)^2/4u_o^2} \tag{18-7}$$

or

$$I_{x1} = j\sqrt{\pi}\, \frac{k}{u_o^2} \sin\theta\cos\phi\, e^{-k^2\sin^2\theta\cos^2\phi/4u_o^2} \tag{18-8}$$

Therefore

$$\bar{E} = (-\bar{u}_\theta \sin\phi - \bar{u}_\phi \cos\theta\cos\phi)\, \frac{e^{-jkR}}{\lambda R} E_1 \sqrt{Tw\lambda/\pi} \cdot \sqrt{\pi}\, \frac{k}{u_o^2} \sin\theta\cos\phi\, e^{-k^2\sin^2\theta\cos^2\phi/4u_o^2} \tag{18-9}$$

For the case $\phi = 0$,

---

81. G. Campbell and R. Foster, Fourier Integrals for Practical Applications, D. Van Nostrand Co., New York, N.Y., 1948, pp. 9, 34, 81.

$$\bar{E} = (-E_1)(\bar{u}_\phi \cos\theta)\frac{e^{-jkR}}{R}\sqrt{Tw/\lambda}\,\frac{k}{u_o^2}\sin\theta e^{-k^2\sin^2\theta/4u_o^2} \tag{18-10}$$

This is a field strength pattern that is antisymmetric in θ. The pattern is however omnidirectional in the yz plane just as the pattern for the n=o mode is. The corresponding pattern of the power density S is,

$$S_{n=1}\Big|_{\phi=0} = E_1^2\cos^2\theta\,\frac{Tw}{\eta\lambda R^2}\sin^2\theta e^{-k^2\sin^2\theta/2u_o^2} \tag{18-11}$$

The gain G of the antenna excited in the n=1 mode will now be determined. In order to do this an expression for the total power radiated must first be obtained. Now for a slot antenna of slot width w, Eq. 16-34 yields

$$P_{rad} = \frac{1}{\eta}\,Tw\int_{-\infty}^{\infty} E_n^2(x)\,dx \tag{18-12}$$

For the n=1 mode

$$\int_{-\infty}^{\infty} E_{n=1}^2(x)\,dx = E_1^2\int_{-\infty}^{\infty} He_{n=1}^2(2u_o x)e^{-2u_o x^2}\,dx \tag{18-13}$$

Evaluating this integral gives,

$$\int_{-\infty}^{\infty} E_{n=1}^2(x)\,dx = E_1^2\,(n!/u_o)\sqrt{\frac{\pi}{2}} = E_1^2\sqrt{\frac{\pi}{2}}\,\frac{1}{u_o} \tag{18-14}$$

Similarly for the n=o mode

$$\int_{-\infty}^{\infty} E_{n=o}^2(x)\,dx = E_o^2\,(0!/u_o)\sqrt{\frac{\pi}{2}} = E_o^2\sqrt{\frac{\pi}{2}}\,\frac{1}{u_o} \tag{18-15}$$

Then using Eqs. 18-12, 14 and 15 in the general gain equation 16-32

$$G = 4\pi R^2\,S_{max}/P_{rad} \tag{18-16}$$

yields

$$\frac{G_{n=1}}{G_{n=o}} = \frac{S_{max\ n=1}/E_1^2}{S_{max\ n=o}/E_o^2} \tag{18-17}$$

The value of S_{max} for the n=o mode is from Eq. 16-37,

$$S_{max\ n=0} = \frac{E_o^2\ Tw}{\eta\lambda u_o^2 R^2} \tag{18-18}$$

Now for the n=1 mode the maximum value of S in Eq. 18-11 can be found by setting the derivative of S with respect to θ equal to zero. Thus,

$$\frac{d}{d\theta}\left[\cos^2\theta\sin^2\theta e^{-k^2\sin^2\theta/2u_o^2}\right]\Bigg|_{\theta=\theta_{max}} = 0 \tag{18-19}$$

Since the range of interest of θ is $|\theta|\leq 8°$ where typically $|\theta_{max}|<8°$, Eq. 18-19 can be simplified by using the approximation that $\cos^2\theta\approx 1$. Then

$$\frac{d}{d\theta}\left[\sin^2\theta e^{-k^2\sin^2\theta/2u_o^2}\right]\Bigg|_{\theta=\theta_{max}} \simeq 0 \tag{18-20}$$

$$\sin^2\theta_{max}\left[-\frac{k^2}{2u_o^2}\,2\sin\theta_{max}\cos\theta_{max}\right] + 2\sin\theta_{max}\cos\theta_{max} \simeq 0$$

or

$$\sin^2\theta_{max} \simeq \frac{2u_o^2}{k^2} \tag{18-21}$$

Then S_{max} becomes

$$S_{max\ n=1} = \frac{E_1^2 Twk^2}{\eta\lambda u_o^4 R^2}\,2\,(u_o^2/k^2)e^{-1} \tag{18-22}$$

or

$$S_{max\ n=1} = \frac{2E_1^2 Tw}{\eta\lambda u_o^2 R^2}\,e^{-1} \tag{18-23}$$

The gain for the n=1 mode is from Eq. 18-17,

$$G_{n=1} = 2e^{-1}G_{n=0} = 0.726G_{n=0} = \frac{8}{\lambda u_o}\sqrt{2\pi}\,e^{-1} \tag{18-24}$$

where the value of $G_{n=o}$ was given previously by Eq. 16-31. Stated in decibels

$$G_{n=1}(db) = G_{n=o}(db) - 1.4 \text{ db} \tag{18.25}$$

These theoretical calculations for antenna pattern and gain are based on the assumption that the slot length L_s is infinite. A finite length slot would result in side lobes in the pattern just as occurs for the case of the n=o mode. The gain should be relatively unchanged when making L_s a finite but reasonable length.

C. Excitation of n=1 Mode by One Probe

The antenna with D = 0.150 inches and described in section XVI of this report was used to test the theory of the n-1 mode excitation. The exciting probe was placed at the point in the resonator where the field strength is a maximum for the n=1 mode. This was accomplished by drilling and tapping a new hole in the antenna resonator at x = 2.34 inches and z = -0.328 inches. A brass plug was inserted in the original probe coupling hole at x = 0. The probe in its new position was adjusted to the proper depth to obtain critical coupling for the n=1 mode at a frequency $f_{n=1}$ = 8.963 GHz.

The preliminary radiation pattern measured at 8.963 GHz is shown in Fig. 18-1. The theoretical or calculated pattern given by Eq. 18-11 is shown also in Fig. 18-1. The agreement between measured and calculated values is excellent for the range $\theta<0^{\circ}$ but only fair for the range $\theta>0^{\circ}$. A possible reason for the asymmetry of the measured pattern is that the n=o mode may have been excited along with the n=1 mode.

The total gain G_T of the antenna was also measured. The gain was 9 db at the peak of the pattern which occurred at $\theta = -5^{\circ}$. The theoretical total gain is $G_T(db) = 11.1-1.4 = 9.7$ db. The calculated and measured gains at $\theta = -5^{\circ}$ are in good agreement.

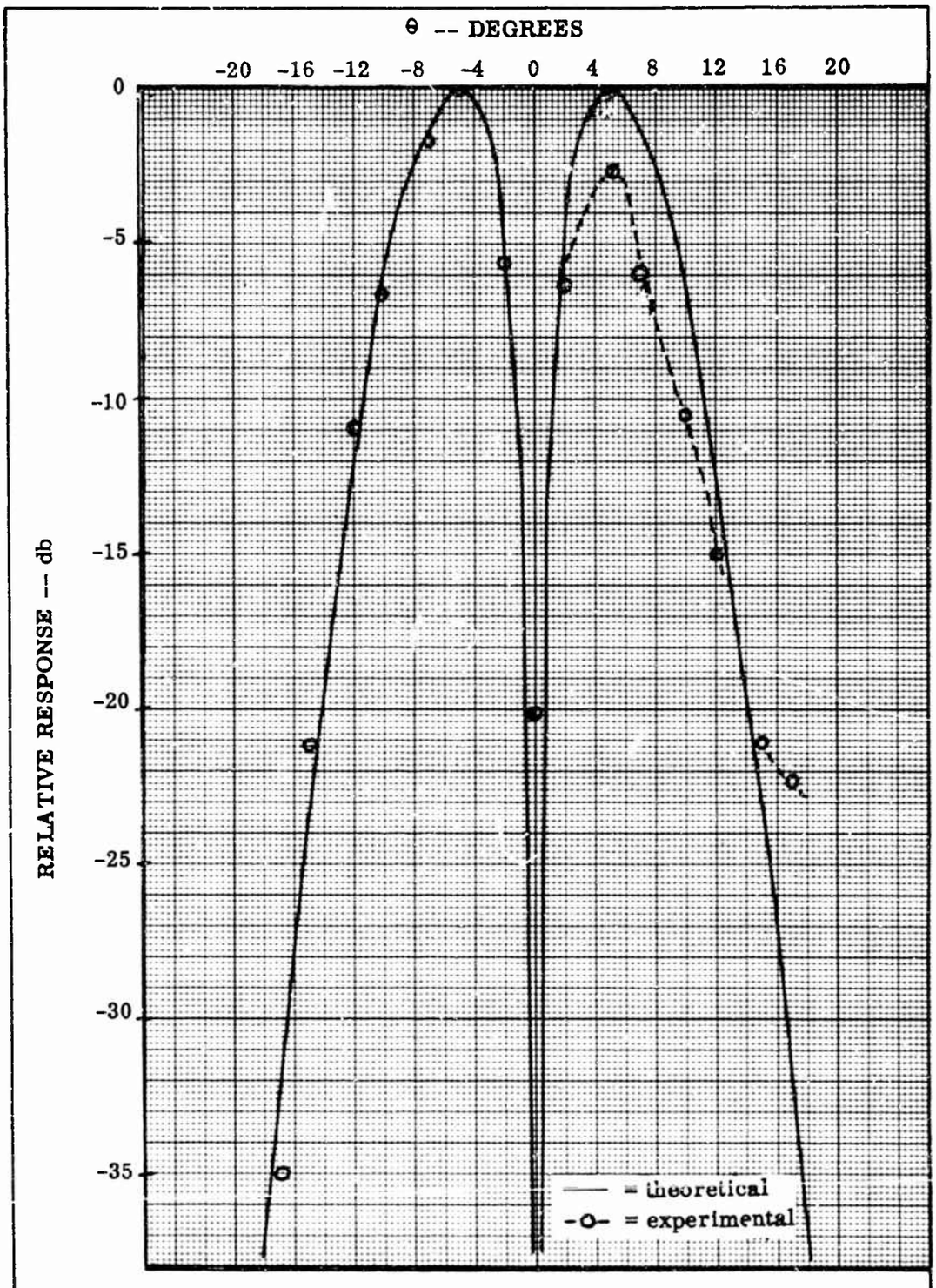

FIG. 18-1. RADIATION PATTERN OF ANTENNA EXCITED IN THE n=1 MODE

Probe at x = +2.34"

It was decided to place the probe on the other side of the antenna, that is, at x = -2.34". The hole at x = +2.34" was closed with a brass bolt. The probe at x = -2.34" was adjusted for critical coupling to the n=1 mode as indicated in Table 18-I. The resulting radiation pattern is shown in Fig. 18-2. Note that this pattern is almost the mirror image of the pattern of Fig. 18-1, that is, the new pattern is asymmetric with its maximum at $\theta = +5°$. The probe placement evidently determines the kind of asymmetry obtained. Note also that for both probe placements the minimum at $\theta = 0$ in Figs. 18-1 and 18-2 is approximately -20 db. Theoretically the value should be $-\infty$ db.

A possible explanation for the difference between the measured and theoretical n=1 radiation patterns is that other modes are present in the resonator. In particular the n=o and n=2 modes may be present due to the closeness of their resonant frequencies to $f_{n=1}$. Figure 18-3a is a sketch of the n=o, n=1, and n=2 modes on a reflectometer display of the power reflected by a single probe at x = ± 2.34". The probe has the depth for critical coupling to the n=1 mode, and the n=o and n=2 modes are therefore undercoupled. The n=o and 2 modes are only moderately undercoupled, however. The loaded Q, Q_L, determines the degree to which the n=o and 2 mode reflectometer curves overlap onto the n=1 curve. If Q_L is high then the n=o and n=2 response curves do not extend much at all toward the frequency $f_{n=1}$ on the reflectometer display. However, for the antenna studied here Q_L is on the order of one half of Q_{oor} or $1/2 \cdot 1000 = 500$ and thus the Q curves overlap slightly as sketched in Fig. 18-3a. Therefore, setting $f = f_{n=1}$ will excite not only the n=1 mode but also to some extent the n=o and n=2 modes.

x Value of Probe Position	Measured Probe Depth	Measured $f_{n=1}$ GHz	Measured $\rho^2 \mid f=f_{n=1}$ db	Radiation Pattern in Fig.	Measured Total Gain db	Theoretical Total Gain db
+2.34"	3.5 mm	8.963	-40	18-1	9.0	9.7*
-2.34"	3.5 mm	8.963	-40	18-2	8.2	9.7*
+2.34"	1.5 mm	8.969	-4.3	18-4	7.5	7.7#

*G_T = 12.6 db + Γ db -(1.5 db since not full ground plane)

#G_T = 12.6 db + Γ db -1.5 db +$(1-\rho^2)$db

TABLE 18-I

ANTENNA OPERATING IN THE n=1 MODE EXCITED BY ONE PROBE

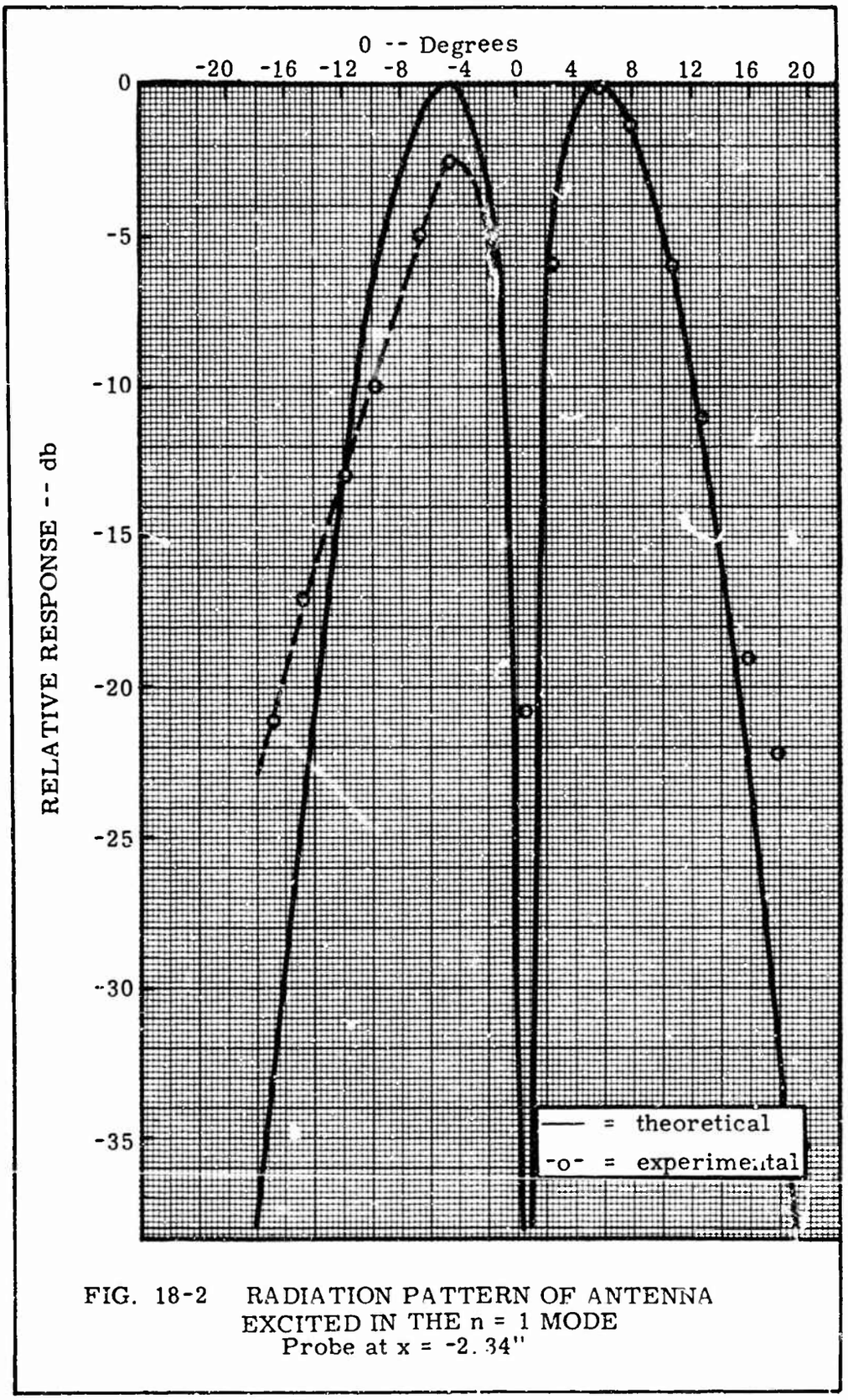

FIG. 18-2 RADIATION PATTERN OF ANTENNA EXCITED IN THE n = 1 MODE
Probe at x = -2.34"

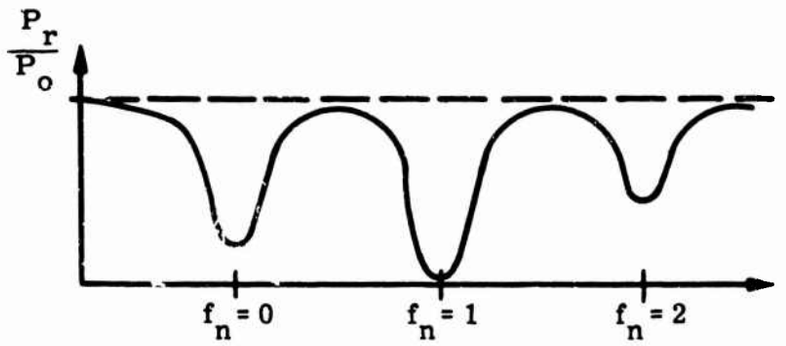

a) Reflectometer Display for a Probe at x = $\pm$2.34"

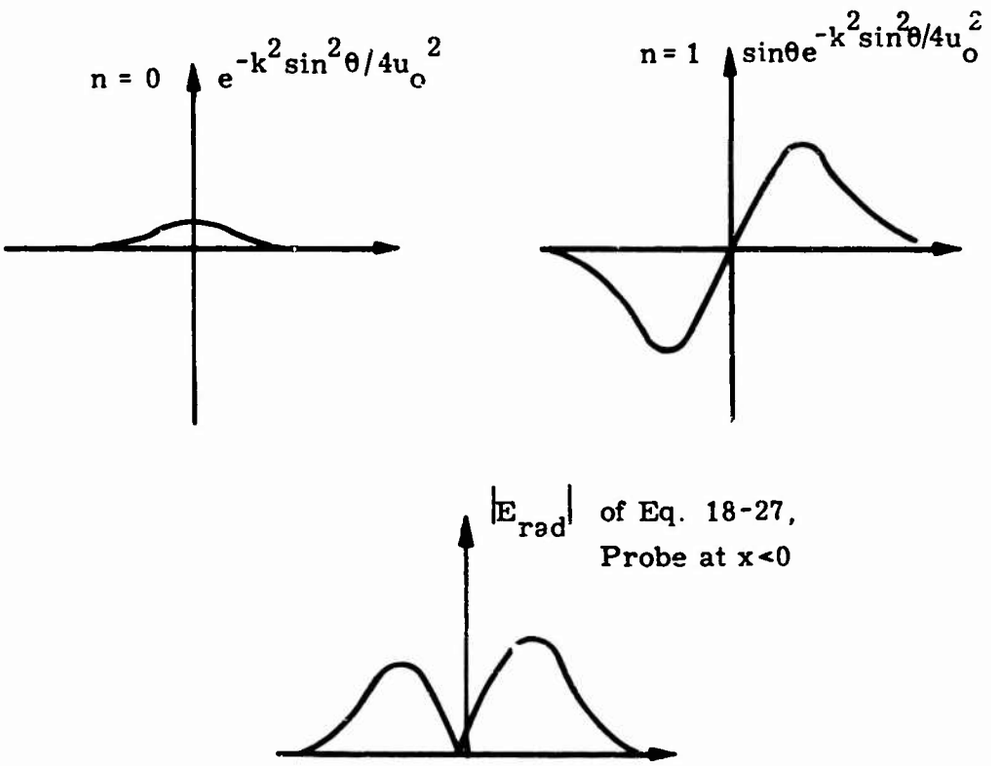

b) Radiated Fields of n = 0 and n = 1 Modes

FIG. 18-3 ADDITION OF n = 1 and n = 0 MODES

Consider for simplicity that the fields in the resonator at frequency $f_{n=1}$ consist only of the n=1 mode plus a small field of the n=o mode. Since the n=o mode is off resonance, its field differs in phase from the n=o mode field by approximately 90°. The equivalent circuit of Fig. 16-1 is essentially an inductor for frequencies above resonance, so the n=o mode fields will lag the excitation by about 90°. Thus the resonator field consists of

$$E = -jE_o e^{-u_o^2 x^2} \pm E_1 2u_o x e^{-u_o^2 x^2} \tag{18-26}$$

where $E_1 >> E_o > 0$

and + corresponds to probe at $x>0$

- corresponds to probe at $x<0$

The resulting radiation field is found with the aid of Eq. 18-8, giving

$$E_{rad} \propto -jE_o e^{-k^2 \sin^2\theta/4u_o^2} \pm jE_1 \sin\theta e^{-k^2 \sin^2\theta/4u_o^2} \tag{18-27}$$

where ϕ has been assumed zero

+ is for the probe at $x>0$

- is for the probe at $x<0$

Figure 18-3b illustrates the summation of these n=o and n=1 patterns to form the pattern of Eq. 18-27 with the - sign, corresponding to the probe at $x<0$. Note that the total pattern has the peak at $\theta<0$ of a higher value than the peak at $\theta>0$. A sketch of Eq. 18-27 with the + sign would give the higher peak at $\theta<0$.

The theoretical predictions of Eq. 18-27 agree qualitatively with the previous experimental graphs of Figs. 18-1 and 18-2. That is, a probe at $x>0$ gives a maximum peak at $\theta<0$, and a probe at $x<0$ gives a maximum at $\theta>0$.

There is one basic disagreement between Eq. 18-27 (as graphed in Fig. 18-3b) and the data of Figs. 18-1 and 18-2. The theoretical graph in Fig. 18-3b has value zero at $\theta=0°$ whereas the experimental curves have a minimum of only -20 db. The explanation is that Eq. 18-27 was derived using two assumptions which are only approximately valid here. First, only the radiation field was assumed present, whereas the measured patterns are only approximately in the radiation field. Thus the j factor contributed by Eq. 18-8 is only approximately valid. Second, Eq. 18-26 assumed that the resonator field of the n=o mode is exactly 90° out of phase, which is not quite true. Hence the fact that the experimental patterns do not have a perfect null seems reasonable.

Improvement in the experimental radiation pattern at the frequency $f_{n=1}$ was sought. One thought was to decrease the probe depth since a smaller probe depth would raise Q_L. Of course a smaller probe depth would also result in undercoupling and a corresponding reflection of some of the incident power at the resonator input. But the increase in Q_L should cause less excitation of the neighboring n=o and n=2 modes and hence should improve the radiation pattern.

The experimental procedure consisted of decreasing the depth of the exciting probe at x = +2.34" while the holes at x = 0 and x = -2.34" were closed with bolts flush with the resonator wall. The probe depth was decreased until the reflection coefficient at resonance was -4.3 db as listed in Table 18-I. The measured radiation pattern is shown in Fig. 18-4. Note that the minimum at $\theta = 0$ now has the very low value of -34 db. The two peaks at $\theta = \pm 5°$ are within 1.1 db of each other. The only angular range for which the measured pattern deviates significantly from theory is for $\theta < -15°$. The measured total gain compares well with the theoretical gain in Table 18-I,

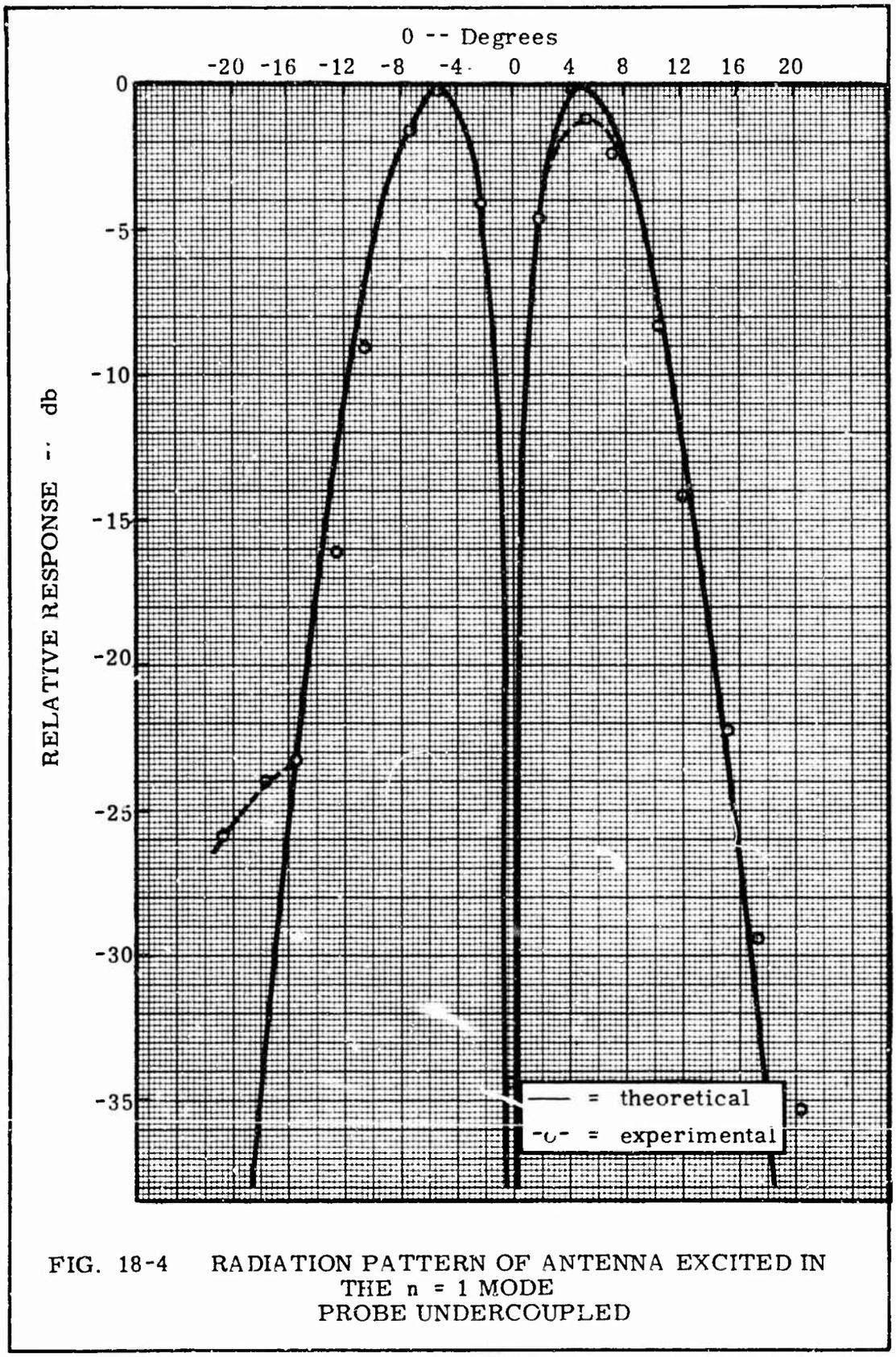

FIG. 18-4 RADIATION PATTERN OF ANTENNA EXCITED IN THE n = 1 MODE
PROBE UNDERCOUPLED

and is 1.5 db less than that measured at critical coupling. In conclusion, the radiation pattern of this antenna is better than the patterns of Figs. 18-1 and 18-2.

D. Excitation of n=1 Mode by Two Probes

Another method of exciting the n=1 mode is to use two probes, one at $x = +x_p$ and the other at $x = -x_p$, where x_p is some distance from $x = 0$. If the probes have the same depth and are fed out of phase, the modes for n odd can be excited while the modes for n even should not be excited. The 180° phase difference between the excitations of the two probes can be provided by a hybrid or "magic" tee.

The excitation circuit is shown in Fig. 18-5. When the two probes are at the same depth then the reflection coefficients at the probes are equal. A hybrid tee has the following important properties:

1) The reflection coefficient at the input port 4 is one half of the sum of the reflection coefficients at ports 1 and 2 (of the probes in this case) for a matched condition at port 3. $[\rho_{in} = 1/2\ (\rho_1+\rho_2)]$
2) The power absorbed by a matched load at port 3 is proportional to the square of the difference between the reflection coefficients at ports 1 and 2. $[P_3 \propto (\rho_1-\rho_2)^2]$

The probe depths were made exactly equal by using the following procedure. Power was fed into port 4 of the hybrid tee using the reflectometer setup to observe the reflected power versus frequency. The frequency was swept from $f_{n=o}$ to $f_{n=2}$ to enable observation of the n=o, 1, and 2 modes. First the probes were inserted to about equal depths and until the n=1 mode was observed to be approximately critically coupled. The reflectometer pattern then showed that the n=o and 2 modes were also being excited, although they were considerably undercoupled. Next the power at port 3 was minimized by adjusting the depth of just one of the probes. After this adjustment the n=o and 2 modes had disappeared from the

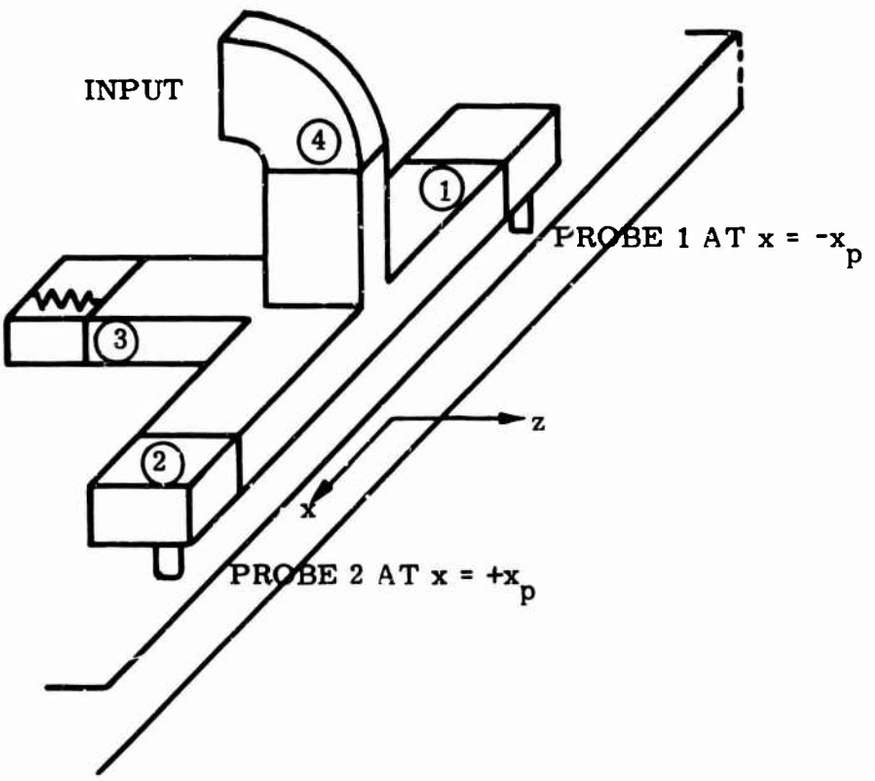

a) APPARATUS

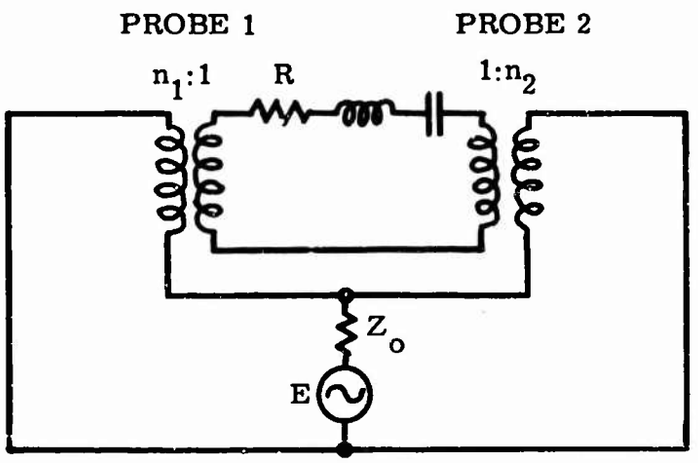

b) EQUIVALENT CIRCUIT

FIG. 18-5 HYBRID TEE AND TWO PROBES EXCITING n = 1 MODE

reflectometer pattern, while the n=1 mode was critically coupled. Althouth the power at port 3 was not zero, it was 22 db below the input power to port 4. The radiation pattern at frequency $f_{n=1}$ was then measured and is plotted in Fig. 18-6. The minimum at $\theta = 0°$ is -22.5 db down, which is somewhat better than the -20 db obtained previously with one critically coupled probe. Recall, however, that -34 db was obtained with the undercoupled probe as shown in 18-4. The measured total gain of the antenna excited by two probes was 9 db for a ground plane extending from y = -7/16" to +7/16". Finally the two probe method produces peaks at $\theta = \pm 5°$ which differ by only 0.6 db. This difference is smaller than that obtained with one probe and shows the merit of the two probe method of excitation.

XIX. CONCLUSIONS AND RECOMMENDATIONS

A closed microwave resonator was developed in which the fields are rectangular beam waveguide modes. The resonator was transformed into an antenna by making one of its walls partially transparent.

The theory of the rectangular beam waveguide resonator was presented in Section XIV. The beam modes resonate between two conducting surfaces which are separated by π radians of phase shift. The modes resonate at distinct frequencies but all have the same unloaded Q. The excitation of the various modes by a probe was analyzed. An experimental resonator was fabricated as described in section XV. An X band reflectometer was used to measure its resonant frequencies, Q's and reflection coefficients at resonance. The measured values agreed very well with those predicted by theory.

The rectangular beam waveguide antenna was proposed in Section XVI. The theories of a slot and of a row of holes as apertures in the wall of the resonator were presented. The radiation pattern of the n=o mode of an antenna of infinite length was shown to be a Gaussian beam. Calculations were also made on the effect

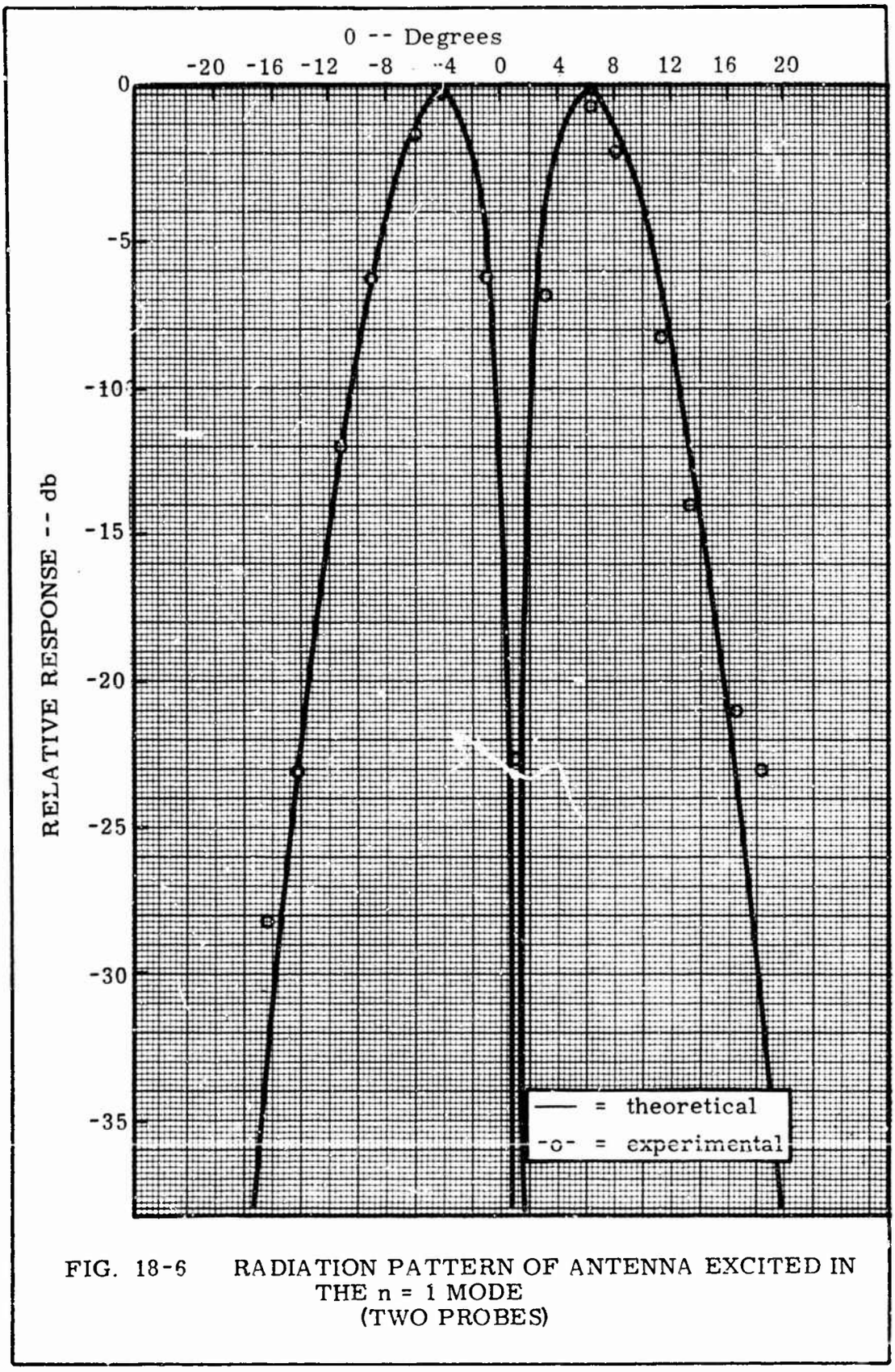

FIG. 18-6 RADIATION PATTERN OF ANTENNA EXCITED IN THE n = 1 MODE (TWO PROBES)

of a finite antenna length on the radiation pattern. The measurements made in Section XVII showed that a sufficiently narrow slot aperture could not be fabricated, but that a row of closely spaced circular holes produced the desired Gaussian radiation pattern. The measured total gain was found to be 12 db in this instance.

The n=1 mode of the antenna was investigated in section XVIII because of its possible application to monopulse radar and tracking. The theoretical antisymmetric radiation pattern of this mode is the derivative of a Gaussian. The pattern was best produced experimentally by exciting the resonator-antenna with either one undercoupled probe or two probes fed out of phase. Experimental work remains to be done in testing a complete monopulse system containing this antenna.

In conclusion, it appears that the rectangular beam waveguide resonator-antenna is practical and has several desirable features. It is small in size, quite easy to fabricate, and low in cost. The n=o mode radiation pattern is a narrow beam Gaussian with the sidelobes down more than 30 db from the peak. The radiation pattern of the n=1 mode is the derivative of a Gaussian. These two radiation patterns, evidently unobtainable until now, are an ideal pair of patterns for use in monopulse radar and tracing.

XX SELECTED BIBLIOGRAPHY

Books

Abramowitz, M., and Stegun, I. (editors), Handbook of Mathematical Functions, National Bureau of Standards, U. S. Government Printing Office, Washington, D. C., 1965.

Altman, J. L., Microwave Circuits, D. Van Nostrand Co., Princeton, N. J., 1964.

Atwater, H. A. , Introduction to Microwave Theory, McGraw-Hill Co., New York, N. Y., 1962.

Campbell, G. A., and Foster, R. M., Fourier Integrals for Practical Applications, D. Van Nostrand Co., New York, N. Y., 1948.

Collin, R. E., Field Theory of Guided Waves, McGraw-Hill Book Co., New York, N. Y., 1960.

Collin, R. E., Foundations for Microwave Engineering, McGraw-Hill Book Co., New York, N. Y., 1966.

Faddayeva, V. N., and Terent'ev, N. M., Tables of the Probability Integral for Complex Argument, Pergamon Press, New York, N. Y., 1961.

Ginzton, E. L., Microwave Measurements, McGraw-Hill Book Co., New York, N. Y., 1957.

Goubau, G., Electromagnetic Waveguides and Cavities, Pergamon Press, New York, N. Y., 1961.

Hansen, R. C., Microwave Scanning Antennas, Vols. I and II, Academic Press, New York, N. Y., 1964, 1966.

Harrington, R. F., Time-Harmonic Electromagnetic Fields, McGraw-Hill Book Co., New York, N. Y., 1961.

Jackson, J. D., Classical Electrodynamics, John Wiley & Sons, New York, N. Y., 1962.

Magnus, W., and Oberhettinger, F., Functions of Mathematical Physics, Chelsea Publishing Co., Toronto, Canada, 1949.

Montgomery, C. G., Techniques of Microwave Measurements, McGraw-Hill Book Co., New York, N. Y., 1947.

Powell, J. L., and Crasemann, B., Quantum Mechanics, Addison-Wesley Publishing Co., Reading, Mass., 1961.

Rhodes, D. R., Introduction to Monopulse, McGraw-Hill Book Co., New York, N. Y., 1959.

Rosser, J. B., Theory and Application of $\int_0^z e^{-x^2} dx$ and $\int_0^z e^{-p^2y^2} dy \cdot \int_0^y e^{-x^2} dx$, Mapleton House, Brooklyn, N. Y., 1948.

Skolnik, M. I., Introduction to Radar Systems, McGraw-Hill Book Co., New York, N. Y., 1962.

Sucher, M., and Fox., J., Handbook of Microwave Measurements, 3rd Ed., Vol. II, Polytechnic Press of the Polytechnic Institute of Brooklyn, Brooklyn, N. Y., 1963.

Periodicals and Papers

Adams, A. T., "Flush Mounted Rectangular Cavity Slot Antennas--Theory and Design," IRE Trans. on Antennas and Propagation, Vol. AP-15, May, 1967, pp. 342-351.

Bartlett, H. E., and Moseley, R. E., "Dielguides--Highly Efficient Low Noise Antenna Feeds," Microwave Journal, Vol. 9, No. 12, December, 1966, pp. 53-58.

Bethe, H. A., "Theory of Diffraction by Small Holes," Physical Review, Vol. 66, Nos. 7 and 8, October 1944, pp. 163-182.

Brown, J., "A Theoretical Analysis of Some Errors in Aerial Measurements, Proceedings of the Institution of Electrical Engineers, Vol. 1050, February, 1958, pp. 343-351.

Dunn, J. H., and Howard, D. D., "Precision Tracking with Monopulse Radar," Electronics, Vol. 33, No. 17, April 22, 1960, pp. 51-56.

Goubau, G., unpublished notes for course given at the University of Wisconsin, 1962.

Goubau, G., and Schwering, F., "On the Guided Propagation of Electromagnetic Wave Beams," IRE Trans. on Antennas and Propagation, Vol. AP-9, May, 1961, pp. 248-256.

Hannan, P. W., "Optimum Feed for All Three Modes of a Monopulse Antenna," IRE Trans. on Antennas and Propagation, Vol. AP-9, September, 1961, pp. 454-461.

Jacobsen, S., Andersen, E., and Gronlund, M., "An Antenna Illuminated by a Cavity Resonator," Proceedings of the IEEE, Vol. 51, November, 1963, pp. 1431-1435.

Kay, Alan F., "Near-Field Gain of Aperture Antennas," IRE Trans. on Antennas and Propagation, Vol. AP-8, November, 1960, pp. 586-593.

Lee, T. C., and Zook, J. D., "Light Beam Deflection with Electrooptic Prisms," IEEE Journal of Quantum Electronics, Vol. QE-4, July, 1968, pp. 442-454.

Lopez, A. R., "Monopulse Networks for Series Feeding an Array Antenna," IEEE Trans. on Antennas and Propagation, Vol. AP-16, July, 1968, pp. 436-440.

Miles, J. W., "On the Diffraction of an Electromagnetic Wave Through a Plane Screen," Journal of Applied Physics, Vol. 20, August, 1949, pp. 760-771.

Morse, P. M., and Rubenstein, P. J., "The Diffraction of Waves by Ribbons and Slits," Physical Review, Vol. 54, December 1, 1938, pp. 895-898.

Page, R. M., "Monopulse Radar," IRE Convention Record, Vol. 3, Part 3, 1955, pp. 132-134.

Redlien, H. W., Jr., "Monopulse Operation with Continuously Variable Beamwidth by Antenna Defocusing," IEEE Trans. on Antennas and Propagation, Vol. AP-16, July 1968, pp. 415-423.

Ricardi, L. J., and Niro, L., "Design of a Twelve-Horn Monopulse Feed," IRE International Convention Record, Part I, 1961, pp. 49-56.

Schwering, F., "Reiterative Wave Beams of Rectangular Symmetry," Archiv der Elektrischen Uebertragung, Vol. 15, December 1961, pp. 555-564.

Takeshima, T., "A Slot Array Antenna for Monopulse Tracking Radar," Microwave Journal, Vol. 9, No. 12, December 1966, pp. 63-65.

Takeshita, S., "Realization of Optimum Aperture Illumination by Gaussian Taper in Small Fresnel Number," IRE Trans. on Antennas and Propagation, Vol. AP-16, January 1968, pp. 1929-130.

Taylor, T. T., "Design of Line-Source Antennas for Narrow Beamwidth and Low Side Lobes," IRE Trans. on Antennas and Propagation, Vol. AP3, January 1955, pp. 16-28.

Walker, S. H., and Osborn, J. D., "Investigation of a Nonambiguous Monopulse Antenna," Microwave Journal, Vol. 10, No. 13, December 1967, pp. 39-44.

Wheeler, H. A., "Antenna Beam Patterns Which Retain Shape with Defocusing," IRE Trans. on Antennas and Propagation, Vol. AP-10, September, 1962, pp. 573-580.

Unclassified

Security Classification

DOCUMENT CONTROL DATA - R&D

(Security classification of title, body of abstract and indexing annotation must be entered when the overall report is classified)

1. ORIGINATING ACTIVITY (Corporate author)	2a. REPORT SECURITY CLASSIFICATION
University of Wisconsin Department of Electrical Engineering Madison, Wisconsin	2b. GROUP

3. REPORT TITLE

Waveguide, Waveguide Circuit and Antenna Research Study

4. DESCRIPTIVE NOTES (Type of report and inclusive dates)

Final Report - 1 September 1964 to 31 January 1969

5. AUTHOR(S) (Last name, first name, initial)

Scheibe, Elmer H.

6. REPORT DATE	7a. TOTAL NO. OF PAGES	7b. NO. OF REFS
February 28, 1969	290	81

8a. CONTRACT OR GRANT NO.	9a. ORIGINATOR'S REPORT NUMBER(S)
DA 36-039 AMC-02261 (E) b. PROJECT NO. 3A99-25-004 c. d.	N/A 9b. OTHER REPORT NO(S) (Any other numbers that may be assigned this report) ECOM-02261-F

10. AVAILABILITY/LIMITATION NOTICES

This document is subject to special export controls and each transmittal to foreign governments or foreign nationals may be made only with prior approval of the Commanding General, U.S. Army Electronics Command, Fort Monmouth, N.J., AMSEL XL-C

11. SUPPLEMENTARY NOTES	12. SPONSORING MILITARY ACTIVITY
N/A	U.S. Army Electronics Command Fort Monmouth, New Jersey 07703

13. ABSTRACT

The research work that was carried out under this contract was a continuation of, but over and beyond, the studies made under Contract No. DA-36-039-sc-85188. This final report covers the period from September 1, 1964 to January 31, 1969. During this period three distinct studies were carried out. Two of these studies dealt with topics closely related to the beam waveguide. The third study was a separate one and was concerned with the theory and design of a new type of filter called a cut-off coupled microwave filter.

Part 1 of the report describes the general study made of beam waveguide resonators at millimeter wavelengths. An important result of this study was the derivation of the equivalent circuits for resonators with input and output coupling. An extensive bibliography on guided electromagnetic wave beams, beam waveguides, beam waveguide antennas, beam waveguide resonators, and Fabry-Perot resonators is included in Part 1 of this report.

Part 2 of ~~this report~~ describes a new type of waveguide filter called a cut-off coupled microwave filter. The theory, design and febrication of these filters as well as the measurements made on them is described in some detail.

Part 3 of ~~this~~ report deals with two general applications of the beam waveguide of rectangular symmetry. One of the studies was concerned with the rectangular beam waveguide resonator and the other with a rectangular beam waveguide antenna formed from the resonator.

DD FORM 1 JAN 64 1473

Unclassified

Security Classification

Unclassified
Security Classification

14. KEY WORDS	LINK A		LINK B		LINK C	
	ROLE	WT	ROLE	WT	ROLE	WT
Antennas						
Beam Waveguides						
Electromagnetic Waves						
Filters						
Guided Wave Beams						
Microwaves						
Measurements						
Propagation						
Resonators						
Waves						

INSTRUCTIONS

1. ORIGINATING ACTIVITY: Enter the name and address of the contractor, subcontractor, grantee, Department of Defense activity or other organization *(corporate author)* issuing the report.

2a. REPORT SECURITY CLASSIFICATION: Enter the overall security classification of the report. Indicate whether "Restricted Data" is included. Marking is to be in accordance with appropriate security regulations.

2b. GROUP: Automatic downgrading is specified in DoD Directive 5200.10 and Armed Forces Industrial Manual. Enter the group number. Also, when applicable, show that optional markings have been used for Group 3 and Group 4 as authorized.

3. REPORT TITLE: Enter the complete report title in all capital letters. Titles in all cases should be unclassified. If a meaningful title cannot be selected without classification, show title classification in all capitals in parenthesis immediately following the title.

4. DESCRIPTIVE NOTES: If appropriate, enter the type of report, e.g., interim, progress, summary, annual, or final. Give the inclusive dates when a specific reporting period is covered.

5. AUTHOR(S): Enter the name(s) of author(s) as shown on or in the report. Enter last name, first name, middle initial. If military, show rank and branch of service. The name of the principal author is an absolute minimum requirement.

6. REPORT DATE: Enter the date of the report as day, month, year; or month, year. If more than one date appears on the report, use date of publication.

7a. TOTAL NUMBER OF PAGES: The total page count should follow normal pagination procedures, i.e., enter the number of pages containing information.

7b. NUMBER OF REFERENCES: Enter the total number of references cited in the report.

8a. CONTRACT OR GRANT NUMBER: If appropriate, enter the applicable number of the contract or grant under which the report was written.

8b, 8c, & 8d. PROJECT NUMBER: Enter the appropriate military department identification, such as project number, subproject number, system numbers, task number, etc.

9a. ORIGINATOR'S REPORT NUMBER(S): Enter the official report number by which the document will be identified and controlled by the originating activity. This number must be unique to this report.

9b. OTHER REPORT NUMBER(S): If the report has been assigned any other report numbers *(either by the originator or by the sponsor)*, also enter this number(s).

10. AVAILABILITY/LIMITATION NOTICES: Enter any limitations on further dissemination of the report, other than those imposed by security classification, using standard statements such as:

(1) "Qualified requesters may obtain copies of this report from DDC."

(2) "Foreign announcement and dissemination of this report by DDC is not authorized."

(3) "U. S. Government agencies may obtain copies of this report directly from DDC. Other qualified DDC users shall request through _____."

(4) "U. S. military agencies may obtain copies of this report directly from DDC. Other qualified users shall request through _____."

(5) "All distribution of this report is controlled. Qualified DDC users shall request through _____."

If the report has been furnished to the Office of Technical Services, Department of Commerce, for sale to the public, indicate this fact and enter the price, if known.

11. SUPPLEMENTARY NOTES: Use for additional explanatory notes.

12. SPONSORING MILITARY ACTIVITY: Enter the name of the departmental project office or laboratory sponsoring *(paying for)* the research and development. Include address.

13. ABSTRACT: Enter an abstract giving a brief and factual summary of the document indicative of the report, even though it may also appear elsewhere in the body of the technical report. If additional space is required, a continuation sheet shall be attached.

It is highly desirable that the abstract of classified reports be unclassified. Each paragraph of the abstract shall end with an indication of the military security classification of the information in the paragraph, represented as *(TS)*, *(S)*, *(C)*, or *(U)*.

There is no limitation on the length of the abstract. However, the suggested length is from 150 to 225 words.

14. KEY WORDS: Key words are technically meaningful terms or short phrases that characterize a report and may be used as index entries for cataloging the report. Key words must be selected so that no security classification is required. Identifiers, such as equipment model designation, trade name, military project code name, geographic location, may be used as key words but will be followed by an indication of technical context. The assignment of links, rules, and weights is optional.

Unclassified
Security Classification